THE DIATOM HOLOBIONT IN A CHANGING ARCTIC OCEAN

2024

JAKOB K. GIESLER

Examination Committee

Date of colloquium: 19.12.2025

1. Examiner: Prof. Dr. Kai Bischof
University of Bremen

2. Examiner: Prof. Dr. Tilmann Harder
University of Bremen

3. Examiner: Prof. Dr. Astrid Gärdes
Hochschule Bremerhaven; Alfred Wegener Institute, Helmholtz Center for Polar and Marine Research

1. Reviewer: Dr. Sylke Wohlrab
Alfred Wegener Institute, Helmholtz Center for Polar Marine Research; Helmholtz Institute for Functional Marine Biodiversity

2. Reviewer: Prof. Dr. Eva Sonnenschein
Swansea University

3. Reviewer: Prof. Dr. Silke Langenheder
Uppsala University

The diatom holobiont in a changing Arctic Ocean

Dissertation zur Erlangung des akademischen Grades
Doktor der Naturwissenschaften

Dr. rer. nat.

Jakob K. Giesler

November, 2024

Table of contents

Acknowledgments

I dedicate this work to the many people who supported me during the last three years. Firstly, I would like to thank my supervisors Sylke Wohlrab and Tilmann Harder for putting their trust in me to let me work on this exciting project. I thank Sylke for her endless support, patience, excellent scientific guidance, and countless coffee breaks with lots of laughter in her office, at train stations, and on research vessels in stunning landscapes, which I will never forget. I thank Tilmann for his mentoring, clear scientific vision, and for supporting me in my scientific career in any possible way. I am deeply grateful for having had the opportunity to learn from such inspirational humans. Furthermore, I thank the great people who review this thesis including Eva Sonnenschein and Silke Langenheder for their willingness and time. I also thank Uwe John for his continuous support, encouragement, and optimism.

During my studies, I had the opportunity to work with inspiring and excellent scientists. Special thanks go to Dedmer Van de Waal, Mridul Thomas, and Florian Koch for being such amazing co-authors. I thank my great thesis advisory committee, including Cedric Munier, Gunnar Gerdts, and Marine Vallet for their scientific advice and for always keeping me on track. Moreover, I thank everyone in the 'Ecological Chemistry' section for contributing to this productive work environment, particularly Scarlett Trimborn and Boris Koch for keeping it all together. I also thank my lab-mates Avril Hoyningen, Cora Hörstmann, and Konstantinos Anestis for funny times and stupid jokes in the office. Furthermore, none of this work would have been possible without the excellent technical assistance from Nancy Kühne, Annegret Müller, Jennifer Bergemann, and Stefan Neuhaus.

Working on this thesis gave me the opportunity to travel to places I never thought I would be able to visit. I thank everyone who supported me on these adventures, most of all Thomas Juul-Pedersen, Luka Šupraha, and Charlotte Volpe.

During the last three years, I made amazing friends along the way that I hope to keep in touch with for many, many years. Thank you, Antonia Ahme, Linda Rehder, Ruben Schulte-Hillen, Carla Pein, Kristof Möller, Frederik Bussmann, Joel Bose, Marrit Jacob, and Benjamin Ahme, for being these awesome humans you are and for always motivating me to keep going.

Finally, my deepest gratitude goes to my parents, my brother, my sister, my nephew, and most of all Anika Happe, my partner in crime. These last three years would not have been possible without your love, care, and unconditional support.

Summary

Interactions between diatoms and bacteria are crucial for marine ecosystem functioning and the global climate as they largely govern primary production in marine systems and drive global biogeochemical cycles. Zooming in on the immediate surroundings of a diatom cell, a microhabitat for a diverse and overall mutualistic bacterial community can be found that enables reciprocal exchanges of metabolites benefiting both the diatom and its associated bacteria, which together form a discrete ecological unit – the holobiont. Despite considerable advancements in the molecular understanding of specific diatom-bacteria interactions, little is known about how diatom holobionts adapted to the multifactorial abiotic environment they naturally experience or how they jointly respond to environmental stress. Considering the profound effects of the microbiome on diatom growth, the potential dependency of the underlying mechanisms on abiotic drivers may have important implications for diatom adaptative potential to climate change in the rapidly warming Arctic and warming-induced distributional poleward range shifts of temperate diatoms. To address this knowledge gap, this thesis aims to understand diatom adaptation and responses to their abiotic environment from a holobiont perspective employed by stepwise laboratory experiments:

After a general introduction (chapter 1), chapter 2 identifies habitat-specific genetic adaptations of two closely related Arctic (*Thalassiosira gravida*) and temperate (*Thalassiosira rotula*) diatoms and the functional traits characterizing their responses to different levels of temperature, photoperiod, and nitrate as single drivers. The outcome suggests that besides habitat-specific thermal adaptations, the photoperiodic range is a previously neglected factor relevant to diatom biogeographic adaptation. This is based on the highly conserved competitive advantage under extremely short or long photoperiods of the Arctic diatom compared to the temperate diatom that showed the highest growth rates under intermediate photoperiods. The resulting competitive disadvantage for the temperate diatom under the extreme photoperiods that are characteristic for Arctic latitudes could constrain its potential for warming-induced poleward range shifts. Subsequently, in chapter 3, the net effect of the bacterial microbiome on diatom growth is decoupled from the holobiont. In a comparative approach, axenic and xenic cultures of the Arctic and temperate diatoms were exposed to specific factorial combinations of temperature (4; 9; 13.5°C) and photoperiod (4; 16; 24h) identified as crucial for Arctic adaptation and poleward range shifts based on the outcome of chapter 2. The results demonstrate a positive-net effect of the bacterial microbiome on host diatom growth that is particularly important at the margins of the respective diatom's fundamental niches, thus

substantially shaping their realized niches. However, the outcome of the study did not only reveal treatment-dependent patterns of growth-supporting effects but also highlighted risks for tipping points of diatom mutualistic microbiomes towards growth-inhibitory effects under certain multi-stressor conditions. Building on the previously generated knowledge, chapter 4 explores how specific temperature-photoperiod combinations employed in chapter 3 affect the diatom-associated bacterial microbiome community composition and the underlying host-microbiome interactions on the molecular level. Therefore, xenic and axenic cultures of the Arctic diatom *T. gravida* were exposed to a selected subset of temperature (9; 13.5°C) combined with photoperiod (16; 24h). The outcome repeatedly demonstrated a positive net effect of the bacterial microbiome on host growth and a mostly compositionally stable microbiome community. However, the 13.5°C/16:8h treatment differed from all other treatments in terms of microbiome composition as well as (meta)transcriptomics of the microbiome and the diatom host, coinciding with the loss of the *Sulfitobacter* clade as a key microbiome member. A combined diatom-bacteria transcriptome cluster analysis revealed tightly linked host-microbiome co-expression patterns that were driven by main and interactive effects of temperature and photoperiod. Despite the general resilience in terms of diatom growth rates, increased microbiome compositional shifts and potential bacterial cell detachment from the host highlight the risk for microbiome dysbiosis under thermal stress. In chapter 5 a novel method is introduced that enables the collection of urgently needed data about species-specific diatom microbiomes in natural systems. This is achieved by an effective approach that allows studying the diatom-associated microbiome community composition on the individual host cell level. Additionally, the study demonstrates coordinated microbiome dynamics for individual diatom host cells of *T. gravida* in response to nitrate or vitamin limitation that reproducibly result in compositional increases of distinct bacterial microbiome members.

Overall, this thesis highlights the value of stepwise experimental designs. Narrowing down highly resolved single drivers to relevant and carefully chosen multifactorial conditions in combination with multi-omics techniques provided systematic insights into how diatoms and their associated bacterial microbiomes jointly respond to their abiotic environment. Ultimately, the outcome improves our understanding of how diatom holobionts adapted to occupy Arctic or temperate niches and to which extent diatom-associated bacterial microbiomes help to adapt their host under environmental conditions relevant to climate change and associated climate change-mediated poleward range shifts.

Zusammenfassung

Die Interaktionen zwischen Diatomeen und Bakterien sind von entscheidender Bedeutung für marine Ökosysteme und das globale Klima, da sie die Primärproduktion in marinen Systemen regulieren und globale biogeochemische Kreisläufe steuern. Betrachtet man die unmittelbare Umgebung einer Diatomeenzelle, findet man ein Mikrohabitat für eine vielfältige und insgesamt mutualistische Bakteriengemeinschaft, die einen wechselseitigen Austausch von Metaboliten ermöglicht, von dem sowohl die Diatomee als auch die mit ihr assoziierten Bakterien profitieren. Zusammen bilden sie somit eine eigenständige ökologische Einheit - den Holobionten. Trotz jüngster Fortschritte im molekularen Verständnis spezifischer Diatomeen-Bakterien-Interaktionen ist wenig darüber bekannt, wie sich Diatomeen-Holobionten an die multifaktorielle abiotische Umwelt anpassen, der sie natürlicherweise ausgesetzt sind, oder wie sie gemeinsam auf Umweltstress reagieren. In Anbetracht der tiefgreifenden Auswirkungen des Mikrobioms auf das Wachstum von Diatomeen, könnte die mögliche Abhängigkeit dieser Mechanismen von abiotischen Faktoren essenziell für die Anpassungsfähigkeit von Diatomeen sein. Dies betrifft nicht nur das Anpassungspotenzial von Diatomeen an den Klimawandel in der sich schnell erwärmenden Arktis, sondern auch die durch die Erwärmung bedingte Verschiebung der Verbreitungsgebiete von temperaten Diatomeen in Richtung der Pole. Um diese Wissenslücke zu schließen, zielt diese Arbeit darauf ab, die Anpassung von Diatomeen und ihre Reaktionen auf die abiotische Umwelt aus einer Holobionten-Perspektive zu verstehen. Dies wird durch aufeinander aufbauende Laborexperimente umgesetzt:

Nach einer allgemeinen Einführung (Kapitel 1) werden in Kapitel 2 die lebensraumspezifischen genetischen Anpassungen von zwei eng verwandten Arktischen (*Thalassiosira gravida)* und temperaten (*Thalassiosira rotula*) Diatomeen identifiziert. Zudem werden funktionelle Merkmale, die ihre Reaktionen auf unterschiedliche Temperatur-, Photoperioden- und Nitratwerte als separate Faktoren charakterisieren, bestimmt. Die Ergebnisse zeigen, dass neben den lebensraumspezifischen thermischen Anpassungen die Photoperiode ein bisher vernachlässigter Faktor ist, der für die biogeographische Anpassung von Diatomeen relevant ist. Dies basiert auf dem stark konservierten kompetitiven Vorteil von Arktischen Diatomeen unter extrem kurzen oder langen Photoperioden im Vergleich zu temperaten Diatomeen, die die höchsten Wachstumsraten bei mittleren Photoperioden zeigten. Der daraus resultierende kompetitive Nachteil für temperate Diatomeen unter den für Arktische Breitengrade charakteristischen extremen Photoperioden könnte ihr Potenzial für polwärts gerichtete Verschiebungen ihres Verbreitungsgebiets einschränken. Anschließend wird in Kapitel 3 der

Nettoeffekt des bakteriellen Mikrobioms auf das Diatomeenwachstum vom Holobionten entkoppelt. In einem vergleichenden Ansatz wurden axenische und xenische Kulturen der Arktischen und temperaten Diatomeen ausgewählten Faktorenkombinationen von Temperatur (4; 9; 13,5°C) und Photoperiode (4; 16; 24h) ausgesetzt, die auf der Grundlage der Ergebnisse in Kapitel 2 als entscheidend für ihre Anpassung an die Arktis und die polwärts gerichtete Verschiebung von Verbreitungsgebieten identifiziert wurden. Die Ergebnisse zeigen einen meist positiven Nettoeffekt des bakteriellen Mikrobioms auf das Wachstum der Wirtsdiatomee, der vor allem an den Rändern der fundamentalen Nischen der jeweiligen Diatomeen von Bedeutung ist und somit wesentlich ihre realisierten Nischen prägt. Die Ergebnisse der Studie zeigen jedoch nicht nur wachstumsfördernde Effekte, sondern weisen auch auf die Gefahr hin, dass sich das Mikrobiom von Diatomeen unter bestimmten Multi-Stressor-Bedingungen auch negativ auf das Diatomeenwachstum auswirken kann. Aufbauend auf den zuvor gewonnenen Erkenntnissen wird in Kapitel 4 untersucht, wie sich spezifische Temperatur-Photoperioden-Kombinationen aus Kapitel 3 auf die Zusammensetzung von Diatomeen-assoziierten Mikrobiomgemeinschaften sowie auf die zugrunde liegenden molekularen Wirt-Mikrobiom-Interaktionen auswirken. Dazu wurden xenische und axenische Kulturen der Arktischen Diatomee *T. gravida* ausgewählten Kombinationen von Temperatur (9; 13,5°C) und Photoperiode (16; 24h) ausgesetzt. Die Ergebnisse bestätigten einen positiven Nettoeffekt des bakteriellen Mikrobioms auf das Wachstum des Wirts und eine in ihrer Zusammensetzung größtenteils stabile Mikrobiomgemeinschaft. Die 13,5°C/16:8h-Bedingung unterschied sich jedoch von allen anderen getesteten Bedingungen in Bezug auf die Zusammensetzung des Mikrobioms sowie die Mikrobiom- und Wirts- (Meta-)Transkriptomik, was mit dem Verlust der *Sulfitobacter*-Gruppe als bakterielles Schlüsselmitglied des Mikrobioms zusammenfiel. Eine kombinierte Transkriptom-Cluster-Analyse von Diatomeen und Bakterien ergab eng verknüpfte Koexpressionsmuster zwischen Wirt und Mikrobiom, die durch Haupt- und Interaktionseffekte von Temperatur und Photoperiode bestimmt wurden. Trotz der durch das Mikrobiom gegebenen allgemeinen Widerstandsfähigkeit in Bezug auf die Wachstumsraten der Diatomeen verdeutlichen Verschiebungen in der Mikrobiomzusammensetzung sowie die potenzielle Ablösung von Bakterienzellen von der Wirtsdiatomee das Risiko einer Mikrobiom-Dysbiose unter Temperaturstress. In Kapitel 5 wird ein eigens entwickelter methodischer Ansatz vorgestellt, der es ermöglicht, die dringend benötigten Informationen über artspezifische Diatomeen-Mikrobiome in natürlichen Systemen zu erheben. Dies wird ermöglicht durch eine effektive Methode zur Untersuchung der Zusammensetzung der Diatomeen-assoziierten Mikrobiom-Gemeinschaft auf der Ebene von einzelnen Wirtsindividuen. Darüber hinaus zeigt

die Studie koordinierte Mikrobiom-Dynamiken für einzelne Wirtszellen, welche als Reaktion auf Nitrat- oder Vitamin-Limitierung reproduzierbar zu einer Zunahme bestimmter bakterieller Gruppen des Mikrobiom führten.

Insgesamt unterstreicht diese Arbeit den Wert einer schrittweisen experimentellen Umsetzung. Die Eingrenzung hoch aufgelöster einzelner abiotischer Einflussfaktoren auf relevante und sorgfältig ausgewählte multifaktorielle Bedingungen in Kombination mit Multi-Omics-Techniken ermöglichte systematische Einblicke, wie Diatomeen und ihre bakteriellen Mikrobiome gemeinsam auf ihre abiotische Umwelt reagieren. Die gewonnenen Erkenntnisse verbessern unser Verständnis darüber, wie sich Diatomeen-Holobionten an die Besiedlung Arktischer oder temperater Nischen angepasst haben und inwieweit Diatomeen-Mikrobiome ihre Wirte an Umweltbedingungen anpassen, die für den Klimawandel und die damit verbundene polwärts gerichtete Verschiebungen ihrer Verbreitungsgebiete relevant sind.

Abbreviations

AHL	N-acyl-Homoserine Lactone
ASV	Amplicon Sequence Variant
CAAS	Convergent Amino Acid Substitution
CTD	Conductivity Temperature Depth
DAPI	4`,6-Diamidin-2-phenylindol
DHPS	2,3-dihydroxypropane- 1-sulfonate
DNA	Deoxyribonucleic acid
DOC	Dissolved Organic Carbon
DOM	Dissolved Organic Matter
HGT	Horizontal Gene Transfer
HMW	High Molecular Weight
IAA	Indole-3-acetic acid
ITS	Internal Transcribed Spacer
$K_{1/2}$	Half-saturation constant
LMW	Low Molecular Weight
MAG	Metagenome Assembled Genome
POC	Particulate Organic Carbon
RCP	Representative Concentration Pathway
RDOC	Refractory Dissolved Organic Carbon
RNA	Ribonucleic acid
ROS	Reactive Oxygen Species
TEP	Transparent Exopolymeric Particles
T_{max}	Thermal maximum
T_{min}	Thermal minimum
T_{opt}	Thermal optimum
Trp	Tryptophan
µm	micrometer

1 Introduction

1 INTRODUCTION

1.1 Marine microbes and their importance for global biogeochemical cycles

The vast majority of life in the oceans is invisible to the human eye. Yet, marine microorganisms which comprise of prokaryotes and unicellular eukaryotes make up ~70% of the total marine biomass (Bar-On et al., 2018). Their intricate functions and interactions have driven evolutionary innovations, nutrient cycling, and ecosystem stability, fundamentally shaping the planet's biosphere and enabling diverse life forms to thrive in various environments (Falkowski, 1994, Field et al., 1998, Azam and Malfatti, 2007, Jiao et al., 2024). After the emergence of prokaryotes almost 4 billion years ago in an alkaline hydrothermal vent (Lane et al., 2010), the endosymbiosis of two prokaryotes gave rise to ancient eukaryotic life approximately 1.8 billion years ago (Sagan, 1967, Parfrey et al., 2011). The subsequent eukaryotic evolution has not only enabled human life but also led to a large taxonomic diversity of unicellular eukaryotes, also called protists, that still dominate the eukaryotic tree of life today (Worden et al., 2015). Among marine protists, particularly phytoplankton are crucial for sustaining the marine food web and contribute as much as 50% to global primary productivity (Field et al., 1998) by transforming inorganic carbon into biomass using solar light energy and a few macro- and micronutrients.

The different evolutionary pathways of eukaryotes were shaped by hard and soft selection pressures, adapting them to their abiotic environment but also to one another. Despite their different evolutionary trajectories, eukaryotes never became fully independent from prokaryotes and, for some essential processes, still rely on their genetic functions (e.g., biosynthesis of certain vitamins and nitrogen fixation). Therefore, the solitary eukaryote does not exist. Consequently, this applies also to phytoplankton whose interactions with other marine microbes are of particular importance due to their key role in shaping aquatic ecosystems and the global climate.

Since the introduction of the term ‘plankton’ (Greek for wanderers) in 1889 by Prof. Victor Hensen, who led the first expedition to study these suspended (i.e., drifting) aquatic organisms, the understanding of their importance for global biogeochemical cycles has continuously grown. This includes the vital role of these organisms for the Earth’s climate, chemistry and ecosystem dynamics by cycling of essential elements including carbon, nitrogen, sulfur and oxygen (Falkowski, 1994, Falkowski et al., 2008).

One way how phytoplankton drives global biogeochemical cycles is their key role in the global carbon cycle as they fuel the biological carbon pump (Fig. 1.1, Field et al., 1998, Nowicki et al., 2022). Besides the physical carbon pump, which draws dissolved carbon dioxide to deeper

layers by deep water formation (Macdonald and Wunsch, 1996), the biological carbon pump refers to the biological sequestration of carbon from the atmosphere to the deep ocean sediments, where it is stored for geologically relevant time scales (Nowicki et al., 2022). Generally, the processes that are comprised in the biological carbon pump start with the uptake of dissolved carbon dioxide by phytoplankton, transferring the inorganic carbon into organic biomass by photosynthesis. As phytoplankton cells decay or are consumed by higher trophic levels (e.g., zooplankton), their remains sink to deeper layers of the ocean, along with the fecal pellets of their consumers, effectively transporting carbon away from the atmosphere (Chisholm, 2000). However, as during this process, the sinking particulate organic carbon (POC) is degraded by heterotrophic bacteria, it is estimated that only ~1% of the original amount of carbon reaches long-term storage in deep-sea sediments (DeVries, 2022, Friedlingstein et al., 2022).

Besides phytoplankton, also bacteria, archaea, and viruses play complex but important roles in global carbon cycling and sequestration (Jiao et al., 2010, Jiao et al., 2024). Bacteria and archaea utilize labile dissolved organic matter (DOC) released by phytoplankton and zooplankton fecal pellets and are subsequently grazed by microzooplankton. Thereby, the contained carbon is returned back into the food chain in a particulate form – a process that was already introduced as the microbial loop in 1983 (Azam et al.). At the same time, these marine microbes convert labile, bioavailable DOC into much more complex, less bioavailable forms of carbon called recalcitrant DOC (RDOC). This conversion is mediated either by direct exudation, degradation of POC, or by cell lysis and subsequent release of microbial cell surface macromolecules (Jiao et al., 2010). RDOC can persist for millennia and therefore also represents a large reservoir of carbon in the ocean comparable to the atmospheric CO_2 reservoir (Jiao et al., 2024). This mechanism has been termed ‘microbial carbon pump’ and is fueled further by viruses that provide fresh labile DOC to the system by lysing other marine microbes – the so called ‘viral shunt’ (Wilhelm and Suttle, 1999, Jiao et al., 2010). However, the viral lysis of phytoplankton also results in the sedimentation of their cellular debris (‘viral shuttle’), thus further supporting the downward carbon flux of the biological carbon pump (Kolundzija et al., 2022).

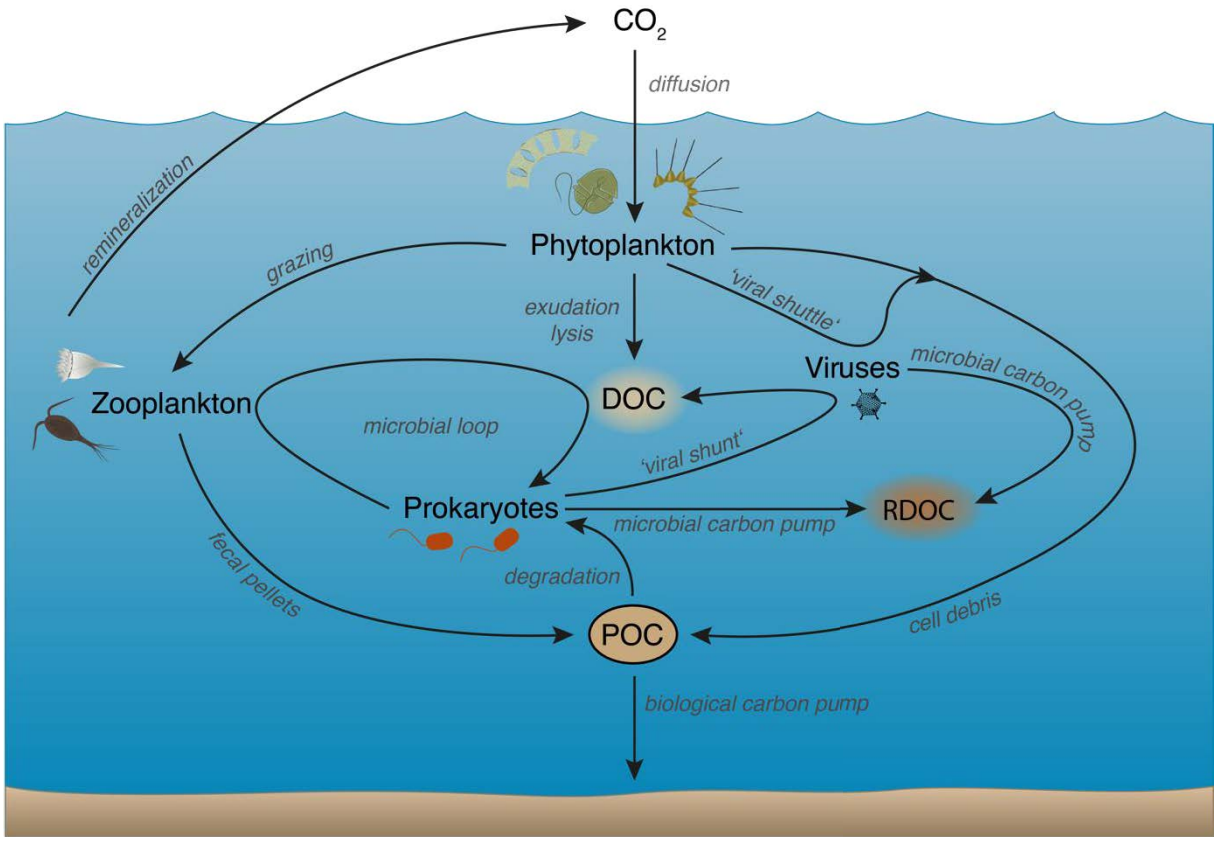

Fig. 1.1: Key biological processes in global ocean carbon cycling. Important marine planktonic and microbial groups (phytoplankton, zooplankton, prokaryotes, and viruses) are labeled black and the processes that mediate carbon cycling and export between these organisms are labeled grey. The scheme includes processes related to the biological carbon pump (i.e., phytoplankton primary production, zooplankton grazing and respective POC export in terms of sedimentation of cellular debris and zooplankton fecal pellets. Microbial carbon pump (production of RDOC by bacteria and viruses), the microbial loop, and import viral processes (viral shunt and viral shuttle).

Although the biological carbon pump is equivalent to about 10.2 gigatons of stored carbon per year and has thereby significantly shaped global climate over geological timescales (Nowicki et al., 2022), anthropogenic carbon dioxide emissions far exceed its capacity, as it takes the biological carbon pump approximately one million years to store the anthropogenic carbon emissions of a single year (Falkowski, 2015).

1.2 Poleward-shifting habitats in a warming world

Due to human activity, the Earth's climate is warming at a rate unprecedented for millennia (IPCC, 2023). Following industrialization, the emission of greenhouse gases led to an average global temperature increase of 1.1°C at a mean warming rate of 0.06°C per decade since 1850 (IPCC, 2023). Atmospheric carbon dioxide concentrations rose to 422 ppm (= parts per million, August 2024), thus far exceeding pre-industrial values of 280 ppm and prior maximum concentrations of the past 800.000 years (NOAA, 2024). Impacts of climate warming on the biosphere have been documented on every continent and every ocean basin (Rosenzweig et al., 2008). However, the magnitude of climate warming is not equally distributed across the globe (Fig. 1.2). This concerns particularly the Arctic, which is warming multiple times faster than the global average (Maturilli et al., 2013, Rantanen et al., 2022). At the Arctic Svalbard archipelago, a time series of air temperature measurements even recorded an average warming rate of 1.35°C per decade (Maturilli et al., 2013). This phenomenon, also known as 'Arctic amplification', is largely driven by the ice-albedo effect, which describes the feedback mechanism of how ice and snow reflect sunlight, but as they melt, darker surfaces absorb more heat, thereby accelerating the feedback by further warming and ice loss (Bintanja and Krikken, 2016). Furthermore, the observed shifts in isotherms are significantly larger in the marine realm compared to terrestrial environments (Burrows et al., 2011).

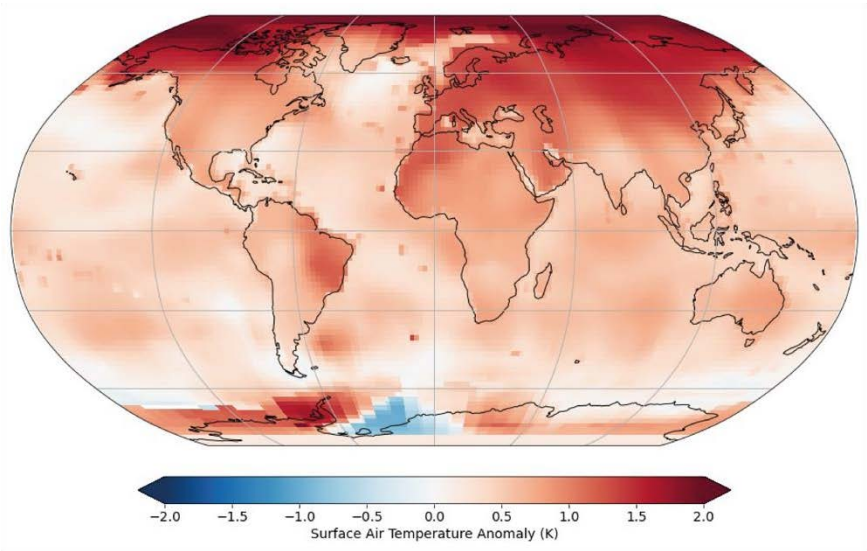

Fig. 1.2: Global surface air temperature anomaly in kelvin (K) for the 1991-2020 time period, relative to the 1951-1980 baseline period. *Taken from Lenssen et al. (2019).*

As most marine organisms are ectotherms, they respond very sensitively to these thermal changes. Although there have already been warmer episodes in the Earth's history (Huber et al.,

2018, Hearing et al., 2018, Retallack, 2013), the unnaturally rapid temperature increase particularly challenges marine organisms' potential for adaptation to keep track with these changes (Munday et al., 2013). As a consequence (among many others), climate warming alters species distributional ranges, i.e., the geographical area in which a species occurs during the entirety of its lifetime (Poloczanska et al., 2013, Hodapp et al., 2023). In general, the limits of these distributional ranges are defined where emigration and death exceed the rates of immigration and birth (Gaston, 1990). Already in 1958, it was noticed that these boundaries of a species' distributional range are set by the respective abiotic factor for which it has the smallest tolerance (Bartholomew, 1958). Nowadays, however, it is increasingly accepted that to comprehensively define a species' geographic range, also complex biotic interactions and interacting environmental drivers have to be taken into account (Lynch et al., 2014, Eckhart et al., 2011).

With progressing global warming, species' distributional ranges will shift poleward as they track suitable thermal conditions (Poloczanska et al., 2013, Burrows et al., 2014). It is assumed that tropical habitats will become increasingly inhospitable and temperate regions will experience tropicalization, leading to a global reorganization of species (Hodapp et al., 2023). Following the spatial patterns of global climate warming, species distributional range shifts are projected to happen four times faster in marine systems compared to the terrestrial environment (Sorte et al., 2010, Burrows et al., 2011, Poloczanska et al., 2013). This is not only due to lower dispersal constraints in marine environments but also due to smaller thermal safety margins of marine organisms (i.e., the difference between organismal temperature and critical lethal temperature) compared to terrestrial organisms (Pinsky et al., 2019). For this reason, marine organisms track temperature changes more closely (Antao et al., 2020).

Habitat suitability models attempt to project these range shifts by considering forecasted temperature increases in concert with as many other environmental factors as possible that define species' fundamental niches. Yet, the accuracy of these models depends to a large extent on the underlying knowledge of these niches, which is often very limited and does also not account for the complex biotic interactions that ultimately define the actual realized niche of a species (Wisz et al., 2013). A habitat suitability model by Hodapp et al (2023) estimated that half of all marine species will eventually lose 50% of their core habitat under the IPCC high emission scenario RCP 8.5 (Fig. 1.3). In addition to the migration towards higher latitudes, contiguous habitats are expected to become more fragmented, thus decreasing effective population sizes (Hodapp et al., 2023).

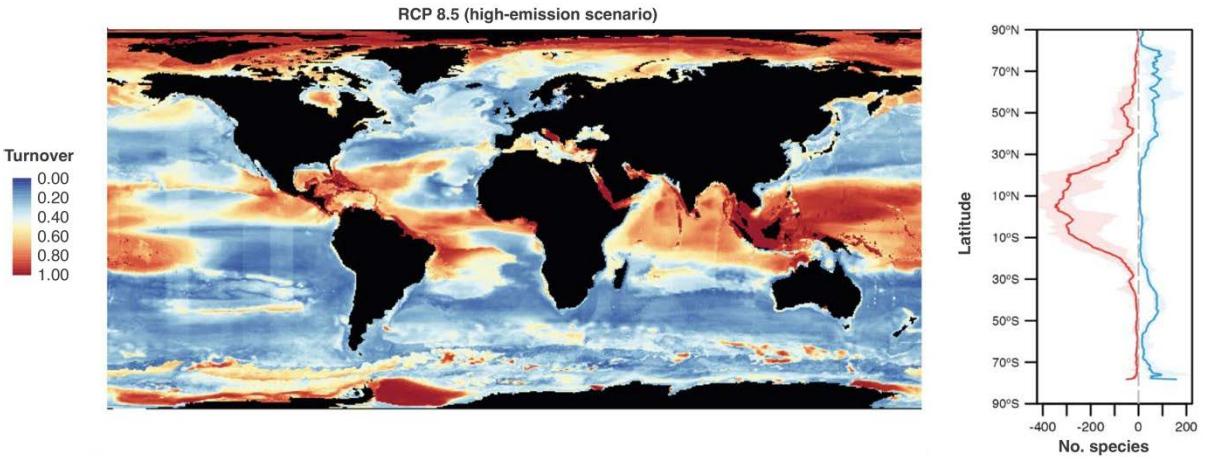

Fig. 1.3: Global map of modeled turnover in marine species composition (containing 33,500 marine species) from the beginning to ending of the 21st century under the RCP 8.5 (i.e., high-emission) scenario. Turnover values of 0 refer to no compositional changes while a value of 1 refers to the complete loss or replacement of all species. The plot panel on the right shows the projected median number of species that is gained (blue) or lost (red) across latitudes and the respective 50% quantiles (shaded error margins). *Modified after Hodapp et al (2023).*

Consequences of poleward range shifts affect the marine ecosystem at many levels, not only by altering physiological processes directly but also by changing biological interactions. This involves the introduction of new predators (Hodapp et al., 2023) but has also consequences for the very base of the food web in terms of changing planktonic abundances, diversity, and community composition (Benedetti et al., 2021). In the North Atlantic, it has been shown that climate change-mediated range shifts of zooplankton significantly lowered the effectivity of the biological carbon pump over the last 55 years (Brun et al., 2019). However, particularly range shifts of phototrophic phytoplankton are of concern due to their crucial role in the marine ecosystem (Field et al., 1998). Despite large differences in the estimated speed of phytoplankton poleward migration ranging from 35 km per decade (Benedetti et al., 2021) up to hundreds of km per decade (Li et al., 2017) both empirical evidence of historical phytoplankton distribution patterns as well as species distribution models agree on the existence of this major restructuring of phytoplankton communities. However, it is important to consider that climate-mediated range shifts may be highly variable among species, thus further complicating their predictions (Chivers et al., 2017).

Despite Arctic amplification and the resulting fast environmental changes at high latitudes which therefore increasingly become thermally inhabitable for temperate species, phytoplankton range shifts towards Arctic habitats are critically understudied. Thus, knowledge about how Arctic-characteristic conditions such as the extreme polar light regime may constrain fundamental niches of temperate phytoplankton interactively with other environmental drivers

and biotic interactions is urgently needed. This mechanistic understanding is crucial for predictions about how phytoplankton will respond and potentially adapt to changing or novel environmental conditions imposed by climate change and associated range shifts.

1.3 Responding and adapting to a changing environment

On the physiological level, phytoplankton growth is driven by environmental conditions such as temperature and essential resources including light, macronutrients (i.e., phosphorous, nitrogen, silicate), and micronutrients such as vitamins and various trace metals (Guillard, 1975, Behrenfeld et al., 2008). If only one of these resources is not available in a sufficient ratio to the other resources, phytoplankton growth is limited (Liebig's law of the minimum, Liebig, 1840). Under constant conditions, a single winner species would outcompete all other species based on the respective lowest demand for a given critical resource (Tilman, 1977). However, as these conditions and resources are highly variable in natural systems, constantly responding to a variety of abiotic and biotic drivers shapes interspecific competition of phytoplankton, fostering a diverse community ('paradox of the plankton', Hutchinson, 1961, Sommer, 1996, Descamps-Julien and Gonzalez, 2005). Within a given range for each driver (i.e., an organism's plasticity), phytoplankton can respond rapidly to changes in their environment, allowing them to adjust their traits and growth rates on short timescales of hours to days (Weisse et al., 2016, Schaum et al., 2022, Ferreira et al., 2020, Lutz et al., 2001). These responses are steered by changes in gene expression and biochemical processes on the individual level rather than genetic changes in the population (Shilova et al., 2020, Hong et al., 2023). In its very essence, adaptation refers to evolutionary changes in phytoplankton populations that occur over longer timescales of months to years, driven by natural selection pressures acting on genetic variation (Padfield et al., 2016, Irwin et al., 2015, Filatov and Kirkpatrick, 2024). Through adaptation, phytoplankton populations can evolve traits that suit their changing environment, thus increasing their fitness and allowing them to thrive under these new conditions. Therefore, adaptation results in the alteration of an organism's plasticity.

1.3.1 Phytoplankton responses to single and multiple drivers

Studying an organism's response to an abiotic factor or a given resource's availability is the prerequisite to predict its response in, e.g., habitat suitability models. To determine the plasticity for a specific factor, reaction norm experiments can be conducted, which describe a pattern of

phenotypic expression of a single genotype across an environmental gradient (Oomen and Hutchings, 2022). In the context of phytoplankton responses, typically a fitness-related parameter (e.g., growth rate, nutrient uptake, photosynthetic rate) is measured across a gradient of the environmental parameter of interest (Eppley and Thomas, 1969, Boyd et al., 2013, Thomas et al., 2017, Fig. 1.4a, b). Due to their known profound effect on phytoplankton physiology, a lot of studies investigated phytoplankton reaction norms for temperature, light intensity, and nutrient availability, with each of these reaction norms following distinct shapes:

Temperature reaction norms (also known as thermal performance curves) are described by unimodal, left-skewed functions, i.e., the performance gradually increases until a thermal optimum (T_{opt}) is reached, followed by a sharp decline in performance (Eppley, 1972). The reaction norm for light intensity starts with a steep incline until an optimum irradiance (I_{opt}) (Litchman and Klausmeier, 2008). Thereafter, detrimental effects of high light intensity (photoinhibition) can have damaging effects and thus increasingly impair the performance (Ryther, 1956). Reaction norms of nutrient availability typically follow a saturating function. The half-saturation constant ($K_{1/2}$) describes the nutrient concentration at which 50% of the maximum growth rate or maximum nutrient uptake rate is achieved (Eppley and Thomas, 1969).

Despite the general applicability of these reaction norm functions for phytoplankton, the range of the resulting response curves as well as the exact position on the parameter scale may vary not only between different species, or differently adapted genotypes of the same species, but even for the same genotype depending on pre-experimental acclimation to the respective conditions (Thomas et al., 2012, Boyd et al., 2013).

Compared to the number of studies devoted to phytoplankton responses for temperature, nutrient availability or light intensity, other factors such as the effect of photoperiod on phytoplankton growth, have been barely studied (Theus et al., 2022). Despite the recognized importance of photoperiod on the cellular level by steering phytoplankton circadian rhythms (Annunziata et al., 2019) as well as driving phytoplankton community turnover (Longobardi et al., 2022), there is currently no generally applicable mathematical model that describes the relationship between photoperiod and growth. To some extent, this might be owed to the fact that studying the effect of photoperiod on phytoplankton growth is complicated in terms of experimental design. Either the amounts of photons per day differ between different photoperiodic levels if the light intensity is kept the same, or if this is compensated for by

adjusting the light intensity between the levels, interactive effects of photoperiod and light intensity are introduced (Theus et al., 2022).

As an environmental driver is never acting in isolation but is always part of a multifactorial environment, it is important to consider interactive effects between different drivers (Thomas et al., 2017, Edwards et al., 2016, Heinrichs et al., 2024). More precisely, the response of a phytoplankton cell to a respective abiotic factor may be affected by the given level of another abiotic factor in a non-linear manner and may even be reversed in some cases. Multifactorial experiments that test the response of an organism towards multiple factors simultaneously by employing different combinations of the respective factors can identify these interactions and display them as a response surface (e.g., Thomas et al., 2017, Theus et al., 2022, Heinrichs et al., 2024).

For phytoplankton growth, multiple of these interaction effects have been identified in laboratory experiments. For instance, an interactive effect of light intensity and temperature on phytoplankton growth was demonstrated by Edwards et al. (2016), resulting in a decrease in T_{opt} of ~5°C under light limitation. A similar interaction effect on phytoplankton growth has been identified for temperature and nitrate availability. Precisely, T_{opt} is a saturating function of nitrate concentration, leading to a decrease in T_{opt} of ~4°C under nitrate limitation (Thomas et al., 2017, Fig. 1.4c). Also, interactive effects of nutrient availability and light intensity were found and are based on the interdependency and consequential co-limitation of these resources (Cloern, 1999, Dickman et al., 2006). On the cellular level, the reasons for these interactions are complex but may include links of physiological processes (e.g., nitrate uptake and reduction to NH_4 is coupled to photosynthetic pigment biosynthesis) (Kanda et al., 1989) as well as energy reallocation between different cellular pathways (Thomas et al., 2017). Also, combinations of these interactions with more than two factors are possible and contribute to more realistic predictions of phytoplankton population growth (Spilling et al., 2015, Brennan and Collins, 2015, Boyd et al., 2016). Overall, the responses of phytoplankton to their naturally multifactorial environment are an important piece of the puzzle to understanding their realized niche and thus their global biogeography.

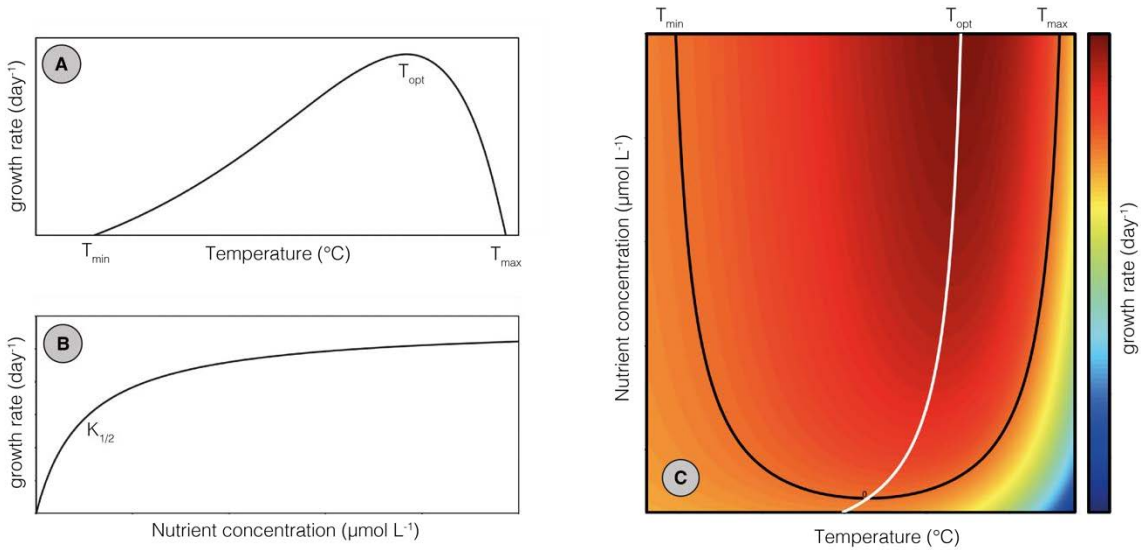

Fig. 1.4: Population growth response to temperature and nitrogen as single drivers and their combined effects in a multiple-driver context. (A) illustrates the population growth response to a thermal gradient (i.e., its thermal reaction norm), highlighting the respective thermal minimum (T_{min}), optimum (T_{opt}), and maximum (T_{max}). (B) demonstrates population growth across a gradient of nutrient concentrations (the curve also applies to nutrient uptake instead of growth as a dependent variable). The half-saturation constant ($K_{1/2}$) is labeled. (C) depicts the interactive effect of temperature and nutrients on the population growth rate, highlighting that T_{opt} (white line) is a saturating function of nutrient concentration. The black line ranging from T_{min} to T_{max} shows the zero net growth isocline. *Modified after Thomas et al. (2017).*

1.3.2 Phytoplankton adaptation across latitudinal gradients

While some abiotic factors that drive phytoplankton growth appear to be rather unstructured globally and act on smaller spatial scales (e.g., salinity, nutrients) (Richon and Tagliabue, 2021), other factors that are driven by solar radiation such as surface temperature or annual photoperiodic ranges generally follow a latitudinal gradient. Consequently, understanding the role of these factors and their potential interactions with other abiotic factors in shaping phytoplankton eco-evolutionary adaptation at a given latitude is crucial to improve predictions about climate change-mediated poleward range shifts.

Thermal adaptation of phytoplankton has been extensively studied and the existing global patterns are comparably well defined. Although the temperature optima, maxima and minima of phytoplankton species across different latitudes clearly reflect a decreasing pattern towards the poles (Fig. 1.5, Thomas et al., 2012, Chen, 2015), the thermal optima are usually several degrees higher than the average environmental temperature they experience (Thomas et al., 2012). This is likely owed to the fact that living below T_{opt} is a 'safer' ecological strategy, as even small temperature fluctuations beyond T_{opt} can have detrimental effects on ectothermic organisms due to the sharp decline of temperature reaction norms beyond T_{opt} (Martin and Huey,

2008). A clear imprint of latitudinal differences in annual environmental temperature amplitudes is also reflected in the finding that the T_{opt} of phytoplankton species in tropical regions is much closer to their mean environmental temperature compared to that of temperate and polar phytoplankton (Thomas et al., 2012). Regarding the breadth of an organism's thermal niche, for terrestrial organisms, it generally increases with latitude based on the poleward increasing climate variability ('Janzen's hypothesis', Janzen, 1967). For phytoplankton, however, this trend is weaker (Chen, 2015, Thomas et al., 2016). This could potentially be explained by the discrepancy in global patterns of climate variability between aquatic and terrestrial systems. In aquatic systems, thermal variability is largest in temperate regions due to constrained minimum temperatures in polar waters that are around the freezing point of seawater.

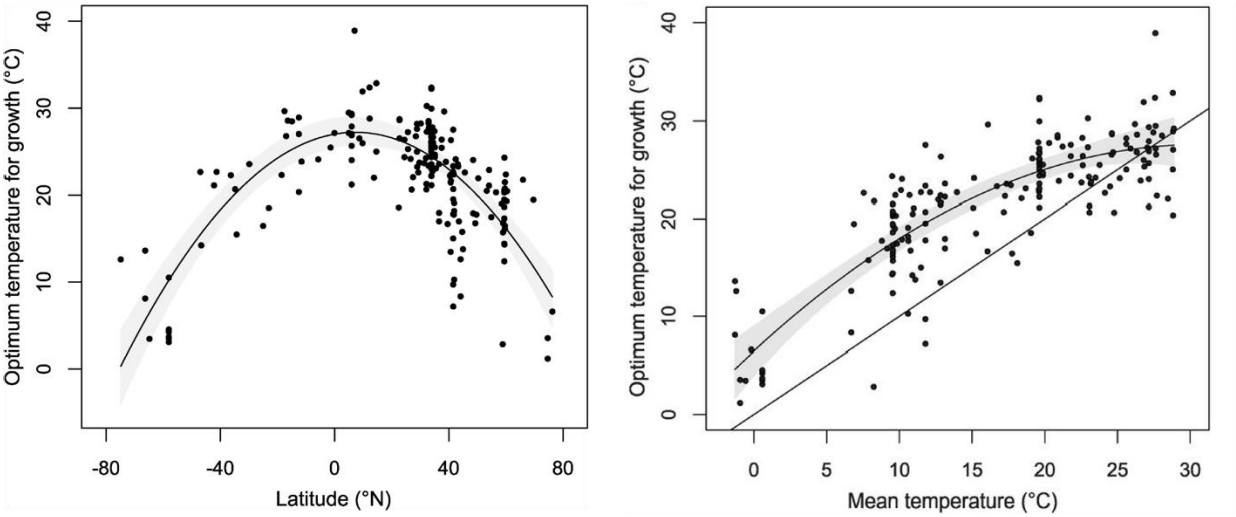

Fig. 1.5: Global patterns of phytoplankton thermal adaptation. Left: Thermal optima of 194 marine and estuarine phytoplankton species across a latitudinal gradient of their isolation origin (black points). A regression line (black line) is displayed along 95% confidence bands (grey shaded area). Right: Thermal optima across the respective mean environmental temperatures at the isolation origin of the respective phytoplankton species (black points), along with a regression line (black curved line) and the respective 95% confidence bands (grey-shaded area). The straight black line illustrates a 1:1 relationship as a comparison. Thermal optima were derived from temperature reaction norm experiments. *Modified after Thomas et al. (2012).*

In contrast to the numerous studies about the thermal adaptation of phytoplankton, comparably little is known about their adaptation to different photoperiodic ranges across latitudinal gradients and how this affects phytoplankton biogeography (Theus et al., 2022). This applies particularly to extreme photoperiods that are imposed by polar night and polar day at high latitudes (Fig. 1.6). While in tropical regions, phytoplankton experience only small differences in photoperiods over the year, the annual photoperiodic range increases towards the poles. At the extremes, the transition phase from complete darkness to continuous light takes less than 4

weeks (e.g., beyond 85°N). Consequently, in high-latitude ecosystems, phytoplankton species not only need to tolerate these extreme ranges but also need to be able to adapt their physiological processes quickly enough to cope with the rate of changes in photon flux. On the cellular level, as a consequence of this extreme polar light regime in terms of photoperiods but also light intensity and spectrum, polar phytoplankton evolved a highly adaptive photosynthetic machinery (Croteau et al., 2021, Svenning et al., 2024). With regard to potential interactive effects of photoperiod with other drivers, the few existing studies point towards interactive effects of irradiance and temperature on phytoplankton growth (Theus et al., 2022). However, the existing studies mostly did not cover the full range of possible photoperiods and/or did not compare species or genotypes from different latitudes. Moreover, interactions with biotic factors, e.g., symbiotic relationships that potentially affect species realized niches are currently unknown. Consequently, the lack of knowledge about the response of phytoplankton towards these extreme light regimes represents considerable uncertainty in the projection of poleward range shifts (Tougeron, 2021).

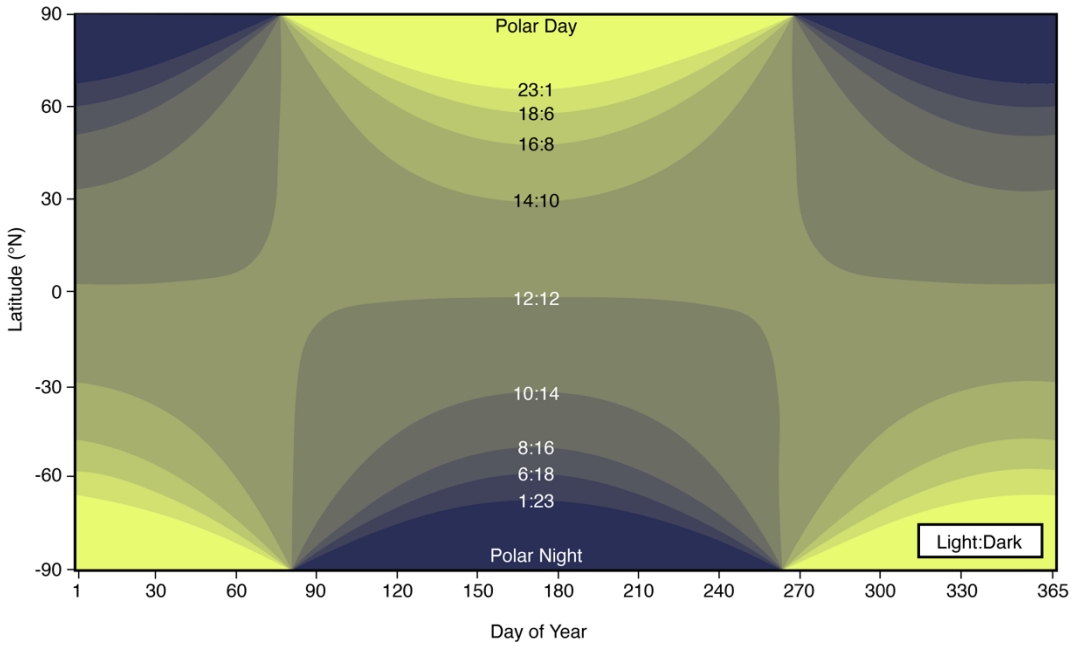

Fig. 1.6: Contour plot for hours of daylight (illustrated as colored areas as a function of latitude and time (day of the year). Edges between differentially colored areas represent iso-lines of equal daylengths that are labeled with photoperiods as hours (light:dark). *Based on Jahren (2007).*

1.4 Diatoms: key players of phytoplankton

Among phytoplankton, diatoms are one of the most diverse and abundant groups consisting of approximately 200,000 species (Armbrust, 2009, Kooistra and Medlin, 2007). As part of the supergroup of Stramenopiles, diatoms are related to brown algae such as the giant kelp. After their emergence about 250 million years ago, they evolved into various shapes and occur as solitary single cells or chain-like colonies (Fig. 1.7), spanning a size range of three orders of magnitude from 2µm to 2000µm (Mann, 1999, Mann and Vanormelingen, 2013). Today, diatoms occupy a diverse range of ecological niches and occur in almost every aquatic environment from freshwater to marine habitats across all latitudes (Malviya et al., 2016). However, their comparably high demand for inorganic nutrients particularly facilitates their abundance in nutrient-rich waters such as temperate to polar regions as well as coastal regions and upwelling areas (Cermeño et al., 2008, Malviya et al., 2016). Therein, diatoms build up massive spring blooms each year when light limitation is alleviated and the mixing of water masses in winter has replenished nutrients until mainly silica limitation terminates this phenomenon (Krause et al., 2019).

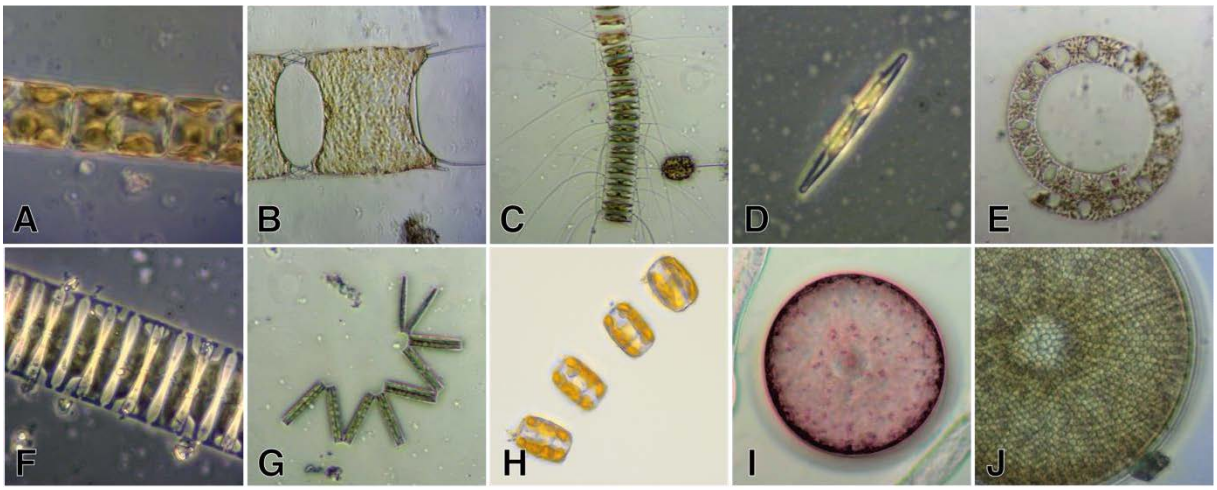

Fig. 1.7: Morphological diversity of various diatoms including *Guinardia* sp. (A), *Odontella* sp. (B), *Chaetoceros* sp. (C), *Cylindrotheca* sp. (D), *Eucampia* sp. (E), *Plagiogrammopsis* sp. (F), *Thalassionema nitschioides* (G), *Thalassiosira* sp. (H), *Coscinodiscus* sp. (I-J). *Micrographs by J. Giesler.*

The probably most characteristic feature of diatoms is their ornamented silica shell comprised of two box-like frustules. Prior to the rise of molecular methods, the ornament patterns on these frustules were primarily used to identify different diatom species. Despite offering protection against grazers (Hamm et al., 2003), the silica frustules also have implications for the diatom cell size which decreases over generations. This is due to the fact that with each mitotic cell

division cycle, as the two valves of the mother-cell detach, a new smaller valve is formed in each valve of the two mother-cell valves, leading to a gradual decrease in cell size (Medlin et al., 1993). When a critical minimum cell size is reached, which is estimated to happen after two to forty years (Mann, 1988, Jewson, 1992, von Dassow and Montresor, 2011, Holtermann et al., 2010), mitotic cell division is stopped and switched to sexual reproduction. Via the formation of auxospores, large diatom cells are formed again and the cycle renews (Medlin et al., 1993). As diatom sexual reproduction is relatively rare to observe, comparably little is known about this complex process. Besides environmental conditions (Poulíčková and Mann, 2019, Mouget et al., 2009), it has been recognized, that sexual reproduction appears to be facilitated in presence of bacteria, although the exact mechanisms remain elusive (Windler et al., 2014). At the end of their bloom period, diatoms particularly often form heavily silicified resting spores that sink to the sediment and may emerge after years and even decades, when environmental conditions are more favorable (Smetacek, 1985). Thereby, diatoms create their own seed banks, storing genetic variability that may be valuable at a later stage when a specific gene variant could provide the answer to an environmental challenge for the population (Ellegaard and Ribeiro, 2018). Moreover, the silica frustules make diatoms denser than their surrounding water column, thus increasing their sinking speed. Particularly upon bloom termination (e.g., by viral lysis), diatom cellular debris can form fast-sinking aggregates and thereby significantly contribute to the biological carbon pump (Jin et al., 2006). In total, diatoms account for as much as 40% of marine primary production corresponding to 20% of global primary productivity (Field et al., 1998). Thereby, diatoms alone even exceed the Amazon rainforest in carbon fixation and are the major source of organic carbon in the ocean (Benoiston et al., 2017, Field et al., 1998).

1.4.1 A brief characterization of the *Thalassiosira* genus

Within the taxonomic world of diatoms, the *Thalassiosira* genus is particularly species-rich (Liu et al., 2024). After its first mentioning in 1873 (Cleve, 1873), today 179 species have been accepted and described in detail (Liu et al., 2024). *Thalassiosira* species occupy freshwater and marine habitats and have been widely recognized as key primary producers, particularly in temperate and polar waters, where they contribute significantly to the recurring spring blooms (Chappell et al., 2013, Liu et al., 2024).

While some members of the *Thalassiosira* genus can be easily identified microscopically by their unique morphology, other more closely related *Thalassiosira* species only differ by a

single-digit percentage in specific genomic regions, challenging the biological species concept (Whittaker et al., 2012). For instance, this applies to *Thalassiosira gravida* and *Thalassiosira rotula,* which have long been considered conspecific (Sar et al., 2011) until the assessed genomic difference in their internal transcribed spacer (ITS) region led to their general acceptance as distinct species (Whittaker et al., 2012) although they are not distinguishable through common V4-18s barcodes (Supraha et al., 2022). Unlike intensively studied model diatoms such as *Thalassiosira pseudonana*, this close phylogenetic proximity in combination with the different distributional ranges of *T. rotula* (predominantly temperate regions) and *T. gravida* (predominantly polar regions) (Semina, 2004, Sar et al., 2011) offers exiting opportunities to study their biogeographic adaptation on the molecular level. This is because genomic differences due to speciation are comparatively small (Whittaker et al., 2012), and it is reasonable to assume that much of the existing differences can be attributed to the contrasting habitats that have left their marks on the genomes of these two *Thalassiosira* species.

1.4.2 Functional genomics in diatom research

Functional genomics is a relatively young field in diatom research, with its roots in the first diatom genome sequenced approximately 20 years ago (Armbrust et al., 2004). Since then, increasing knowledge and methodological advancements have rapidly expanded our understanding of diatom evolutionary success so that today, diatom ecology and evolution are inseparable from the genomic perspective (Falciatore et al., 2020).

Shortly after the genome of the first centric diatom *Thalassiosira pseudonana* became available (Armbrust et al., 2004), it was complemented by the genome of the pennate diatom *Phaeodactylum tricornutum* (Bowler et al., 2008), and soon these two diatom species became two of the most studied model organisms in algae research (Falciatore et al., 2020). Starting with fundamental insights into their evolutionary origin, ecology, physiology, and metabolic diversity by comparative genomic approaches (Nisbet et al., 2004, Montsant et al., 2005, Montsant et al., 2007, Veluchamy et al., 2014, Levitan et al., 2015, Rastogi et al., 2020), further genomic studies gave important insights into their carbon assimilation processes (Kroth et al., 2008), the formation of their silica shells (Mock et al., 2008, Shrestha et al., 2012), lipid biosynthesis (Sayanova et al., 2017), and horizontal gene transfer from bacteria and even other eukaryotes (Bowler et al., 2008, Vancaester et al., 2020, Dorrell et al., 2021).

In line, the rise of transcriptomic analysis techniques, revealed how diatoms regulate their gene expression in response to abiotic drivers and further enabled the discovery of physiological

marker genes for certain macro- and micronutrient limitations (e.g., Dyhrman et al., 2012, Marchetti et al., 2012, Bender et al., 2014, Caputi et al., 2019). With the expanding knowledge of diatom functional diversity based on the intensively studied model organisms, the discoveries of novel gene variants and environmental responses of natural diatom communities were enabled by amplicon sequencing and metatranscriptomic approaches, respectively (Pearson et al., 2015, Alexander et al., 2016)

Despite these milestone achievements, focusing on only a few model organisms has also been criticized as it might miss important questions, such as the biogeographic adaptation of ecological key diatom species (Falciatore et al., 2020). To address this, an increasing effort is undertaken to make more diatom genomes available and understand their genetic functions (Lommer et al., 2012, Traller et al., 2016, Ogura et al., 2018, Mock et al., 2017). Yet reducing the proportion of non-annotatable genes of diatoms will remain a task of the scientific community for the next decades.

1.5 The diatom holobiont

Like all life on earth, diatoms do not live in isolation. This was recognized already in 1901 when the first empiric evidence of diatom associations with diazotrophic bacteria was discovered (Fig. 1.8, Ostenfeld, 1901). About 35 years later, it was recognized that the dissolved organic matter that is exuded by diatoms is utilized by heterotrophic bacteria (Waksman, 1936). In the following decades, knowledge about diatom-bacteria interactions continuously increased, including the discovery of symbiotic relationships in terms of bacterial provision of essential micronutrients (Haines and Guillard, 1974) as well as parasitic interactions and their respective effects on diatom ecology (Mayali and Azam, 2004). The close associations and co-evolution of diatoms and bacteria for millions of years shaped specific diatom-associated bacterial communities that are also known as diatom microbiomes. Like other host-microbiome systems such as plants or corals, diatom hosts and their associated bacterial microbiomes, can be considered a discrete ecological unit – the holobiont (Margulis and Fester, 1991).

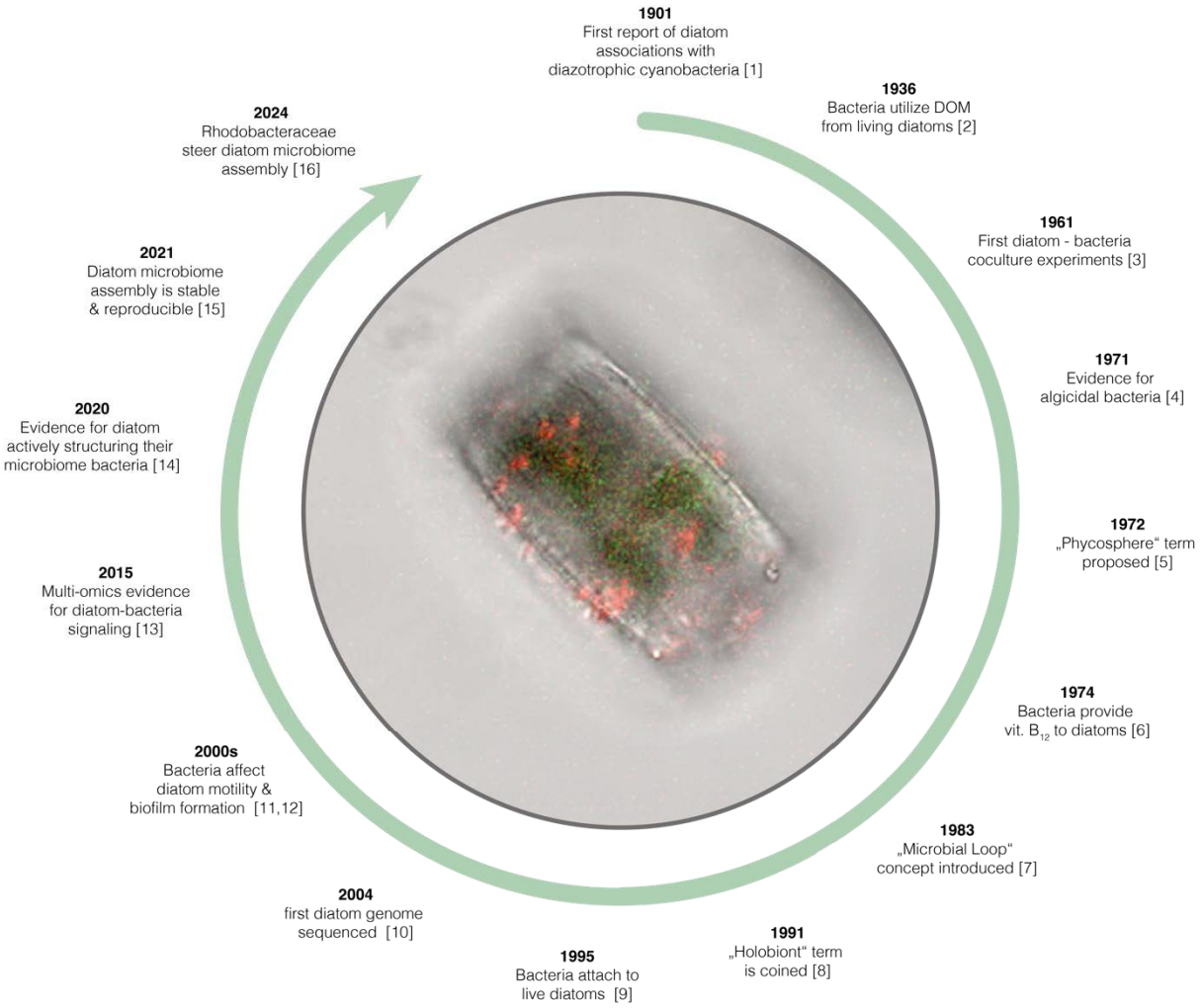

Fig. 1.8: A historical timeline of milestone-discoveries related to diatom holobiont research including (1) Ostenfeld and Schmidt (1901); (2) Waksman and Renn (1936); (3) Moskovits (1961); (4) Mitchell (1971); (5) Bell and Mitchell (1972); (6) Haines and Guillard (1974); (7) Azam et al. (1983); (8) Margulis (1991) (9) Smith et al. (1995); (10) Armbrust et al. (2004); (11) Wigglesworth-Cooksey and Cooksey (2005); (12) Bruckner et al. (2008); (13) Amin et al. (2015); (14) Shibl et al. (2020); (15) Mönnich et al. (2020); (16) Isaac et al. (2024). (*own micrograph,* color-graded image taken with a confocal microscope displaying a *T. gravida* cell in girdle view and its associated microbiome bacteria stained with DAPI). *Based on Helliwell et al. (2022).*

1.5.1 The phycosphere – a marketplace for microbial interactions

As an aquatic equivalent to the rhizosphere of plants, the phycosphere is defined as a diffusive boundary layer immediately surrounding the algal cell, where metabolites are most rapidly exchanged (Seymour et al., 2017, Helliwell et al., 2022). Within this microhabitat, phytoplankton cells can drastically modify the chemical environment in terms of pH levels and oxygen concentrations (Azam and Malfatti, 2007). With increasing distance from the host cell, the distinct chemical microenvironment made up of algae-derived exudates around the host cell

is gradually diluted due to diffusion and turbulence (Amin et al., 2012). Despite only representing a minimal fraction of the water column, this micro-environment is the main meeting place, marketplace, and sometimes also battleground for interkingdom interactions of algae and bacteria in the oceans, which ultimately drive ecosystem productivity and global biogeochemical cycles (Cole, 1982, Seymour et al., 2017). The size of a phytoplankton cell's phycosphere is hard to define, but estimates of organic compound gradients suggest a range of several hundred micrometers up to several millimeters, depending mainly on cell size, exudation rate and concentration (Grosser et al., 2012, Smriga et al., 2016).

The nature of these algal-exuded compounds is not only species-specific but is also determined by the host cells viability (i.e., age and health). In an early growth phase, mainly highly labile low-molecular-weight (LMW) compounds including carbohydrates and amino acids are exuded into the phycosphere to actively mediate chemotaxis (Bjornsen, 1988, Buchan et al., 2014). In later growth phases, more high-molecular-weight (HMW) molecules such as proteins, polysaccharides, lipids, and nucleic acids can be expected due to exudation or cell lysis (Biddanda and Benner, 1997, Fukao et al., 2010, Buchan et al., 2014). Within the phycosphere, the transport mechanism of the respective molecules is largely driven by molecular diffusivity rather than turbulence of the surrounding water column. Therefore, after excretion by either active transport or passive diffusion, LMW and/or hydrophilic compounds with consequentially fast diffusion rates are dispersed away much faster from the phytoplankton cell than HMW and/or hydrophobic compounds (Seymour et al., 2017).

As the exudation of dissolved organic matter is also continued under darkness, it is unlikely that the exudates are only excess photosynthates (Smith and Wiebe, 1976, Seymour et al., 2017). Consequently, the excreted dissolved organic matter (DOM) represents considerable 'costs' in terms of energy and carbon for a phytoplankton cell which have to be outweighed by the benefits they gain from the interactions with attracted bacteria. Among the LMW compounds, many act as potent chemoattractants for diverse bacteria due to their labile nature (Miller et al., 2004, Seymour et al., 2010). However, the HMW compounds act as important sorting tools that shape host-specific bacterial communities as they require specific bacterial enzymatic capabilities for their utilization (Mühlenbruch et al., 2018). Moreover, it has been recognized that the host algal cell actively modulates its DOM composition in terms of the release of specific metabolites that attract certain bacteria that complement its current metabolic need (Shibl et al., 2020).

1.5.2 The formation of a bacterial microbiome: assembly and attachment

The process and underlying mechanism of how diatom-associated bacterial microbiome are established has been intensively studied by steadily growing research community over the recent decades (Helliwell et al., 2022, and references therein). While previously articulated concepts assumed a stochastic assembly process also known as 'lottery assembly' based on random encounters of host phytoplankton cells and functionally suitable bacteria (Burke et al., 2011), increasing evidence has led to the rejection of this hypothesis in favor of a more selective species-specific assembly mechanism (Mönnich et al., 2020, Ahern et al., 2021). One reason for this is that random encounters of diatoms and bacteria are scarce in the marine environment which is comparably dilute compared to the organismal density of terrestrial systems (Amin et al., 2012). Considering average oceanic phytoplankton and bacterial densities, a bacterium may encounter a phytoplankton cell only 0.0035 times per day (Seymour et al., 2017). This low encounter rate is boosted to 9 potential encounters per day if a bacterium is motile and increases even further if the bacterium is attracted to the diatom's phycosphere by chemotaxis, i.e., a directed bacterial movement following a chemical gradient (Sonnenschein et al., 2012, Seymour et al., 2017). The unique DOM fingerprint of different diatoms and their bacteria-specific chemotaxis leads to highly species-specific and even genotype-specific diatom microbiomes (Helliwell et al., 2022, Ahern et al., 2021). Furthermore, despite possible modulation of specific microbiome members (Shibl et al., 2020), generally, the major fraction of bacterial microbiome composition is strongly conserved and characteristic of its host (Seymour et al., 2017, Behringer et al., 2018). Laboratory experiments provided evidence that even when the bacterial microbiome is completely removed from a diatom culture and the diatom host is subsequently exposed to a diverse bacterial consortium, the outcome of the assembly process is reproducible (Mönnich et al., 2020).

Once in the phycosphere, bacteria may either switch from a free-living to a particle-attached lifestyle (Sonnenschein et al., 2012) or continuously track the phycosphere via chemotaxis, however at higher energetic costs (Helliwell et al., 2022). In case of attachment, bacteria can attach directly to the diatom's surface or to transparent exopolymeric particles (TEP), a gel-like substance that works as a sticking agent and can be used as a growth substrate by bacteria (Fig. 1.9, Seymour et al., 2017). Different bacterial attachment mechanisms exist resulting in different attachment strengths including reversible attachment, enabling bacterial disassociation from the diatom phycosphere under non-favorable conditions or host cell senescence (Helliwell et al., 2022). Furthermore, it has been shown that attached microbiome bacteria have a profound

impact on the physical microhabitat as they stimulate diatom TEP production and enhance their aggregation (Gärdes et al., 2011, Sonnenschein et al., 2012). This, in turn, affects the sinking speed of the resulting diatom aggregates and thereby has important implications for the biological carbon pump.

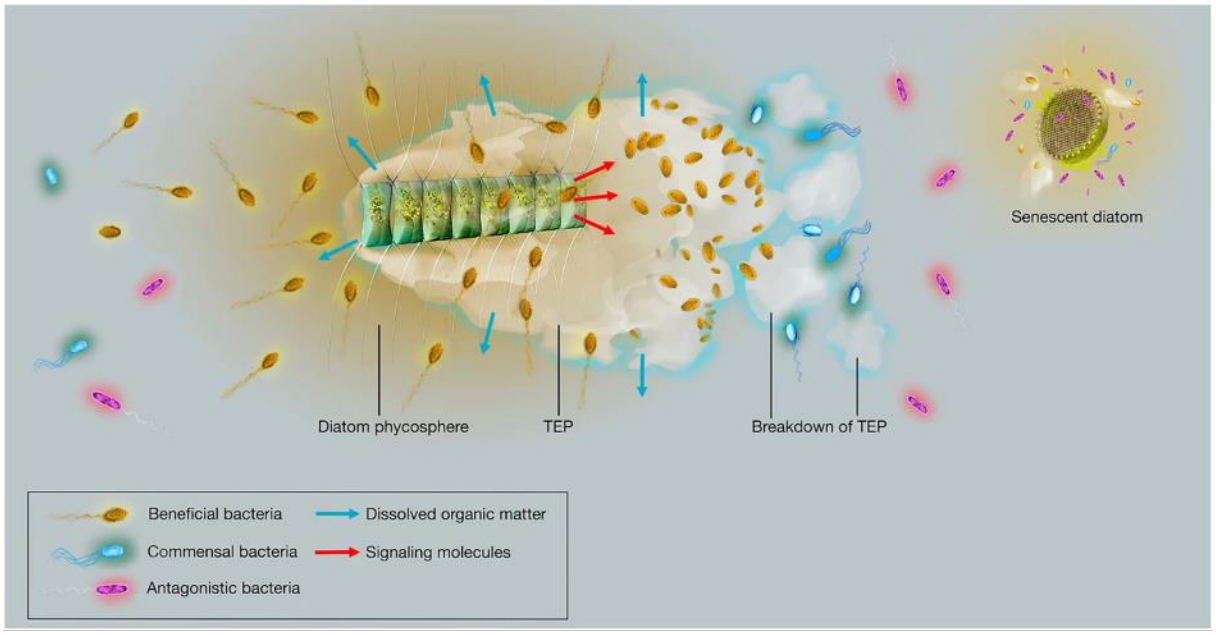

Fig. 1.9: Conceptual figure about diatom microbiome assembly and maintenance. The host diatom cell(s) release DOM (blue arrows) which attracts chemotactic bacteria (including beneficial, commensal, and antagonistic bacteria). Incoming beneficial bacteria colonize diatom-exuded TEP and stimulate its further production by the diatom host. Diatoms excrete secondary metabolites (red arrows) into the phycosphere which work as defense molecules against antagonistic bacteria but also include infochemicals that favor their symbionts. (Top right): Under stress, diatom-associated microbiomes may become out of balance and opportunistic and antagonistic bacteria can lyse diatom cells. *Taken from Helliwell et al. (2022), Image credit: Glynn Gorick.*

1.5.3 Important known interactions of diatoms and bacteria

As noted above, diatoms exude a diverse range of organic substances that are utilized by specific bacterial groups (Helliwell et al., 2022). This enables the diatom host to structure its own bacterial community and engage in interkingdom signaling to interact with distinct microbiome members that are capable of fulfilling specific functions. Multiple of these mechanisms have been elucidated, showing how diatom-associated bacteria provide a fitness advantage to their host or alleviate certain macro- and micronutrient limitations. Other bacteria evolved antagonistic strategies to cover their own metabolic needs (Fig. 1.10).

Among the synergistic interactions, the bacterial provision of macronutrients such as nitrogen has important ecological implications for diatoms, particularly when inorganic nitrogen sources

in the environment are limited (Helliwell et al., 2022). While some diatoms associate with diazotrophic bacteria which can fix atmospheric N_2 and provide it to their host as they convert it to ammonia (Cole, 1982, Zehr, 2015), other bacteria were shown to remineralize ubiquitous organic nitrogen compounds such as methylamines. Laboratory experiments demonstrated that bacterial monomethylamine remineralization into ammonia has the potential to fully cover nitrogen growth demands of a marine diatom, underlining the importance of this function in diatom phycospheres (Suleiman et al., 2016).

One of the most intensively studied examples for synergistic diatom-bacteria interactions is the bacterial provision of vitamins to their host (Haines and Guillard, 1974, Croft et al., 2005, Grant et al., 2014, Durham et al., 2015). Among the three vitamins required by diatoms as enzymatic cofactors (B_1, B_7, and B_{12}), B_{12} auxotrophy is the most widespread with approximately 60% of investigated diatom species requiring an exogenous source for vitamin B_{12} (Croft et al., 2005) as they lack methionine-independent cobalamin synthase (MetE). Laboratory studies and field metatranscriptomic studies demonstrated that certain bacteria are able to synthesize vitamin B_{12}, some of which share this essential micronutrient with their diatom hosts (Sultana et al., 2023). For instance, Durham et al (2015) demonstrated that *Thalassiosira pseudonana* specifically stimulated the growth of the microbiome bacterium *Ruegeria pomeroyi* as a response to B_{12} limitation by the release of an organic sulfur metabolite, 2,3-dihydroxypropane-1-sulfonate (DHPS), after which the bacterium alleviated the diatom's B_{12} deficiency. The demand for this micronutrient has shown to be environmentally relevant as diatom bloom termination correlate with limiting environmental vitamin concentrations (Bertrand et al., 2015).

Another crucial micronutrient that frequently constrains diatom growth is iron. Due to the low solubility of Fe(III) and its complex bounds to organic ligands (Gledhill and Buck, 2012), iron bioavailability to marine microbes is low, resulting in natural competition for this scarce resource (Hassler et al., 2011, Toulza et al., 2012). One strategy evolved by marine bacteria for iron acquisition is the release of siderophores which bind to Fe(III) and facilitate its uptake in the cell's proximity by active transport mechanisms (Chen et al., 2019). Interestingly, despite competing for the same resource with their diatom hosts, some common microbiome bacteria of the *Marinobacter* genus produce an unusual, highly photo-labile siderophore known as vibrioferrin which oxidizes the bound Fe(III) to Fe(II) upon light exposure (Amin et al., 2009). Thereby, the solubility increases and the iron becomes bioavailable, potentially enhancing iron assimilation for the host-diatom, likely in exchange for DOM (Amin et al., 2009).

Further growth-supporting mechanisms of phycosphere-inhabiting bacteria include the provision of growth-stimulating phytohormones such as auxins (Amin et al., 2015). For example, it has been shown that a *Sulfitobacter* species enhances diatom growth by releasing indole-3-acetic acid which it produces by utilizing diatom-secreted tryptophan (Amin et al., 2015). Moreover, some microbiome bacteria may indirectly support host growth, e.g., by suppressing potential pathogenic bacteria (Koedooder et al., 2019) or by detoxifying the phycosphere from reactive oxygen species (Hünken et al., 2008).

Another often neglected nature of diatom-bacteria interactions is the transfer of genetic material from bacteria to diatoms which is also known as horizontal gene transfer (HGT). For instance, it is estimated that 7.4% of the Phaeodactylum genome consists of genes that were originally obtained from prokaryotes, corresponding to a much higher proportion compared to other phytoplankton groups (Bowler et al., 2008). It is noteworthy that the corresponding 784 predicted genes in the Phaeodactylum genome were not assigned to a single prokaryote, but likely originate from various different bacteria and archaea which emphasizes the increased frequency of HGT to diatoms. It was speculated that the cause for this high level of HGT could be found in the bacterial groups to which the respective genes were assigned as those have demonstrated particularly close associations with diatoms (i.e., heterotrophic bacteria and cyanobacteria, especially diazotrophs and planctomycete bacteria) (Bowler et al., 2008). This genetic material has the potential to provide novel metabolic functions to diatoms (e.g., a functioning urea cycle) (Bowler et al., 2008), that may be of considerable advantage for the diatom holobiont.

Some bacteria also evolved antagonistic strategies, exploiting diatoms by causing stress or cell lysis and therefore, along with viruses and parasitic fungi, importantly drive bloom termination of diatoms (Mayali and Azam, 2004). An example of such an algicidal capability was demonstrated in the bacterial genus of *Saprospira*. After the bacterium enters the phycosphere of the diatom, it induces cell aggregation and degrades the diatom cell wall with the aid of fibril-like proteins. Subsequently, the bacteria invade into the diatom cell causing its lysis (Yoshikawa et al., 2008, Furusawa et al., 2003).

Other antagonistic bacterial strategies involve the release of algicidal proteases which e.g., in the case of the bacterium *Kordia algicida* showed to act highly species-specific and involve a quorum sensing mediated strategy: Precisely, upon reaching a specific bacterial density in the diatoms phycosphere, the bacterial production of algicides is started collectively by means of concentration-dependent intraspecific chemical communication through N-acyl-Homoserine

Lactones (AHLs) to kill the diatom host (Paul and Pohnert, 2011). Further, context-dependent or bi-phasic interactions between algae and bacteria have been demonstrated (particularly in the *Phaeobacter* genus) that involve a switch in the bacterial interaction partner from a mutualistic to a pathogenic lifestyle (Seyedsayamdost et al., 2011, Wang et al., 2022). For instance, the bacterium *Phaeobacter gallaeciensis* provides a phytohormone to the coccolithophore *Emiliania huxleyi*, stimulating its growth. Upon host cell senescence which is detected by algae-excreted *p*-coumaric acid, *P. gallaeciensis* switches to the production of roseobacticides leading to cell lysis (Seyedsayamdost et al., 2011).

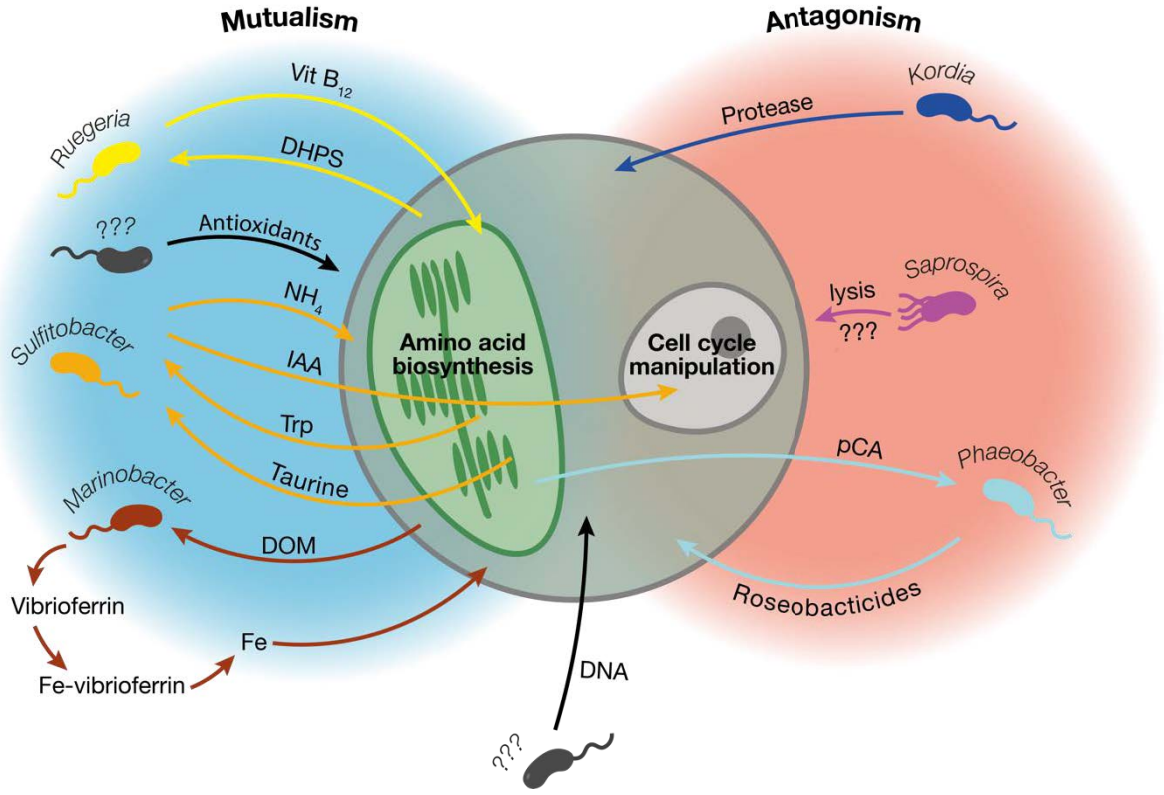

Fig. 1.10: A subset of so far identified mutualistic and antagonistic algae-bacteria interactions. The grey circle depicts a generic algal cell. Bacteria are colored by different genera, unclear/unknown bacterial genera are colored in black. Mutualistic interactions are depicted in the blue-shaded circle, antagonistic interactions in the red-shaded circle. *Ruegeria* provides vit B_{12} and receives 2,3-dihydroxypropane- 1-sulfonate (DHPS) in return. *Sulfitobacter* obtains tryptophan (Trp) and taurine as a carbon source in exchange for ammonium (NH_{4+}) and the phytohormone indole-3-acetic acid (IAA). *Marinobacter* recieves DOM and produces the siderophore vibrioferrin which binds to iron (Fe-vibrioferrin) and makes it bioavailable for the algae (Fe) upon light exposure. Furthermore, bacteria were shown to secrete antioxidants that cleave hydrogen peroxide. Antagonistic interactions include algae cell lysis by *Cordia*-excreted protease, as well as by uncharacterized microtubule-like structures of *Saprospira*. *Based on Seymour et al. (2017).*

Although the knowledge of these diatom-bacteria interactions has considerably improved our understanding of diatom holobionts and the underlying molecular mechanisms, it is likely that the interactions identified so far only represent the tip of the iceberg (Helliwell et al., 2022). On top of that, little is known about how these interactions between diatoms and their associated bacteria change in a dynamic environment or how coevolution of bacteria and diatoms adapt the holobiont to a certain niche space and thereby contribute to its biogeographic adaptation.

1.5.4 Coevolution and adaptation of diatom-bacteria assemblages

As bacteria have evolved mechanisms to communicate with each other and thereby synchronize their behavior (quorum sensing), diatoms have also developed strategies for communication with their bacterial microbiome members (Amin et al., 2015, Stock et al., 2020, Shibl et al., 2020). This interkingdom signaling is mediated through target-specific infochemicals or defense molecules to attract beneficial bacteria and repel pathogens (Shibl et al., 2020). The coordinated and reciprocal nature of many of these finely-tuned interkingdom interactions suggests that, despite living in a fluid and turbulent environment, the host organisms and their microbiomes must maintain spatial proximity over substantial temporal scales to enable this kind of coevolution (Stocker, 2015, Seymour et al., 2017). Laboratory studies have confirmed the long-term stability (Mönnich et al., 2020, Barreto et al., 2021) of diatom-associated microbiomes, that are prerequisites for developing these coevolutive mechanisms.

Considered from a biogeographic perspective, it has been demonstrated in a pole-to-pole survey that algal microbiomes are largely separated into two main groups: polar and non-polar species associations (Martin et al., 2021). Precisely, based on phytoplankton metatranscriptomes and microbial rRNA gene sequencing, the geographic differentiation of co-occurring microbes in algal microbiomes is well explained by the latitudinal temperature gradient and associated break points in beta diversity, separating cold and warm locations (Martin et al., 2021). Other environmental parameters that correlate with temperature and latitude as for instance photoperiodic range might also contribute to this biogeographic differentiation of algal microbiomes.

In the context of other holobiont systems, studies showed that host and microbiomes both significantly contribute to holobiont adaptation to challenging abiotic conditions (Henry et al., 2021, Kim et al., 2023, Petersen et al., 2023). Particularly in novel or changing environments, the microbiome plays an important role in host adaptation due to their small genomes and short

generation cycles which allow more rapid adaptation (Petersen et al., 2023). Bacterial genetic functions that are not needed anymore for survival are eliminated quickly by genome shrinkage suggesting that the existing genetic functions are relevant for their proliferation in a given habitat (Moran, 2002). As in all coevolutive relationships, both host and microbiome exert selective pressure on one another it is likely that also diatom holobionts in polar regions select for microbiome members that fulfill habitat-specific functions which differ from those in temperate regions, resulting in the temperate- and polar-specific microbiomes observed by Martin et al. (2021).

Although the knowledge of these coevolved functions is still in its infancy, a growing research community is dedicated to deciphering the underlying mechanisms at the molecular level. Understanding how evolved microbiome functions foster diatom adaptation in the Arctic or temperate regions, and to which degree these can buffer environmental changes until they are shifted out of balance is crucial knowledge not only for predicting their adaptive capabilities as a response to climate change but also for improving predictions about climate-change-mediated poleward range shifts.

1.6 Aims and outline of this thesis

Despite considerable advancements that have been made in identifying and molecularly unraveling the sophisticated mechanisms of diatom-bacteria interactions, so far, none of these discoveries have been considered in the context of the multifactorial abiotic environment that these organisms naturally experience (Helliwell et al., 2022). Yet, due to the profound effects of these host-microbiome dynamics on diatom physiology and growth, the potential dependency of growth-supporting or -inhibitory effects on abiotic factors may have important implications for diatom holobiont adaptation to climate change in the rapidly warming Arctic and for poleward shifting temperate diatoms.

This thesis aims to improve our understanding of how diatom holobionts adapted to occupy Arctic or temperate niches and to which extent diatom-associated bacterial microbiomes help to adapt their host under environmental conditions relevant to climate change and associated climate change-mediated poleward range shifts. The main objectives are to **(I)** experimentally quantify the response of Arctic and temperate diatoms to abiotic factors that characterize their biogeographic separation and thereby identify potential bottlenecks for adaptation of Arctic diatoms and poleward range shifts of their temperate relatives; **(II)** determine the net effect of the bacterial microbiome on Arctic and temperate diatom growth under multi-driver settings of these factors to understand its role in host adaptation; **(III)** unravel how abiotic conditions affect diatom-associated bacterial microbiome community composition and the underlying host-microbiome interactions **(IV)** develop a methodological strategy to understand diatom-microbiome community dynamics on the single- (host-) cell level to enable necessary species-specific (in-situ) information of natural diatom microbiomes in the future.

These above-listed objectives were addressed with step-wise laboratory experiments that build on each other with increasing complexity using the closely related Arctic and temperate diatom species *Thalassiosira gravida* and *Thalassiosira rotula* as model organisms (Fig. 1.11). In total, the listed objectives resulted in four publications that are structured as the following chapters in this thesis:

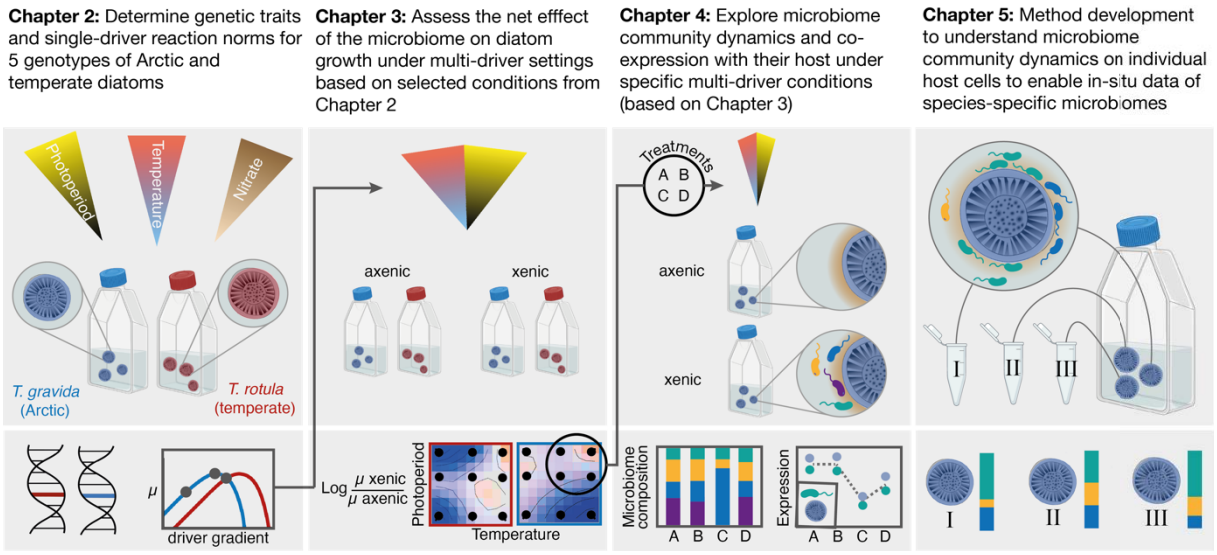

Fig. 1.11: Graphical abstract of the chapters included in this thesis. Detailed outlines about each chapter can be find in the subsequent paragraphs. *Contains elements from BioRender.com*

In **chapter 2** (Publication I), I aim to identify habitat-specific (i.e., Arctic vs. temperate) adaptations of key functional and genetic traits in the chosen model diatoms *T. gravida* and *T. rotula*. Therefore, multiple (xenic) genotypes of each species were exposed to gradients of temperature, photoperiod, and nitrate concentrations under single driver settings to measure fitness-related parameters such as growth rates for temperature or photoperiod reaction norms and nutrient uptake kinetics for nitrate concentration assays. Moreover, habitat-specific genetic adaptations were identified in terms of convergent amino acid substitutions (CAAS) by means of transcriptomic profiles of the investigated diatoms in concert with other publicly available diatom transcriptomes from Arctic and temperate regions. By characterizing what an Arctic or temperate adaptation constitutes and highlighting the most crucial differences, the results are interpreted in the context of the trait-based potential for adaptation to climate warming and associated poleward range shifts.

Chapter 3 (Publication II) addresses the net effect of the bacterial microbiome on Arctic and temperate diatom growth under multi-driver settings with those abiotic factors that are considered crucial for their biogeographic adaptation. The choice of included abiotic factors and their respective levels was based on the outcome of Publication I, which particularly demonstrated the importance of temperature and photoperiod for Arctic and temperate diatom adaptation. Therefore, in a comparative approach, axenic and xenic cultures of one Arctic and one temperate genotype of *T. gravida* and *T. rotula* each were exposed to a factorial experimental design of temperature and photoperiod. The outcome of the study did not only

reveal treatment-dependent patterns of growth-supporting effects but also highlighted risks for tipping points of these mutualistic host-microbiome relationships towards growth-inhibitory effects under certain environmental conditions.

Chapter 4 (publication III) zooms in, to study the underlying host-microbiome dynamics at the molecular level. Therefore, xenic and axenic cultures of the *T. gravida* genotype studied in Publication II were exposed to four selected temperature-photoperiod treatment combinations that were found to result in growth-supporting or inhibitory effects in publication II. To unravel the underlying host-microbiome mechanisms, changes in the bacterial microbiome, community composition were tracked as well as the transcriptomic responses of the host and the bacterial microbiome. After the differences between axenic and xenic diatom transcriptomes were determined, the resulting genes of interest were studied in concert with the microbiome metatranscriptome to identify highly correlating gene clusters of the host diatom and its microbiome and how temperature and photoperiod interactively affect their expression. This allows for detailed insights into the context dependency of host-microbiome interactions and highlights the importance of key microbiome members for diatom holobiont resilience.

Chapter 5 (Publication IV) is a methodological stepping stone towards the urgently needed information about species-specific diatom microbiomes in natural systems by developing a methodological approach to study the diatom-associated microbiome community composition on the single-cell level. Additionally, the study gives detailed insights into coordinated microbiome dynamics for individual host cells belonging to different genotypes of *T. gravida* in response to macro- and micronutrient limitations.

1.7 List of publications and author contributions

Publication I	Giesler, J. K., Van de Waal, D. B., Thomas, M.K., Šupraha, L., Koch, F., Harder, T., Pein, C.M., John, U., Wohlrab, S. (2024): What does it mean to be(come) Arctic? Functional and genetic traits of Arctic- and temperate- adapted diatoms. Under review in *Global Change Biology*.
Chapter 2	

Author contributions: The experiments were planned by SW, TH, MKT, FK and myself. The experiments were conducted by myself with the help of SW, LS, and CMP. Samples were processed by myself with the help of SW and DBVW. Data analysis and manuscript writing was conducted by myself with the help of SW. Manuscript revision was done with the help of all coauthors.

Publication II	Giesler, J. K., Harder, T., Wohlrab, S. (2023): Microbiome and photoperiod interactively determine thermal sensitivity of polar and temperate diatoms. *Biology Letters* 19 (11), doi: 10.1098/rsbl.2023.0151.
Chapter 3	

Author contributions: The experiments were planned by SW, TH and myself. The experiments were conducted by myself. Data analysis and manuscript writing was conducted by myself with the help of SW. Manuscript revision was done with the help of all coauthors.

Publication III	Giesler, J. K., Bussmann, F., Harder, T., Eren, A. M., John, U., Wohlrab, S. (2024): Co-expression of Arctic diatoms and their bacterial microbiomes under thermal and photoperiodic stress. To be submitted.
Chapter 4	

Author contributions: The experiments were planned by SW, TH, FB and myself. The experiments were conducted by myself FB and SW. Data analysis and manuscript writing was conducted by myself with the help of SW and MAE. Manuscript revision was done with the help of all coauthors.

Publication IV	Giesler, J. K.*, Schulte-Hillen, R. L.*, Mock, T., Belshaw, N., John, U., Harder, T., Kühne, N., Neuhaus, S., Wohlrab, S. (2024): A CRISPR-Cas9 assisted analysis of single-cell microbiomes for identifying rare bacterial taxa in phycospheres of diatoms. Under review in *ISME communications*.
Chapter 5	

Author contributions: RLSH and myself contributed equally to this study. The study was planned by SW, RLSH, UJ and myself. The experiments were conducted by myself SW and RLSH. Samples were processed by myself, RLSH, SW, NK, TM, NB, SN. Data analysis and manuscript writing was conducted by myself with the help of SW. Manuscript writing was conducted by myself, RLSH, and SW. Manuscript revision was done with the help of all coauthors.

2 Publication I

What does it mean to be(come) Arctic? Functional and genetic traits of Arctic- and temperate-adapted diatoms

Under review in Global Change Biology

What does it mean to be(come) Arctic? Functional and genetic traits of Arctic- and temperate- adapted diatoms

Jakob K. Giesler*[1], Dedmer B. Van de Waal[2,3], Mridul K. Thomas[4], Luka Šupraha [5,6], Florian Koch[1], Tilmann Harder[1,7], Carla Pein[1], Uwe John[1,8], and Sylke Wohlrab[1,8]

[1)] *Ecological Chemistry Section, Alfred Wegener Institute, Helmholtz Centre for Polar and Marine Research, Bremerhaven, Germany*

[2)] *Department of Aquatic Ecology, Netherlands Institute of Ecology (NIOO-KNAW), Wageningen, The Netherlands*

[3)] *Department of Freshwater and Marine Ecology, Institute for Biodiversity and Ecosystem Dynamics, University of Amsterdam, Amsterdam, The Netherlands*

[4)] *Department. F.-A. Forel for Environmental and Aquatic Sciences & Institute for Environmental Sciences, University of Geneva, Switzerland*

[5)] *Department of Biosciences, University of Oslo, Oslo, Norway*

[6)] *Norwegian Institute for Water Research (NIVA), Oslo, Norway*

[7)] *Department of Biology and Chemistry, University of Bremen, Bremen, Germany*

[8)] *Helmholtz Institute for Functional Marine Biodiversity at the University of Oldenburg (HIFMB), Oldenburg, Germany*

Abstract

Climate change-induced warming is expected to drive phytoplankton poleward as they track suitable thermal conditions. However, successful establishment in new environments requires adaptation to multiple abiotic factors beyond temperature alone. As little is known about how polar species differ in key functional and genetic traits, simple predictions of poleward movement rely on large assumptions about performance in other relevant dimensions than thermal responses (e.g., light regime, nutrient uptake). To identify evolutionary bottlenecks of adaptation, we assessed a range of thermal, resource acquisition and genetic traits for multiple strains of the diatom *Thalassiosira rotula* from the temperate North Sea, as well as multiple strains of the closely related Arctic *Thalassiosira gravida*. We found a broader thermal range for the temperate diatoms and a mean optimum temperature of 10.3 ± 0.8°C and 18.4 ± 2.4°C for the Arctic and temperate diatoms, respectively, despite similar maximum growth rates. Photoperiod reaction norms had an optimum photoperiod of ~17h for temperate diatoms,

whereas the Arctic diatoms exhibited their highest growth performance at a photoperiod of 24h. Nitrate uptake kinetics showed high intraspecific variation without a habitat-specific signal. The screening for convergent amino acid substitutions (CAAS) of the studied diatom strains and other publicly available transcriptomes revealed 26 candidate genes in which potential habitat-specific genetic adaptation occurred. The identified genes include subunits of the DNA polymerase and multiple transcription factors (zinc-finger proteins). Our findings suggest that the thermal range of the temperate diatom would enable poleward migration, while the extreme polar photoperiods might pose a barrier to the Arctic. Additionally, the identified genetic adaptations are particularly abundant in Arctic diatoms as they may contribute to competitive advantages in polar habitats beyond those detected with our physiological assays, hampering the establishment of temperate diatoms in Arctic habitats.

Keywords

range shift, photoperiod, phytoplankton, poleward migration, Thalassiosira, convergent evolution

Introduction

The Arctic Ocean is among the biologically most productive areas in the world (Ardyna et al., 2013), and its resident primary producers are therefore of particular importance for the biological carbon pump and the marine food web (Tremblay et al., 2015). As the Arctic is warming several times faster than the global average (Rantanen et al., 2022, Maturilli et al., 2013), there is growing interest in assessing the short-term adaptive potential of key Arctic primary producers to the predicted consequences of increased temperature (Wolf et al., 2017, Ahme et al., 2023, Biskaborn et al., 2023). However, changes in the Arctic habitat go beyond a mere increase in temperature, due to other correlated abiotic factors fundamental for primary production. For instance, effective annual photoperiods will likely become longer due to further and earlier sea ice decline, increasing the light intensity under the thinning ice cover (Arrigo et al., 2012). Moreover, vertical mixing will weaken, which is expected to result in lower nutrient advection and thus especially challenge Arctic primary producers with a high nutrient demand such as diatoms (Farmer et al., 2021).

In general, such cumulative effects of global change challenge the ability of organisms to adapt in a timely manner, thus currently driving a global reorganization of species (Lenoir et al., 2020). This reorganization involves poleward range shifts of temperate phytoplankton and may alter ecosystem functioning in the Arctic (Brandt et al., 2023, Benedetti et al., 2021). For example, poleward migration and corresponding changes in diversity and cell sizes can affect the efficiency of the biological carbon pump (Ward, 2015, Brun et al., 2019, Tréguer et al., 2018). Although further consequences are largely unknown, the potential replacement of Arctic phytoplankton species by their temperate relatives could impact trophic interactions in terms of elemental ratios, fatty acid profiles and temporal food-web mismatches as reported for metazoans (Falk-Petersen, 2006, Karnovsky et al., 2010, Asch et al., 2019). Consequently, the groundwork for predicting potential changes involves identifying traits that evolved in response to an Arctic or temperate habitat and govern phytoplankton success and their ability for poleward migration.

Capturing evolutionary adaptation remains challenging as each established approach has its specific weaknesses. For example, evolutionary differences between ancestors and their descendants are determined from sedimentary fossil records (Sims et al., 2019, Westacott et al., 2021), which is possible for only some taxa and provides little insight into non-morphological traits. Long-term laboratory incubation experiments (Jin and Agusti, 2018, Zhong et al., 2021) can track evolution, but are limited to fewer generations compared to natural timescales, a simplified selection regime and a small amount of standing genetic variation. Reaction norm experiments (Boyd et al., 2013, Baker et al., 2016, Aranguren-Gassis et al., 2020) can be informative for short-term abiotic tolerances, but may not capture the long-term adaptive potential without resurrecting resting stages from sediments and measuring their response curves, which is only possible for few cyst-forming species (Hattich et al., 2024). Therefore, to identify habitat-specific adaptation, it is necessary to assess multiple traits for the same (or a closely related) species in a contrary habitat (e.g., Arctic vs. temperate) and include multiple genotypes to account for the population's intraspecific variation.

For key primary producers like diatoms, suitable model organisms to implement such a comparative approach can be found in the Arctic species *Thalassiosira gravida* and its closely related temperate counterpart *Thalassiosira rotula*. While it was long debated whether these diatoms represent distinct taxa or are simply different morphotypes of the same species (Sar et al., 2011), genetic differences in their internal transcript spacer 1 (ITS1) sequences support to regard them as separate species (Whittaker et al., 2012). This phylogenetic proximity in

combination with separated geographic distribution makes them specifically suitable for a comparison of inherent habitat-specific key traits. In this study, we compare the reaction norms (temperature, photoperiod, nitrate kinetics) of five strains of Arctic *T. gravida* with five strains of temperate *T. rotula*. This allows us to resolve differences in respective growth-related traits in response to these drivers and analyze implications for poleward migration.

To extend our knowledge beyond key physiological traits, we assessed genetic (i.e., gene-specific) traits to reveal temperate and polar specific adaptations. To this end, we screened the species' transcriptomes together with other publicly available Arctic and temperate diatom transcriptomes for convergent amino acid substitutions (CAAS). Considering there is no generally accepted definition for CAAS (Rey et al., 2019), here we operationally define CAAS as phylogenetically independent changes in amino acid sequences resulting in identical amino acids at specific positions in proteins from species from comparable habitats (Barteri et al., 2023). CAAS reflect convergent evolution on the molecular level and thereby are indicative of adaptation. Therein, similar environmental pressures lead to parallel genetic changes across different species, enabling them to thrive in specific habitats by developing similar phenotypic traits (Ito et al., 2022, Shen et al., 2019). Despite the consequential importance of these molecular adaptations for phytoplankton range shifts, we do not know of CAAS relevant to adaptation to polar temperature, light and other conditions.

Material & Methods

Biological material and culture conditions

The experiments in this study comprise five Arctic adapted strains of *Thalassiosira gravida* obtained from the Norwegian Culture Collection of Algae (NORCCA strain numbers UiO478; UiO483; UiO484; UiO447; UiO448, here called A1, A2, A3, A4, and A5) as well as five temperate adapted strains of *Thalassiosira rotula*. This includes one strain obtained from the Harder Lab (University of Bremen; strain number S16, here called T1) isolated from Helgoland, two strains isolated from the German Bight (strain Wilhelmshaven, strain Sylt, here called T2 and T3), and two strains obtained from the Roscoff Culture Collection (strain numbers RCC-778, RCC-290, here called T4 and T5) isolated from the English Channel. Further details about the strains used in this study can be found in supplementary Table S2.1. The number of strains used differs between experiments because not all strains were available at the time of the

experiment. *T. gravida* and *T. rotula* strains were identified by their ITS sequences based on taxonomic definitions by Whittaker et al. (2012) (see Fig S2.1). Cultures were maintained in climate chambers at a light intensity of 30 µmol photons m^{-2} s^{-1} at a photoperiod of 16:8h light:dark and a temperature of 4°C and 15°C for the Arctic and temperate strains, respectively. Cultures were kept in exponential growth by semi-continuous dilution with K-medium (Keller et al., 2007) that was modified by additional of Si-enrichment (1.06 x 10^{-4} M Na_2SiO_3 x 9 H_2O) and no ammonium addition.

Temperature performance curves

Temperature performance curves (TPCs) were assessed for 5 Arctic strains of *T. gravida* and 5 temperate strains of *T. rotula*. The TPC assays were conducted on a thermal gradient block with a respective temperature gradient for the Arctic (-0.5, 2.3, 5.0, 7.3, 9.9, 12.3, 15°C) and temperate (2.8, 7.0, 11.0, 14.5, 18.0, 21.4, 24.5, 27.8°C) diatoms at a light intensity of 30 µmol photons m^{-2} s^{-1} and a light:dark cycle of 16:8 h. In order to acclimate the cultures to their experimental conditions, 200 mL of batch cultures from each strain were incubated at the mean temperature of the chosen gradient for the Arctic or temperate strains. Over a period of 7 days, the cultures were then gradually heated or cooled until reaching their respective final experimental temperature where they were kept in the exponential growth phase for 8 more days, by semi-continuous dilution with modified K-medium. After this acclimation period, 4 replicates of 50 mL culture flasks (Sarstedt, Germany) were inoculated with the final experimental cultures to an initial cell density of 250 cells mL^{-1} in 40 mL of media. Sampling was conducted daily by fixing 500 µL subsamples from each experimental unit with 2% final concentrated Lugol's solution in a 48-well microplate (Sarstedt, Germany). Samples were quantified microscopically using a Zeiss Axiovert 10C inverted light microscope. Cell densities were tracked daily and the treatments were ended upon reaching stationary phase (i.e., begin of saturation in the logistic growth curve).

Photoperiod reaction norms

To assess the growth response to different photoperiods (1h, 4h, 8h, 16h, 24h), photoperiod reaction norms assays were conducted using 4 Arctic *T. gravida* (A1, A2, A3, A4) and 4 temperate *T. rotula* (T1, T2, T3, T5) strains. These growth assays were conducted in nanocosm

well-plate photobioreactors which allowed for high replication numbers, well-specific programmed light settings and a lab-independent and reproducible experimental setup (Volpe et al., 2021). The experiments were conducted in modified K-medium (see above) at a light intensity of 30 µmol photons m^{-2} s^{-1} and an experimental temperature representing the lowest optimum temperature among the studied genotypes of Arctic and temperate strains assessed in the TPCs (i.e., 9°C for *T. gravida* and 16°C for *T. rotula*). To acclimate the cultures to their experimental conditions, 24 replicates per strain with an experimental volume of 300 µL were inoculated in 96 well-plates at an initial chl-a fluorescence value close to the blank value measured in the medium except for 1h and 4h photoperiod treatments, which were inoculated twice the blank value to obtain sufficient biomass. The microtiter plates were sealed with a gas permeable membrane (Breathe Easy, Sigma Aldrich, USA) and placed in a climate cabinet at the respective experimental temperature. After seven days of acclimation to the experimental conditions, cultures were diluted with temperature-acclimated medium and inoculated in a new well-plate close to their fluorescence blank value for the actual growth experiment. This acclimation duration was chosen as it covers both, short-term and long-term photoacclimation time scales (Lutz et al., 2001), i.e., no further treatment effects on cellular chl-a content can be assumed and robust growth rates can directly be calculated from fluorescence intensity values. Chl-a fluorescence intensity was measured daily at the same time after 10 min of dark acclimation using a photo-spectrometric plate reader at an excitation wavelength of 440 nm and emission of 680 nm (ClarioStar Plus BMG Labtech for Arctic strains; Spark TECAN for temperate strains). Chl-a fluorescence was tracked regularly and the treatments were ended upon reaching stationary phase (i.e., begin of saturation in the logistic growth curve).

Nitrate uptake assays

^{15}N nitrate uptake assays were conducted by means of tracer additions of highly enriched (98%) ^{15}N-labeled nitrate (Mulholland et al., 2002, Mulholland et al., 2009) for 4 Arctic and 3 temperate strains of *Thalassiosira gravida* and *Thalassiosira rotula*, respectively (strains A1, A2, A3, A5 and T1, T2, T3). For precultivation, 2L batch cultures of each strain were grown at a light intensity of 25 µmol photons m^{-2} s^{-1} and a light:dark cycle of 16:8h. Cultures were grown in modified ESAW medium (Harrison et al., 2008) at the lowest respective optimum temperature (9°C for Arctic strains and 16°C for temperate strains). The nitrate concentration in the medium corresponded to 1/5 K-medium (~100 µmol L^{-1}) which was considered necessary to obtain sufficient biomass for the ^{15}N isotope analysis. In the mid-exponential growth phase,

90% of the supernatant of the batch culture flasks was decanted and the sedimented cells were resuspended in nitrate (and ammonia) free modified ESAW medium. Overnight, the cells sedimented again and the procedure was repeated two more times with a time interval of 24 hours in between. This dilution led to a calculated final concentration of 0.1 µmol $NaNO_3$ L^{-1} in the medium at maximum without considering the N uptake of the diatoms in the batch cultures which depleted the dissolved nitrate concentrations even further. This procedure was considered the best possible compromise between a sufficiently dense culture and nitrogen depletion. Moreover, it has been demonstrated that 24 hours of N-starvation were sufficient to trigger high nutrient uptake in the marine diatom *Phaeodactylum tricornutum* (Raimbault et al., 1990). Accordingly, 24 hours after the last dilution step with nitrogen-free medium, the assay was prepared by filling 40 mL culture from the batch cultures into 50 mL culture flasks for the nitrate addition treatments comprising of 7 nitrate levels (n=4) as well as a nitrate deplete control treatment. The chosen seven levels of final nitrate concentrations were 0.1, 0.4, 0.8, 2, 10, 50, 100 µmol $NaNO_3$ L^{-1} at a ratio of 1:1 of ^{14}N:^{15}N for levels ≤ 2µmol $NaNO_3$ L^{-1} and 9:1 for levels > 2 µmol $NaNO_3$ L^{-1}. The experimental units were incubated for 40 minutes at the same culture conditions as the batch cultures (see above) and were then filtered onto pre-combusted glass microfiber filters (Whatman GF/F, Maidstone, UK). After filtration of the experimental unit, another 100 mL of nitrate-free medium was filtered to reduce dissolved ^{15}N contamination on the filter. The filters were dried at 60°C for 48 hours and then folded into tin capsules which were stored in the dark until further analysis. POC/PON and the particulate ^{15}N:^{14}N ratio were measured using an elemental analyzer (Flash 2000, Thermo Scientific, Karlsruhe, Germany) coupled to an isotope ratio mass spectrometer (IRMS, Thermo Scientific, Karlsruhe, Germany; (Morrien et al., 2017)).

Transcriptomic profiles

To assess transcriptomic profiles, a 40 mL culture of each strain was filtered onto a 10 µm nylon filter (Merck Millipore, USA) which was fixed in 1 mL TriReagent (Sigma-Aldrich, St. Louis, USA) with glass beads and immediately frozen at -80 °C until further processing. Cultures were kept as described in the culture conditions section and were harvested in the mid-exponential growth phase. RNA extraction was conducted as described in detail by Wohlrab et al (2017). The subsequent library preparation was conducted using the Illumina Stranded mRNA Prep Ligation Kit (Illumina, San Diego, USA) following the manufacturer's protocol. The resulting

paired-end cDNA libraries were sequenced on a NextSeq 2000 (Illumina, San Diego, USA) using the P3 Reagents kit (2 x 150 cycles).

Statistical analysis of TPCs

To fit strain-specific TPC models, maximum growth rates were determined for each experimental unit (i.e., for each strain at each experimental temperature and each replicate) using the "growthrates" package (Petzoldt et al., 2017). TPC models were fitted to these growth rates across the tested temperatures by means of the "rTPC" package (Padfield, 2023) applying the model of Thomas et al. (2017). Subsequently, non-parametric bootstrapping was conducted to estimate model uncertainty and 95% confidence intervals for TPC parameters (i.e., optimum temperature (T_{opt}), maximum growth rate (μ_{max}), thermal breadth at 80% of μ_{max} (Tb_{80}), and activation energy (E_A). To test for a general difference between Arctic and temperate populations, a Welch t-test was conducted with the mean of the respective TPC parameters (see above) from each strain as dependent variable and the population origin as independent variable.

Statistical analysis of photoperiod growth assays

After the mean blank value of the medium was subtracted from the measured chl-a fluorescence values of the samples, the "growthrates" package (Petzoldt et al., 2017) was used to obtain μ_{max} values for each experimental unit. In order to specifically analyze differences in photoperiod reaction norm shape between Arctic and temperate origin, growth rates of each species were normalized by their respective highest achieved growth rate. To test for shape differences in photoperiod reaction norms, generalized additive models (GAMs) were fitted to each species' data and differences tested by assessing the significance of the difference smooth term between both species.

Calculation and statistical analysis of N-uptake rates

Values for $\delta^{15}N$ were determined by measuring the difference in ^{15}N levels between the sample and a reference gas containing 0.366 atom% ^{15}N. Subsequently, these $\delta^{15}N$ values were

employed in computing absolute nitrate uptake rates (V_{abs}) for the tested nitrate concentrations using the mixing model of Montoya et al. (2002) and using equations from Orcutt et al. (2001). The obtained V_{abs} values (µmol N L^{-1} h^{-1}) for the respective tested concentrations were then normalized by cell density and the parameters of the Michaelis-Menten function were estimated:

$$V = \frac{V_{max}\, S}{K_s + S}$$

where V (µmol N h^{-1} $cell^{-1}$) represents the cell-normalized nitrate uptake rate, V_{max} (µmol N h^{-1} $cell^{-1}$) represents the highest achieved uptake rate, K_s is the half-saturation-constant (µmol L^{-1}) and S is a given nitrate concentration in the growth medium (µmol L^{-1}).

Analysis of transcriptomic data

The Illumina basecall files underwent demultiplexing and were transformed into FASTQ files using the Illumina bcl2fastq conversion tool (version 2.20). Subsequently, the FASTQ files were processed using CLCGenomicsWorkbench (version 21, Qiagen, Hilden) including paired-end mapping, adapter and quality trimming, and *de novo* assembly into contigs with default parameters for Illumina sequence data. Open reading frames (ORFs), coding sequences and amino acid translation were created with transdecoder (Haas, 2013).

For CAAS analysis, additional transcriptomes and metatranscriptomes were obtained from the respective sources listed in Supplementary Table S2.2. This allowed us to more confidently assess convergence due to origin and to distinguish it from speciation events, as well as to assess whether a given CAAS-bearing transcript is expressed in the native habitat (metatranscriptome), i.e., to highlight its ecological significance. In cases where raw reads or nucleotide data were retrieved, processing was as described above for the transcriptome data. Diatom-specific transcripts were filtered and phylogenetically placed using the MMseqs2 taxonomy tool (Mirdita et al., 2021), with a custom-built reference database containing revised sequences from the MMETSP project (Van Vlierberghe et al., 2021) as well as the *T. gravida* strains used in this study. Amino acid sequences were clustered into similarity groups with an identity threshold of 75% with Silix (Miele et al., 2011). Sequences in each cluster were aligned with MAFFT (Katoh and Standley, 2013) and trimmed with the gappyout algorithm implemented in trimAI (Capella-Gutierrez et al., 2009). Trimmed sequences were analysed for convergent amino acid substitutions using CAAStools (Barteri et al., 2023) and filtered

according to the following criteria: I) each substitution must additionally occur in a temperate and an Arctic diatom species other than *T. gravida* and *T. rotula*, and II) each CAAS gene variant must be expressed in both the Arctic and temperate metatranscriptome collections. The position of each CAAS in each alignment was manually checked to ensure reliability, i.e., to occur in an otherwise gapless conserved region. The resulting genes were annotated using eggNOG-mapper version 2.1.12 (Cantalapiedra et al., 2021), including *de novo* screening for the occurrence of PFAM protein domain motifs (Mistry et al., 2020).

Results

Temperature performance curves

For the Arctic strains, the fitted temperature performance curve models displayed an optimum temperature (T_{opt}) ranging from 9.3 ± 0.7°C for strain A4 up to 11.2 ± 1.6°C for strain A2 and an overall mean of 10.3 ± 0.8°C for the Arctic strains (Fig. 2.1). For the temperate strains T_{opt} ranged from 15.7 ± 1.2°C for strain T3 up to 20.8 ± 0.9°C for strain T1 and a mean across strains of 18.4 ± 2.4°C. T_{opt} differed as a response to Arctic or temperate origin (Table 2.1). With regard to the maximum achieved growth rate across all tested temperatures (μ_{max}), Arctic and temperate strains had a mean μ_{max} of 0.60 ± 0.07 and 0.59 ± 0.08, respectively and showed no significant difference by origin. Furthermore, the thermal breadth was compared at a level of 80% of μ_{max} (Tb_{80}) and revealed a significant origin-specific difference between the studied diatom strains with the Arctic strains showing a narrower breadth (7.82 ± 0.75°C) compared to the temperate strains (11.35 ± 2.44°C). The activation energies (E_a) of the fitted TPCs range from 0.32 ± 0.10 eV for strain T1 to 1.00 ± 0.45 eV for strain T5. However, no origin-specific differences could be detected.

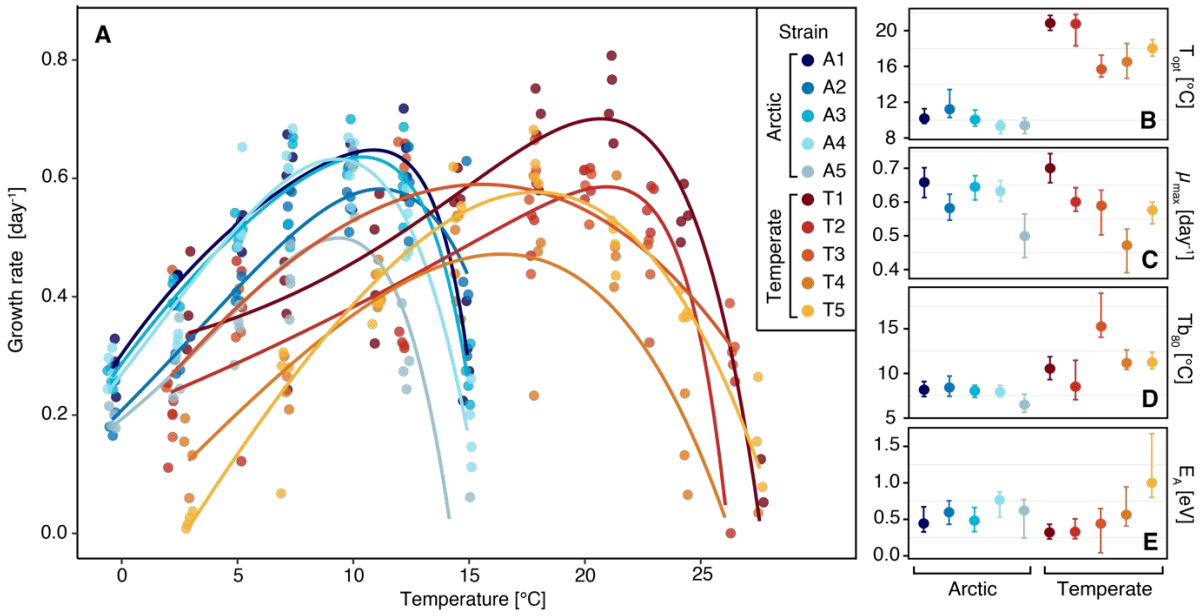

Fig. 2.1: Temperature performance curves and associated parameters for *T. gravida* (strains A1-A5) and *T. rotula* (strains T1-T5) indicated by color with (A) fitted TPC models to growth rate on the y-axis and temperature on the x-axis; (B) optimum temperature (T_{opt}); (C) maximum growth rate (μ_{max}); (D) thermal breadth at 80% of μ_{max} (Tb_{80}); and (E) activation energy (E_A). TPC parameters (panel B-E) are given as mean ± 95% confidence intervals as error bars. For visibility, x-axis jittering was added to the points.

Table 2.1: Welch T-test results on differences across Arctic and temperate strain origin for the TPC parameters optimum temperature (T_{opt}), maximum growth rate (μ_{max}), thermal breadth at 80% of μ_{max} and activation energy (E_A). T and p-values are reported for each effect. Values marked with an asterisk (*) indicate significant effects ($p < 0.05$).

		Arctic vs. Temperate		
parameter	*df*	*t*	*p*	
T_{opt}	4.8	-7.443	<0.001	*
μ_{max}	7.6	0.335	0.747	
Tb_{80}	4.8	-3.086	0.029	*
E_A	5.6	0.369	0.726	

Photoperiod reaction norms

The photoperiod reaction norms that were fitted as GAMs to the normalized growth rates of the tested Arctic and temperate diatom strains displayed distinct shapes which differed significantly ($p < 0.001$, Table S2.3) between the species, i.e., between Arctic and temperate origin (Fig. 2.2). The reaction norm for the Arctic strains was a saturating function, achieving the highest growth

rates at photoperiods of 24h. During the initial phase of the reaction norm, the strains A1, A2, and A4 immediately increase with photoperiod while strain A3 followed a sigmoidal shape. Contrastingly, for the temperate diatom strains, photoperiod reaction norms showed a linear to sigmoidal shaped increase of the reaction norm followed by a modeled local optimum at a photoperiod of 17.3 ± 0.2h after which growth decreases towards the 24h photoperiod.

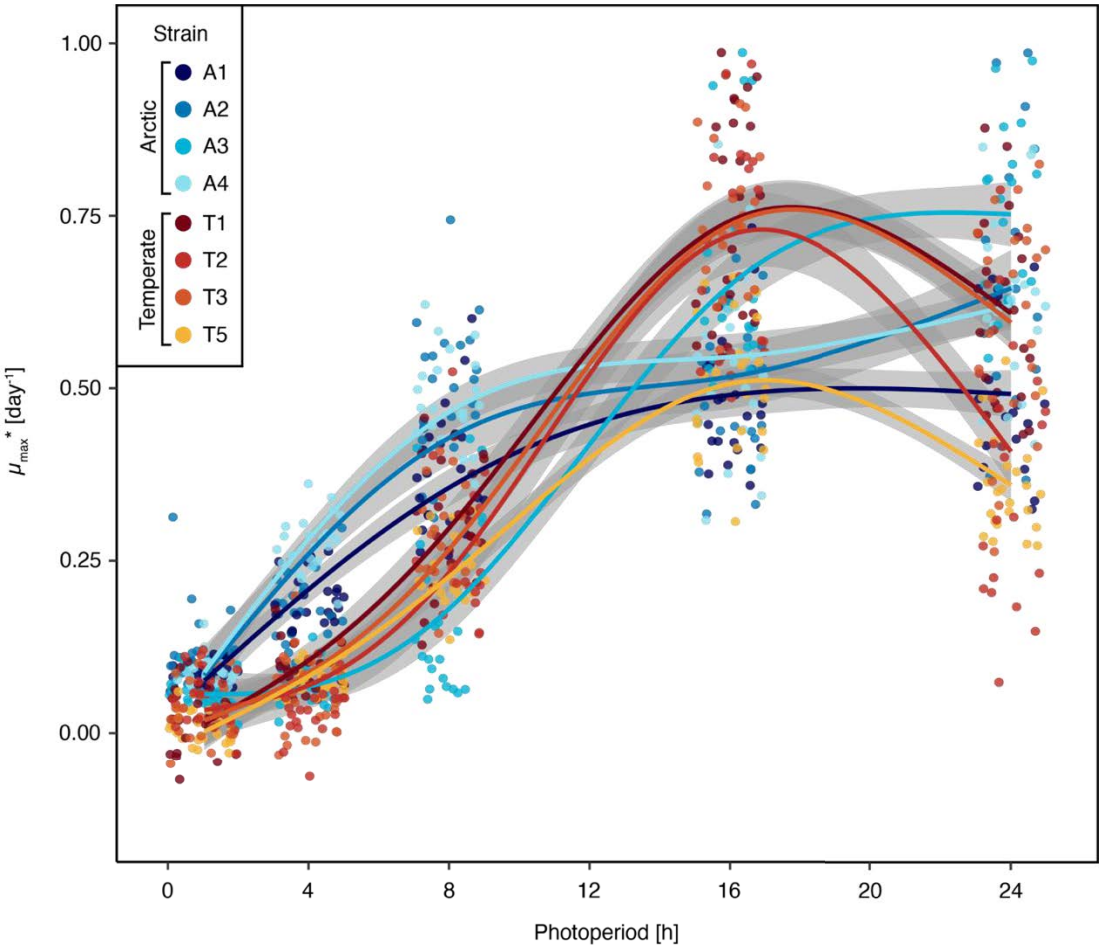

Fig. 2.2: Photoperiod reaction norms of 4 strains of *T. gravida* (A1-A4) and *T. rotula* (T1-T3; T5), respectively, with normalized maximum growth rate on the y-axis (μ_{max}*) and applied photoperiod (in hours) on the x-axis. GAMs ± SE are fitted to the data points for each strain. For visibility, x-axis jittering was added to the points (GAMs were fit to unjittered data).

Nitrate Uptake rates

The nitrate uptake kinetics showed a wide range of maximum uptake rates (V_{max}) among the strains (Fig. 2.3) ranging from $0.29 \pm 0.08 \times 10^{-7}$ µmol N cell^{-1} h^{-1} in the Arctic strain A3 up to $5.82 \pm 0.30 \times 10^{-7}$ µmol N cell^{-1} h^{-1} in the temperate strain T1. Despite generally higher V_{max} values for most temperate diatom strains, we did not find strong evidence for differences

between latitudes (p = 0.14). Similarly, half saturation constants (Ks) showed high intraspecific variability, particularly in strain A3, resulting in no significant differences (p = 0.70).

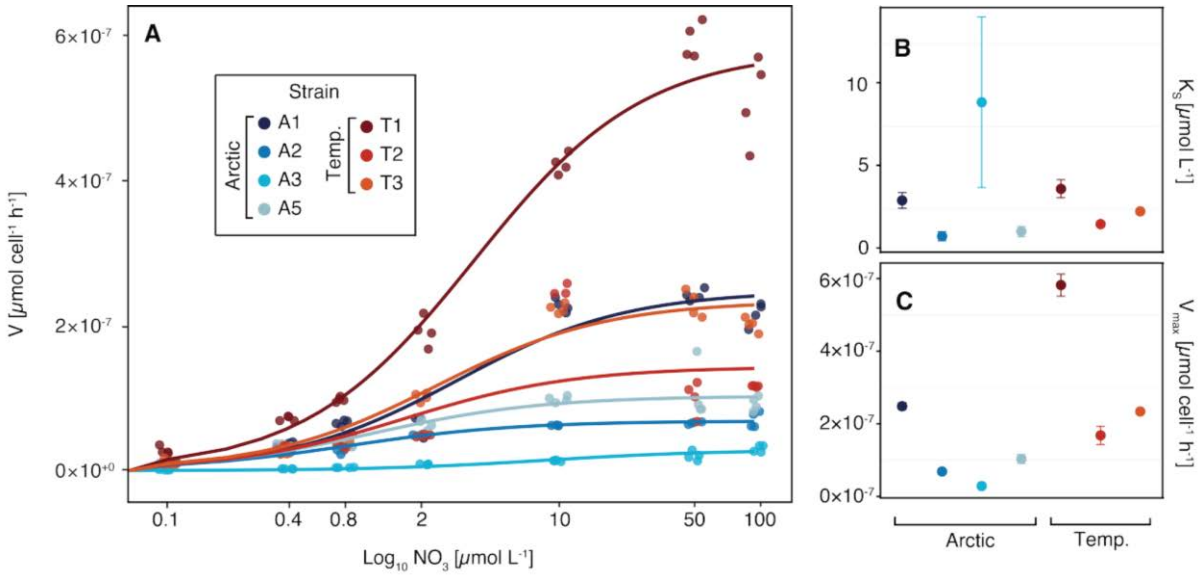

Fig. 2.3: Nitrate uptake kinetics and associated parameters for *T. gravida* (strains A1, A2, A3 and A5) and *T. rotula* (strains T1, T2, T3) indicated by color with (A) cell-normalized nitrate uptake rates across the tested nitrate concentrations fitted to the Michaelis-Menten function plotted on a logarithmic x-axis; (B) half-saturation constant (K_S); and (C) maximum uptake rate (V_{max}). Uptake parameters (panel B-C) are given as mean ± SD. Note that uptake experiments for Arctic and temperate strains had to be performed at different temperatures (9°C vs. 16°C, see methods) and so may not be directly comparable.

Convergent Amino Acid Substitutions

After quality filtering, we identified 26 candidate gene alignments with specific CAAS, i.e., convergence towards a specific amino acid at a specific alignment position as a response to Arctic or temperate origin of the sequence (Fig. 2.4, Table 2.2). In total, 12 of these candidate gene alignments could be functionally annotated. For convenience, members of each candidate gene alignment are collectively called 'IDs' in the following sections. Of the 12 functionally annotated IDs, 6 IDs are annotated as being involved in the central dogma processes (i.e., fundamental processes of the flow of genetic information: DNA replication, transcription, and translation that are responsible for the maintenance and expression of genes within an organism). A further 5 IDs are annotated as being involved in metabolic functions, including the often interrelated functions of lipid- and secondary metabolism. Among all 26 identified IDs, 22 of those exclusively contained CAAS in the Arctic diatom sequences (i.e., one unique

AA shared between all identified Arctic diatom sequences, while temperate sequences show different AAs at the respective alignment position, e.g., Fig. 2.4c). For 3 IDs, CAAS were identified only in temperate sequences and 1 ID showed a CAAS for both origins simultaneously (i.e., one unique AA for Arctic and temperate sequence, respectively, at the same alignment position, Fig. 2.4b). With regard to taxonomic coverage, the Arctic-origin CAAS with the highest number of diatom species was found in a sugar transporter (gene ID 7700) shared among *Thalassiosira gravida*, *Thalassiosira oceanica*, *Shionodiscus bioculatus* and *Detonula confervaceae*. For the temperate CAAS the highest taxonomic coverage was found in one of the zinc finger gene families (Sec23/Sec24, gene ID 6123) shared across seven diatom species (*Thalassiosira rotula*, *Minidiscus spinulatus*, *Minidiscus variabilis*, *Minidiscus comicus*, *Detonula confervaceae*, *Leptocylindrus danicus*, *Chaetoceros* sp.).

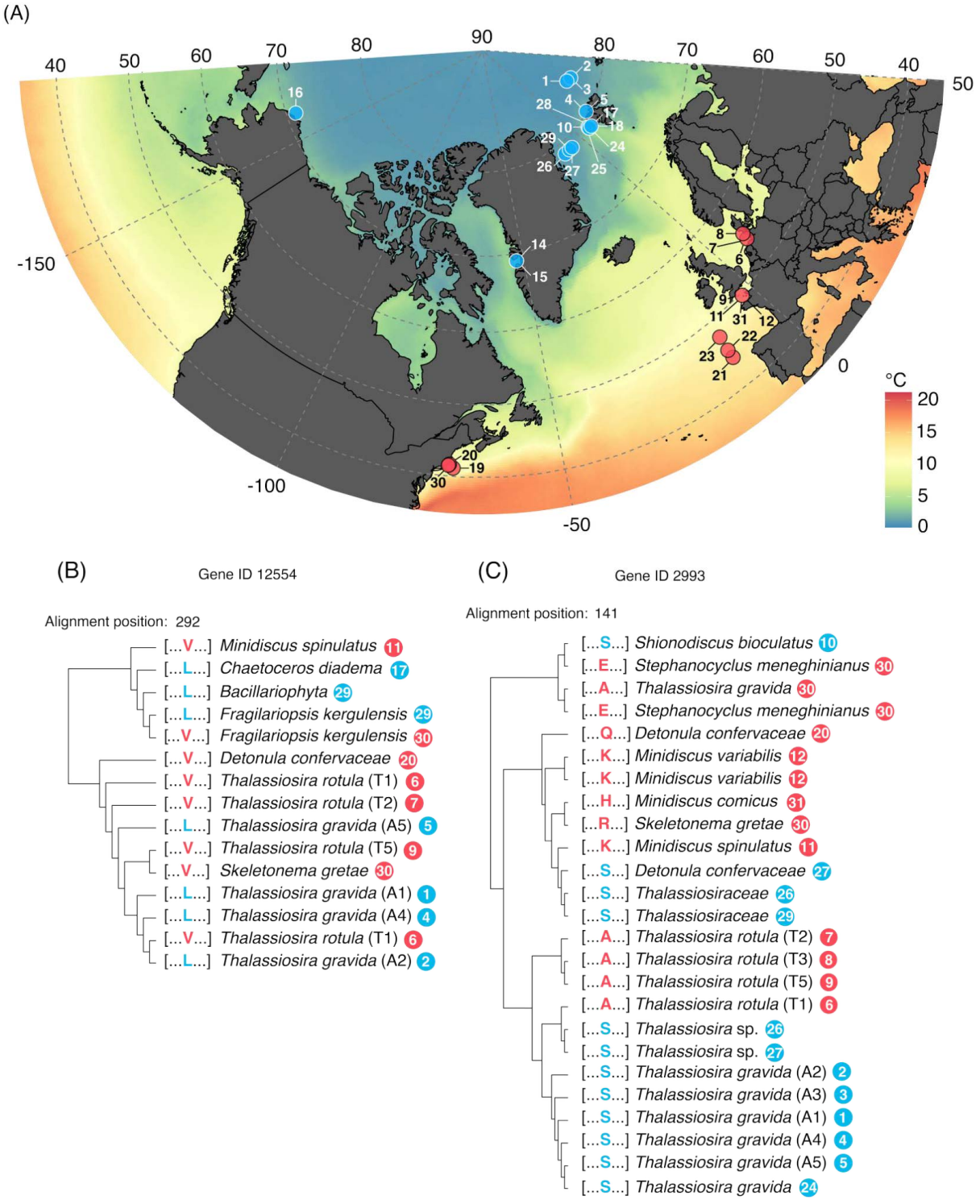

Fig. 2.4: Map of origin for metatranscriptomes and culture isolate RNA-seq datasets used in the CAAS analysis (see details and references for datasets in Table S2), colored by annual mean sea surface temperature (modified after NASA, 2013). RNA-seq datasets from Arctic and temperate ocean provinces are marked as blue and red dots, respectively and are numbered with a location code (A). Exemplary midpoint rooted phylogenetic trees of two candidate genes resulting from the CAAS analysis are shown for gene ID 12554 with habitat-specific amino acids in Arctic and temperate diatoms at alignment position 292 (B) and gene ID 2993 with CAAS only in Arctic diatoms at alignment position 141 while showing diverse amino acids in temperate diatoms (C). Phylogenetic trees highlight phylogenetic independence of the found CAAS. Tips are labeled with the respective amino acid (one-letter code) at the corresponding CAAS site, the assigned taxonomy, and the location code of the respective RNA-seq data set. CAAS and station code are colored blue or red for Arctic or temperate origin, respectively.

Table 2.2: Results of CAAS analysis. For each alignment ID reported by CAAStools that passed quality filtering and manual quality control, alignment position (Pos.), amino acid of Arctic sequences (Arctic AA) and temperate sequences (Temperate AA) as well as the functional annotation from the eggNOG-mapper results are given.

Alignment ID	Pos.	Arctic AA	Temperate AA	Functional annotation	Functional group
9895	384	N	D, F, K, T	Methylation of tRNAs	[J] Translation, ribosomal structure and biogenesis
1375	52	S	A, D, P, V	Zinc finger, C3HC4 type	[K] Transcription
2720	413	N	Q, S	Zinc finger, Nab2-type	[K] Transcription
6123	30	A, I	V	Sec23/Sec24 zinc finger	[K] Transcription
2998	749	E	C, G, I, Q, R, S, T	DNA mismatch repair protein Mlh1	[L] Replication, recombination and repair
7630	448	E	K, Q, S	DNA polymerase alpha/epsilon subunit B	[L] Replication, recombination and repair
7700	423	V	E, G, S, T	Sugar transporter	[G] Carbohydrate transport and metabolism
5037	269	Q	E, K, R	Membrane-bound acyltransferase	[I] Lipid transport and metabolism
5781	218	K	E, G, S, V	Oxidation-reduction (dehydrogense)	[I] Lipid transport and metabolism & [Q] Secondary metabolites biosynthesis, transport and catabolism
6653	168	E	D, G, Q	All-trans-retinol 13,14-reductase	[I] Lipid transport and metabolism & [Q] Secondary metabolites biosynthesis, transport and catabolism
8045	893	S	A, V	ABC transporter	[Q] Secondary metabolites biosynthesis, transport and catabolism
8045	1162	V	A, I		
8045	1259	A	I, K, V		
631	616	W	A, F, H, L, Y	Chitinase class I	[R] General function prediction only
557	16	L	A, F, I, S, T	-	[S] Function unknown

908	158	D, F, T	S	-	[S] Function unknown
2702	371	C	F, S, Y	-	[S] Function unknown
2993	141	S	A, E, H, K, Q, R	-	[S] Function unknown
3485	150	S	A, D, E, T	-	[S] Function unknown
4072	662	M	A, G, L, P, S, T, V	-	[S] Function unknown
4756	49	A	E, N, T, V	-	[S] Function unknown
4990	33	E	A, D, K, N, Q, S, T, V	-	[S] Function unknown
6457	27	A	K, P, S	-	[S] Function unknown
10130	156	N	D, F, G, L, S	-	[S] Function unknown
11282	276	N	K, L, R, V	-	[S] Function unknown
11341	215	M	I, K, L, S	-	[S] Function unknown
12554	333	L	V	-	[S] Function unknown
13375	292	A, F, I	V	-	[S] Function unknown

Discussion

The Arctic and temperate diatoms showed distinct temperature reaction norms with significant differences in T_{opt} and thermal breadth but no significant differences in E_A and μ_{max}. With regard to photoperiod-dependent growth, reaction norm shapes varied between short photoperiods and diverged at 24h of photoperiod for Arctic and temperate strains. Large trait variability was observed in nitrate uptake parameters V_{max} and K_S. In terms of genetic traits, a screening of available (meta-) transcriptomes for CAAS revealed 26 candidate genes pointing to habitat-specific molecular adaptations, most of which were found in Arctic diatoms. The CAAS proteins with functional annotations were dominated by central dogma processes, followed by functions in lipid and secondary metabolism.

Adaptation of thermal traits

The TPCs of the Arctic and temperate diatom strains differed as expected for these contrary thermal habitats, which is reflected across the studied thermal traits. While for the temperate diatoms an optimum temperature of 18.4°C lies at the upper range of their habitat's annual temperature amplitude (Wiltshire and Manly, 2004), a T_{opt} of around 10°C for the Arctic strains

might seem surprisingly high, given the fact that these water temperatures are neither reached nor surpassed in the Arctic Ocean (Timmermanns and Labe, 2022). However, there are two likely explanations for this seemingly high T_{opt}, which are not mutually exclusive. Firstly, organisms that live below their T_{opt} are buffered against temperature fluctuations that would be detrimental if T_{opt} was exceeded. This pattern has previously been described by Thomas et al. (2012) who showed the T_{opt} of polar and temperate phytoplankton to be several degrees higher than the annual mean water temperatures of their respective habitat while in tropical habitats, species live very close to their optimum temperature. Secondly, it has been demonstrated that T_{opt} is interactively affected by other stressors such as nitrate concentration (Thomas et al., 2017) or light intensity (Edwards et al., 2016) that can lower T_{opt} by up to 4°C or 5°C, respectively. Given the fact that in this study, both nutrient and light conditions were replete, this might lead to an overestimation of T_{opt} compared to natural systems that frequently experience resource limitation (Reid et al., 1990, Elser et al., 2007). Considering thermal traits beyond T_{opt}, habitat-specific adaptation can also be observed in differences of the thermal breadth of the TPCs of Arctic and temperate diatom strains. The temperate diatom strains which are subject to much larger annual temperature variation (Wiltshire and Manly, 2004) exhibited much broader TPCs compared to the narrower thermal breadth of the Arctic strains. This corresponds to the eurytherm and stenotherm lifestyles imposed by the different temperature amplitudes of Arctic and temperate habitats.

With regard to poleward migration potential, the thermal range of the temperate diatom strains would allow them to proliferate in Arctic habitats, but they would grow slower than existing Arctic diatoms at the low temperatures and so they would likely be at a competitive disadvantage. However, considering the known interactive effects of temperature dependent growth with nitrate and light intensity (Thomas et al., 2017, Edwards et al., 2016), causing a decrease of T_{opt} when resources are limited (see above), this may affect the competitive outcome. Particularly in a scenario of elevated temperatures in combination with resource-limitation, Arctic diatoms may be pushed beyond their T_{opt}, leading to detrimental effects on the population while the temperate diatoms likely would not surpass their respective T_{opt} (Thomas et al., 2017).

Adaptation to photoperiods

The photoperiod reaction norms assessed in this study showed habitat-specific adaptations which reflect an imprint of a chronobiological background that is strongly conserved even after years of laboratory cultivation at a constant intermediate photoperiod (Giesler et al., 2023). While the temperate strains displayed a photoperiod optimum of ~17h, mirroring a habitat characterized by intermediate daylengths, the Arctic strains showed specific competitive advantages at both extreme long and extreme short photoperiods. This response is likely a consequence of the polar day and polar night. In contrast to the light regimes of temperate regions, intermediate photoperiods only correspond to a transitional phase lasting a few weeks in Arctic habitats. As the photoperiod reaction norm assays were conducted as a single driver experiment (i.e., close to the respective populations T_{opt}), interactive effects of photoperiod and temperature were not considered in our study. Yet, another study by Giesler et al. (2023) investigated the interactive responses of one Arctic and temperate strain each used in this study and showed that the Arctic strain may lose its ability to cope with 24h photoperiods at temperatures beyond their T_{opt}. Other studies found that the response to photoperiod interacted with temperature, light intensity (Theus et al., 2022), and cell size (Li et al., 2017) thus highlighting that reaction norms are only a snapshot of the multifactorial reality. Despite the interactive nature of most abiotic drivers, the response of the tested conditions in this study showed to be reproducible across strains from the same origin and also had comparable responses at the respective experimental conditions and strains in the study by Giesler et al. (2023).

On the cellular level, prolonged photoperiods cause oxidative stress (Roeber et al., 2021) to which Arctic diatoms fine-tune specific adaptations in terms of their photosynthetic machinery (Croteau et al., 2020), their lipidome (Svenning et al., 2024), and even symbiotic interactions with associated bacteria to reduce ROS stress (Hunken et al., 2008). The decreased growth performance for temperate diatoms at a 24h photoperiod compared to Arctic diatoms suggests the lack of these adaptations, resulting in decreasing growth performance. As a consequence, extreme day lengths in polar regions may pose an additional barrier to poleward range shift of temperate diatoms. Current species distribution models project a median speed of 35 km per decade for poleward migration of temperate phytoplankton (Benedetti et al., 2021) but do not consider required adaptation to polar light regimes which might slow down the speed of poleward range shifts. This underlines the need for further studies to investigate whether temperate diatoms can adapt to an extreme polar light regime and if so, whether there are trade-

offs associated with this. Given that the Arctic diatom strains experienced a constant photoperiod of 14:10h light:dark during long-term cultivation in the culture collection (Table S2.1), and still maintain a strong adaptive signal to extreme Arctic photoperiods, this suggests that photoperiodic adaptation is likely to be costly and a rather long-term process.

Nitrate uptake traits

The maximum uptake rate of nitrate as well as the half saturation constant showed high variability across the tested diatom strains. Yet it has to be considered how the results are affected by the different temperatures at which the assays had to be conducted for Arctic and temperate diatoms. Previous studies demonstrated that an organisms' nitrate affinity decreases at temperatures below its optimum (Nedwell, 1999, Reay et al., 1999). Therefore, direct comparisons between the determined nitrate uptake traits and resulting implications for competitive advantages are complicated. Nevertheless, the observed large intraspecific variability for both Arctic and temperate diatoms suggests a relatively low selective pressure on nitrate uptake rates compared to other, more stable environmental drivers. Indeed, environmental nitrate concentrations in Arctic and temperate habitats both show large annual variation, ranging from near zero concentrations in the late summer months up to ~10 µmol L^{-1} and ~20 µmol L^{-1} during winter/early spring in northeast Svalbard (Arctic) and Helgoland (North Sea), respectively (Randelhoff et al., 2015, Wiltshire, 2011). Thus, due to trade-offs of nutrient uptake with other metabolic processes (Ward et al., 2016), it might be beneficial to maintain high variability in nutrient uptake related traits in a population to quickly respond to these nutrient fluctuations (Raimbault et al., 1990). To maintain this variability in the context of poleward range shifts, the temperate diatoms membrane lipids and uptake transporters likely require specific molecular adaptations as their flexibility and effectiveness decreases with temperature (Nedwell, 1999). The presence of these habitat specific adaptations in Arctic diatoms is indicated by the CAAS analysis in which multiple transporters and lipid-related gene candidates with molecular adaptations were identified (see below).

Convergent amino acid substitutions

The analysis of the temperate and Arctic diatom transcriptomes in concert with other available Arctic and temperate diatom (meta-) transcriptomes allowed the identification of 26 proteins

with habitat-specific convergent amino acid substitutions (CAAS). These molecular adaptations likely contribute to the found differences in diatom adaptation to different thermal and light regimes. Most of these CAAS showed selection towards an identical amino acid in Arctic diatoms while the temperate diatoms had different and variable amino acids at the respective alignment position. These molecular adaptations indicate hard selection pressure favoring the fixation of these substitutions in Arctic populations and species. Consequently, the resulting traits of these adaptations likely facilitate their distribution in Arctic habitats (Birkeland et al., 2020).

The majority of the CAAS bearing proteins are involved in central dogma processes that transfer genetic information within cells. To some extent, it is reasonable to assume that thermal differences in the respective habitats may have contributed to the natural selection of these CAAS, coordinating transcription and translation to ensure cellular homeostasis in coherence with further environmental factors (Knapp and Huang, 2022). In this context, the convergent modulation of zinc finger transcription factor sequences could potentially contribute to cellular homeostasis by e.g., altering their binding affinities to promoter regions (Knapp and Huang, 2022). Functionally, the identified zinc finger transcription factors are known to be involved in abiotic stress responses in plants (Han et al., 2022) and in the regulation of growth and photosynthesis in diatoms (Ye et al., 2022). The CAAS discovered in DNA polymerase and DNA mismatch repair proteins also suggest a functionally coherent parallel adaptation of these related processes (i.e., synthesizing nucleotide strands and correcting for potential errors). The discovery of CAAS in a membrane-bound acyltransferase and in the all-trans-retinol 13,14-reductase suggests additional adaptations and merits further investigation. In general, membrane-bound acyltransferases are involved in the modification and synthesis of complex membrane lipids, which may indeed reflect temperature adaptation (Nedwell, 1999). The CAAS in the all-trans-retinol 13,14-reductase may likely influence photobiological regulation, as it provides both the chromophore for rhodopsin photoreceptors and molecules for photoprotection in diatoms, and is thus involved in photoreception and cellular energy regulation (Marchetti et al., 2012, Dong et al., 2016).

We note that many of the identified CAAS-bearing proteins could not be functionally annotated, leaving their specific contribution to the polar adaptation of diatoms open. This highlights a crucial gap in our understanding of ecologically important functions of diatoms. Without this knowledge, we cannot fully assess the potential consequences and possibilities of eventual range shifts. Indeed, the functional complexity of the proteins in which CAAS are detected

raises questions about the extent to which migration and long-term persistence of temperate *Thalassiosira* populations in the Arctic is possible in response to immediate or current global change conditions. Zinc, for example, has been shown to be important for the evolution of Arctic phytoplankton species (Ye et al., 2022) and is therefore likely to challenge the competitive ability of migrating diatoms that do not carry specific adaptations. Particularly for zinc-finger protein domains, an adaptive expansion in polar regions and an accelerated rate of evolution was revealed in line with our finding of multiple zinc finger gene families with CAAS (Asch et al., 2019). The same applies to polar light regimes, for which adaptations are reflected not only in the photoperiod reaction norms discussed above, but potentially also in transcription factors regulating photosynthesis and growth, as well as in enzymes crucial for photobiological regulation.

Although the degree to which a respective CAAS is essential for a specific diatom population to establish in an Arctic habitat may differ among the identified proteins, the sum of habitat-specific functional genetic modifications represent potential bottlenecks of adaptation that can hamper poleward migration of temperate diatoms. Yet, as a consequence of ocean warming, CAAS that are the result of thermal adaptation may become less important while genetic adaptations to more stable physical parameters unique to Arctic latitudes, such as the extreme light regimes, will prevail.

Conclusion

This study highlights different facets of Arctic adaptation. These include adaptations to polar photoperiods and temperatures that are shaped by molecular adaptations that ensure information flow from DNA to proteins, and molecular adaptations within lipid-, carbohydrate- and secondary metabolism. The assessed thermal traits indicate the potential for poleward range shifts of temperate diatoms in response to the ongoing warming of the Arctic, but the different photoperiod response norms highlight barriers that are not yet considered in species distribution models. In addition, the identified candidate genes in which adaptation to Arctic habitats is most evident provide a first comparative insight into the convergent evolution of Arctic diatoms, but also underline our lack of knowledge of ecologically important gene functions governing polar adaptation. Finally, our results open new targets for further studies to investigate the consequences of global warming on marine primary producers, and to estimate adaptation speed under polar day scenarios to gain a more realistic understanding of poleward range shifts.

Acknowledgements

We thank Nancy Kühne, Charlotte Volpe and Nico Helmsing for technical and logistical support in the lab, as well as Antonia Ahme and Ruben Schulte-Hillen for their help during experimental sampling.

References

AHME, A., VON JACKOWSKI, A., MCPHERSON, R. A., WOLF, K. K. E., HOPPMANN, M., NEUHAUS, S. & JOHN, U. 2023. Winners and Losers of Atlantification: The Degree of Ocean Warming Affects the Structure of Arctic Microbial Communities. *Genes (Basel),* 14.

ARANGUREN-GASSIS, M., LITCHMAN, E. & MOISANDER, P. 2020. Thermal performance of marine diatoms under contrasting nitrate availability. *Journal of Plankton Research*.

ARDYNA, M., BABIN, M., GOSSELIN, M., DEVRED, E., BÉLANGER, S., MATSUOKA, A. & TREMBLAY, J. É. 2013. Parameterization of vertical chlorophyll a in the Arctic Ocean: impact of the subsurface chlorophyll maximum on regional, seasonal, and annual primary production estimates. *Biogeosciences,* 10**,** 4383-4404.

ARRIGO, K. R., PEROVICH, D. K., PICKART, R. S., BROWN, Z. W., VAN DIJKEN, G. L., LOWRY, K. E., MILLS, M. M., PALMER, M. A., BALCH, W. M., BAHR, F., BATES, N. R., BENITEZ-NELSON, C., BOWLER, B., BROWNLEE, E., EHN, J. K., FREY, K. E., GARLEY, R., LANEY, S. R., LUBELCZYK, L., MATHIS, J., MATSUOKA, A., MITCHELL, B. G., MOORE, G. W., ORTEGA-RETUERTA, E., PAL, S., POLASHENSKI, C. M., REYNOLDS, R. A., SCHIEBER, B., SOSIK, H. M., STEPHENS, M. & SWIFT, J. H. 2012. Massive phytoplankton blooms under Arctic sea ice. *Science,* 336**,** 1408.

ASCH, R. G., STOCK, C. A. & SARMIENTO, J. L. 2019. Climate change impacts on mismatches between phytoplankton blooms and fish spawning phenology. *Glob Chang Biol,* 25**,** 2544-2559.

BAKER, K. G., ROBINSON, C. M., RADFORD, D. T., MCINNES, A. S., EVENHUIS, C. & DOBLIN, M. A. 2016. Thermal Performance Curves of Functional Traits Aid Understanding of Thermally Induced Changes in Diatom-Mediated Biogeochemical Fluxes. *Frontiers in Marine Science,* 3.

BARTERI, F., VALENZUELA, A., FARRE, X., DE JUAN, D., MUNTANE, G., ESTEVE-ALTAVA, B. & NAVARRO, A. 2023. CAAStools: a toolbox to identify and test Convergent Amino Acid Substitutions. *Bioinformatics,* 39.

BENEDETTI, F., VOGT, M., ELIZONDO, U. H., RIGHETTI, D., ZIMMERMANN, N. E. & GRUBER, N. 2021. Major restructuring of marine plankton assemblages under global warming. *Nat Commun,* 12**,** 5226.

BIRKELAND, S., GUSTAFSSON, A. L. S., BRYSTING, A., BROCHMANN, C. & NOWAK, M. 2020. Multiple Genetic Trajectories to Extreme Abiotic Stress Adaptation in Arctic Brassicaceae. *Molecular biology and evolution,* 37.

BISKABORN, B. K., FORSTER, A., PFALZ, G., PESTRYAKOVA, L. A., STOOF-LEICHSENRING, K., STRAUSS, J., KRÖGER, T. & HERZSCHUH, U. 2023. Diatom responses and geochemical feedbacks to environmental changes at Lake Rauchuagytgyn (Far East Russian Arctic). *Biogeosciences,* 20**,** 1691-1712.

BOYD, P. W., RYNEARSON, T. A., ARMSTRONG, E. A., FU, F., HAYASHI, K., HU, Z., HUTCHINS, D. A., KUDELA, R. M., LITCHMAN, E., MULHOLLAND, M. R., PASSOW, U., STRZEPEK, R. F., WHITTAKER, K. A., YU, E. & THOMAS, M. K. 2013. Marine phytoplankton temperature versus growth responses from polar to tropical waters--outcome of a scientific community-wide study. *PLoS One,* 8**,** e63091.

BRANDT, S., WASSMANN, P. & PIEPENBURG, D. 2023. Revisiting the footprints of climate change in Arctic marine food webs: An assessment of knowledge gained since 2010. *Frontiers in Marine Science,* 10.

BRUN, P., STAMIESZKIN, K., VISSER, A. W., LICANDRO, P., PAYNE, M. R. & KIORBOE, T. 2019. Climate change has altered zooplankton-fuelled carbon export in the North Atlantic. *Nat Ecol Evol,* 3**,** 416-423.

CANTALAPIEDRA, C. P., HERNANDEZ-PLAZA, A., LETUNIC, I., BORK, P. & HUERTA-CEPAS, J. 2021. eggNOG-mapper v2: Functional Annotation, Orthology Assignments, and Domain Prediction at the Metagenomic Scale. *Mol Biol Evol,* 38**,** 5825-5829.

CAPELLA-GUTIERREZ, S., SILLA-MARTÍNEZ, J. & GABALDÓN, T. 2009. TrimAl: a tool for automated alignment trimming in large-scale phylogenetic analyses. *Bioinformatics (Oxford, England),* 25**,** 1972-3.

CROTEAU, D., GUÉRIN, S., BRUYANT, F., FERLAND, J., CAMPBELL, D. A., BABIN, M. & LAVAUD, J. 2020. Contrasting nonphotochemical quenching patterns under high light and darkness aligns with light niche occupancy in Arctic diatoms. *Limnology and Oceanography,* 66.

DONG, H. P., DONG, Y. L., CUI, L., BALAMURUGAN, S., GAO, J., LU, S. H. & JIANG, T. 2016. High light stress triggers distinct proteomic responses in the marine diatom Thalassiosira pseudonana. *BMC Genomics,* 17**,** 994.

EDWARDS, K. F., THOMAS, M. K., KLAUSMEIER, C. A. & LITCHMAN, E. 2016. Phytoplankton growth and the interaction of light and temperature: A synthesis at the species and community level. *Limnology and Oceanography,* 61**,** 1232-1244.

ELSER, J. J., BRACKEN, M. E., CLELAND, E. E., GRUNER, D. S., HARPOLE, W. S., HILLEBRAND, H., NGAI, J. T., SEABLOOM, E. W., SHURIN, J. B. & SMITH, J. E. 2007. Global analysis of nitrogen and phosphorus limitation of primary producers in freshwater, marine and terrestrial ecosystems. *Ecol Lett,* 10**,** 1135-42.

FALK-PETERSEN, S., PAVLOV, V., TIMOFEEV, S. & SARGENT, J. R. 2006. Climate variability and possible effects on arctic food chains: The role of *Calanus*. *In:* ØRBÆK, J. B., KALLENBORN, R., TOMBRE, I., HEGSETH, E. N., FALK-

PETERSEN, S. & HOEL, A. H. (eds.) *Arctic Alpine Ecosystems and People in a Changing Environment.* Berlin, Heidelberg: Springer Berlin Heidelberg.

FARMER, J. R., SIGMAN, D. M., GRANGER, J., UNDERWOOD, O. M., FRIPIAT, F., CRONIN, T. M., MARTÍNEZ-GARCÍA, A. & HAUG, G. H. 2021. Arctic Ocean stratification set by sea level and freshwater inputs since the last ice age. *Nature Geoscience,* 14**,** 684-689.

GIESLER, J. K., HARDER, T. & WOHLRAB, S. 2023. Microbiome and photoperiod interactively determine thermal sensitivity of polar and temperate diatoms. *Biol Lett,* 19**,** 20230151.

HAAS, B. 2013. TransDecoder (Find Coding Regions Within Transcripts). https://github.com/TransDecoder/transdecoder.github.io.

HAN, G., QIAO, Z., LI, Y., YANG, Z., WANG, C., ZHANG, Y., LIU, L. & WANG, B. 2022. RING Zinc Finger Proteins in Plant Abiotic Stress Tolerance. *Front Plant Sci,* 13**,** 877011.

HARRISON, P. J., WATERS, R. E. & TAYLOR, F. J. R. 2008. A Broad Spectrum Artificial Sea Water Medium for Coastal and Open Ocean Phytoplankton1. *Journal of Phycology,* 16**,** 28-35.

HATTICH, G. S. I., JOKINEN, S., SILDEVER, S., GAREIS, M., HEIKKINEN, J., JUNGHARDT, N., SEGOVIA, M., MACHADO, M. & SJÖQVIST, C. 2024. Temperature optima of a natural diatom population increases as global warming proceeds. *Nature Climate Change,* 14.

HUNKEN, M., HARDER, J. & KIRST, G. O. 2008. Epiphytic bacteria on the Antarctic ice diatom *Amphiprora kufferathii* Manguin cleave hydrogen peroxide produced during algal photosynthesis. *Plant Biol (Stuttg),* 10**,** 519-26.

ITO, R. K., HARADA, S., TABATA, R. & WATANABE, K. 2022. Molecular evolution and convergence of the rhodopsin gene in *Gymnogobius*, a goby group having diverged into coastal to freshwater habitats. *J Evol Biol,* 35**,** 333-346.

JIN, P. & AGUSTI, S. 2018. Fast adaptation of tropical diatoms to increased warming with trade-offs. *Sci Rep,* 8**,** 17771.

KARNOVSKY, N., HARDING, A., WALKUSZ, W., KWASNIEWSKI, S., GOSZCZKO, I., WIKTOR, J., JR., ROUTTI, H., BAILEY, A., MCFADDEN, L., BROWN, Z., BEAUGRAND, G. & GRÉMILLET, D. 2010. Foraging distributions of little auks Alle alle across the Greenland Sea: implications of present and future Arctic climate change. *Marine Ecology Progress Series,* 415**,** 283-293.

KATOH, K. & STANDLEY, D. 2013. Katoh K, Standley DM.. MAFFT Multiple Sequence Alignment Software Version 7: Improvements in performance and usability. Mol Biol Evol 30: 772-780. *Molecular biology and evolution,* 30.

KELLER, M. D., SELVIN, R. C., CLAUS, W. & GUILLARD, R. R. L. 2007. Media for the Culture of Oceanic Ultraphytoplankton1,2. *Journal of Phycology,* 23**,** 633-638.

KNAPP, B. D. & HUANG, K. C. 2022. The Effects of Temperature on Cellular Physiology. *Annu Rev Biophys,* 51**,** 499-526.

LENOIR, J., BERTRAND, R., COMTE, L., BOURGEAUD, L., HATTAB, T., MURIENNE, J. & GRENOUILLET, G. 2020. Species better track climate warming in the oceans than on land. *Nature Ecology & Evolution,* 4**,** 1044-1059.

LI, G., TALMY, D. & CAMPBELL, D. A. 2017. Diatom growth responses to photoperiod and light are predictable from diel reductant generation. *J Phycol,* 53**,** 95-107.

MARCHETTI, A., SCHRUTH, D. M., DURKIN, C. A., PARKER, M. S., KODNER, R. B., BERTHIAUME, C. T., MORALES, R., ALLEN, A. E. & ARMBRUST, E. V. 2012. Comparative metatranscriptomics identifies molecular bases for the physiological responses of phytoplankton to varying iron availability. *Proc Natl Acad Sci U S A,* 109**,** E317-25.

MATURILLI, M., HERBER, A. & KÖNIG-LANGLO, G. 2013. Climatology and time series of surface meteorology in Ny-Ålesund, Svalbard. *Earth System Science Data,* 5**,** 155-163.

MIELE, V., PENEL, S. & DURET, L. 2011. Ultra-fast sequence clustering from similarity networks with SiLiX. *BMC bioinformatics,* 12**,** 116.

MIRDITA, M., STEINEGGER, M., BREITWIESER, F., SODING, J. & LEVY KARIN, E. 2021. Fast and sensitive taxonomic assignment to metagenomic contigs. *Bioinformatics,* 37**,** 3029-3031.

MISTRY, J., CHUGURANSKY, S., WILLIAMS, L., QURESHI, M., SALAZAR, GUSTAVO A., SONNHAMMER, E., TOSATTO, S., PALADIN, L., RAJ, S., RICHARDSON, L., FINN, R. & BATEMAN, A. 2020. Pfam: The protein families database in 2021. *Nucleic Acids Research,* 49.

MONTOYA, J. P., CARPENTER, E. J. & CAPONE, D. G. 2002. Nitrogen fixation and nitrogen isotope abundances in zooplankton of the oligotrophic North Atlantic. *Limnology and Oceanography,* 47**,** 1617-1628.

MORRIEN, E., HANNULA, S. E., SNOEK, L. B., HELMSING, N. R., ZWEERS, H., DE HOLLANDER, M., SOTO, R. L., BOUFFAUD, M. L., BUEE, M., DIMMERS, W., DUYTS, H., GEISEN, S., GIRLANDA, M., GRIFFITHS, R. I., JORGENSEN, H. B., JENSEN, J., PLASSART, P., REDECKER, D., SCHMELZ, R. M., SCHMIDT, O., THOMSON, B. C., TISSERANT, E., UROZ, S., WINDING, A., BAILEY, M. J., BONKOWSKI, M., FABER, J. H., MARTIN, F., LEMANCEAU, P., DE BOER, W., VAN VEEN, J. A. & VAN DER PUTTEN, W. H. 2017. Soil networks become more connected and take up more carbon as nature restoration progresses. *Nat Commun,* 8**,** 14349.

MULHOLLAND, M. R., BONEILLO, G. E., BERNHARDT, P. W. & MINOR, E. C. 2009. Comparison of Nutrient and Microbial Dynamics over a Seasonal Cycle in a Mid-Atlantic Coastal Lagoon Prone to *Aureococcus anophagefferens* (Brown Tide) Blooms. *Estuaries and Coasts,* 32**,** 1176-1194.

MULHOLLAND, M. R., GOBLER, C. J. & LEE, C. 2002. Peptide hydrolysis, amino acid oxidation, and nitrogen uptake in communities seasonally dominated by *Aureococcus anophagefferens*. *Limnology and Oceanography,* 47**,** 1094-1108.

NEDWELL, D. B. 1999. Effect of low temperature on microbial growth: lowered affinity for substrates limits growth at low temperature. *Fems Microbiology Ecology,* 30**,** 101-111.

ORCUTT, K. M., LIPSCHULTZ F., GENDERSEN, K. 2001. A seasonal study of the significance of N_2 fixation by *Trichodesmium* spp. at the Bermuda Atlantic Time-series Study (BATS) site. *Deep-Sea Research II*, 48, 1583-1608.

PADFIELD, D. O. S., H. 2023. rTPC: Fitting and Analysing Thermal Performance Curves. https://github.com/padpadpadpad/rTPC.

PETZOLDT, T., KNEIS, D. & SEILER, C. 2017. Maximum Growth Rates Estimation with R Package 'growthrates'.

RAIMBAULT, P., SLAWYK, G. & GENTILHOMME, V. 1990. Direct Measurements of Nanomolar Nitrate Uptake by the Marine Diatom *Phaeodactylum tricornutum* (Bohlin) - Implications for Studies of Oligotrophic Ecosystems. *Hydrobiologia,* 207**,** 311-318.

RANDELHOFF, A., SUNDFJORD, A. & REIGSTAD, M. 2015. Seasonal variability and fluxes of nitrate in the surface waters over the Arctic shelf slope. *Geophysical Research Letters,* 42**,** 3442-3449.

RANTANEN, M., KARPECHKO, A. Y., LIPPONEN, A., NORDLING, K., HYVÄRINEN, O., RUOSTEENOJA, K., VIHMA, T. & LAAKSONEN, A. 2022. The Arctic has warmed nearly four times faster than the globe since 1979. *Communications Earth & Environment,* 3.

REAY, D. S., NEDWELL, D. B., PRIDDLE, J. & ELLIS-EVANS, J. C. 1999. Temperature dependence of inorganic nitrogen uptake: reduced affinity for nitrate at suboptimal temperatures in both algae and bacteria. *Appl Environ Microbiol,* 65**,** 2577-84.

REID, P. C., LANCELOT, C., GIESKES, W. W. C., HAGMEIER, E. & WEICHART, G. 1990. Phytoplankton of the North Sea and its dynamics: A review. *Netherlands Journal of Sea Research,* 26**,** 295-331.

REY, C., LANORE, V., VEBER, P., GUEGUEN, L., LARTILLOT, N., SEMON, M. & BOUSSAU, B. 2019. Detecting adaptive convergent amino acid evolution. *Philos Trans R Soc Lond B Biol Sci,* 374**,** 20180234.

ROEBER, V. M., SCHMULLING, T. & CORTLEVEN, A. 2021. The Photoperiod: Handling and Causing Stress in Plants. *Front Plant Sci,* 12**,** 781988.

SAR, E. A., SUNESEN, I., LAVIGNE, A. S. & LOFEUDO, S. 2011. *Thalassiosira rotula*, a heterotypic synonym of Thalassiosira gravida: morphological evidence. *Diatom Research,* 26**,** 109-119.

SHEN, X., PU, Z., CHEN, X., MURPHY, R. W. & SHEN, Y. 2019. Convergent Evolution of Mitochondrial Genes in Deep-Sea Fishes. *Front Genet,* 10**,** 925.

SIMS, P. A., MANN, D. G. & MEDLIN, L. K. 2019. Evolution of the diatoms: insights from fossil, biological and molecular data. *Phycologia,* 45**,** 361-402.

SVENNING, J. B., VASSKOG, T., CAMPBELL, K., BAEVERUD, A. H., MYHRE, T. N., DALHEIM, L., FORGEREAU, Z. L., OSANEN, J. E., HANSEN, E. H. & BERNSTEIN, H. C. 2024. Lipidome Plasticity Enables Unusual Photosynthetic Flexibility in Arctic vs. Temperate Diatoms. *Mar Drugs,* 22.

THEUS, M. E., LAYDEN, T. J., MCWILLIAMS, N., CRAFTON-TEMPEL, S., KREMER, C. T. & FEY, S. B. 2022. Photoperiod influences the shape and scaling of freshwater phytoplankton responses to light and temperature. *Oikos,* 2022.

THOMAS, M. K., ARANGUREN-GASSIS, M., KREMER, C. T., GOULD, M. R., ANDERSON, K., KLAUSMEIER, C. A. & LITCHMAN, E. 2017. Temperature-nutrient interactions exacerbate sensitivity to warming in phytoplankton. *Glob Chang Biol,* 23**,** 3269-3280.

THOMAS, M. K., KREMER, C. T., KLAUSMEIER, C. A. & LITCHMAN, E. 2012. A global pattern of thermal adaptation in marine phytoplankton. *Science,* 338**,** 1085-8.

TIMMERMANS, M. & LABE, Z. 2022. Sea Surface Temperature. in "Arctic Report Card 2022".

TRÉGUER, P., BOWLER, C., MORICEAU, B., DUTKIEWICZ, S., GEHLEN, M., AUMONT, O., BITTNER, L., DUGDALE, R., FINKEL, Z., IUDICONE, D., JAHN, O., GUIDI, L., LASBLEIZ, M., LEBLANC, K., LEVY, M. & PONDAVEN, P. 2018. Influence of diatom diversity on the ocean biological carbon pump. *Nature Geoscience,* 11**,** 27-37.

TREMBLAY, J. É., ANDERSON, L. G., MATRAI, P., COUPEL, P., BÉLANGER, S., MICHEL, C. & REIGSTAD, M. 2015. Global and regional drivers of nutrient supply, primary production and CO_2 drawdown in the changing Arctic Ocean. *Progress in Oceanography,* 139**,** 171-196.

VAN VLIERBERGHE, M., DI FRANCO, A., PHILIPPE, H. & BAURAIN, D. 2021. Decontamination, pooling and dereplication of the 678 samples of the Marine Microbial Eukaryote Transcriptome Sequencing Project. *BMC Res Notes,* 14**,** 306.

VOLPE, C., VADSTEIN, O., ANDERSEN, G. & ANDERSEN, T. 2021. Nanocosm: a well plate photobioreactor for environmental and biotechnological studies. *Lab Chip,* 21**,** 2027-2039.

WARD, B., MARANON, E., SAUTEREY, B., RAULT, J. & CLAESSEN, D. 2016. The Size Dependence of Phytoplankton Growth Rates: A Trade-Off between Nutrient Uptake and Metabolism. *The American Naturalist,* 189**,** 000-000.

WARD, B. A. 2015. Temperature-Correlated Changes in Phytoplankton Community Structure Are Restricted to Polar Waters. *PLoS One,* 10**,** e0135581.

WESTACOTT, S., PLANAVSKY, N. J., ZHAO, M. Y. & HULL, P. M. 2021. Revisiting the sedimentary record of the rise of diatoms. *Proc Natl Acad Sci U S A,* 118.

WHITTAKER, K. A., RIGNANESE, D. R., OLSON, R. J. & RYNEARSON, T. A. 2012. Molecular subdivision of the marine diatom *Thalassiosira rotula* in relation to geographic distribution, genome size, and physiology. *BMC Evol Biol,* 12**,** 209.

WILTSHIRE, K. H. 2011. Hydrochemistry at time series station Helgoland Roads, North Sea, in 2010. *In: Wiltshire, Karen Helen; Carstens, Kristine; Ecker, Ursula; Kirstein, Inga V: Hydrochemistry at time series station Helgoland Roads, North Sea since 1873 [dataset publication series]. Alfred Wegener Institute - Biological Institute Helgoland, PANGAEA, https://doi.pangaea.de/10.1594/PANGAEA.960375 (dataset in review).* PANGAEA.

WILTSHIRE, K. H. & MANLY, B. F. J. 2004. The warming trend at Helgoland Roads, North Sea: phytoplankton response. *Helgoland Marine Research,* 58**,** 269-273.

WOHLRAB, S., SELANDER, E. & JOHN, U. 2017. Predator cues reduce intraspecific trait variability in a marine dinoflagellate. *BMC Ecol,* 17**,** 8.

WOLF, K. K. E., HOPPE, C. J. M. & ROST, B. 2017. Resilience by diversity: Large intraspecific differences in climate change responses of an Arctic diatom. *Limnology and Oceanography,* 63**,** 397-411.

YE, N., HAN, W., TOSELAND, A., WANG, Y., FAN, X., XU, D., VAN OOSTERHOUT, C., SEA OF CHANGE, C., GRIGORIEV, I. V., TAGLIABUE, A., ZHANG, J., ZHANG, Y., MA, J., QIU, H., LI, Y., ZHANG, X. & MOCK, T. 2022. The role of zinc in the adaptive evolution of polar phytoplankton. *Nat Ecol Evol,* 6**,** 965-978.

ZHONG, J., GUO, Y., LIANG, Z., HUANG, Q., LU, H., PAN, J., LI, P., JIN, P. & XIA, J. 2021. Adaptation of a marine diatom to ocean acidification and warming reveals constraints and trade-offs. *Sci Total Environ,* 771**,** 145167

3 Publication II

Microbiome and photoperiod interactively determine thermal sensitivity of polar and temperate diatoms

Published in Biology Letters (2023)

BIOLOGY LETTERS

royalsocietypublishing.org/journal/rsbl

Research

Cite this article: Giesler JK, Harder T, Wohlrab S. 2023 Microbiome and photoperiod interactively determine thermal sensitivity of polar and temperate diatoms. *Biol. Lett.* **19**: 20230151.
https://doi.org/10.1098/rsbl.2023.0151

Received: 30 March 2023
Accepted: 26 October 2023

Subject Category:
Marine biology

Subject Areas:
ecology, evolution, molecular biology

Keywords:
phytoplankton, microbiome, holobiont, diatom, light, temperature

Author for correspondence:
Jakob K. Giesler
e-mail: jakob.giesler@awi.de

Electronic supplementary material is available online at https://doi.org/10.6084/m9.figshare.c.6922305.

THE ROYAL SOCIETY PUBLISHING

Microbiome and photoperiod interactively determine thermal sensitivity of polar and temperate diatoms

Jakob K. Giesler[1], Tilmann Harder[1,2] and Sylke Wohlrab[1,3]

[1]Section Ecological Chemistry, Alfred Wegener Institute, Helmholtz Centre for Polar and Marine Research, 27570 Bremerhaven, Germany
[2]Marine Chemistry, Department of Chemistry and Biology, University of Bremen, 28359 Bremen, Germany
[3]Helmholtz Institute for Functional Marine Biodiversity at the University of Oldenburg (HIFMB), 23129 Oldenburg, Germany

JKG, 0000-0001-6674-5249; TH, 0000-0003-3173-6806; SW, 0000-0003-3190-0880

The effect of temperature on ectothermic organisms in the context of climate change has long been considered in isolation (i.e. as a single driver). This is challenged by observations demonstrating that temperature-dependent growth is correlated to further factors. However, little is known how the chronobiological history of an organism reflected in its adaptation to re-occurring cyclic patterns in its environment (e.g. annual range of photoperiods in its habitat) and biotic interactions with its microbiome, contribute to shaping its realized niche. To address this, we conducted a full-factorial microcosm multi-stressor experiment with the marine diatoms *Thalassiosira gravida* (polar) and *Thalassiosira rotula* (temperate) across multiple levels of temperature (4°C; 9°C; 13.5°C) and photoperiod (4 h; 16 h; 24 h), both in the presence or absence of their microbiomes. While temperature-dependent growth of the temperate diatom was constrained by short and long photoperiods, the polar diatom coped with a 24 h photoperiod up to its thermal optimum (9°C). The algal microbiomes particularly supported host growth at the margins of their respective fundamental niches except for the combination of the warmest temperature tested at 24 h photoperiod. Overall, this study demonstrates that temperature tolerances may have evolved interactively and that the mutualistic effect of the microbiome can only be determined once the multifactorial abiotic niche is defined.

1 Introduction

Rising ocean temperatures lead to a global reorganization of species that move to track their thermal habitat. Accordingly, numerous studies of thermal adaptation capacities at different levels of biological organization have been published and used to estimate species vulnerability to global warming. While this research provided valuable insights into potential future range shifts and consequences at different ecological scales [1–3], the multifactorial nature of changing environmental conditions on temperature-driven range shifts has been largely neglected [4,5]. For example, diurnal and annual latitudinal light regimes are one of the most stable environmental signals, and chronobiological adaptations may limit the capacity for thermal range shifts due to photic mismatches, especially in photosynthetic organisms whose light regimes have imprinted a strong signal in the adaptive history and consequently coordinate various cellular functions [4,6].

Similarly, it is rarely considered in the context of temperature-driven range shifts that species do not occur as isolated entities and that their adaptations have evolved in concert with species interactions. On a small scale, a species interacts with its microbiome in complex and dynamic ways. Thus, a species'

microbiome reflects a tight association in which the holobiont may have evolved to respond in a coordinated manner to changing conditions, often increasing the host fitness and resilience [7–9]. However, beneficial associations to cope with environmental conditions beyond the range of the evolved mutualism can be reversed, thereby amplifying negative effects, which can even cascade to higher levels of the respective biological system [10–14].

The goal of this study was to determine if diatom thermal performance is interactively affected by the organism's microbiome and the locally evolved chronobiology (i.e. tolerance to different photoperiods). To address this, we monitored growth of a temperate and a polar strain of the marine diatom *Thalassiosira* spp. in response to a gradual combination of temperatures and photoperiods both in the presence and absence of their native microbiomes.

2 Methods

(a) Cultures and culture conditions

The polar *Thalassiosira gravida* (central Arctic Ocean) was obtained from the Norwegian culture collection of algae (NORCCA strain number UIO 478). The temperate *Thalassiosira rotula* from the German bight, was provided by the Harder Lab (University of Bremen; strain *T. rotula*_S16). Both strains were identified by their ITS1 sequences (electronic supplementary material, figure S1) and an axenic culture was rendered following the protocol of Mönnich *et al.* [15]. Axenicity of a culture was referred to as continuous absence of any contaminants stained with SYBR Green by regular (i.e. every 5–7 days) epifluorescence microscopy at 400× magnification (electronic supplementary material, figure S2). All cultures were maintained in climate chambers at a photoperiod of 16 : 8 h, a light intensity of 50 µmol photons m^{-2} s^{-1} and a temperature of 4°C and 15°C for the polar and temperate strains, respectively. Cultures were grown in filter-sterilized artificial seawater medium (ESAW) containing 1/5 of the vitamin concentration proposed by Harrison *et al.* [16] and kept in exponential growth by semi-continuous dilution.

(b) Temperature–photoperiod growth assay

The growth of axenic and xenic strains of *T. gravida* and *T. rotula* was studied under multifactorial combinations of photoperiod [4 h; 16 h; and 24 h at 50 µmol photons m^{-2} s^{-1}] and temperature [4°C; 9°C and 13.5°C] with the chosen levels based on previously assessed fully resolved thermal reaction norms. Cultures were pre-acclimatized to experimental conditions for a fixed acclimatization period of 7 days by inoculating 40 ml batch cultures with 500 cells ml^{-1} (2000 cells ml^{-1} for treatments with 4 h photoperiod to obtain sufficient biomass) which were grown at each of the nine treatment conditions to allow acclimatization of fluorophores. The actual subsequent multifactorial experiment was conducted in white 96-well plates (Greiner, Germany) with 300 µl experimental units and 48 replicates per treatment. After chlorophyll-a fluorescence of the acclimatized stock cultures was measured with a photo-spectrometric plate reader (ClarioStar Plus BMG Labtech, excitation 440 nm, emission 680 nm) plates were inoculated at twice the initial fluorescence units of the blank value measured in the growth medium. To maintain sterile conditions, the 96-well plates were sealed with a gas-permeable membrane (Breathe-Easy, Sigma-Aldrich, USA). Plates were incubated in climate cabinets at the respective experimental temperature and were placed onto LED tables emitting 50 µmol m^{-2} s^{-1} under the photoperiod settings above. Fluorescence intensity was measured daily at the same time after not more than 5 min of dark acclimation to not disturb photoperiod as an experimental factor. The experiment was terminated after 7 days.

(c) Statistical analysis

After blank values of fluorescence in the growth medium were subtracted from the raw experimental fluorescence data, maximum growth rates (μ_{max}) were calculated for each experimental unit by fitting nonlinear models to the data using the 'growthrates' package [17]. To test for main and interactive effects, a three-way ANOVA (type III SS) was conducted for *T. gravida* and *T. rotula*, respectively, with μ_{max} as dependent, and temperature, photoperiod and the presence/absence of the native microbiome as independent variables. Groups were weighted by the inverse of their variance to account for heteroscedasticity. *Post-hoc* analyses were conducted with Games–Howell tests. The effect sizes of the main effects and the three-way interaction were calculated with the 'variancePartition' package [18] which reports the fraction of explained variance to be attributed to each variable while correcting for all other variables. All statistical analyses and graphs were performed with the R environment 4.2.2 [19].

3. Results

For both, the polar and temperate diatom strain, temperature, photoperiod and the presence/absence of their respective microbiome had significant main effects on maximum growth rate, and showed a statistically significant three-way interaction ($p < 0.001$). The effect sizes of the independent variables differed largely in treatments with temperate and polar diatoms strains (table 1).

For the polar strain, the temperature main effect explained 2.2% of the total variance in the dataset, but adding the factors of photoperiod and microbiome presence increased the explained variance by 45.7% and 18.3%, respectively. Thus, all main effects explained the variance by 66.1%. The analysis revealed an interactive effect of all terms, i.e. the effect of photoperiod and bacteria on temperature-dependent growth was not uniform. Including this interactive effect increased the explained variance by 31.2%, finally explaining 97.3% of the variability in the dataset.

For the temperate strain the temperature main effect accounted for 35.7% of the variance, while the effect size of photoperiod and microbiome presence explained 33.9% and 11.2% of the variance, respectively. Also, for the temperate diatom the maximum growth rate was not only affected by additive main effects, but also by their interactive effect, explaining 16.6% of the variance, adding up the total explained variance to 97.4%.

In terms of the direction of these effects, the xenic polar diatom had its optimum growth conditions at 9°C and a 16 h photoperiod (figure 1*a*). The axenic polar diatom strain did not show this clear optimum and revealed decreased maximum growth rates with increasing temperature and decreasing photoperiod (figure 1*b*). This growth pattern was also reflected in the log response ratios where the difference in maximum growth rates between the xenic and axenic polar strain increased with increasing temperature and decreasing photoperiod (figure 1*c*). Although the xenic polar strain generally had higher maximum growth rates than the axenic strain, this pattern was reversed at 13.5°C in combination with a 24 h photoperiod. Here, the axenic polar strain showed significantly higher maximum growth rates than the xenic strain ($p < 0.001$).

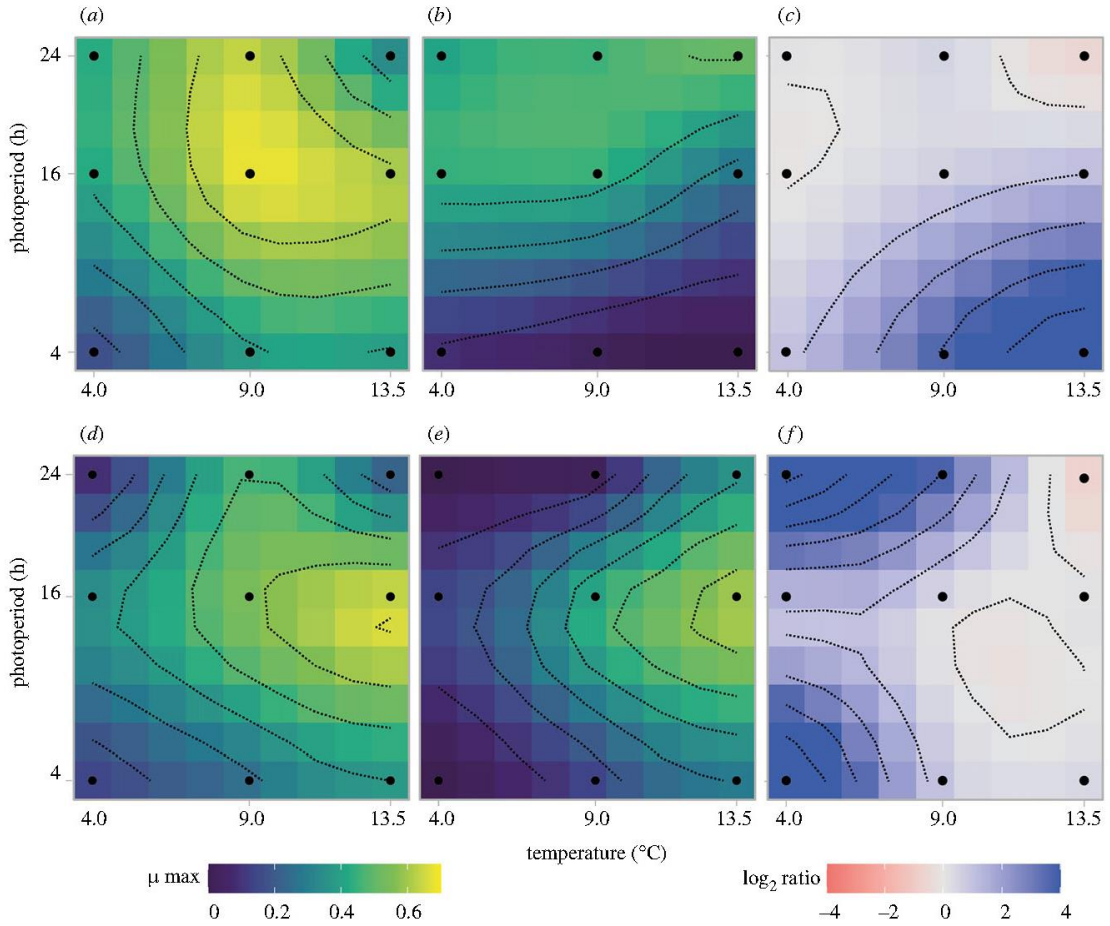

Figure 1. Maximum growth rates for the polar *T. gravida* (upper panel) and the temperate *T. rotula* (lower panel). Interpolated response surface plots of the effects of temperature and photoperiod on (*a*,*d*) maximum growth rates (μ_{max} day^{-1} indicated by colour) of the xenic strain and (*b*,*e*) the axenic strain as well as (*c*,*f*) the $\log_2$-response ratio (LRR indicated by colour) of xenic divided by axenic maximum growth rates displaying positive (blue) and negative (red) microbiome effects. Black lines indicate isolines of the displayed variable (bin width of 0.1 for μ_{max} and bin width of 1.2 for the log-ratio). Black dots represent tested experimental conditions.

Table 1. ANOVA results and effect sizes of temperature, photoperiod and presence/absence of diatom microbiome on maximum growth rates (μ_{max}) of *T. gravida* and *T. rotula*. Degrees of freedom (*d.f.*), *F* and *p*-values are given for each effect. Asterisk (*) indicate significant effects ($p < 0.05$). Effect sizes are given as % fraction of the total variance attributed to each factor.

	T. gravida (polar)				*T. rotula* (temperate)		
		μ_{max}			μ_{max}		
effect	*d.f.*	effect size	*F*	*p*	effect size	*F*	*p*
temp.	2	2.2	442.4	<0.001*	35.7	5444.2	<0.001*
photoperiod	2	45.7	5778.4	<0.001*	33.9	2837.3	<0.001*
bacteria	1	18.3	2381.5	<0.001*	11.9	2080.4	<0.001*
temp. × photoperiod × bacteria	4	31.2	377.2	<0.001*	16.6	448.2	<0.001*

For the temperate diatom, both the xenic and axenic strains exhibited highest growth rates at 13.5°C under a 16 h photoperiod (figure 1*d*,*e*). The xenic temperate diatom showed overall higher maximum growth rates than the axenic strain, especially at 9°C and a 24 h photoperiod (figure 1*f*). Yet, just like for the polar diatom, at 13.5°C and a photoperiod of 24 h, the axenic temperate strain showed significantly higher maximum growth rates than the xenic strain ($p < 0.001$).

4 Discussion

Both the polar and temperate *Thalassiosira* strains showed specific adaptations to their respective chronobiological and climatic geographical history, reflected in their growth response across multiple levels of temperature and photoperiod. This study revealed that the presence of the diatom microbiome enhanced maximum diatom growth rates especially at the margins of their respective niche, except for the warmest temperature under the 24 h photoperiod.

While the temperate axenic and xenic diatom did not reach their thermal optimum in this experimental design, the polar (xenic) diatom displayed its highest growth rates at 9°C, a water temperature rarely reached in the Arctic Ocean [20]. However, it was demonstrated by Thomas *et al.* [21] that especially at high latitudes, planktonic organisms do not live at their thermal optimum but rather at the onset of their temperature reaction norm (unimodal, left-skewed function describing an ectothermic organism's growth/fitness in response to temperature). This may be beneficial to survive heat waves, and is also logical as the fundamental niche is constrained by further drivers shaping the organism's realized niche. For example, high growth rates at elevated temperatures may be associated with unsustainable resource depletion, i.e. the two factors may not scale linearly. In a natural environment, this limits the allocation of energy to crucial pathways that maintain growth in response to multiple abiotic or biotic factors, and maximum growth may therefore not pay off [22,23].

Interactive effects of light and temperature on photosynthesis are comparatively well understood in plants. Here, prolonged photoperiods exacerbate the negative effects of elevated temperatures on photosynthesis by triggering oxidative burst-like reactions that additionally affect temperature-impaired electron transport capacities [24]. Our study showed that the polar strain coped with short and long photoperiods until its temperature optimum was reached. By contrast, the temperate strain was more sensitive to 24 h light exposure as its growth rate was significantly affected prior to the optimum temperature. Biogeographically determined adaptations of the strains, such as photoperiod-dependent physiology and cell division regulated by the molecular circadian clock, may cause the observed growth rate patterns. The more flexible response of the polar compared to the temperate diatom to the photoperiods tested may therefore be linked to their evolved chronobiology. Diverse polar species, e.g. marine zooplankton [4], fruit flies [25] and reindeer [26], were found to have plastic molecular clocks, whereas their temperate representatives remain entrained in their rhythmicity [25,26]. While this flexibility has not been reported for polar diatoms, entrainment in rhythmicity is at least known for the temperate diatom *Phaeodactylum*. Here, rhythmic gene expression of a key circadian clock regulator and associated cellular functions persist under constant light (and dark) conditions [27]. This supports the conclusion that due to the synergistic nature of light and temperature stress, in tandem with the control of light stress by the circadian rhythm, the chronobiological background of the strains tested did affect their sensitivity to temperature. With regard to the microbiome, this is further supported by studies that found diel cycle dependent patterns of highly coordinated gene expression [28] and metabolite production [29] between the host and its microbiome for key resources shared within the phytoplankton holobiont.

Bacteria provide various services to diatoms which impact their growth and survival, such as nutrient recycling [30], biofilm formation [31] or the synthesis of vitamins [32] and growth stimulating compounds [33]. The present study provides evidence that the positive net effects of the microbiome were not equally distributed across multiple temperature and photoperiod levels. Hence, the growth supporting effect of the microbiome come into play at specific environmental conditions that are at least biogeographically determined, if not even genotype-specific [34,35]. For the polar xenic diatom, the growth supporting effect occurred especially at temperatures above its thermal optimum in combination with short photoperiods. For the xenic temperate diatom, the microbiome enhanced its growth towards its thermal minimum, especially in combination with extreme photoperiods, i.e. the 4 h and 24 h photoperiod. Yet, it must be taken into account that the experimental units used in this study are a closed system that do not allow the assembly of a new microbiome, potentially more beneficial at specific environmental settings as demonstrated for plants and their soil microbiomes [36]. However, a prior study investigating the microbiome reassembly of 81 strains of *T. rotula* in a common garden experiment under consideration of environmental stressors, observed a much stronger association of the microbiome to its respective host's genetic population than explained with environmental factors alone [34]. This suggested an association of diatoms and their microbiomes for long time frames, up to decades, which thus may limit the capacity of host cells to recruit new microbiome bacteria.

Since DIC concentrations were not measured, the possibility of carbon limitation must be considered, especially in the axenic cultures in the absence of bacterial respiration. To reduce this possibility, the experimental duration was short and a very dilute inoculum was used. This is evidenced by the low starting fluorescence value, as recommended for nanocosm approaches according to Volpe *et al.* [37].

Since axenicity was verified by epifluorescence microscopy, the putative presence of bacteria on algal cells outside examined fields of view cannot be completely ruled out. However, the effect of these potential minimal contaminations on a diatom culture are considered to be negligible, firstly because bacteria-derived compounds affecting phytoplankton–bacteria interactions are concentration dependent [38,39], and secondly because bacterial densities in xenic cultures would be six orders of magnitude higher than minute bacterial contaminations in pseudo-axenic cultures [40].

In contrast to the observed growth enhancement in the presence of the microbiomes at the described conditions, both axenic diatom strains exhibited higher maximum growth rates than the xenic strains under a combination of 13.5°C and 24 h photoperiod. This indicates a reversal of the overall mutualistic relationship of the diatom microbiome at this environmental condition, which exceeds the pure loss of symbiotic biotic interactions, an observation known from different holobiont systems like plants [7], corals [41] or human holobionts [42], commonly referred to as microbiome dysbiosis [7]. Especially when exposed to several stressors, a stochastic reassembly of the hosts microbiome (Anna Karenina Principle) often encompassing bacterial taxa that reduce the hosts fitness, can occur [7]. For the polar diatom strain, the sensitivity to prolonged photoperiods increased at temperatures beyond its physiological optimum could therefore potentially increase the vulnerability to microbiome dysbiosis

under these conditions. For the temperate diatom strain, this sensitivity to a prolonged photoperiod generally seemed to increase with higher temperatures already prior to the thermal optimum.

Considering the closed system design of this study, potential dysbiosis is limited either to a change in the relative composition of the microbiome (i.e. parasitic species are already present in the system at low abundance), or to a reversal of mutualistic relationships as demonstrated for opportunistic microbiome bacteria that first produce growth stimulating compounds for their host cell and eventually turn parasitic and switch to production of algicides when the fitness of their host is decreasing [43,44]. This underlines the importance to consider mutualistic relationships as context dependent.

The outcome of this study underlines that the thermal sensitivity of diatoms is an integrated response to multifactorial parameters. Specifically, temperature-dependent growth is interactively influenced by the photoperiod in a chronobiological context and biotic interactions, namely co-occurring microbiome bacteria. In addition, we demonstrated the importance of the microbiome in supporting growth of host diatoms, particularly under unfavourable conditions at the margins of their fundamental niches. We suggest that future studies of species adaptability should consider that tolerances are defined and emerge interactively. This is an important aspect for identifying critical thresholds, determining species resilience, and assessing potential adaptive capabilities. In particular, the question of which factor (temperature sensitivity, chronobiology, or biotic interactions) is more evolutionarily constrained is crucial for modelling future habitat shifts of arctic and temperate phytoplankton species. Detailed knowledge of their regulation and evolutionary history is therefore required to assess how future adaptive capacities are possible given the multifactorial nature of changing environmental conditions.

Ethics. This work did not require ethical approval from a human subject or animal welfare committee.

Data accessibility. All data and codes as well as their respective detailed descriptions (metadata) to fully reproduce this study are available from the Dryad Digital Repository: https://doi.org/10.5061/dryad.x95x69pqf [45].

Data available as part of the electronic supplementary material [46].

Declaration of AI use. We have not used AI-assisted technologies in creating this article.

Authors' contributions. J.K.G.: conceptualization, formal analysis, investigation, methodology, visualization, writing—original draft, writing—review and editing; T.H.: conceptualization, funding acquisition, supervision, writing—review and editing; S.W.: conceptualization, formal analysis, writing—original draft, writing—review and editing.

All authors gave final approval for publication and agreed to be held accountable for the work performed therein.

Conflict of interest declaration. We declare we have no competing interests.

Funding. This research was funded by the Helmholtz research programme 'Changing Earth, Sustaining our Future' (subtopic 6.2 'Adaptation of marine life: from genes to ecosystems' in topic 6 'Marine and Polar Life') of the Alfred Wegener Institute Helmholtz Centre for Polar and Marine Research, Germany. Furthermore, we acknowledge the support by the Open Access Publication Funds of Alfred-Wegener-Institut Helmholtz-Zentrum für Polar- und Meeresforschung.

Acknowledgements. The authors thank Jennifer Bergemann for her assistance in the lab, Luka Supraha for providing the Arctic diatoms, and Uwe John for logistic and technical support.

References

1. Benedetti F, Vogt M, Elizondo UH, Righetti D, Zimmermann NE, Gruber N. 2021 Major restructuring of marine plankton assemblages under global warming. *Nat. Commun.* **12**, 5226. (doi:10.1038/s41467-021-25385-x)
2. Lenoir J, Bertrand R, Comte L, Bourgeaud L, Hattab T, Murienne J, Grenouillet G. 2020 Species better track climate warming in the oceans than on land. *Nat. Ecol. Evol.* **4**, 1044–1059. (doi:10.1038/s41559-020-1198-2)
3. Pinsky ML, Selden RL, Kitchel ZJ. 2020 Climate-driven shifts in marine species ranges: scaling from organisms to communities. *Ann. Rev. Mar. Sci.* **12**, 153–179. (doi:10.1146/annurev-marine-010419-010916)
4. Häfker NS, Andreatta G, Manzotti A, Falciatore A, Raible F, Tessmar-Raible K. 2023 Rhythms and clocks in marine organisms. *Ann. Rev. Mar. Sci.* **15**, 509–538. (doi:10.1146/annurev-marine-030422-113038)
5. Litchman E, Thomas MK. 2023 Are we underestimating the ecological and evolutionary effects of warming? Interactions with other environmental drivers may increase species vulnerability to high temperatures. *Oikos* **2023**, e09155. (doi:10.1111/oik.09155)
6. Huffeldt NP. 2020 Photic barriers to poleward range-shifts. *Trends Ecol. Evol.* **35**, 652–655. (doi:10.1016/j.tree.2020.04.011)
7. Arnault G, Mony C, Vandenkoornhuyse P. 2023 Plant microbiota dysbiosis and the Anna Karenina Principle. *Trends Plant Sci.* **28**, 18–30. (doi:10.1016/j.tplants.2022.08.012)
8. Dittami SM, Duboscq-Bidot L, Perennou M, Gobet A, Corre E, Boyen C, Tonon T. 2016 Host–microbe interactions as a driver of acclimation to salinity gradients in brown algal cultures. *ISME J.* **10**, 51–63. (doi:10.1038/ismej.2015.104)
9. Seymour JR, Amin SA, Raina J-B, Stocker R. 2017 Zooming in on the phycosphere: the ecological interface for phytoplankton–bacteria relationships. *Nat. Microbiol.* **2**, 17065. (doi:10.1038/nmicrobiol.2017.65)
10. Akbar S, Gu L, Sun Y, Zhang L, Lyu K, Huang Y, Yang Z. 2022 Understanding host–microbiome–environment interactions: insights from *Daphnia* as a model organism. *Sci. Total Environ.* **808**, 152093. (doi:10.1016/j.scitotenv.2021.152093)
11. Das B, Nair GB. 2019 Homeostasis and dysbiosis of the gut microbiome in health and disease. *J. Biosci.* **44**, 117. (doi:10.1007/s12038-019-9926-y)
12. Jiménez RR, Sommer S. 2017 The amphibian microbiome: natural range of variation, pathogenic dysbiosis, and role in conservation. *Biodiv. Conserv.* **26**, 763–786. (doi:10.1007/s10531-016-1272-x)
13. Sentenac H, Loyau A, Leflaive J, Schmeller DS. 2022 The significance of biofilms to human, animal, plant and ecosystem health. *Funct. Ecol.* **36**, 294–313. (doi:10.1111/1365-2435.13947)
14. Thurber V *et al.* 2020 Deciphering coral disease dynamics: integrating host, microbiome, and the changing environment. *Front. Ecol. Evol.* **8**, 575927. (doi:10.3389/fevo.2020.575927)
15. Monnich J, Tebben J, Bergemann J, Case R, Wohlrab S, Harder T. 2020 Niche-based assembly of bacterial consortia on the diatom *Thalassiosira rotula* is stable and reproducible. *ISME J.* **14**, 1614–1625. (doi:10.1038/s41396-020-0631-5)
16. Harrison PJ, Waters RE, Taylor FJR. 1980 A broad spectrum artificial sea water medium for coastal and open ocean phytoplankton. *J. Phycol.* **16**, 28–35. (doi:10.1111/j.0022-3646.1980.00028.x)
17. Petzoldt T. 2020 growthrates: Estimate Growth Rates from Experimental Data, version 0.8.2. See https://CRAN.R-project.org/package=growthrates.

18. Hoffman GE, Schadt EE. 2016 variancePartition: interpreting drivers of variation in complex gene expression studies. *BMC Bioinf.* **17**, 483. (doi:10.1186/s12859-016-1323-z)
19. R Development Core Team. 2022 *R: a language and environment for statistical computing*. Vienna, Austria: R Foundation for Statistical Computing.
20. Timmermans M-L, Labe ZM. 2022 Sea surface temperature. In *Arctic report card 2022* (eds ML Druckenmiller, RL Thoman, TA Moon). Washington, DC: National Oceanic and Atmospheric Administration (NOAA).
21. Thomas MK, Kremer CT, Klausmeier CA, Litchman E. 2012 A global pattern of thermal adaptation in marine phytoplankton. *Science* **338**, 1085–1088. (doi:10.1126/science.1224836)
22. Edwards KF, Thomas MK, Klausmeier CA, Litchman E. 2016 Phytoplankton growth and the interaction of light and temperature: a synthesis at the species and community level. *Limnol. Oceanogr.* **61**, 1232–1244. (doi:10.1002/lno.10282)
23. Thomas MK, Aranguren-Gassis M, Kremer CT, Gould MR, Anderson K, Klausmeier CA, Litchman E. 2017 Temperature–nutrient interactions exacerbate sensitivity to warming in phytoplankton. *Glob. Change Biol.* **23**, 3269–3280. (doi:10.1111/gcb.13641)
24. Roeber VM, Bajaj I, Rohde M, Schmülling T, Cortleven A. 2021 Light acts as a stressor and influences abiotic and biotic stress responses in plants. *Plant Cell Environ.* **44**, 645–664. (doi:10.1111/pce.13948)
25. Bertolini E, Schubert FK, Zanini D, Sehadova H, Helfrich-Forster C, Menegazzi P. 2019 Life at high latitudes does not require circadian behavioral rhythmicity under constant darkness. *Curr. Biol.* **29**, 3928. (doi:10.1016/j.cub.2019.09.032)
26. van Oort BEH, Tyler NJC, Gerkema MP, Folkow L, Blix AS, Stokkan KA. 2005 Circadian organization in reindeer. *Nature* **438**, 1095–1096. (doi:10.1038/4381095a)
27. Annunziata R *et al.* 2019 bHLH-PAS protein RITMO1 regulates diel biological rhythms in the marine diatom *Phaeodactylum tricornutum*. *Proc. Natl Acad. Sci. USA* **116**, 13 137–13 142. (doi:10.1073/pnas.1819660116)
28. Frischkorn K, Haley S, Dyhrman S. 2018 Coordinated gene expression between *Trichodesmium* and its microbiome over day–night cycles in the North Pacific Subtropical Gyre. *ISME J.* **12**, 997–1007. (doi:10.1038/s41396-017-0041-5)
29. Uchimiya M, Schroer W, Olofsson M, Edison A, Moran MA. 2022 Diel investments in metabolite production and consumption in a model microbial system. *ISME J.* **16**, 1306–1317. (doi:10.1038/s41396-021-01172-w)
30. Azam F, Fenchel T, Field JG, Gray JS, Meyer-Reil LA, Thingstad F. 1983 The ecological role of water-column microbes in the sea. In *Foundations of ecology II* (eds EM Thomas, T Joseph), pp. 384–390. Chicago, IL: University of Chicago Press.
31. Koedooder C, Stock W, Willems A, Mangelinckx S, De Troch M, Vyverman W, Sabbe K. 2019 Diatom–bacteria interactions modulate the composition and productivity of benthic diatom biofilms. *Front. Microbiol.* **10**, 1255. (doi:10.3389/fmicb.2019.01255)
32. Croft MT, Lawrence AD, Raux-Deery E, Warren MJ, Smith AG. 2005 Algae acquire vitamin B12 through a symbiotic relationship with bacteria. *Nature* **438**, 90–93. (doi:10.1038/nature04056)
33. Amin SA *et al.* 2015 Interaction and signalling between a cosmopolitan phytoplankton and associated bacteria. *Nature* **522**, 98–101. (doi:10.1038/nature14488)
34. Ahern OM, Whittaker KA, Williams TC, Hunt DE, Rynearson TA. 2021 Host genotype structures the microbiome of a globally dispersed marine phytoplankton. *Proc. Natl Acad. Sci. USA* **118**, e2105207118. (doi:10.1073/pnas.2105207118)
35. Sison-Mangus M, Jiang S, Tran K, Kudela R. 2013 Host-specific adaptation governs the interaction of the marine diatom, *Pseudo-nitzschia* and their microbiota. *ISME J.* **8**, 63–76. (doi:10.1038/ismej.2013.138)
36. Lau JA, Lennon JT. 2012 Rapid responses of soil microorganisms improve plant fitness in novel environments. *Proc. Natl Acad. Sci. USA* **109**, 14 058–14 062. (doi:10.1073/pnas.1202319109)
37. Volpe C, Vadstein O, Andersen G, Andersen T. 2021 Nanocosm: a well plate photobioreactor for environmental and biotechnological studies. *Lab. Chip* **21**, 2027–2039. (doi:10.1039/d0lc01250e)
38. Sauvage J, Wikfors G, Dixon M, Kapareiko D, Sabbe K, Li X, Joyce A. 2022 Bacterial exudates as growth-promoting agents for the cultivation of commercially relevant marine microalgal strains. *J. World Aquac. Soc.* **53**, 1101–1119. (doi:10.1111/jwas.12910)
39. Cirri E, Pohnert G. 2019 Algae–bacteria interactions that balance the planktonic microbiome. *New Phytol.* **223**, 100–106. (doi:10.1111/nph.15765)
40. Di Caprio F, Posani S, Altimari P, Concas A, Pagnanelli F. 2021 Single cell analysis of microalgae and associated bacteria flora by using flow cytometry. *Biotechnol. Bioprocess Eng.* **26**, 898–909. (doi:10.1007/s12257-021-0054-9)
41. MacKnight NJ *et al.* 2021 Microbial dysbiosis reflects disease resistance in diverse coral species. *Commun. Biol.* **4**, 679. (doi:10.1038/s42003-021-02163-5)
42. Belizário JE, Faintuch J. 2018 Microbiome and gut dysbiosis. In *Metabolic interaction in infection* (eds R Silvestre, E Torrado), pp. 459–476. Cham, Switzerland: Springer International Publishing.
43. Seyedsayamdost MR, Case RJ, Kolter R, Clardy J. 2011 The Jekyll-and-Hyde chemistry of *Phaeobacter gallaeciensis*. *Nat. Chem.* **3**, 331–335. (doi:10.1038/nchem.1002)
44. Wang RR, Gallant E, Wilson MZ, Wu YH, Li AR, Gitai Z, Seyedsayamdost MR. 2022 Algal p-coumaric acid induces oxidative stress and siderophore biosynthesis in the bacterial symbiont *Phaeobacter inhibens*. *Cell Chem. Biol.* **29**, 670. (doi:10.1016/j.chembiol.2021.08.002)
45. Giesler JK, Harder T, Wohlrab S. 2023 Data from: Microbiome and photoperiod interactively determine thermal sensitivity of polar and temperate diatoms. Dryad Digital Repository. (doi:10.5061/dryad.x95x69pqf)
46. Giesler JK, Harder T, Wohlrab S. 2023 Microbiome and photoperiod interactively determine thermal sensitivity of polar and temperate diatoms. Figshare. (doi:10.6084/m9.figshare.c.6922305)

4 Publication III

Co-expression of Arctic diatoms and their bacterial microbiomes under thermal and photoperiodic stress

To be submitted

Co-expression of Arctic diatoms and their bacterial microbiomes under thermal and photoperiodic stress

Jakob K. Giesler[1], Frederik Bussmann[1], Tilmann Harder[1,2], A. Murat Eren[3], and SylkeWohlrab[1, 3]

[1)] Ecological Chemistry Section, Alfred Wegener Institute, Helmholtz Centre for Polar and Marine Research, Bremerhaven, Germany

[2)] Department of Biology and Chemistry, University of Bremen, Bremen, Germany

[3)] Helmholtz Institute for Functional Marine Biodiversity at the University of Oldenburg (HIFMB), Oldenburg, Germany

Abstract

Phytoplankton-bacteria interactions govern marine primary productivity and can play a crucial role in host adaptation to challenging environments like the Arctic. Although the Arctic habitat is characterized by an extreme light regime and currently experiences an increased rate of ocean warming, little is known about how this will affect the phytoplankton holobiont. To understand how phytoplankton-bacteria interactions change with thermal stress in the context of extreme polar photoperiods, we conducted a factorial laboratory experiment investigating host growth, microbiome community composition, and co-expression of the Arctic diatom *Thalassiosira gravida* and its associated bacteria at 9°C (close to optimum temperature) and 13.5°C (thermal stress) in combination with 16h (intermediate) and 24h (extreme) photoperiods. The results showed an overall positive net effect of the microbiome on host growth. At 9°C, no effects of photoperiod on host transcriptomics, microbiome composition, and microbiome metatranscriptomics were observed, while pronounced photoperiod-depending differences were found under thermal stress. Particularly, the 13.5°C/16:8 treatment differed from all other treatments, coinciding with the loss of the important Sulfitobacter clade as a key microbiome member for microbiome stability. A combined diatom-bacteria cluster analysis revealed co-expression patterns that were driven by main- and interactive effects of temperature and photoperiod. Among others, the diatom-bacteria co-expression patterns included genes associated with biofilm formation, quorum sensing, cobalamin biosynthesis, and microbiome antioxidant production synchronized with oxidative stress gene expression in the diatom host. Despite the microbiome-mediated general resilience in terms of diatom growth rates, increased

compositional shifts and variability, as well as potential bacterial cell detachment, highlight the risk for microbiome dysbiosis under thermal stress.

Keywords

phytoplankton, microbiome, co-expression, dysbiosis, symbiosis, Sulfitobacter

Introduction

Eukaryotic organisms have evolved in concert with associated prokaryotes that form their microbiome (Cirri and Pohnert, 2019, Henry et al., 2021) and together can be considered a discrete ecological unit called holobiont (Margulis and Fester, 1991). The tightly connected interactions between the host and its microbiome span all symbiotic relationships from mutualism to parasitism and can determine host (and microbial) growth and survival (Drew et al., 2021). While significant progress has been made in the understanding of several well-studied plant and mammal host-microbiome model systems (Uehara et al., 2024, Guo et al., 2022, Kudjordjie Enoch et al., 2022), interactions between bacteria and unicellular eukaryotic phytoplankton are critically understudied considering their relevance for the marine food web (Armengol et al., 2019, Rodríguez-Gálvez et al., 2023) and global carbon fixation (Litchman et al., 2015).

Therein, diatoms are particularly important given their contribution of 20% to annual global primary production – twice the fraction of the Amazon rain forest (Field et al., 1998). The manifold inter-kingdom relationships within the diatom holobiont are not only reflected in host species-specific and genotype-specific microbiome compositions (Ahern et al., 2021, Baker and Kemp, 2014) and reproducible assembly (Ahern et al., 2021, Monnich et al., 2020), but also in the ability of diatoms to structure their microbiome community actively (Shibl et al., 2020). The underlying host-microbiome interactions are explained by specific enzymatic capabilities as well as reciprocal needs of bacteria and phytoplankton for essential trace elements, micro-, and macronutrients (Cirri and Pohnert, 2019). The interaction space is the phycosphere, a microscale mucus region rich in organic matter surrounding the phytoplankton cell analogous to the rhizosphere in plants (Seymour et al., 2017). The unique DOM exudated by the diatom attracts chemotactic bacteria that colonize the host diatom in a continuum from tight to loose

attachment strengths (Falciatore and Möck, 2022). By providing co-factors including vitamins (e.g., cobalamin), ammonium, auxin, and potentially iron (Amin et al., 2012) and by detoxifying the phycosphere from reactive oxygen species (Hünken et al., 2008) the microbiome has often been identified to stimulate host growth (Monnich et al., 2020, Biondi et al., 2018, Mukherjee, 2021, Scholz, 2014).

Previous findings also show that this overall mutualistic relationship is context dependent due to possible switches from mutualistic to opportunistic and parasitic behavior of specific bacteria which can negatively affect host fitness (Wang et al., 2022, Seyedsayamdost et al., 2011). Yet, the underlying mechanisms and their dependence on interacting abiotic drivers are largely unknown. This is of particular concern for highly productive ocean provinces like the Arctic which is experiencing an increased rate of warming compared to the global average (Rantanen et al., 2022). Depending on the degree of holobiont resilience, thermal stress in combination with the extreme Arctic light regime could bring mutually beneficial diatom-bacteria interactions out of balance (Giesler et al., 2023a) with severe implications for gross primary productivity (Abada et al., 2023).

This knowledge gap can partly be explained by the lack of studies investigating transcriptomic responses of both the host and its microbiome. However, to detect and understand specific host-microbiome interactions, standard differential gene expression analysis alone is not sufficient, as the interacting partners are studied separately. Additionally, known diatom-bacteria interactions mostly rely on only a single environmental condition they were identified in. Yet, previous host-microbiome studies from related fields showed that microbiome composition and functioning are co-driven by abiotic conditions (Agler et al., 2016, Uehara et al., 2024).

To obtain a better understanding of which cellular processes the diatom-associated microbiome is involved in and how those processes are affected by global warming in the context of the extreme Arctic light regime, we conducted a multi-stressor laboratory experiment. Therein, we assessed the growth rates and transcriptomes of axenic and xenic cultures of the Arctic diatom *Thalassiosira gravida* as well as the microbiome metatranscriptome across a two-factorial experimental design of temperature and photoperiod. Chosen temperature levels comprise 9°C (closely below the optimum temperature of this *T. gravida* strain) and 13.5°C (beyond thermal optimum). Photoperiodic levels were chosen as 16:8h (intermediate) and 24:0h (extreme). After the identification of microbiome-driven host organismal processes based on transcriptomic differences of xenic and axenic diatom cultures, the respective genes of interest underwent cluster analysis and were correlated with microbiome gene clusters. To detect and correlate

changes in host performance and host-microbiome co-expression with potential changes in microbiome composition we further conducted 16S rRNA amplicon sequencing of the diatom-associated bacterial community.

Methods

Culture conditions

A polar strain of *Thalassiosira gravida* was obtained from the Norwegian culture collection of algae (NORCCA, strain ID UIO 478) and cultured at 4°C with 50 µmol photons m^{-2} s^{-1} at a photoperiod of 16:8h. The culture was grown in sterile ESAW medium with only 1/5 of the original vitamin concentration proposed by Harrison et al. (2008) and kept in exponential growth phase by semi continuous dilution with ESAW medium.

Axenization

An axenic culture was established by employing an antibiotic treatment according to the protocol described in Monnich et al. (2020). Axenicity was verified by weekly epifluorescence microscopy after SYBR Green staining as well as 16S rRNA gene sequencing (see below). The axenization treatment was conducted at least 5 months before the start of the experiment to avoid any effects of the antibiotics on the growth of the axenic culture.

Experimental design

The chosen relevant levels of temperature and photoperiod are based on a previous study which determined the relevant experimental levels for temperature and photoperiod by means of thermal and photoperiod reaction norm experiments (Giesler et al. in prep.). Moreover, a microcosm multi-stressor experiment was conducted to determine relevant interactions of thermal sensitivity with photoperiod (Giesler et al., 2023a). Based on the outcome of these preliminary experiments, the final levels for temperature and photoperiod were set to 9°C and 13.5°C for temperature and 16:8h and 24:0h (light:dark) for photoperiod, respectively.

Experimental conduction

To acclimate the cultures to the experimental conditions, 500 ml stock cultures of xenic and axenic *T. gravida* were inoculated at 5000 cells ml^{-1} in combusted 500 ml Erlenmeyer flasks (sealed with combusted aluminum caps) and grown at 9°C or 13.5°C, respectively, in combination with different photoperiods (24:0h and 16:8h) at a light intensity of 55 µmol photons m^{-2} s^{-1}. During the acclimation phase, the stock cultures were semi-continuously diluted with sterile modified ESAW medium (see above). After seven days of acclimation, 200 ml experimental units were inoculated from the stock cultures at an initial cell density of 1500 cells ml^{-1} in combusted and sealed 250 ml Erlenmeyer flasks at a replication of n=5. Twice per day, the Erlenmeyer flasks were carefully homogenized and randomized. For each treatment, replicate 5 was sampled daily in terms of three 0.5 ml subsamples for microscopical cell density quantification to determine the harvest time point for the respective treatment. The other treatments were kept sealed to avoid contamination of the axenic treatments. Treatments were harvested at ~15000 cells ml^{-1} or the latest after 7 days. However, the treatments were always harvested at the same day time to avoid between-group differences that are based on daily cellular cycles.

2.5 *Diatom growth rates*

Cell densities of diatom culture were determined microscopically using an inverted light microscope (Zeiss Axiovert 10C) following the procedure described in detail in Giesler et al. (2023b). Specific growth rates (µ day^{-1}) were determined using the formula

$$\mu = \frac{ln(X_{end}) - ln(X_{start})}{\Delta t}$$

where X_{end} represents the cell density (cells ml^{-1}) at the end of the experiment, X_{start} refers to the start/inoculation cell density (cells ml^{-1}), and Δt refers to the experimental duration in days.

DNA sampling and processing

For DNA sampling of the diatom-associated bacteria and verification of axenic cultures (i.e., 10µm fraction), 20 ml culture of each replicate were filtered onto a 10 µm nylon filter. The flow-through was filtered onto another 0.2µm PC filter to analyze the free-living bacterial community. Filters were stored in extraction buffer and immediately frozen at -20°C until

further processing. DNA extraction was conducted following the manufactures protocol (NucleoSpin Soil extraction kit, Macherey-Nagel GmbH, Düren, Germany). After dilution of the DNA product to 5ng μl^{-1}, replicate samples from the free-living bacterial fraction and axenic 10µm fraction sample replicates were pooled, respectively. Subsequently, amplicon sequencing of the variable V4 region of the 16S rRNA gene was conducted according to the standard Illumina protocol (16S Metagenomic Sequencing Library Preparation # 15044223 B, Illumina, San Diego, CA, United States) using the primers MS_v4_515F_N: 5'-TCGTCGGCAGCGTCAGATGTGTATAAGAGACAG + GTGCCAGCMGCCGCGGTAA-3' (forward primers), and: MS_v4_806R_1: 5'-GTCGTCGGCAGCGTCAGATGTGTATAAGAGACAG + GGACTACHVGGGTWTCTAAT-3' (reverse primers) (Parada et al., 2016). 16S libraries were sequenced on a Next NextSeq 2000 instrument (Illumina, San Diego, CA, United States) using the P1 Reagents kit with 2 x 300 cycles (paired end).

Microbiome community analysis

After the Illumina basecall files were demultiplexed and converted into FASTQ files using the Illumina bcl2fastq conversion tool v.2.20, adapter sequences were removed using cutadapt v.4.4 (Martin, 2011). Further processing was conducted using DADA2 v.1.18 (Callahan et al., 2016). The derived amplicon sequence variants (ASVs) were taxonomically annotated using the SILVA reference database nr.99 v138.1 (Quast et al., 2013). After blank correction, samples with a sequencing depth < 20000 were removed and samples were scaled to the lowest sequencing depth by ranked subsampling (Beule and Karlovsky, 2020). Non-bacterial ASVs, and ASVs with a count of fewer than ten reads in replicate sample means were excluded from analysis. Data were processed in the R statistical environment (R Development Core Team, 2023) and visualized using the phyloseq package (McMurdie and Holmes, 2013). For statistical analysis, the centered log-ratio transformed data were used for principal component analysis (PCA) using the microViz package (Barnett et al., 2021).

RNA sampling and sample processing

For RNA sampling, 20 ml of each replicate were filtered onto a 10 µm nylon filter which was immediately stored in 1ml Trizol (Sigma-Aldrich, St. Louis, USA), carefully inverted, and frozen at -80°C until further analysis. RNA was extracted using the "RNA Clean & Concentrator -5" extraction kit (Zymo Research, United States) following the manufactures protocol. For diatom (i.e., host) transcriptomics, a poly-A selected library was constructed using the "Illumina Stranded mRNA Prep Ligation" kit (Illumina, San Diego, United States). For microbiome meta-transcriptomics (i.e., diatom-attached bacteria retained on the same 10 µm filter) a fraction of the RNA extraction product was processed individually using the "Illumina Stranded Total RNA Prep Ligation with Ribo-Zero Plus" kit (Illumina, San Diego, United States) to reduce the proportion of rRNA. The produced paired-end cDNA libraries underwent sequencing on a NextSeq 2000 instrument (Illumina, San Diego, CA, United States) using the P3 Reagents kit with a cycle configuration of 2 x 150 cycles.

RNA-seq raw data processing

The Illumina basecall files were demultiplexed and converted into FASTQ files using the Illumina bcl2fastq conversion tool (version 2.20). Raw FASTQ files were quality checked using FastQC v.0.12.1 (Andrews, 2010) and underwent quality processing in terms of the removal of rRNA sequences using sortmeRNA v.4.3.6 (Kopylova et al., 2012), as well as adapter trimming, PhiX removal and final quality filtering using BBmap v.39.01 (Bushnell, 2014). Subsequently, a de-novo assembly was conducted to create a reference transcriptome using SPAdes v.3.15.5 (Bankevich et al., 2012). Open reading frames were predicted using TransDecoder v.5.7.0 (Haas, 2013) and prokka v.1.14 (REF) for the diatom transcriptome and bacterial meta-transcriptome, respectively. (Meta-) transcriptomes were annotated using eggNOG-mapper v.2 (Cantalapiedra et al., 2021). Paired-end reads were mapped back to the reference transcriptome using Bowtie2 v.2.5.1 (Langmead and Salzberg, 2012). Expression count tables were created using SubRead v.2.0.6 (Liao et al., 2014).

Diatom transcriptome analysis

Significantly different expressed (up- and down regulated, $p < 0.05$) host genes as response to bacterial presence were determined with DESeq2 (Love et al., 2014) and grouped into clusters of orthologous groups (COG) categories and sub-categories (Tatusov et al., 2000) based on their eggNOG annotations. Subsequently, a functional enrichment/ depletion analysis was conducted by comparing the relative proportion of COG subcategories within significantly up- and downregulated genes to their respective proportions in the reference transcriptome (containing all assembled contigs). Significant enrichments/depletions of COG sub-categories were determined by means of a hypergeometric test. All differentially expressed genes belonging to a significantly enriched or depleted COG sub-category were considered of particular interest and used for further downstream analysis in terms of host-microbiome co-expression.

Host-microbiome co-expression analysis

To analyze host-microbiome co-expression, a K-means cluster analysis was performed which identified clusters of the previously determined differentially expressed and functionally enriched/depleted host genes and how these clusters correlate with bacterial gene clusters (also determined by K-means cluster analysis) in terms of their expression profiles across experimental treatments. Briefly, the bacterial metatranscriptome was cleaned from non-bacterial genes by removing eukaryotic, viral and archaeal genes using the taxonomic annotation obtained from eggNOG-mapper v.2 (Cantalapiedra et al., 2021). Genes without taxonomic annotation were kept only when they were found on the same contig as other genes with a bacterial annotation. Differentially expressed bacterial genes were determined using DESeq2 (Love et al., 2014) by factorial testing across all experimental treatments (Anova-like approach). Further, the cleaned and subset host and microbiome gene count tables underwent variance stabilizing transformation (VST) and were scaled to z-scored expression values. After the transformation, the expression profile of each bacterial and host gene had a mean of 0 and a standard deviation of 1. For both, host and microbiome scaled gene expression data, distance matrices were calculated. To determine an appropriate number of clusters (K) for host and microbiome genes, the elbow of the intra-cluster sum-of-squares curve of K-means was estimated (for host and microbiome data separately) which suggested an appropriate K of 11 host gene clusters and 16 microbiome gene clusters. Bacterial gene clusters underwent functional enrichment/depletion analysis as described for the host transcriptome (see above).

Correlation coefficients between host and microbiome clusters were calculated. Significant correlations ($p<0.05$) with a correlation coefficient of ≥ 0.8 or ≤ -0.8 were determined which indicate a strong relationship, i.e., co-expression. This threshold has been demonstrated to be suitable to reliably identify host-microbiome interactions in other studies (Uehara et al., 2024, Yu et al., 2023). Connected correlating gene clusters are referred to as interaction modules.

Results

Bacterial community composition

After strict quality control, the analysis of the bacterial community composition revealed 107 bacterial ASVs across 29 genera (Fig. 4.1). Comparing the diatom-attached and free-living bacterial community compositions, a clear separation of the two filter size fractions can be observed in the PCA (Fig. 4.2a). This is also reflected in the large relative proportions of the genera *Colwellia* and *Methylophaga* in the free-living bacterial community as well as it's lower mean evenness (0.85 ± 0.03) compared to the diatom-attached bacteria (0.73 ± 0.08). Regarding the temperature and photoperiod treatment effects, at 9°C, the photoperiod level did not affect bacterial community composition for both bacterial filter size fractions. In contrast, in the 13.5°C treatments, the respective photoperiod treatment affected the community composition more strongly. This pattern applies for both, free-living- and diatom-associated bacterial communities.

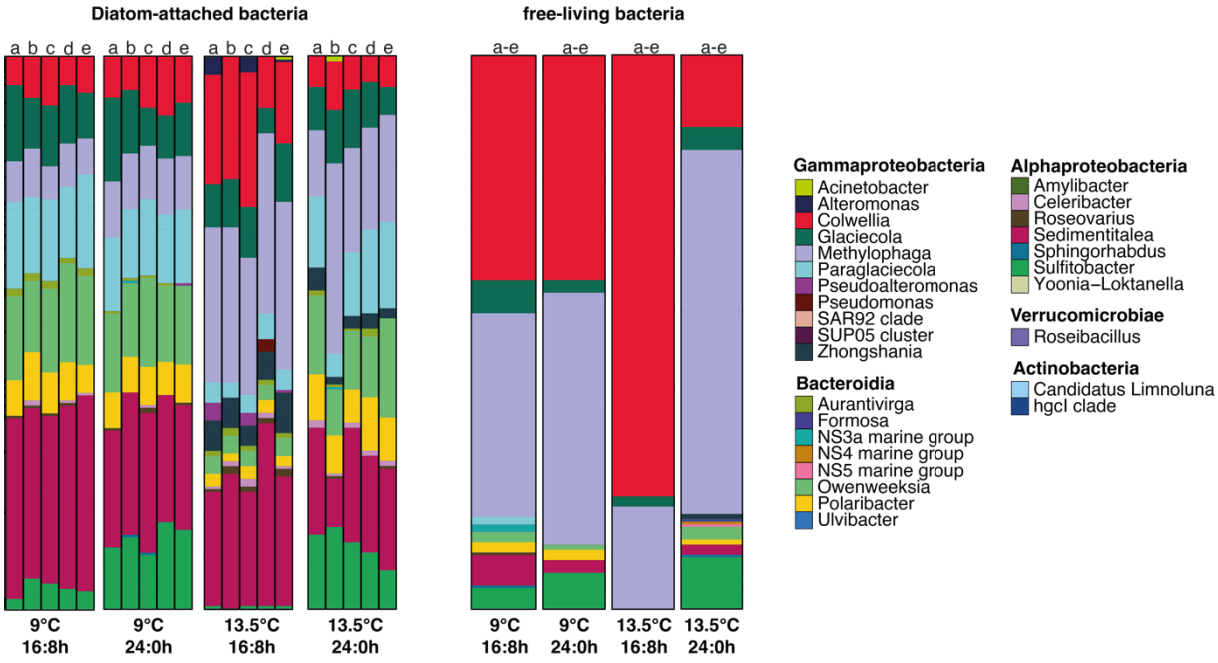

Fig. 4.1: Relative abundance of diatom-attached microbiome bacteria on the genus level (ordered by class) for all replicates (left) and free-living bacteria (right) across all treatment combinations of temperature and photoperiod on the genus level after strict quality filtering.

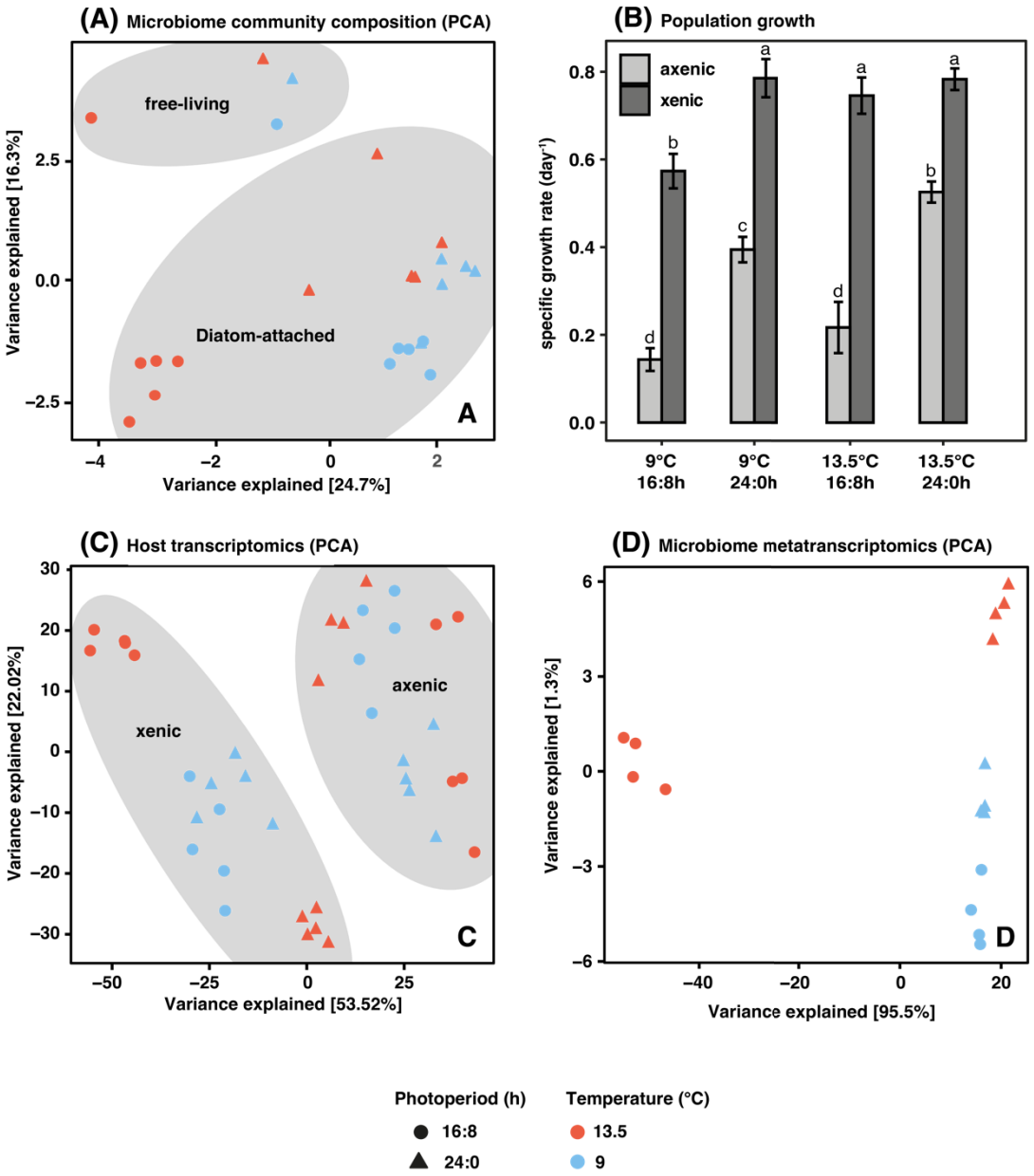

Fig. 4.2: PCA of bacterial community composition. Photoperiod treatments are represented by shape, temperature treatments are represented by color. Ellipses mark the two filter size fractions, i.e., free-living bacteria and diatom-attached bacteria (A). Mean specific growth rates ± SD for xenic (dark grey) and axenic (light grey) *T. gravida* cultures across the two levels of temperature and photoperiod with compact letter display (CLD) showing statistically homogeneous subsets as labels on top of the respective bars (B). PCA of the 500 most variable expressed genes of the diatom host transcriptome (C) and the microbiome metatranscriptome (D). Photoperiod treatments are represented by shape, temperature treatments are represented by color. In the diatom transcriptome (C), ellipses mark xenic and axenic diatom cultures.

Diatom growth rates

The diatom growth rates were significantly higher in all xenic cultures (Fig. 4.2b, Table S4.1). Moreover, a significant main effect of photoperiod and temperature was found as well as a three-way interactive effect of bacterial presence, temperature and photoperiod (i.e., the effect of bacterial presence depends on the temperature and photoperiodic level). The highest observed growth rate was 0.79 ± 0.04 for the xenic cultures at 9°C and a 24h photoperiod while the lowest growth rate of 0.14 ± 0.03 was found for the axenic cultures at 9°C and a photoperiod of 16h.

Transcriptomics

Comparing differentially expressed host genes in response to bacterial presence, 826 significantly upregulated and 733 significantly downregulated genes were identified in consensus across all xenic versus all axenic cultures (Fig. S4.2). These differences in host transcriptomics were also reflected in its respective PCA (Fig. 4.2c), which showed a clear separation of the 500 most variable expressed genes between axenic and xenic diatoms. Moreover, particularly for the xenic diatom cultures, the PCA showed a clustering of the transcriptomes sampled from 9°C irrespective of photoperiodic level. However, at 13.5°C the different photoperiodic levels resulted in strong treatment-specific divergence. Similarly, the microbiome metatranscriptome PCA also revealed strong divergence of the 13.5°C/16:8h treatment (Fig. 4.2d). Narrowing down the differences between xenic and axenic diatom transcriptomes to particular genes of interest, the functional enrichment analysis identified 11 COG sub-categories that were significantly enriched or depleted compared to the reference transcriptome (Fig. 4.3) comprising a total of 189 genes (Table S4.2).

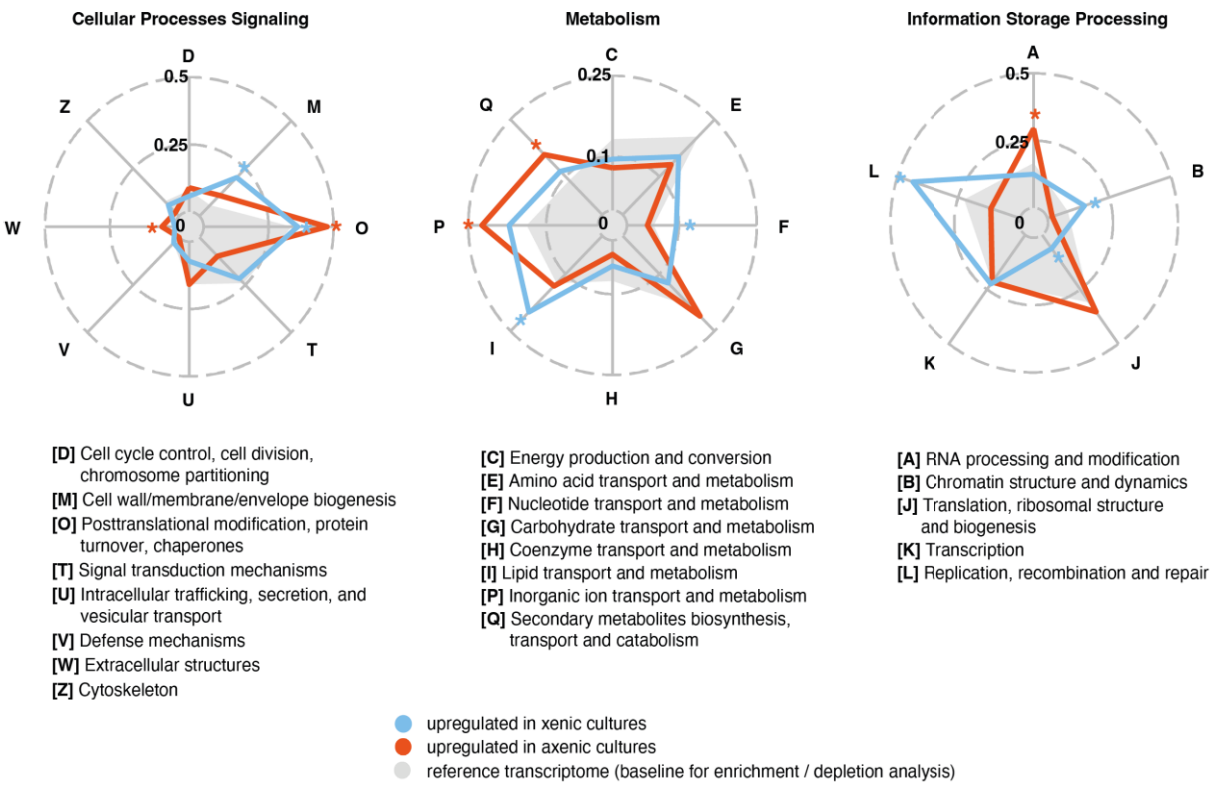

Fig. 4.3: Functional enrichment/depletion analysis of gene clusters of orthologous group (COG) sub-categories for significantly upregulated genes in xenic diatom cultures (blue) and axenic diatom cultures (red) compared to the reference transcriptome (grey polygon). The data includes only genes that were significantly different expressed in response to bacterial presence across all treatments of temperature and photoperiod. Significant enrichment or depletion of COG categories are marked with an asterisk (*) following the same color code.

Co-expression analysis

K-means clustering was conducted with the previously identified 189 differentially expressed and functionally enriched/depleted host genes of interest and 5335 differentially expressed bacterial genes (K=11 for host genes, K=16 for microbiome genes). Considering only the significant (interkingdom) correlations among clusters passing the correlation coefficient thresholds of ≥ 0.8 and ≤ -0.8, four intra-connected host-microbiome modules were identified (module 1-4) (Fig. 4.5). Module size ranged from two gene clusters in module 1 (one host cluster, one microbiome cluster) to six clusters in module 2 (two host clusters, four microbiome clusters). In total, 2431 of the 5335 differentially expressed bacterial genes (i.e., 45.5%) were significantly co-expressed with 159 of 189 (i.e., 84.1%) host genes of interest.

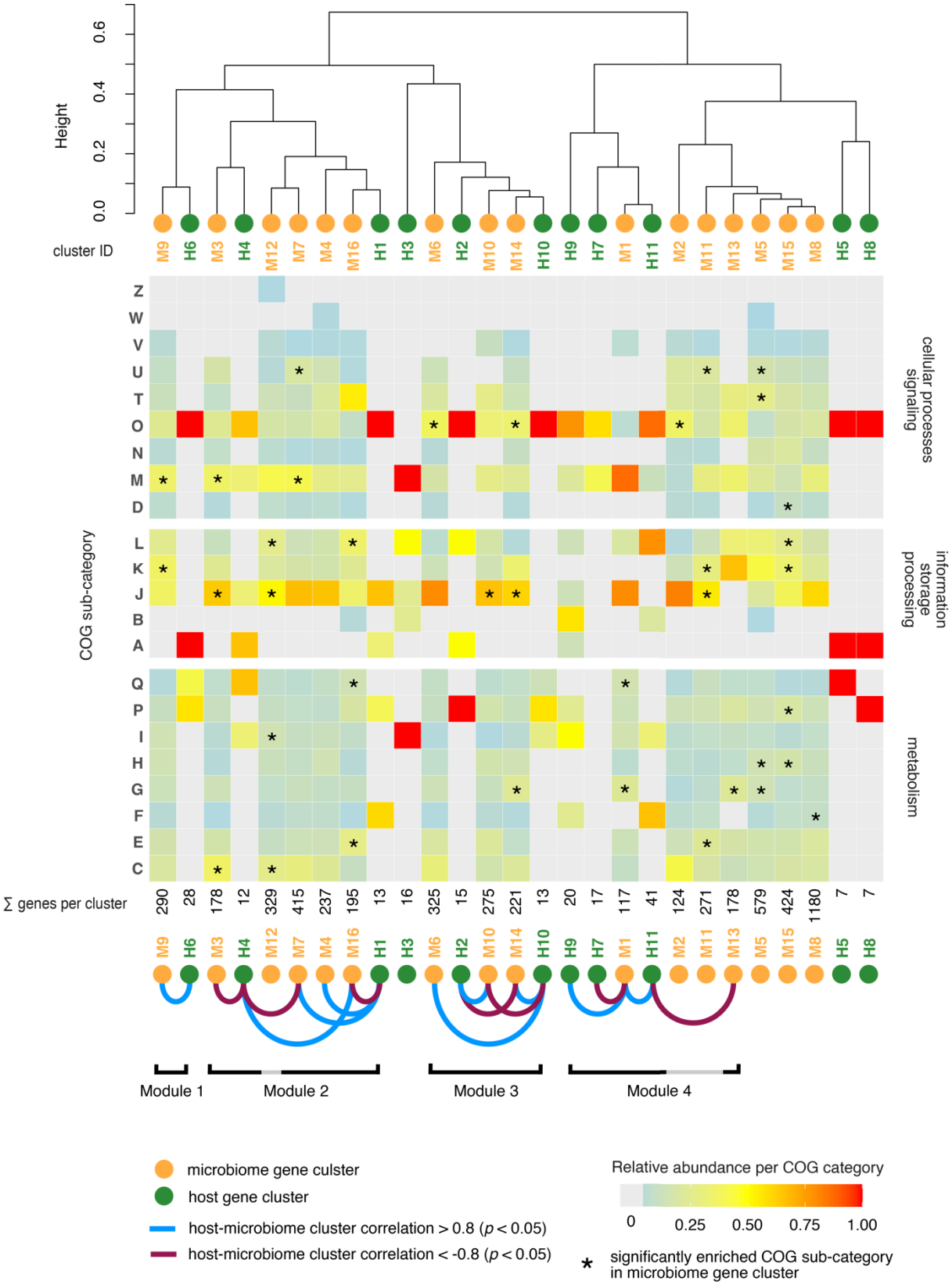

Fig. 4.4: Dendrogram of absolute correlation coefficients of host- and microbiome gene clusters (determined by k-means clustering of scaled gene expression values) (top). Host gene clusters are marked with green dots, microbiome gene clusters with orange dots at the tips, respectively. Cluster IDs are given for each host- and microbiome gene cluster following the same color code. The heatmap shows the relative abundance of COG subcategories (illustrated by continuous color gradient) per COG category (horizontal facets) for each cluster. A

detailed description for each COG subcategory can be found in Fig. 4.3. Significantly enriched/depleted COG subcategories within microbiome gene clusters are marked with an asterisk (*). The total number of genes per cluster is given at the bottom of the heatmap. Significant correlations ($p < 0.05$) between host and microbiome gene clusters exceeding the chosen threshold are connected by blue (correlation ≥0.8) or red (correlation ≤-0.8) threats at the bottom of the heatmap. Interconnected clusters which form a host-microbiome co-expression module are marked with parentheses below and are numbered, respectively.

Co-expression module 1 consisted of host gene cluster H6 and microbiome gene cluster M9. The scaled expression pattern of both clusters followed a strong positive correlation with high scaled expression at 9°C/16:8h photoperiod and coordinated decreased expression towards the higher temperature and longer photoperiod treatments (Fig. 4.5). The host gene cluster H6 contained (among others) ABC-transportersm (ABC_tran), cation transporters (Cation_ATPase_C), alginic acid biosynthesis, chitin recognition (Chitin_bind_1), trypsin, peptidase (Peptidase_S8, M11), RNA recognition motifs, and Dnaj (heatshock proteins) (Table S4.2). The correlating microbiome cluster M9 was taxonomically dominated by the bacterial classes of *Bacteroidia* followed by *Gammaproteobacteria*. Whithin its enriched COG-subcategories (Fig. 4.5), the microbiome cluster particularly contained genes related to carbohydrate metabolism in terms of diverse glycosyltransferases (Glyco_transf), sugar metabolism (GDP, UDPG), transcriptional regulation/signalling (Sigma70, Response_reg, LysR, LytTR, AraC), membrane transporters (OEP, Porin_2), cell adhesion (fasciclin, cadherin_3) and protein modification/degradation (peptidase, epimerase).

Co-expression module 2 consisted of two host gene clusters (H1 and H4) and four microbiome gene clusters (M3, M4, M7, M16) comprising both, positive and negative correlations (Fig. 4.5). Taxonomically, microbiome clusters M3 and M16 were dominated by *Alpha-* and *Gammaproteobacteria*, while cluster M4 and M7 were dominated by *Bacteroidia*. In terms of co-expression patterns, clusters showed relatively stable expresseion at 9°C but diverged in scaled expression at the 13.5°C treatments. Particularly at the 13.5°/24:0h treatment, clusters H1, M3, M4, and M7 decreased strongly while clusters H4 and M16 strongly increased (Fig. 4.5). Host cluster H4 (among others) contained ABC transporters (ABC2), mechanosensitive ion channels, trypsin, and helicase (DEAD). The positive correlated microbiome gene cluster M16 contained diverse methyltransferases, amino oxidase and cysteine synthase/excretion related proteins (PALP, CAP) within its enriched COG-subcategoires. The conversely negative correlated host gene cluster H1 contained mainly methyltransferase (Methyltransf_21), peptidase, adenylate kinase (ADK), and fucoxanthin. Its corresponding synchronously expresssed microbiome cluster M3 contained (among others)

ATP-synthase (ATP_synth), cytochrome, cytochrome oxidase (COX), iron-sulfur containing proteins (Fe-S_biosyn, Fer4, Fer11), outer membrane proteins (Omp), and glycosyltransferase within its significantly enriched COG-subcategories. Microbiome cluster M4 did not show any significant enrichments in COG-subcategories but importantly contained peroxidase, superoxide dismutase, and multiple signaling proteins belonging to two-component systems such as response regulators (Response_Reg, HATPase_c), TonB-dependent receptors (TonB_dep_Rec), and Sigma70. Microbiome cluster M7 which followed the same decreased expression profile as M3, M4, and H1 towards the 13.5°C/24:0h treatment, was containing particularly outer membrane proteins (Omp), cell wall formation proteins (Mur_Ligase), Porin_4, and diverse glycosyltransferase within its respective enriched COG-subcategories.

Within co-expression module 3, all five gene clusters showed oscillating scaled expression patterns with photoperiodic treatment irrespective of applied temperature treatment. Precisely, host cluster H2 and microbiome cluster M10 correlated positively with photoperiodic increase, while conversely, host cluster H10 and microbiome clusters M6 and M14 showed negative correlation with increasing photoperiod (Fig. 4.5). Host cluster H2 contained predominantly helicase, AAA domain, thioredoxin, and a programmed cell death protein (PDCD2_C). The synchrously expressed microbiome cluster M10 which contained genes from many different bacterial clades contained mostly ribosomal RNA in its enriched COG_subcategory. However, beyond that, the cluster (among others) also contained thiamine synthesis (ThiS), cobalamine synthesis (CobN-Mg_chel), glutaredoxin, and cytochrome-b. The counteracting host cluster H10 contained mostly chlorophyll-a/b (Chloroa_b-bind), trypsin, membrane-bound acyltransferase (MBOAT) and peptide-methionine (R)-S-oxide reductase. Its corresponding synchronously expressed microbiome gene clusters M6 and M14 which were dominated by *Alphaproteobacteria*, *Gammaproteobacteria*, and *Bacteroidia* contained (among others) antioxidant enzymes (Redoxin, diverse thioredoxins, Alkyl hydroperoxide reductase (AhpC-TSA), glutaredoxin) as well as lactamase and cytochrome-c.

Co-expression module 4 consisted of host clusters H7, H9, and H11 as well as microbiome clusters M1 and M13. The scaled expression profiles showed an interactive effect of temperature and photoperiod, i.e. the effect of increasing photoperiod depended on temperature. This was reflected in the effect of increasing photoperiod leading to increased expression at 9°C but decreased expression at 13.5°C for gene clusters H9, H11, and M1. Therein, host clusters H9 and H11 most importantly comprised growth- related genes such as PCNA, DNA polymerase, and replication proteins. The synchronously expressed microbiome cluster M1

which comprised genes of diverse bacterial clades contained mostly methyltransferases (Methyltransf_21) and PEP-utilizers within its enriched COG-subcategories. Gene clusters H7 and M13 showed the inverse of this interactive effect, i.e., scaled expression in response to increasing photoperiod decreased at 9°C but increased at 13.5°C. Therein, host cluster H7 contained mostly betaine/carnitine/choline family transporters (BCCT), trypsin, and peptidase. The corresponding co-expressed microbiome cluster M13 which showed a diverse taxonomic composition contained mainly epimerase and transmembrane transporters (MFS_1) within the found enriched COG-categories.

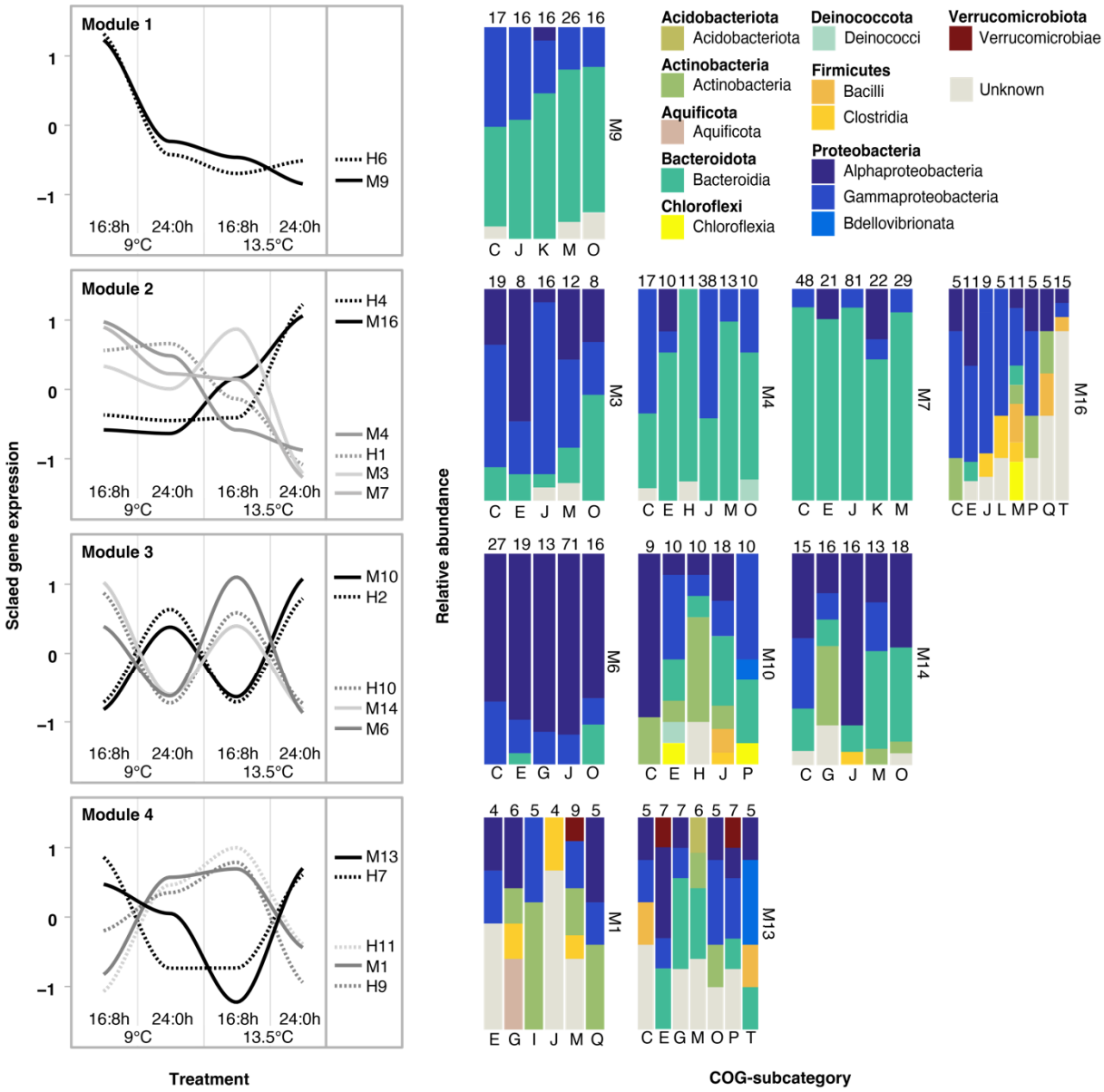

Fig. 4.5 Left: Simplified illustration of scaled expression profiles of host- and microbiome- gene clusters (resulting from the K-means cluster analysis across the experimental treatments of temperature (9°C, 13.5°C) and photoperiod (16:8h, 24:0h) for each host-microbiome co-expression module (Module 1-4, vertical facets). For each module, cluster identity is represented by different shades of grey. Host clusters are depicted as dashed lines, microbiome clusters are depicted as solid lines. Right: Relative taxonomic composition on the class level of the 5 most dominant COG-subcategories (bottom) for each microbiome cluster. The total number of genes per COG-subcategory for each microbiome cluster is given (top). Detailed description for COG subcategory can be found in Fig. 4.3.

Discussion

The results of this study demonstrated a positive net effect of the bacterial microbiome on diatom growth across all experimental conditions. Microbiome community composition, host transcriptomics, and microbiome metatranscriptomics showed little differences between the two photoperiodic treatments at 9°C but strongly diverged at 13.5°C. Host transcriptomics revealed differences between xenic and axenic transcriptomes in 11 COG subcategories, and the majority of the respective genes were significantly co-expressed with specific bacterial genes. The identified host-microbiome co-expression modules showed main- and interactive effects of photoperiod and temperature.

The found positive net effect of bacterial presence on host growth demonstrates an overall mutualistic-symbiotic relationship of the diatom holobiont as already reported in many other examples of algae-associated microbiomes (Mönnich et al., 2020). This observation was reflected at the level of gene expression data, with an enrichment of genes involved in nucleotide metabolism and replication in the xenic treatment, suggesting an overall increase in division rates.

Relatively, this contribution of bacterial presence to host growth was smallest under combined thermal and photoperiodic stress (13.5°C/24:0h) in line with the study of Giesler et al (2023), where however, the microbiome effect for the same diatom strain was not only smallest but even turned negative in this respective treatment conditions (Giesler et al. 2023). The microbiome community associated with this *T. gravida* strain constituted of some Arctic-typical psychrophilic bacteria, e.g., *Colwellia* (Konstantinos et al., 2009), *Polaribacter* (Kim et al., 2013), or *Glaciecola* (Zhang et al., 2007), and some rather cosmopolitan/temperate bacteria also commonly found on temperate diatom microbiomes such as *Sulfitobacter* (Monnich et al., 2020) and *Methylophaga* (Zhang et al., 2014). The found bacterial community composition demonstrated an overall higher evenness in the diatom-attached bacterial fraction compared to the free-living fraction, which was clearly dominated by *Colwellia* and *Methylophaga*, showing that many of the other bacteria that were isolated together with the initial diatom cell of this strain prefer a particle-associated lifestyle.

The identified co-expression modules demonstrate various distinct interaction processes between the host diatom and diverse microbiome members. This reflects the role of the diatom holobiont as a metabolic hotspot offering numerous niches to a diverse bacterial consortium (Kuhlisch et al., 2023). Co-expression module 1 generally reflects the inverse pattern of xenic

diatom growth rates across the treatments and thus may either be the cause or the consequences of the found growth pattern. Therein, with increasing photoperiod and temperature, diatoms reduce the expression of various transporter genes, membrane-embedded chitin recognition proteins, and genes annotated as alginic acid biosynthesis. Alginic acid, a major polysaccharide of brown algae (Percival, 1979), plays a crucial role in their biofilm formation (Reinhardt et al., 2019). The observed synchronous decreasing expression of Bacteroidia cell adhesion mechanisms (i.e., fasciclin), sugar metabolism, membrane transporters, and quorum sensing two-component signaling systems suggest a similar function as extracellular polymeric substance (EPS) for diatoms. Overall, this co-expression module reflects a potential decline of biofilm formation between the host diatom and microbiome members of the Bacteroidia clade (here mainly *Polaribacter* and/or *Owenweeksia*) that appear to be particularly dependent on this niche within the diatom holobiont. This is supported by field studies that showed high niche specificity of *Polaribacter* spp. in utilizing highly specific algal-derived polysaccharides (Avci et al., 2020).

Co-expression module 2 reflects, that differences in microbiome composition and metatranscriptomes mainly occurred under thermal stress (i.e., the 13.5°C treatments). Particularly the 13.5°C/16:8h treatment differed the most from all other treatments. Most strikingly, in this specific treatment, the *T. gravida* microbiome seems to have lost the *Sulfitobacter* clade. Previous studies showed that *Sulfitobacter* is a key microbiome bacterial clade to diatoms, providing growth hormones and ammonium (Behringer et al., 2018, Shibl et al., 2020, Amin et al., 2015), with the ability to switch between mutualistic and pathogenic life styles (Barak-Gavish et al., 2023). Moreover, recent findings showed that particularly the *Sulfitobacter* is essential for microbiome assembly and stability due to close associations with other bacteria (Isaac et al., 2024). Consequently, the loss of *Sulfitobacter* could lead to a less stable and less diverse microbial community. This is indeed reflected in the simultaneous increase of *Zhongshania*, the decline of Bacteroidia (i.e., *Polaribacter* and *Owenweeksia*) and the overall high variability in bacterial community composition between the replicates within the 13.5°C/16:8h treatment. Furthermore, taking into account the metabolic shift within the microbiome community as revealed by increased sulfide oxidation in this treatment, this emphasizes the risk for microbiome dysbiosis. However, in this study, negative consequences likely were buffered by the remaining microbiome members, as interestingly host growth rates were not negatively affected. This suggests that community interactions between the host and its microbiome, and within the microbiome, are flexible enough to allow coordinated responses to changing external conditions that at least increase or maintain host performance. Yet, it is

important to consider that due to the closed-system design, neither the potential recruitment of new microbiome members nor the arrival of pathogens in the phycosphere could be studied (Ahern et al., 2021). Thus, the diatom holobiont resilience to warming in natural systems may diverge.

The oscillating expression patterns with photoperiodic treatments in co-expression module 3 reflect the joint response of the diatom and its microbiome to an extreme Arctic light regime. In diatoms, extended light exposure causes excessive excitation of photosystems, leading to the formation of reactive oxygen species (ROS), while simultaneously depleting the diatom's antioxidant defenses and repair mechanisms, ultimately resulting in oxidative damage to cellular components (Li et al., 2017). The polar adapted *T. gravida* acquired specific adaptations, allowing this diatom species to tolerate and even thrive under polar day scenarios that can have detrimental effects on comparable temperate-adapted diatoms such as *T. rotula* (Giesler et al. under review). Here, in the respective diatom gene clusters, intracellular adaptation to prolonged photoperiods is reflected by a strong decrease in cellular Chl-a gene content. However, also increasing oxidative stress defense can be assumed in terms of an increase in antioxidant enzymes and a programmed cell death-driving gene (Lin et al., 2017). The highly correlated bacterial gene cluster M10 shows synchronized expression of antioxidant enzymes (e.g., Glutarredoxin). However, also negatively correlated bacterial gene clusters contained important antioxidants (e.g., glutathione peroxidase). Previous studies showed that some microbiome bacteria significantly enhanced the growth of an Antarctic diatom by cleaving hydrogen peroxide in the diatom phycosphere (Hünken et al., 2008). Interestingly, in the respective study by Hünken et al., (2008) this function was identified in the presence of the bacterial clades *Colwellia* and *Sulfitobacter*, which are also dominant microbiome members in the *T. gravida* microbiome and thus also may contribute to the observed growth enhancement in the xenic diatom cultures. Unfortunately, the low resolution of taxonomic annotation for the respective expressed genes does not allow a clear assignment of this mechanism to *Colwellia* or *Sulfitobacter*.

Co-expression module 4 demonstrates the interactive effect of temperature and photoperiod and thus includes host and microbiome genes of which the response to photoperiod reverses at different temperatures. For the diatom host, this importantly comprises multiple proxies for cell growth including cell replication proteins and PCNA (Liu et al., 2005). Taking into account co-expressed bacterial gene clusters, this indicates bacterial genes that are likely to be coupled to diatom growth. For instance, the significant enrichment in bacterial genes related to

carbohydrate metabolism in the microbiome gene cluster M1 shows that bacterial DOC consumption is related to diatom growth. This is supported by field observations that underline the dependence of the here-found key microbiome members such as *Colwellia*, *Methylophaga*, and *Sulfitobacter* on diatom-exuded organic matter (Landa et al., 2018).

With regard to other known diatom-bacteria interactions such as the possible bacterial provision of cobalamin (Vitamin B_{12}) to the diatom host (Amin et al., 2012), cobalamin biosynthesis-related genes within significant correlating host-microbiome co-expression modules were identified for three bacterial clades, namely Bacilli, Alpha- and Gammaproteobacteria in three different microbiome gene clusters (M16, M10, and M13). These three clusters complement each other in their expression patterns in 3 of the 4 treatments, suggesting that cobalamin production within the microbiome community can be maintained stable over a range of environmental conditions. However, for the 13.5°C/24:0h treatment, all gene clusters have an increased expression rate, suggesting an increased demand for cobalamin from either or both the host and the microbiome. Further, although due to (micro-) nutrient-replete conditions, these processes likely did not substantially drive host growth in this experiment, it is worth noting that cobalamin synthesis and its potential provision by each of these bacterial groups follows unique (and partially contrary) co-expression profiles and therefore is likely involved in different host-microbiome interaction processes which in turn are differently affected by environmental conditions. As it has previously been shown that not all cobalamin-producing bacteria actually share vitamin B_{12} with their host algae (Sultana et al., 2023) we can extent this knowledge, showing that the production and potential provision can also be inhibited or facilitated by certain (at least clade-specific) abiotic conditions.

Conclusion

Overall, this study underlines the positive net effect of the mutualistic diatom-associated microbiome, likely based on an overall flexible interaction network as indicated by the metatranscriptome and microbiome community composition. The results also showed that algae-bacteria interactions should always be considered in the context of the given environmental conditions, which independently drive specific host-microbiome interaction processes. In the context of a warming Arctic Ocean, the dependence of the diatom holobiont stability on certain key bacterial clades such as *Sulfitobacter*, which may be negatively affected under these conditions, highlight the risk for microbial ecological tipping points that may bring

these mutually beneficial interactions out of balance. Despite the observed diatom resilience in terms of growth rates in this experimental context, more studies are needed to investigate if this resilience is compromised in the presence of naturally occurring pathogens.

References

ABADA, A., BEIRALAS, R., NARVAEZ, D., SPERFELD, M., DUCHIN-RAPP, Y., LIPSMAN, V., YUDA, L., COHEN, B., CARMIELI, R., BEN-DOR, S., ROCHA, J., HUANG ZHANG, I., BABBIN, A. R. & SEGEV, E. 2023. Aerobic bacteria produce nitric oxide via denitrification and promote algal population collapse. *ISME J,* 17**,** 1167-1183.

AGLER, M. T., RUHE, J., KROLL, S., MORHENN, C., KIM, S.-T., WEIGEL, D. & KEMEN, E. M. 2016. Microbial Hub Taxa Link Host and Abiotic Factors to Plant Microbiome Variation. *PLOS Biology,* 14**,** e1002352.

AHERN, O. M., WHITTAKER, K. A., WILLIAMS, T. C., HUNT, D. E. & RYNEARSON, T. A. 2021. Host genotype structures the microbiome of a globally dispersed marine phytoplankton. *Proc Natl Acad Sci U S A,* 118.

AMIN, S. A., HMELO, L. R., VAN TOL, H. M., DURHAM, B. P., CARLSON, L. T., HEAL, K. R., MORALES, R. L., BERTHIAUME, C. T., PARKER, M. S., DJUNAEDI, B., INGALLS, A. E., PARSEK, M. R., MORAN, M. A. & ARMBRUST, E. V. 2015. Interaction and signalling between a cosmopolitan phytoplankton and associated bacteria. *Nature,* 522**,** 98-101.

AMIN, S. A., PARKER, M. S. & ARMBRUST, E. V. 2012. Interactions between diatoms and bacteria. *Microbiol Mol Biol Rev,* 76**,** 667-84.

ANDREWS, S. 2010. FastQC: A Quality Control Tool for High Throughput Sequence Data. Available online at: http://www.bioinformatics.babraham.ac.uk/projects/fastqc/.

ARMENGOL, L., CALBET, A., FRANCHY, G., RODRIGUEZ-SANTOS, A. & HERNANDEZ-LEON, S. 2019. Planktonic food web structure and trophic transfer efficiency along a productivity gradient in the tropical and subtropical Atlantic Ocean. *Sci Rep,* 9**,** 2044.

AVCI, B., KRUGER, K., FUCHS, B. M., TEELING, H. & AMANN, R. I. 2020. Polysaccharide niche partitioning of distinct *Polaribacter* clades during North Sea spring algal blooms. *ISME J,* 14**,** 1369-1383.

BAKER, L. J. & KEMP, P. F. 2014. Exploring bacteria–diatom associations using single-cell whole genome amplification. *Aquatic Microbial Ecology,* 72**,** 73-88.

BANKEVICH, A., NURK, S., ANTIPOV, D., GUREVICH, A. A., DVORKIN, M., KULIKOV, A. S., LESIN, V. M., NIKOLENKO, S. I., PHAM, S., PRJIBELSKI, A. D., PYSHKIN, A. V., SIROTKIN, A. V., VYAHHI, N., TESLER, G., ALEKSEYEV,

M. A. & PEVZNER, P. A. 2012. SPAdes: a new genome assembly algorithm and its applications to single-cell sequencing. *J Comput Biol,* 19**,** 455-77.

BARAK-GAVISH, N., DASSA, B., KUHLISCH, C., NUSSBAUM, I., BRANDIS, A., ROSENBERG, G., AVRAHAM, R. & VARDI, A. 2023. Bacterial lifestyle switch in response to algal metabolites. *eLife,* 12**,** e84400.

BARNETT, D., ARTS, I. & PENDERS, J. 2021. microViz: an R package for microbiome data visualization and statistics. *Journal of Open Source Software,* 6.

BEHRINGER, G., OCHSENKUHN, M. A., FEI, C., FANNING, J., KOESTER, J. A. & AMIN, S. A. 2018. Bacterial Communities of Diatoms Display Strong Conservation Across Strains and Time. *Front Microbiol,* 9**,** 659.

BEULE, L. & KARLOVSKY, P. 2020. Improved normalization of species count data in ecology by scaling with ranked subsampling (SRS): application to microbial communities. *PeerJ,* 8**,** e9593.

BIONDI, N., CHELONI, G., RODOLFI, L., VITI, C., GIOVANNETTI, L. & TREDICI, M. 2018. *Tetraselmis suecica* F&M-M33 growth is influenced by its associated bacteria. *Microbial Biotechnology,* 11**,** 211-223.

BUSHNELL, B. 2014. BBMap: A Fast, Accurate, Splice-Aware Aligner. Computer Science Biology.

CALLAHAN, B. J., MCMURDIE, P. J., ROSEN, M. J., HAN, A. W., JOHNSON, A. J. A. & HOLMES, S. P. 2016. DADA2: High-resolution sample inference from Illumina amplicon data. *Nature Methods,* 13**,** 581-583.

CANTALAPIEDRA, C. P., HERNANDEZ-PLAZA, A., LETUNIC, I., BORK, P. & HUERTA-CEPAS, J. 2021. eggNOG-mapper v2: Functional Annotation, Orthology Assignments, and Domain Prediction at the Metagenomic Scale. *Mol Biol Evol,* 38**,** 5825-5829.

CIRRI, E. & POHNERT, G. 2019. Algae-bacteria interactions that balance the planktonic microbiome. *New Phytol,* 223**,** 100-106.

DREW, G. C., STEVENS, E. J. & KING, K. C. 2021. Microbial evolution and transitions along the parasite-mutualist continuum. *Nat Rev Microbiol,* 19**,** 623-638.

FALCIATORE, A. & MÖCK, T. 2022. *The molecular life of diatoms,* Cham, Switzerland, Springer.

FIELD, C. B., BEHRENFELD, M. J., RANDERSON, J. T. & FALKOWSKI, P. 1998. Primary Production of the Biosphere: Integrating Terrestrial and Oceanic Components. *Science,* 281**,** 237-240.

GIESLER, J. K., HARDER, T. & WOHLRAB, S. 2023a. Microbiome and photoperiod interactively determine thermal sensitivity of polar and temperate diatoms. *Biol Lett,* 19**,** 20230151.

GIESLER, J. K., LEMLEY, D. A., ADAMS, J. B. & MOORTHI, S. D. 2023b. Interactive effects of salinity, temperature and food web configuration on performance and

harmfulness of the raphidophyte *Heterosigma akashiwo*. *Frontiers in Marine Science,* 10.

GUO, X., TANG, P., HOU, C., CHONG, L., ZHANG, X., LIU, P., CHEN, L., LIU, Y., ZHANG, L. & LI, R. 2022. Integrated Microbiome and Host Transcriptome Profiles Link Parkinson's Disease to Blautia Genus: Evidence From Feces, Blood, and Brain. *Front Microbiol,* 13**,** 875101.

HAAS, B. 2013. TransDecoder (Find Coding Regions Within Transcripts). https://github.com/TransDecoder/transdecoder.github.io.

HARRISON, P. J., WATERS, R. E. & TAYLOR, F. J. R. 2008. A Broad Spectrum Artificial Sea Water Medium for Coastal and Open Ocean Phytoplankton1. *Journal of Phycology,* 16**,** 28-35.

HENRY, L. P., BRUIJNING, M., FORSBERG, S. K. G. & AYROLES, J. F. 2021. The microbiome extends host evolutionary potential. *Nat Commun,* 12**,** 5141.

HÜNKEN, M., HARDER, J. & KIRST, G. 2008. Epiphytic bacteria on the Antarctic ice diatom *Amphiprora kufferathii* Manguin cleave hydrogen peroxide produced during algal photosynthesis. *Plant biology (Stuttgart, Germany),* 10**,** 519-26.

ISAAC, A., MOHAMED, A. & AMIN, S. 2024. Rhodobacteraceae are key players in microbiome assembly of the diatom *Asterionellopsis glacialis*. *Applied and Environmental Microbiology,* 90**,** e0057024.

KIM, B.-C., OH, H., KIM, H., PARK, D.-S., HONG, S. G., LEE, H. K. & BAE, K. S. 2013. Polaribacter sejongensis sp. nov., isolated from Antarctic soil, and emended descriptions of the genus *Polaribacter, Polaribacter butkevichii* and *Polaribacter irgensii*. *International journal of systematic and evolutionary microbiology,* 63.

KONSTANTINIDIS KONSTANTINOS, T., BRAFF, J., KARL DAVID, M. & DELONG EDWARD, F. 2009. Comparative Metagenomic Analysis of a Microbial Community Residing at a Depth of 4,000 Meters at Station ALOHA in the North Pacific Subtropical Gyre. *Applied and Environmental Microbiology,* 75**,** 5345-5355.

KOPYLOVA, E., NOE, L. & TOUZET, H. 2012. SortMeRNA: fast and accurate filtering of ribosomal RNAs in metatranscriptomic data. *Bioinformatics,* 28**,** 3211-7.

KUDJORDJIE ENOCH, N., HOOSHMAND, K., SAPKOTA, R., DARBANI, B., FOMSGAARD INGE, S. & NICOLAISEN, M. 2022. *Fusarium oxysporum* Disrupts Microbiome-Metabolome Networks in *Arabidopsis thaliana* Roots. *Microbiology Spectrum,* 10**,** e01226-22.

KUHLISCH, C., SHEMI, A., BARAK-GAVISH, N., SCHATZ, D. & VARDI, A. 2023. Algal blooms in the ocean: hot spots for chemically mediated microbial interactions. *Nat Rev Microbiol*.

LANDA, M., BLAIN, S., HARMAND, J., MONCHY, S., RAPAPORT, A. & OBERNOSTERER, I. 2018. Major changes in the composition of a Southern Ocean bacterial community in response to diatom-derived dissolved organic matter. *FEMS Microbiology Ecology,* 94**,** fiy034.

LANGMEAD, B. & SALZBERG, S. L. 2012. Fast gapped-read alignment with Bowtie 2. *Nat Methods,* 9**,** 357-9.

LI, G., TALMY, D. & CAMPBELL, D. A. 2017. Diatom growth responses to photoperiod and light are predictable from diel reductant generation. *J Phycol,* 53**,** 95-107.

LIAO, Y., SMYTH, G. K. & SHI, W. 2014. featureCounts: an efficient general purpose program for assigning sequence reads to genomic features. *Bioinformatics,* 30**,** 923-30.

LIN, Q., LIANG, J.-R., HUANG, Q.-Q., LUO, C.-S., ANDERSON, D. M., BOWLER, C., CHEN, C.-P., LI, X.-S. & GAO, Y.-H. 2017. Differential cellular responses associated with oxidative stress and cell fate decision under nitrate and phosphate limitations in *Thalassiosira pseudonana*: Comparative proteomics. *PLOS ONE,* 12**,** e0184849.

LITCHMAN, E., DE TEZANOS PINTO, P., EDWARDS, K. F., KLAUSMEIER, C. A., KREMER, C. T., THOMAS, M. K. & AUSTIN, A. 2015. Global biogeochemical impacts of phytoplankton: a trait-based perspective. *Journal of Ecology,* 103**,** 1384-1396.

LIU, J., JIAO, N., HONG, H., LUO, T. & CAI, H. 2005. Proliferating cell nuclear antigen (PCNA) as a marker of cell proliferation in the marine dinoflagellate *Prorocentrum donghaiense* Lu and the green alga *Dunaliella salina* Teodoresco. *Journal of Applied Phycology,* 17**,** 323-330.

LOVE, M. I., HUBER, W. & ANDERS, S. 2014. Moderated estimation of fold change and dispersion for RNA-seq data with DESeq2. *Genome Biol,* 15**,** 550.

MARGULIS, L. S. & FESTER, R. Symbiosis as a source of evolutionary innovation : speciation and morphogenesis. 1991.

MARTIN, M. 2011. Cutadapt removes adapter sequences from high-throughput sequencing reads. *2011,* 17**,** 3.

MCMURDIE, P. J. & HOLMES, S. 2013. phyloseq: an R package for reproducible interactive analysis and graphics of microbiome census data. *PLoS One,* 8**,** e61217.

MONNICH, J., TEBBEN, J., BERGEMANN, J., CASE, R., WOHLRAB, S. & HARDER, T. 2020. Niche-based assembly of bacterial consortia on the diatom *Thalassiosira rotula* is stable and reproducible. *ISME J,* 14**,** 1614-1625.

MUKHERJEE, A. 2021. Compounds derived from bacteria enhance marine diatom growth. *Plant Physiology,* 186**,** 827-828.

PARADA, A. E., NEEDHAM, D. M. & FUHRMAN, J. A. 2016. Every base matters: assessing small subunit rRNA primers for marine microbiomes with mock communities, time series and global field samples. *Environ Microbiol,* 18**,** 1403-14.

PERCIVAL, E. 1979. The polysaccharides of green, red and brown seaweeds: Their basic structure, biosynthesis and function. *British Phycological Journal,* 14**,** 103-117.

QUAST, C., PRUESSE, E., YILMAZ, P., GERKEN, J., SCHWEER, T., YARZA, P., PEPLIES, J. & GLOCKNER, F. O. 2013. The SILVA ribosomal RNA gene database

project: improved data processing and web-based tools. *Nucleic Acids Res,* 41**,** D590-6.

R DEVELOPMENT CORE TEAM 2023. R: A language and environment for statistical computing. Vienna, Austria: R Foundation for Statistical Computing.

RANTANEN, M., KARPECHKO, A. Y., LIPPONEN, A., NORDLING, K., HYVÄRINEN, O., RUOSTEENOJA, K., VIHMA, T. & LAAKSONEN, A. 2022. The Arctic has warmed nearly four times faster than the globe since 1979. *Communications Earth & Environment,* 3.

REINHARDT, T., MOELZNER, J., NEU, T. R. & FINK, P. 2019. Biofilm pads—an easy method to manufacture artificial biofilms embedded in an alginate polymer matrix. *Limnology and Oceanography: Methods,* 18**,** 1-7.

RODRÍGUEZ-GÁLVEZ, S., MACÍAS, D., PRIETO, L. & RUIZ, J. 2023. Top-down and bottom-up control of phytoplankton in a mid-latitude continental shelf ecosystem. *Progress in Oceanography,* 217**,** 103083.

SCHOLZ, B. 2014. Purification and culture characteristics of 36 benthic marine diatoms isolated from the Solthörn tidal flat (Southern North Sea). *Journal of Phycology,* 50**,** 685-697.

SEYEDSAYAMDOST, M. R., CASE, R. J., KOLTER, R. & CLARDY, J. 2011. The Jekyll-and-Hyde chemistry of *Phaeobacter gallaeciensis*. *Nature Chemistry,* 3**,** 331-335.

SEYMOUR, J., AMIN, S., RAINA, J.-B. & STOCKER, R. 2017. Zooming in on the phycosphere: The ecological interface for phytoplankton-bacteria relationships. *Nature Microbiology,* 2.

SHIBL, A. A., ISAAC, A., OCHSENKUHN, M. A., CARDENAS, A., FEI, C., BEHRINGER, G., ARNOUX, M., DROU, N., SANTOS, M. P., GUNSALUS, K. C., VOOLSTRA, C. R. & AMIN, S. A. 2020. Diatom modulation of select bacteria through use of two unique secondary metabolites. *Proc Natl Acad Sci U S A,* 117**,** 27445-27455.

SULTANA, S., BRUNS, S., WILKES, H., SIMON, M. & WIENHAUSEN, G. 2023. Vitamin B12 is not shared by all marine prototrophic bacteria with their environment. *The ISME Journal,* 17**,** 836-845.

TATUSOV, R. L., GALPERIN, M. Y., NATALE, D. A. & KOONIN, E. V. 2000. The COG database: a tool for genome-scale analysis of protein functions and evolution. *Nucleic Acids Research,* 28**,** 33-36.

UEHARA, M., INOUE, T., HASE, S., SASAKI, E., TOYODA, A. & SAKAKIBARA, Y. 2024. Decoding host-microbiome interactions through co-expression network analysis within the non-human primate intestine. *mSystems,* 9**,** e01405-23.

WANG, R., GALLANT, É., WILSON, M. Z., WU, Y., LI, A., GITAI, Z. & SEYEDSAYAMDOST, M. R. 2022. Algal p-coumaric acid induces oxidative stress and siderophore biosynthesis in the bacterial symbiont *Phaeobacter inhibens*. *Cell Chemical Biology,* 29**,** 670-679.e5.

YU, H., WANG, Q., TANG, J., DONG, L., DAI, G., ZHANG, T., ZHANG, G., XIE, K., WANG, H. & ZHAO, Z. 2023. Comprehensive analysis of gut microbiome and host transcriptome in chickens after *Eimeria tenella* infection. *Front Cell Infect Microbiol,* 13**,** 1191939.

ZHANG, D.-C., YU, Y., CHEN, B., WANG, H.-X., LIU, H.-C., DONG, X.-Z. & ZHOU, P.-J. 2007. *Glaciecola psychrophila* sp. nov., a novel psychrophilic bacterium isolated from the Arctic. *International journal of systematic and evolutionary microbiology,* 56**,** 2867-9.

ZHANG, L., GAO, G., TANG, X. & SHAO, K. 2014. Can the freshwater bacterial communities shift to the "marine-like" taxa? *Journal of basic microbiology,* 54.

5 Publication IV

A CRISPR-Cas9 assisted analysis of single-cell microbiomes for identifying rare bacterial taxa in phycospheres of diatoms

Under review in ISME communications

A CRISPR-Cas9 assisted analysis of single-cell microbiomes for identifying rare bacterial taxa in phycospheres of diatoms

Jakob K. Giesler*[1,2], Ruben Schulte-Hillen*[1,3,4], Thomas Mock[5], Nigel Belshaw[5], Uwe John[1], Tilmann Harder[1,2], Nancy Kühne[1], Stefan Neuhaus[1], and Sylke Wohlrab[1,6]

* These authors contributed equally to this work and share first authorship.

[1)] *Alfred Wegener Institute, Helmholtz Centre for Polar and Marine Research, Bremerhaven Germany*

[2)] *Universität Bremen, Bremen, Germany*

[3)] *Max Planck Institute for Marine Microbiology, Bremen, Germany*

[4)] *Albert-Ludwigs-Universität Freiburg, Freiburg, Germany*

[5)] *University of East Anglia, School of Environmental Sciences, Norwich, UK*

[6)] *Helmholtz Institute for Functional Marine Biology at the University of Oldenburg (HIFMB), Oldenburg, Germany*

Competing Interests:

The authors declare there is no conflict of interest

Abstract

Primary production in aquatic systems is governed by interactions between microalgae and their associated bacteria. Most of our knowledge about algal microbiomes stems from natural mixed communities or isolated algal monocultures, which therefore does neither address the role of genotypic diversity among the algal host cells nor do they reveal how this host diversity impacts the assembly process of associated bacteria. To overcome this knowledge gap, we developed a single-cell 16S sequencing approach in combination with CRISPR-Cas9 guided depletion of host 16S contaminations from the chloroplast. The validity of this novel method was tested by comparing bacterial communities of 144 single-cells across three genotypes of the Arctic marine diatom *Thalassiosira gravida* grown under different environmental conditions. From these, 62 single-cells were additionally sequenced after CRISPR-Cas9 treatment. Due to the

improved sequencing depth, bacterial richness associated with individual diatom cells was increased by up to 56%. By applying this CRISPR-Cas9 treatment we not only revealed intraspecific host-genotype associations but also rare bacterial taxa that were not detected by standard 16S rRNA gene metabarcoding. Thus, the CRISPR-Cas9 assisted single-cell approach developed in this study advances our understanding on how the intraspecific diversity among algal hosts impacts the assembly process of their associated bacteria. This knowledge is essential to understand the co-evolution and adaptation of species in algal microbiomes.

Introduction

The role and function of interactions between individuals in microbial communities is increasingly recognized in microbiome research (Margulis, 1991, Dittami et al., 2021), which coined the term 'holobiont' describing an assemblage of a host (e.g., microalga) and associated microbes (e.g., bacteria). As the main primary producers in aquatic ecosystems, both uni- and multicellular algae have been studied from a holobiont perspective because their associated microbiomes substantially affect algal physiology, growth and resilience (Amin et al., 2012, Giesler et al., 2023). For example, interactions between host algae and bacteria are underpinned by specific bacterial enzymes as well as reciprocal nutritional requirements for essential trace elements, micro-, and macronutrients (Amin et al., 2012, Kodama and Fujishima, 2022).

Given the recognized importance of microalgae for diverse ecosystem functions (Cirri and Pohnert, 2019, Kuhlisch et al., 2023) methods to accurately determine their associated microbial communities are of considerable value. Current strategies to assess the bacterial composition associated with microalgae predominantly rely on laboratory monocultures or natural field communities, introducing uncertainties such as culture artifacts and biases due to single-cell isolation and filtration. Moreover, clonality in microalgal populations usually is short-lived as sub-populations arise due to genetic drift leading to clonal interference. How this intraspecific host diversity impacts the diversity of associated bacterial communities has rarely been studied and is therefore largely unknown. Natural algal microbiomes, on the other hand, are difficult to study in a natural community context due to challenges in assigning bacteria to specific hosts for revealing their interactions (Martin et al., 2021). To address these challenges, single-cell-based metabarcoding has recently been developed to assesses the microbial diversity associated with single-cells of host protists such as choanoflagellates and ciliates (Needham et al., 2022, Boscaro et al., 2023, Rossi et al., 2019). However, this single-cell sequencing strategy comes

with several challenges. For instance, sequencing small amounts of DNA isolated from a proximity of the host protist might introduce a bias due to significant variability between single host cells in terms of the success of DNA extraction and amplification (Schmitz et al., 2021). Although microbiomes on single sand grains have been successfully studied despite low DNA concentrations (Probandt et al., 2018), similar microbiome analyses using single-celled algal microbiomes have been challenging due to the presence of 16S rRNA gene copies encoded in the algal chloroplast genomes, which can account for up to 99% of all sequence reads (Lundberg et al., 2012, Zarraonaindia et al., 2015).

This predominance of 16S rRNA gene copies encoded in chloroplast genomes reduces the sequencing depth of the 16S copies from the associated microbiomes. This caveat is adding to challenges imposed by overall low quantities of DNA, spatial heterogeneity and potential other methodological biases (see above). One strategy to reduce contamination by host 16S rRNA gene sequences from chloroplasts is PCR clamping, a method to suppress a particular allele during PCR (Orum et al., 1993). Yet, this strategy has its own biases, i.e., species-specific suppression of PCR amplification (Jackrel et al., 2017, Baker and Kemp, 2014). Here, we address these biases with a novel approach, **S**ingle-**C**ell **Ho**lobiont **C**as9-**O**ptimised-**Seq**uencing (SCHoCO-Seq), which employs a Cas9 nuclease together with a target-specific guide RNA to dissect the 16S rRNA gene sequences of oceanic microalgae. Our approach is thus methodologically complementary to the approach developed by Song and Xie (2020), who used Cas9 to dissect the 16sRNA gene copies of rice chloroplasts from bulk leaf samples. However, we further extended this method to the single-cell level. In addition, as our approach is not restricted to a single species, it can be used to gain insight into a wide range of natural microbiomes associated with diverse single-cell host organisms.

We have compared this novel SCHoCO-seq approach with CRISPR/Cas9 untreated single-cell control microbiomes (further referred to as SC-Seq) of the diatom *Thalassiosira gravida* under different culture conditions. This workflow of SCHoCO-seq is based on single-cell isolation, optional DNA extraction, subsequent nested low template PCR and Cas9-mediated, target-specific cleavage of the diatom chloroplast 16S rRNA gene amplicons, followed by amplicon metabarcoding of the associated prokaryotic community. Furthermore, controls were conducted to test for contaminations and off-target activity.

Material and methods

Three strains of the Arctic diatom *T. gravida* were grown under different culture conditions. Single-cells were manually isolated and washed to remove free-living bacteria leaving mainly diatom-associated bacteria. The isolated single diatom cells were processed according to the workflow in Figure 5.1 and described in detail below. Two different pre-processing protocols are presented: a direct PCR method, which is less labor intensive, and a method involving a single-cell DNA extraction step, which has the advantage of retaining the DNA for additional analysis.

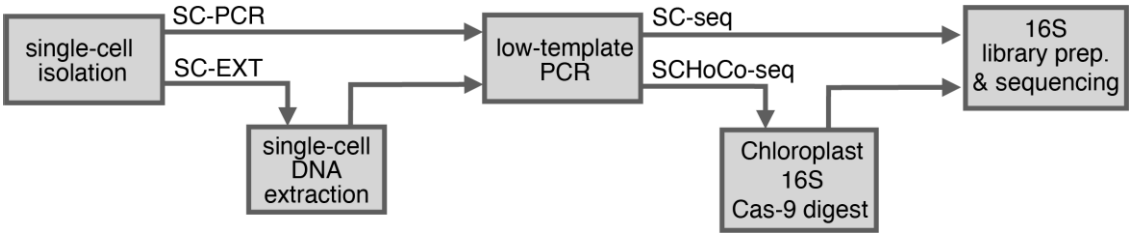

Figure 5.1: Schematic overview of the laboratory workflow. After single-cell isolation, samples were either subjected to DNA extraction (SC-EXT) or processed directly to low template PCR without prior DNA extraction (SC-PCR). A subset of low-template PCR products from all samples (62 out of 144) were treated with Cas9 to dissect the chloroplast 16S rRNA gene (SCHoCO-seq) prior to library preparation.

Culture Conditions

Diatom cultures of *Thalassiosira gravida* strains (UIO 478; UIO 483; UIO 448, table S5.1) were obtained from the Norwegian Culture Collection of Algae (NORCCA). Here, we refer to UIO 478 as A1, UIO 483 as A2, and UIO 448 as A5. Stock cultures were maintained in three culture media based on a modified and silica-enriched K-medium (20) (table S5.2), a nitrogen-deplete medium (table S5.3), and a vitamin-deplete medium (table S4). Cultures were grown at 4°C and 50 µmol photons m^{-2} s^{-1} under a light:dark period of 16:8 h.

Single-cell Isolation

To study the diversity of diatom-associated microbiomes among conspecific host cells across genotypes, single-cells of *T. gravida* strains A1, A2 and A5 cultured under different conditions (see above) were isolated (n = 8). To remove the free-living bacteria, Individual diatom cells were picked and sequentially washed five times by pipetting 3 µL into two separate 30 µL drops of PBS buffer (PBS CellPure, Roth, Karlsruhe, Germany), followed by three washings in 30

µL of PCR-grade water under an inverted light microscope. To validate the absence of free-living bacteria, 3 µL culture blanks (without diatom cells) were sampled from all strains and treated identical to the single-cell samples undergoing single-cell DNA extraction (see below). Cells were stored either in 30 µL 2xT&C lysis buffer of the MasterPure Complete DNA & RNA Purification Kit (Lucigen, Wisconsin, USA) or in 10 µL PCR-grade water. Cells in PCR-grade water were used directly as DNA template for a nested, low template PCR (see below). Cells stored in 2xT&C lysis buffer were used to generate a PCR product after DNA extraction (see below).

DNA Extraction from Isolated Single-cells (SC-EXT)

To extract DNA from the single-cellular diatom microbiomes, a modified protocol of the DNA MasterPure Complete DNA & RNA Purification Kit was employed (SC-EXT). The changes to the manufacturer instructions were: (i) smaller buffer volumes, (ii) added pellet dye, and (iii) rinsing of pipette tips. (details in Table S5.5)

Nested Low Template PCR of Single Diatom Cell Holobionts

During the low template PCR, the hypervariable V1-V9 region of the 16S rRNA gene was targeted by Primer 27F (5'-AGAGTTTGATYMTGGCTCAG-3') (Frank et al., 2008) and 1492R (5'-TACGGYTACCTTGTTACGACTT-3') (Lane D, 1991). PCR reactions for single-cell samples were set up to 50 µL per reaction containing 5 µL 10 x Hotmaster Taq Buffer (Qiagen, Hilden, Germany), 0.5 µL Primer 27F (10 mM), 0.5 µL Primer 1492R (10 mM), 0.5 µL dNTPs (10 mM), 0.1 µL bovine serum albumin (BSA, 10 mg/mL), 0.5 Taq Polymerase (Qiagen), 32.9 µL H_2O and 10 µL Single-Cell Sample (SC-PCR) or 2.5 µL extracted DNA (SC-EXT) plus 7.5 µL H_2O. PCR protocols for SC-PCR and SC-EXT differed only in the duration of the initial denaturation phase of 94°C for 1.5 min (SC-EXT) and 10 min (SC-PCR), respectively. Both protocols consisted of 35 cycles; denaturation: 94°C for 1.5 min primer annealing: 55°C for 1.5 min, elongation: 68°C for 2 min, final elongation: 68°C for 10 min. PCR products were cleaned with the MinElute PCR Purification kit (Qiagen). All culture blanks (without diatom cell) showed no bands during the gel-electrophoresis (Fig. S5.1).

Cas9 digest of chloroplast-derived 16S-rRNA gene amplicons

The 16S rRNA gene amplicons generated by nested low template PCR were cloned into pCR 4-TOPO vectors and transferred into competent *E. coli* cells of the TOPO TA cloning kit (Thermo Fisher, Massachusetts, USA). Plasmids of single colonies were purified with the Plasmid Plus Midi Sample Kit (Qiagen). PCR products were sequenced on an ABI 3130xl Genetic Analyzer; obtained sequences were searched for chloroplast 16S rRNA gene sequences by BLAST search in the PhytoRef database (Decelle et al., 2015). Plasmids containing the respective *Thalassiosira* chloroplast 16S rRNA gene and respective sequences were used for the design of the gRNA.

Design of gRNA

Guide RNAs (gRNAs) were designed for the *T. gravida* chloroplast 16S rRNA gene according to Hopes et al. (2017). Five gRNA sequences were selected for in vitro testing by comparison with endosymbiotic derived 16S rRNA gene amplicons and gRNAs lacking homology in the PAM sequences and therefore not cut by the gRNA mediated Cas9 (Hsu et al., 2013). Subsequently, the selected gRNAs were tested for their efficiency in directing Cas9 digestion of the *T. gravida* chloroplast 16S rRNA gene by OmicronCR, Norwich, UK.

Selection of the most suitable gRNA

The five gRNA sequences were aligned to the chloroplast sequence of a total of 15 diatom families retrieved from the PhytoREF plastidal 16S rRNA database (Decelle et al., 2015). The gRNA which cut the central V4 region of chloroplast ASV-16S RNA sequences in a highly conserved region was selected (Fig. S5.2). To determine the general utility of SCHoCO-seq for diverse diatom taxa, we searched for matching crRNA target sequences in the full PhytoREF database (Decelle et al., 2015). In addition, we searched the SILVA database V138 (Quast et al., 2013) for potential off-target sequences to further test whether a loss of microbial 16S rRNAs occurred due to unwanted Cas9 digestions. We allowed two mismatches to include potential off-targets with a 4% probability given the low mismatch tolerance of CRISPR-Cas9 (Anderson et al., 2015). Furthermore, we evaluated in-silico the phylogenetic range of the diatom chloroplast sequences not only regarding matching gRNA, but also regarding the outer and

inner primers of the SCHoCO-seq approach. For this purpose, we also relied on the PhytoREF database. Chloroplast sequences with 100% matches to all primers and the gRNA were aligned with kalign (Lassmann, 2019) and an unrooted phylogenetic tree was built with FastTree (Price et al., 2009). Taxonomic annotations were transferred from the PhytoREF database (Decelle et al., 2015).

Synthesis of sgRNA

The single guide RNA (sgRNA) comprised two specific sequences: the CRISPR RNA (crRNA) containing the complementary sequence to the target sequence, and the trans-activating-crRNA (tracrRNA) guiding and stabilizing the Cas9 nuclease (Hiranniramol et al., 2020). Both parts were derived from respective oligonucleotides (universal oligo: 5'-AAAAAAGCACCGACTCGGTGCCACTTTTTCAAGTTGATAACGGACTAGCCTTATTTTAACTTGCTATTTCT-3', specific oligo: 5'-TAATACGACTCACTATAGGAAGTCAACTGTTAAATCTTGGTTTTAGAGCTAGAAATAG-3') (Eurofins, Hamburg, Germany) which were grafted together and amplified in a PCR forming the double-stranded sgRNA template. For this reaction to succeed the two oligonucleotides must share a common overlapping sequence (linker) as well as binding sequences for a forward and reverse primer (Fig S5.2).

PCR was set up to 50 µL, containing 5 x Phusion Plus buffer (10 µL), a sgRNA specific oligo (1 µL, 0.1 µM), T7 sgRNA oligo 2 (1 µL, 0.1 µM), T7sgRNA Forward (3.75 µL, 10 µM), T7sgRNA Reverse (3.75 µL, 10 µM), dNTPs (1.5 µL 10 µM), Phusion polymerase (0.5 µL) and PCR grade water (28.5 µL) (all Jena Bioscience, Germany). PCR conditions were: initial denaturing (98°C, 30 s), 30 cycles of denaturing (98°C, 10 s), annealing (51°C, 10 s), and elongation (72°C, 15 s); final elongation (72°C, 10 min.). The sgRNA was synthesized by *in-vitro* transcription as followed: 20 µL containing High Yield T7 reaction buffer (2 µL), DTT (2 µL, 100 mM), ATP, GTP, CTP, UTP (each 1.5 µL, 100 mM), High Yield T7 RNA Polymerase Mix (2 µL), template DNA (2 µL) and PCR grade water (4 µL) (Jena Bioscience, Germany). The reaction mix was incubated for 11 h at 37.5 °C, followed by a DNAse I digest (1 µL RNAse free DNAse I, Jena Bioscience) for 15 min at 37°C. The sgRNA was purified using the RNA clean & concentrator-5 kit (Zymo Research, USA) and the gRNA synthesis was checked for correct product size with an RNA Nano Chip Assay on a 2100 Bioanalyzer device (Agilent Technologies, Santa Clara, California, USA).

In-vitro digestion of 16S amplicons using Cas9 and gRNA

The Cas9 digest was performed after the amplification and purification of the V1-V9 region of the prokaryotic 16S rRNA and prior to the 16s rRNA V4 amplicon sequencing library preparation. The Cas9 Nuclease (New England Biolabs, USA) and the gRNA were assembled in a 27 µL reaction containing PCR grade Water (20 µL), Cas9 Buffer (3.5 µL), gRNA (150 nM, 3 µL) and Cas9 (1 µM, 0.5 µL) by incubating at 25°C for 10 min. The 16S rRNA gene was digested by adding 3 µL of 15 nM target DNA to the mixture and incubating it at 37°C overnight (~11 h).

The sample was cleaned with the MinElute PCR Purification kit (Qiagen).

Illumina Sequencing of partial 16S rRNA genes

The amplicon library was constructed according to the manufacturer's protocol for 16S metagenomic sequencing library preparation, described in Ahme et al. (2023). The library was sequenced on the MiSeq System (Illumina, San Diego, USA) according to the MiSeq Reagent Kit v3 (600 cycles) (Illumina). Forward Primer: MS_v4_515F_N: 5'-TCGTCGGCAGCGTCAGATGTGTATAAGAGACAG+GTGCCAGCMGCCGCGGTAA-3' (Apprill et al., 2015), Reverse Primer: MS_v4_806R_1: 5'-GTCGTCGGCAGCGTCAGATGTGTATAAGAGACAG+GGACTACHVGGGTWTCTAAT-3' (Parada et al., 2016).

Processing of sequence data

FASTQ files were demultiplexed according to the 'Generate FASTQ workflow' of the MiSeq sequencer software. Primers were removed with cutadapt v2.8 (Martin, 2011), and sequence data were processed with the DADA2 R package (quality trimming, denoising, merging, removal of chimeras, Callahan et al., 2016). The resulting Amplicon Sequence Variants (ASVs) were taxonomically annotated with the SILVA v138 database (Quast et al., 2013). Details about the FASTQ and ASV data processing pipeline are described in Ahme et al. (2023). Statistical analyses were performed in R version 4.1.2 (R Studio, Inc. 2021; www.r-project.org).

Analysis of single-cell diversity and bacterial community composition:

ASVs were excluded from a sample if 1) their relative contribution to the respective sample was smaller than 0.25% as recommended by Reitmeier et al (2021) 2) ASVs represent common contaminants according to Sheik et al. (2018) 3) ASVs were known to be derived from non-marine sources (see supplemental Table S5.6). Samples with sequencing depths contained in the lower 10% quantile of the whole dataset, or below 10000 reads, were excluded from the analysis. ASV count tables were scaled by subsampling using the SRS package (Beule and Karlovsky, 2020) and normalized by power transformation ($X^{0.25}$). Graphical representation was done with the Phyloseq package (McMurdie and Holmes, 2013).

Statistical analysis of single-cell samples:

Richness and Shannon diversity of the *T. gravida* single-cell samples were determined using the "microbiome" package (Lahti, 2017). To test for significant effects on ASV richness and Shannon diversity as a response to strain identity (A1; A2; A5), culture condition (full medium; -N; -Vit) and DNA processing method (SC-EXT; SC-PCR), three-way ANOVAs were calculated with subsequent Tukey's post-hoc tests. To evaluate differences in microbiome community composition across *T. gravida* strains and culture conditions, a Bray-Curtis distance matrix was calculated from the down-sampled and normalized ASV count data, serving as input for ordination of a principal component analysis. PERMANAOVA was applied on the Bray-Curtis distance matrix as dependent variable, and strain identity and culture condition as independent variables using the "adonis2" function of the "vegan" package (Oksanen et al., 2013). To obtain a more detailed analysis on microbiome composition and its drivers, bacterial ASVs were aggregated and subset to the genus level. Normalized count subsets for each genus were tested for differences across strains and culture conditions using two-way ANOVAs.

Analysis of SCHoCO-seq samples:

Bacterial ASV data of single-cells of *T. gravida* strains A1, A2 and A5 were quality-filtered, down-sampled and normalized as described above. After richness calculation, an ANOVA was conducted to test for differences in bacterial ASV richness as a response to SCHoCO-seq treatment (compared to SC-seq control treatment). The respective diatom single-cell ID (of

which the DNA product for both treatments originated) was treated as a random factor. To test for differences in relative proportions of bacterial ASVs, chloroplast ASVs, and mitochondrial ASVs as a response to SCHoCO-seq, a t-test was conducted to compare the relative proportion of each ASV category compared to the control treatment. To evaluate the effect of sequencing depth on the relative proportion of bacterial, chloroplast, and mitochondrial ASVs, 1000 replicates of random subsamples (each containing 500, 1000, 5000, and 10000 ASVs) were generated from each sample.

The incidence rate ratio (IRR) represents the probability of detecting a bacterial family with SCHoCO-seq compared to SC-seq. The IRR was estimated by comparing the ASV counts per family using a generalized linear model with Poisson regression and log-link function in R at a significance level of $p < 0.05$. Positive values indicate a significant increase in the detection probability, while negative values indicate a significant decrease in the detection probability.

Results

Single-cell diversity & bacterial community composition analysis

The 16S rRNA ASV richness and Shannon diversity of the *T. gravida* single-cell microbiomes was strain specific and impacted by culture condition, but not affected by single-cell DNA processing methods (Table S5.7, Fig. S5.3). The differences were mainly caused by strain A1 which showed a significantly higher richness and Shannon diversity in the nitrogen- and vitamin-deplete media compared to the full medium (Fig. S5.4).

Moreover, the 16S rRNA gene ASV community composition of the single-cell *T. gravida*-associated microbiomes differed significantly in response to strain identity and culture conditions (Table S5.8). The genotypic specificity regarding microbiome community composition was reflected on the single-cell level, particularly for highly abundant bacterial groups. This is supported by distinct genotype-specific clustering in the principal component analysis (PCA) (Fig. 5.1). However, normalized read counts for multiple bacterial genera differed significantly between diatom strains and culture conditions (Table S5.9). Furthermore, no bacterial genus was consistently present across all analyzed single-cell replicates and strains (Fig. 5.2). Yet, 8 of the 48 detected bacterial genera occurred across all tested strains, but with differences in abundance and frequency between single-cells. Within the fraction of shared bacterial genera, the *Sulfitobacter, Colwellia* and *Roseobacter* clades showed the highest

normalized reads and were particularly abundant in strain A1. Moreover, strain A1 shared three bacterial genera exclusively with strain A2 (most importantly *Glaciecola* and *Paraglaciecola*) and four bacterial genera exclusively with strain A5, of which *Polaribacter* was the most abundant genus. In strain A1, eight unique bacterial genera were found, with *Aurantivirga* as the most abundant genus. For strain A2 and A5, ten unique bacterial genera were found each, of which *Lentilitoribacter* showed the highest abundance in strain A2 and *Octadecabacter* clade in strain A5.

Multiple bacterial groups showed significantly different abundance under specific culture conditions (Table S5.9, Fig. 5.2). This was evident for *Marinobacter*, which increased in abundance in vitamin-deplete treatments, as well as *Colwellia* showing an increase in abundance under nitrogen-deplete culture conditions.

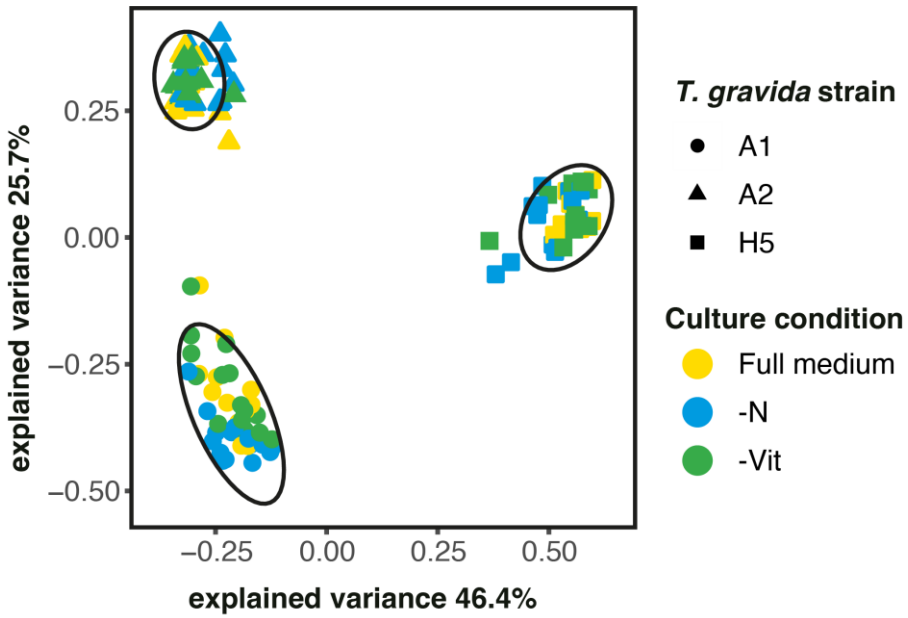

Figure 5.2: Principal component analysis of Bray-Curtis distances from *T. gravida* single-cell microbiomes in different culture media, including Full K medium (yellow), nitrogen -deplete medium (-N, blue), and vitamin-deplete medium (-Vit, green) based on normalized 16S ASV data. Ellipses (confidence level = 0.95) show clusters of the respective *T. gravida* strain (indicated by shape).

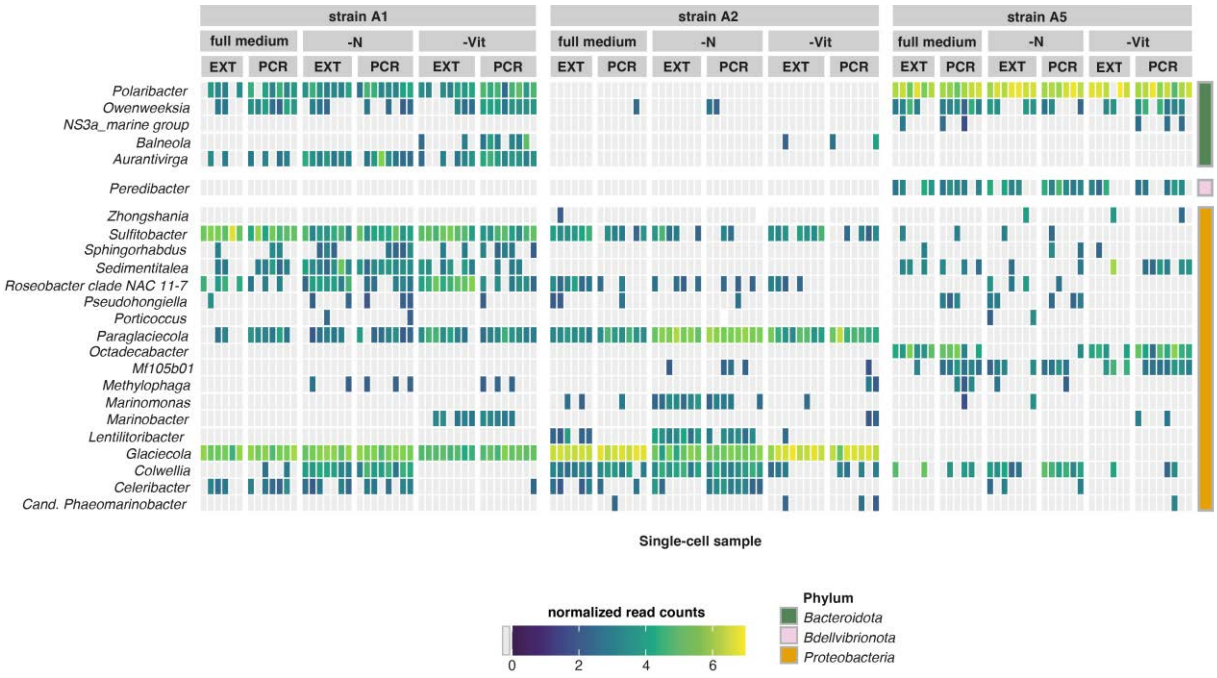

Figure 5.3: Normalized (subsampled and power-transformed [$X^{0.25}$]) 16S rRNA gene ASV read counts (indicated by continuous color scale, gray = not detected) summarized on the genus level (y-axis) across *T. gravida* single-cell samples (x-axis). *T. gravida* strains and culture conditions are indicated by vertical facets. Genera are ordered by Phylum (displayed as discrete color scale (right). Genera occurring in less than 4 samples were excluded from the plot. Single-cell sample treatments indicated with; full medium = modified K medium, -Vit = Vitamin limited Medium, -N = Nitrogen limited medium, EXT = Single-cell DNA extraction (SC-EXT), PCR = direct Single-Cell PCR (SC-PCR)

SCHoCO-seq results

The SCHoCO-seq treatment significantly affected the relative proportions of all ASV categories (bacterial, chloroplast, and other ASVs) of the single-cell microbiomes (Table 5.1, Fig. 5.4). On average, chloroplast ASVs in a given single diatom-cell accounted for 71.4 ± 14.3% of total reads in SC-seq control treatments, but were reduced in the SCHoCO-seq treatment to 17.5 ± 12.8%. Bacterial ASVs, which on average accounted for 25.9 ± 14.7% in the SC-seq control, increased to 71.0 ± 16.7% in the SCHoCO-seq treatment. Random subsampling across ranges of sequencing depth showed that with increasing sequencing depth mostly bacterial 16S ASVs were detected in a theoretical ASV composition in the SCHoCO-seq treatment, whereas increasing sequencing depth in the SC-seq control treatment mainly resulted in more chloroplast ASV reads.

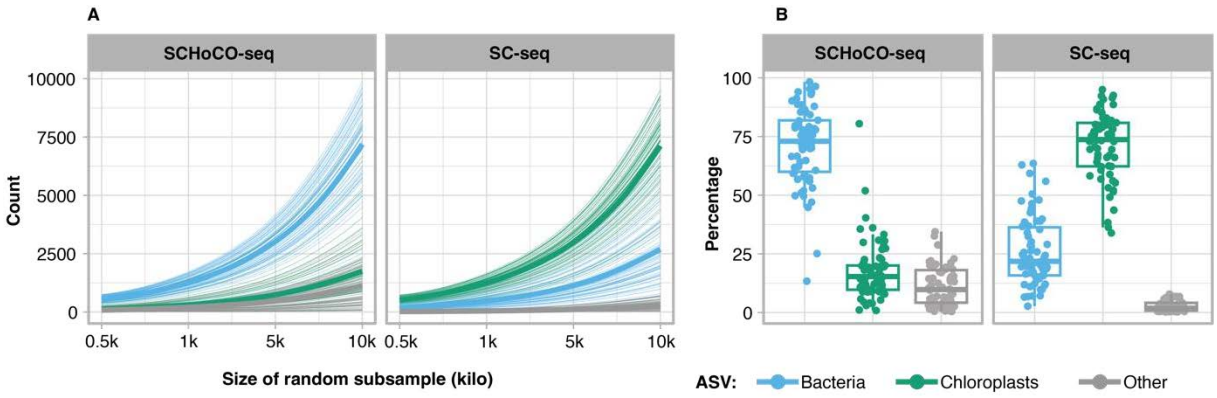

Figure 5.4: Effect of Cas9 plastidal 16S rRNA gene amplicon digest on total read composition and as a function of a range of assumed sequencing depths. The line plots show the theoretical composition of each sample if it was sequenced at different depths (obtained from random subsamples of the original dataset). Thin lines represent the ASV composition of each of the 62 samples after (SCHoCO-seq) and prior (SC-seq) to the cas9 digest. Bold lines are means obtained from the respective ASV compositions (A). Boxplots represent the percentage of the actual read composition of the ASVs, summed by annotation. 'Bacteria' refers to all bacterial ASVs after removal of a) potential contamination and b) ASVs without annotations at least at the order level. 'Chloroplasts' refers to all ASVs annotated as chloroplasts, and 'Others' refers to mitochondria-derived ASVs and ASVs with no annotation at least at the order level (B).

Table 5.1: Results of Welch t-tests on relative proportions of the ASV categories bacteria, chloroplasts and other 16S rRNA gene ASVs as a response to SCHoCO-seq. Bacteria refer to all bacterial ASVs after removal of a) potential contamination and b) ASVs without annotations at least at the order level. Chloroplasts refer to all ASVs annotated as chloroplasts, and 'Other' refer to mitochondria-derived ASVs and ASVs with no annotation at least at the order level. Mean proportions of ASV-categories are given in percent ± standard deviation. T- and p-values are reported for the treatment effect for each ASV category. Values marked with an asterisk (*) indicate significant effects ($p < 0.05$).

	% in Cas9 sample	% in No Cas9 sample	*p*-value	*t*-value
Bacteria	71.0 ± 16.7	25.9 ± 14.7	<0.001	15.94
Chloroplast	17.5 ± 12.8	71.4 ± 14.3	<0.001	-22.11
Other	11.5 ± 8.3	2.7 ± 2.1	<0.001	8.17

By increasing the overall proportion of bacterial ASV reads (Fig. 5.4), SCHoCO-seq significantly increased the probability of detecting several bacterial families compared to SC-seq (Fig. 5.5A). There was no significant decrease in the detection probability for any bacterial family. The increase in IRR values was particularly pronounced for *Sphingomonadaceae*, where the ASV counts were approximately 16 times higher compared to SC-seq. *Methylophilaceae, Rhizobiaceae, Parvibaculaceae* and *Cryomorphaceae* also showed comparably high IRR values with IRRs > 5. The SCHoCO-seq approach additionally identified the bacterial phylum

Verrucomicrobiota, which was not covered by the SC-seq control (Fig. 5.2). Consistently, there was a significant increase in the IRR value for a total of six families within these phyla.

In line, the ANOVA results indicated a significant effect of SCHoCO-seq treatment on bacterial ASV richness (Fig. 5.5B, Table S5.10). Single-cell samples without Cas9 digest (SC-seq) had a mean ASV richness of 10.4 ± 3.2 (strain A1), 6.5 ± 3.3 (strain A2), and 5.6 ± 1.8 (strain A5). In SCHoCO-seq treatments, richness increased to 15.0 ± 3.7 (strain A1), 8.4 ± 3.4 (strain A2), and 8.1 ± 1.5 (strain A5), corresponding to a richness increase of 51%, 53%, and 56%, respectively.

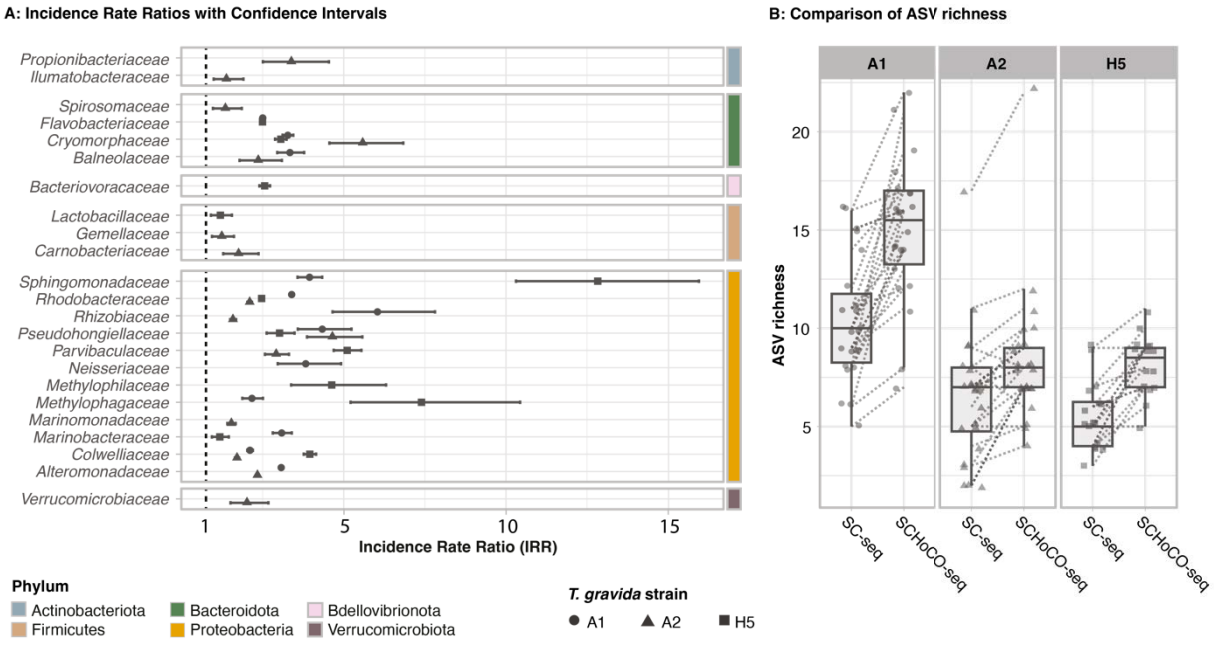

Figure 5.5: Performance comparison of 62 SCHoCO-seq and SC-seq sample pairs on A: the differences in the probability of detecting a given bacterial family level based on ASV counts per sample and B) the actual total ASV richness. In A, bacterial families for which a significant change in the Incidence Rate Ratio could be detected are shown, with error bars representing the 95% confidence interval. The dotted line marks the boundary between a decrease in IRR (<1) and an increase in IRR (>1).

In-silico gRNA specificity

The selected gRNA and the search for corresponding crRNA target sequences in the full PhytoREF databases resulted in a perfect match (100%) with 969 of the 1068 available diatom sequences (~90%), spanning various taxonomic lineages (Fig. 5.6A). Of 99 sequences not matching the crRNA, 85 had at least no genus-level annotation, rendering their taxonomic

identification elusive. Identification of potential Cas9 off-targets based on the 16S rRNA gene SSU sequences obtained from the SILVA V138 database resulted in 100% matches to only 644 sequences annotated as chloroplast and one mitochondrial hit. However, there were no other matches to any of the 451,459 16S rRNA gene SSU sequences, indicating no potential Cas9 off-targets for the selected gRNA. Low-probability potential off-targets (i.e., considering a gRNA sequence match of 96%, (Hsu et al., 2013)) were identified for 117 16S rRNA gene SSUs, representing only a fraction of 0.025% of the sequence representatives in the SILVA V138 database. The evaluation of the phylogenetic range of the diatom chloroplast sequences based on the crRNA target sequence and the outer and inner primers used for SCHoCO-seq resulted in 62 matches, spanning at least 3 families and 12 orders (Fig. 5.6B). It should be noted that this relatively low number compared to the gRNA matches is due to the fact that only ~20% of sequences in PhytoREF are long enough to fully cover both primer binding sites.

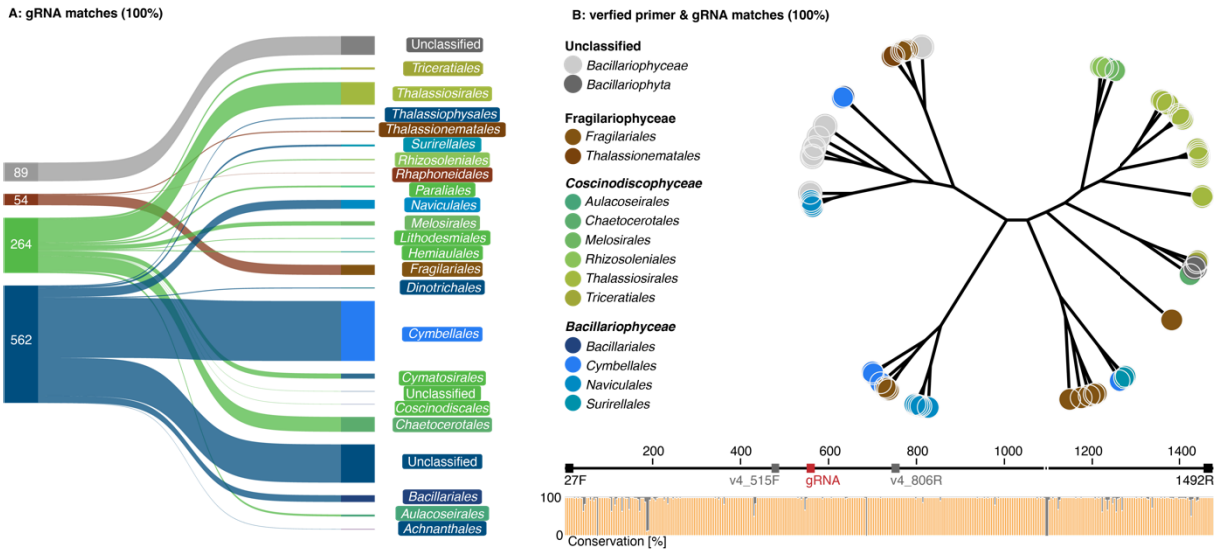

Figure 5.6: Coverage of taxonomic lineages with perfect gRNA sequence matches (A) and perfect matches with all primer pairs used in this study (B). Numbers in (A) refer to the gRNA chloroplast sequence matches for each diatom family. The bottom panel in (B) shows the primer binding sites and nucleotide conservation of 62 diatom chloroplast sequences; the corresponding unrooted phylogenetic tree shows the order-level annotations as indicated in the PhytoREF database.

Discussion

This study demonstrated that diatom microbiomes under investigation were mostly strain-specific and that the different micro-/macronutrient limitations treatments modulated the abundance of single microbiome members. The SCHoCO-seq treatment enabled in depth assessment of the microbial diversity in algal microbiomes on single-cell host level by reducing

chloroplast ASV reads while increasing sequencing depth for bacterial ASVs. Consequently, SCHoCO-seq led to increased microbiome richness and detected rare microbial taxa which were not found with standard 16S rRNA gene single-cell metabarcoding. Our *in-silico* analyses identified a 100% match to 969 of the potential 1068 crRNA target sequences in PhytoREF databases, suggesting the newly developed protocol to be applicable to a wide range of diatom species with no apparent 16S rRNA gene off-target effects.

With respect to genotype-specific microbiomes of *T. gravida*, strain A1 and A2 were more similar to each other than to strain A5. Despite differing dates of isolation, variations in microbiome composition were most likely explained by the biogeographic distance of their sampling origin (table S1), as microbiomes of laboratory cultures have been shown to be stable over long periods of time (Barreto Filho et al., 2021). Yet, although strain A1 and A2 originated from the same location, their microbiomes still showed differences in richness and diversity, highlighting the necessity for a single-cell perspective when profiling natural phytoplankton microbiomes.

Previous studies discussed the possibility of a core microbiome, i.e., a fraction of microbiome bacteria consistently present across diatom genotypes (Behringer et al., 2018, Monnich et al., 2020). However, the probability to detect a core microbiome likely decreases with increasing sampling size, biogeographic distance and region. For example, Ahern et al. (2021) found no shared ASVs across 85 *Thalassiosira rotula* strains from various ocean provinces. Yet, for the *T. gravida* strains in this study, a shared core community across the studied genotypes was indeed found, although not consistently across all single-cell replicates. This finding reflects the diatom's Arctic origin, where host-microbe associations are more stable due to co-evolution under hard selection compared to the soft selection in temperate regions (Malmstrom et al., 2007). Remarkably, the shared core microbial community consisted of the genera *Colwellia*, *Roseobacter clade NAC11-7 lineage* as well as *Sulfitobacter,* also belonging to the *Roseobacter* group. Particularly the *Sulfitobacter* genus evolved complex mutualistic-symbiotic interactions with phytoplankton of which the underlying mechanisms are comparably well understood and include bacteria-derived provision of auxin and ammonium for their host (Amin et al., 2015, Segev et al., 2016), as well as specific antibiotics to protect the holobiont from parasitic bacteria (Beiralas et al., 2023). In exchange, *Sulfitobacter* receive various forms of exudated organic carbon from the diatom host, as well as dimethylsulfoniopropionate (DMSP) for sulfur oxidation, and amino acids like tryptophan and taurine as organic nitrogen source (Amin et al., 2015, Segev et al., 2016, Yang et al., 2021).

Moreover, the *T. gravida* microbiomes responded to nitrogen- or vitamin-limited culture conditions with compositional changes of few specific bacterial genera. Considering that the nitrogen- and vitamin-limited cultures were inoculated from a full medium culture, the fact that certain bacterial groups were only retrieved in the limitation treatments suggests that these rare microbiome taxa may become abundant only during abiotic stress. This is exemplified for strain A1, where *Marinobacter* increased in abundance in the vitamin-limited treatments. *Marinobacter* are known for their ability to produce siderophores, potentially providing iron to their host (Amin et al., 2009, Butler et al., 2021). *Marinobacter* have also been associated with potential vitamin supply for the marine dinoflagellate *Lingulodinium polyedrum* (Cruz-Lopez and Maske, 2016). For the genus *Balneola*, an increase in the nutrient-limited treatments was observed for *T. gravida* strain A1. However, these increases were not necessarily due to a mutualistic interaction but may also indicate opportunistic mechanisms. In fact, Zhu et al. (Zhu et al., 2021) hypothesized that *Balneola* has the ability to degrade specific organic compounds released by plants and potentially also phytoplankton upon encounter of nutrient stress. Moreover, diatoms have been shown to regulate their microbiome by target-specific secondary metabolites like rosmarinic acid or azelaic acid (Shibl et al., 2020), yet whether this was the case in our experiments remains elusive.

Studying microbiome diversity in laboratory cultures is influenced not only by the fact that most heterotrophic bacteria cannot be cultured (Vartoukian et al., 2010), but also by the dynamics of the microbiome community itself. Certain culture conditions may favor the growth of specific bacterial groups, thus underestimating bacterial richness. Conversely, shifts in evenness may allow the detection of bacterial groups that perform essential services for their host and represent an insurance for the holobiont in case of perturbations, while others remain undetected. This highlights the importance of considering microbiome community dynamics and the potential for different culture conditions to reveal distinct aspects of the microbiome's diversity and functional roles. Additionally, considering the isolation bias in terms of species- and even genotype-specificity of microbiome composition (Baker and Kemp, 2014, Ahern et al., 2021), our findings underline the necessity for (semi-) quantitative *in-situ* single-cell data on microbiome composition.

The bacterial richness in *T. gravida* microbiomes obtained in this study at the single-cell level by SCHoCO-seq agrees with richness data obtained from bulk diatom samples ranging from 1 to 125 ASVs or OTUs, respectively (Baker and Kemp, 2014, Behringer et al., 2018, Ahern et al., 2021, Sison-Mangus et al., 2014). To recover the full bacterial community richness on a

given single diatom cell (preceding the SCHoCO-seq protocol), both the SC-PCR and SC-EXT methods developed in this study have been equally accurate as reflected by insignificant statistical test results. Both single-cell methods are therefore applicable depending on the research objective. For example, the SC-EXT approach offers the advantage of enabling multiple PCR reactions for further genomic DNA based investigations, such as metagenomics or host identification via 18S sequencing, and the long-term storage of the sample (Hallmaier-Wacker et al., 2018).

The SCHoCO-seq approach is a promising strategy to accurately analyze diatom host-associated microbiome ASVs. This is largely due to the reduction of chloroplast reads, which in turn boost the detection and resolution of the microbiome richness. Furthermore, our subsampling approach showed that the increase of microbiome ASVs over various sequencing depths by SCHoCO-seq was higher than the corresponding increase in chloroplast ASVs (Fig. 3). Importantly, this pattern was the opposite without Cas9 treatment, suggesting that merely increasing the sequencing depth is not an efficient strategy to recover rare microbiome ASVs. Therein, SCHoCO-seq is particularly valuable in resolving the bacterial diversity of diatom microbiomes that harbor low bacterial abundance in their phycosphere. Thus, especially due to its potential to reveal higher community richness and identify potentially rare bacterial taxa in the phycosphere, SCHoCO-seq has the potential to become the preferred method in diatom microbiome diversity research. Indeed, by identifying rare bacterial taxa, taxon shifts, gains and losses, the overall genetic diversity in diatom microbiomes can be more accurately assessed, thereby increasing our knowledge of microbiome community assembly (Monnich et al., 2020), regulation and modulation. As microbiome genetic diversity and variation are aligned to selection (Baltar et al., 2019), these capabilities are particularly relevant under current global change conditions. SCHoCO-seq therefore bears potential to assess and distinguish diatom microbiome responses to environmental change, e.g., plasticity, resilience, functional redundancy and dysbiosis of diatom holobionts (Baltar et al., 2019, Graham et al., 2016).

Conclusion

This study revealed a) genotype-specific diatom microbiomes identified through single-cell isolation and b) that diatom holobionts respond to macro- and micro-nutrient limitations with compositional changes of their microbiome. To increase the discovery of rare bacterial taxa as part of diatom microbiomes, we have developed SCHoCO-seq which increases the bacterial

biodiversity (richness) by reducing the chloroplast 16S ASVs. Thus, this novel single-cell microbiome analysis may serve as an important steppingstone towards *in-situ* single-cell microbiome analysis. The latter will help to understand how phytoplankton-associated microbiomes function in natural systems. In addition, the method presented here for reducing host DNA contamination with the aid of Cas9 can be applied to various other host-microbiome systems by adapting the sequence of the guide RNA.

Acknowledgments

The authors thank the working group for their support.

Study Funding

This research was funded by the Helmholtz research program 'Changing Earth, Sustaining our Future' (subtopic 6.2 'Adaptation of marine life: from genes to ecosystems' in topic 6 'Marine and Polar Life') of the Alfred Wegener Institute Helmholtz Centre for Polar and Marine Research, Germany. Furthermore, we acknowledge the support by the Open Access Publication Funds of Alfred-Wegener-Institut Helmholtz-Zentrum für Polar- und Meeresforschung.

Author Contributions

Ruben Schulte-Hillen and Jakob Giesler contributed equally to this work and share first authorship. For the purposes of applications, proposals and outreach, either author may list themselves first.

Data availability

All raw sequence data used in this study will be made available upon publication.

References

AHERN, O. M., WHITTAKER, K. A., WILLIAMS, T. C., HUNT, D. E. & RYNEARSON, T. A. 2021. Host genotype structures the microbiome of a globally dispersed marine phytoplankton. *Proc Natl Acad Sci U S A,* 118.

AHME, A., VON JACKOWSKI, A., MCPHERSON, R. A., WOLF, K. K. E., HOPPMANN, M., NEUHAUS, S. & JOHN, U. 2023. Winners and Losers of Atlantification: The Degree of Ocean Warming Affects the Structure of Arctic Microbial Communities. *Genes (Basel),* 14.

AMIN, S. A., GREEN, D. H., KUPPER, F. C. & CARRANO, C. J. 2009. Vibrioferrin, an unusual marine siderophore: iron binding, photochemistry, and biological implications. *Inorg Chem,* 48**,** 11451-8.

AMIN, S. A., HMELO, L. R., VAN TOL, H. M., DURHAM, B. P., CARLSON, L. T., HEAL, K. R., MORALES, R. L., BERTHIAUME, C. T., PARKER, M. S., DJUNAEDI, B., INGALLS, A. E., PARSEK, M. R., MORAN, M. A. & ARMBRUST, E. V. 2015. Interaction and signalling between a cosmopolitan phytoplankton and associated bacteria. *Nature,* 522**,** 98-101.

AMIN, S. A., PARKER, M. S. & ARMBRUST, E. V. 2012. Interactions between diatoms and bacteria. *Microbiol Mol Biol Rev,* 76**,** 667-84.

ANDERSON, E. M., HAUPT, A., SCHIEL, J. A., CHOU, E., MACHADO, H. B., STREZOSKA, Z., LENGER, S., MCCLELLAND, S., BIRMINGHAM, A., VERMEULEN, A. & SMITH, A. 2015. Systematic analysis of CRISPR-Cas9 mismatch tolerance reveals low levels of off-target activity. *J Biotechnol,* 211**,** 56-65.

APPRILL, A., MCNALLY, S., PARSONS, R. & WEBER, L. 2015. Minor revision to V4 region SSU rRNA 806R gene primer greatly increases detection of SAR11 bacterioplankton. *Aquatic Microbial Ecology,* 75**,** 129-137.

BAKER, L. J. & KEMP, P. F. 2014. Exploring bacteria–diatom associations using single-cell whole genome amplification. *Aquatic Microbial Ecology,* 72**,** 73-88.

BALTAR, F., BAYER, B., BEDNARSEK, N., DEPPELER, S., ESCRIBANO, R., GONZALEZ, C. E., HANSMAN, R. L., MISHRA, R. K., MORAN, M. A., REPETA, D. J., ROBINSON, C., SINTES, E., TAMBURINI, C., VALENTIN, L. E. & HERNDL, G. J. 2019. Towards Integrating Evolution, Metabolism, and Climate Change Studies of Marine Ecosystems. *Trends Ecol Evol,* 34**,** 1022-1033.

BARRETO FILHO, M. M., WALKER, M., ASHWORTH, M. P. & MORRIS, J. J. 2021. Structure and Long-Term Stability of the Microbiome in Diverse Diatom Cultures. *Microbiol Spectr,* 9**,** e0026921.

BEHRINGER, G., OCHSENKUHN, M. A., FEI, C., FANNING, J., KOESTER, J. A. & AMIN, S. A. 2018. Bacterial Communities of Diatoms Display Strong Conservation Across Strains and Time. *Front Microbiol,* 9**,** 659.

BEIRALAS, R., OZER, N. & SEGEV, E. 2023. Abundant Sulfitobacter marine bacteria protect *Emiliania huxleyi* algae from pathogenic bacteria. *ISME Commun,* 3**,** 100.

BEULE, L. & KARLOVSKY, P. 2020. Improved normalization of species count data in ecology by scaling with ranked subsampling (SRS): application to microbial communities. *Peerj,* 8.

BOSCARO, V., MANASSERO, V., KEELING, P. J. & VANNINI, C. 2023. Single-cell Microbiomics Unveils Distribution and Patterns of Microbial Symbioses in the Natural Environment. *Microb Ecol,* 85**,** 307-316.

BUTLER, A., HARDER, T., OSTROWSKI, A. D. & CARRANO, C. J. 2021. Photoactive siderophores: Structure, function and biology. *J Inorg Biochem,* 221**,** 111457.

CALLAHAN, B. J., MCMURDIE, P. J., ROSEN, M. J., HAN, A. W., JOHNSON, A. J. A. & HOLMES, S. P. 2016. DADA2: High-resolution sample inference from Illumina amplicon data. *Nature Methods,* 13**,** 581-+.

CIRRI, E. & POHNERT, G. 2019. Algae-bacteria interactions that balance the planktonic microbiome. *New Phytol,* 223**,** 100-106.

CRUZ-LOPEZ, R. & MASKE, H. 2016. The Vitamin B1 and B12 Required by the Marine Dinoflagellate *Lingulodinium polyedrum* Can be Provided by its Associated Bacterial Community in Culture. *Front Microbiol,* 7**,** 560.

DECELLE, J., ROMAC, S., STERN, R. F., BENDIF EL, M., ZINGONE, A., AUDIC, S., GUIRY, M. D., GUILLOU, L., TESSIER, D., LE GALL, F., GOURVIL, P., DOS SANTOS, A. L., PROBERT, I., VAULOT, D., DE VARGAS, C. & CHRISTEN, R. 2015. PhytoREF: a reference database of the plastidial 16S rRNA gene of photosynthetic eukaryotes with curated taxonomy. *Mol Ecol Resour,* 15**,** 1435-45.

DITTAMI, S. M., ARBOLEDA, E., AUGUET, J. C., BIGALKE, A., BRIAND, E., CARDENAS, P., CARDINI, U., DECELLE, J., ENGELEN, A. H., EVEILLARD, D., GACHON, C. M. M., GRIFFITHS, S. M., HARDER, T., KAYAL, E., KAZAMIA, E., LALLIER, F. H., MEDINA, M., MARZINELLI, E. M., MORGANTI, T. M., NUNEZ PONS, L., PRADO, S., PINTADO, J., SAHA, M., SELOSSE, M. A., SKILLINGS, D., STOCK, W., SUNAGAWA, S., TOULZA, E., VOROBEV, A., LEBLANC, C. & NOT, F. 2021. A community perspective on the concept of marine holobionts: current status, challenges, and future directions. *PeerJ,* 9**,** e10911.

FRANK, J. A., REICH, C. I., SHARMA, S., WEISBAUM, J. S., WILSON, B. A. & OLSEN, G. J. 2008. Critical evaluation of two primers commonly used for amplification of bacterial 16S rRNA genes. *Applied and Environmental Microbiology,* 74**,** 2461-2470.

GIESLER, J. K., HARDER, T. & WOHLRAB, S. 2023. Microbiome and photoperiod interactively determine thermal sensitivity of polar and temperate diatoms. *Biology Letters,* 19.

GRAHAM, E. B., KNELMAN, J. E., SCHINDLBACHER, A., SICILIANO, S., BREULMANN, M., YANNARELL, A., BEMAN, J. M., ABELL, G., PHILIPPOT, L., PROSSER, J., FOULQUIER, A., YUSTE, J. C., GLANVILLE, H. C., JONES, D. L., ANGEL, R., SALMINEN, J., NEWTON, R. J., BURGMANN, H., INGRAM, L. J., HAMER, U., SILJANEN, H. M., PELTONIEMI, K., POTTHAST, K., BANERAS, L., HARTMANN, M., BANERJEE, S., YU, R. Q., NOGARO, G., RICHTER, A., KORANDA, M., CASTLE, S. C., GOBERNA, M., SONG, B., CHATTERJEE, A., NUNES, O. C., LOPES, A. R., CAO, Y., KAISERMANN, A., HALLIN, S.,

STRICKLAND, M. S., GARCIA-PAUSAS, J., BARBA, J., KANG, H., ISOBE, K., PAPASPYROU, S., PASTORELLI, R., LAGOMARSINO, A., LINDSTROM, E. S., BASILIKO, N. & NEMERGUT, D. R. 2016. Microbes as Engines of Ecosystem Function: When Does Community Structure Enhance Predictions of Ecosystem Processes? *Front Microbiol,* 7**,** 214.

HALLMAIER-WACKER, L. K., LUEERT, S., ROOS, C. & KNAUF, S. 2018. The impact of storage buffer, DNA extraction method, and polymerase on microbial analysis. *Sci Rep,* 8**,** 6292.

HIRANNIRAMOL, K., CHEN, Y. H., LIU, W. J. & WANG, X. W. 2020. Generalizable sgRNA design for improved CRISPR/Cas9 editing efficiency. *Bioinformatics,* 36**,** 2684-2689.

HOPES, A., NEKRASOV, V., BELSHAW, N., GROUNEVA, I., KAMOUN, S. & MOCK, T. 2017. Genome Editing in Diatoms Using CRISPR-Cas to Induce Precise Bi-allelic Deletions. *Bio Protoc,* 7**,** e2625.

HSU, P. D., SCOTT, D. A., WEINSTEIN, J. A., RAN, F. A., KONERMANN, S., AGARWALA, V., LI, Y. Q., FINE, E. J., WU, X. B., SHALEM, O., CRADICK, T. J., MARRAFFINI, L. A., BAO, G. & ZHANG, F. 2013. DNA targeting specificity of RNA-guided Cas9 nucleases. *Nature Biotechnology,* 31**,** 827-+.

JACKREL, S. L., OWENS, S. M., GILBERT, J. A. & PFISTER, C. A. 2017. Identifying the plant-associated microbiome across aquatic and terrestrial environments: the effects of amplification method on taxa discovery. *Mol Ecol Resour,* 17**,** 931-942.

KODAMA, Y. & FUJISHIMA, M. 2022. Endosymbiotic *Chlorella variabilis* reduces mitochondrial number in the ciliate *Paramecium bursaria*. *Scientific Reports,* 12.

KUHLISCH, C., SHEMI, A., BARAK-GAVISH, N., SCHATZ, D. & VARDI, A. 2023. Algal blooms in the ocean: hot spots for chemically mediated microbial interactions. *Nat Rev Microbiol*.

LAHTI, L., SHETTY, S. 2017. Tools for microbiome analysis in R. http://microbiome.github.com/microbiome.

LANE D, J. 1991. 16S/23S rRNA sequencing. *Nucleic Acid Techniques in Bacterial Systematics***,** 125-175.

LASSMANN, T. 2019. Kalign 3: multiple sequence alignment of large data sets. *Bioinformatics,* 36**,** 1928-9.

LUNDBERG, D. S., LEBEIS, S. L., PAREDES, S. H., YOURSTONE, S., GEHRING, J., MALFATTI, S., TREMBLAY, J., ENGELBREKTSON, A., KUNIN, V., DEL RIO, T. G., EDGAR, R. C., EICKHORST, T., LEY, R. E., HUGENHOLTZ, P., TRINGE, S. G. & DANGL, J. L. 2012. Defining the core *Arabidopsis thaliana* root microbiome. *Nature,* 488**,** 86-90.

MALMSTROM, R., STRAZA, T., COTTRELL, M. T. & KIRCHMAN, D. 2007. Diversity, abundance, and biomass production of bacterial groups in the western Arctic Ocean. *Aquatic Microbial Ecology - AQUAT MICROB ECOL,* 47**,** 45-55.

MARGULIS, L. 1991. Evolution of Eukaryotes. *American Scientist,* 79**,** 187-188.

MARTIN, K., SCHMIDT, K., TOSELAND, A., BOULTON, C. A., BARRY, K., BESZTERI, B., BRUSSAARD, C. P. D., CLUM, A., DAUM, C. G., ELOE-FADROSH, E., FONG, A., FOSTER, B., FOSTER, B., GINZBURG, M., HUNTEMANN, M., IVANOVA, N. N., KYRPIDES, N. C., LINDQUIST, E., MUKHERJEE, S., PALANIAPPAN, K., REDDY, T. B. K., RIZKALLAH, M. R., ROUX, S., TIMMERMANS, K., TRINGE, S. G., VAN DE POLL, W. H., VARGHESE, N., VALENTIN, K. U., LENTON, T. M., GRIGORIEV, I. V., LEGGETT, R. M., MOULTON, V. & MOCK, T. 2021. The biogeographic differentiation of algal microbiomes in the upper ocean from pole to pole. *Nat Commun,* 12**,** 5483.

MARTIN, M. 2011. CUTADAPT removes adapter sequences from high-throughput sequencing reads. *EMBnet.journal,* 17.

MCMURDIE, P. J. & HOLMES, S. 2013. phyloseq: an R package for reproducible interactive analysis and graphics of microbiome census data. *PLoS One,* 8**,** e61217.

MONNICH, J., TEBBEN, J., BERGEMANN, J., CASE, R., WOHLRAB, S. & HARDER, T. 2020. Niche-based assembly of bacterial consortia on the diatom *Thalassiosira rotula* is stable and reproducible. *ISME J,* 14**,** 1614-1625.

NEEDHAM, D. M., POIRIER, C., BACHY, C., GEORGE, E. E., WILKEN, S., YUNG, C. C. M., LIMARDO, A. J., MORANDO, M., SUDEK, L., MALMSTROM, R. R., KEELING, P. J., SANTORO, A. E. & WORDEN, A. Z. 2022. The microbiome of a bacterivorous marine choanoflagellate contains a resource-demanding obligate bacterial associate. *Nat Microbiol,* 7**,** 1466-1479.

OKSANEN, J., BLANCHET, F. G., KINDT, R., LEGENDRE, P., MINCHIN, P., O'HARA, R. B., SIMPSON, G., SOLYMOS, P., STEVENS, M. H. H. & WAGNER, H. 2013. Vegan: Community Ecology Package. R Package Version. 2.0-10. *CRAN*.

ORUM, H., NIELSEN, P. E., EGHOLM, M., BERG, R. H., BUCHARDT, O. & STANLEY, C. 1993. Single base pair mutation analysis by PNA directed PCR clamping. *Nucleic Acids Res,* 21**,** 5332-6.

PARADA, A. E., NEEDHAM, D. M. & FUHRMAN, J. A. 2016. Every base matters: assessing small subunit rRNA primers for marine microbiomes with mock communities, time series and global field samples. *Environmental Microbiology,* 18**,** 1403-1414.

PRICE, M. N., DEHAL, P. S. & ARKIN, A. P. 2009. FastTree: computing large minimum evolution trees with profiles instead of a distance matrix. *Mol Biol Evol,* 26**,** 1641-50.

PROBANDT, D., EICKHORST, T., ELLROTT, A., AMANN, R. & KNITTEL, K. 2018. Microbial life on a sand grain: from bulk sediment to single grains. *ISME J,* 12**,** 623-633.

QUAST, C., PRUESSE, E., YILMAZ, P., GERKEN, J., SCHWEER, T., YARZA, P., PEPLIES, J. & GLOCKNER, F. O. 2013. The SILVA ribosomal RNA gene database project: improved data processing and web-based tools. *Nucleic Acids Res,* 41**,** D590-6.

REITMEIER, S., HITCH, T. C. A., TREICHEL, N., FIKAS, N., HAUSMANN, B., RAMER-TAIT, A. E., NEUHAUS, K., BERRY, D., HALLER, D., LAGKOUVARDOS, I. & CLAVEL, T. 2021. Handling of spurious sequences affects the outcome of high-throughput 16S rRNA gene amplicon profiling. *ISME Communications,* 1.

ROSSI, A., BELLONE, A., FOKIN, S. I., BOSCARO, V. & VANNINI, C. 2019. Detecting Associations Between Ciliated Protists and Prokaryotes with Culture-Independent Single-Cell Microbiomics: a Proof-of-Concept Study. *Microb Ecol,* 78**,** 232-242.

SCHMITZ, T. C., DEDE EREN, A., SPIERINGS, J., DE BOER, J., ITO, K. & FOOLEN, J. 2021. Solid-phase silica-based extraction leads to underestimation of residual DNA in decellularized tissues. *Xenotransplantation,* 28**,** e12643.

SEGEV, E., WYCHE, T. P., KIM, K. H., PETERSEN, J., ELLEBRANDT, C., VLAMAKIS, H., BARTENEVA, N., PAULSON, J. N., CHAI, L., CLARDY, J. & KOLTER, R. 2016. Dynamic metabolic exchange governs a marine algal-bacterial interaction. *Elife,* 5.

SHEIK, C. S., REESE, B. K., TWING, K. I., SYLVAN, J. B., GRIM, S. L., SCHRENK, M. O., SOGIN, M. L. & COLWELL, F. S. 2018. Identification and Removal of Contaminant Sequences From Ribosomal Gene Databases: Lessons From the Census of Deep Life. *Front Microbiol,* 9**,** 840.

SHIBL, A. A., ISAAC, A., OCHSENKUHN, M. A., CARDENAS, A., FEI, C., BEHRINGER, G., ARNOUX, M., DROU, N., SANTOS, M. P., GUNSALUS, K. C., VOOLSTRA, C. R. & AMIN, S. A. 2020. Diatom modulation of select bacteria through use of two unique secondary metabolites. *Proc Natl Acad Sci U S A,* 117**,** 27445-27455.

SISON-MANGUS, M. P., JIANG, S., TRAN, K. N. & KUDELA, R. M. 2014. Host-specific adaptation governs the interaction of the marine diatom, *Pseudo-nitzschia* and their microbiota. *ISME J,* 8**,** 63-76.

SONG, L. & XIE, K. 2020. Engineering CRISPR/Cas9 to mitigate abundant host contamination for 16S rRNA gene-based amplicon sequencing. *Microbiome,* 8**,** 80.

VARTOUKIAN, S. R., PALMER, R. M. & WADE, W. G. 2010. Strategies for culture of 'unculturable' bacteria. *FEMS Microbiol Lett,* 309**,** 1-7.

YANG, Q., GE, Y. M., IQBAL, N. M., YANG, X. & ZHANG, X. L. 2021. *Sulfitobacter alexandrii* sp. nov., a new microalgae growth-promoting bacterium with exopolysaccharides bioflocculanting potential isolated from marine phycosphere. *Antonie Van Leeuwenhoek,* 114**,** 1091-1106.

ZARRAONAINDIA, I., OWENS, S. M., WEISENHORN, P., WEST, K., HAMPTON-MARCELL, J., LAX, S., BOKULICH, N. A., MILLS, D. A., MARTIN, G., TAGHAVI, S., VAN DER LELIE, D. & GILBERT, J. A. 2015. The soil microbiome influences grapevine-associated microbiota. *mBio,* 6.

ZHU, Z., MENG, R., SMITH, W. O., JR., DOAN-NHU, H., NGUYEN-NGOC, L. & JIANG, X. 2021. Bacterial Composition Associated With Giant Colonies of the Harmful Algal Species *Phaeocystis globosa*. *Front Microbiol,* 12**,** 737484.

6 Synthesis

6 SYNTHESIS

This thesis aimed to improve our understanding of how diatoms adapted to occupy Arctic and temperate habitats not only from an abiotic perspective but also interactively with their microbiomes. The outcome demonstrates the importance of considering interactive effects in holobiont research and gives insights into the common evolutionary history of the studied diatoms and their associated bacteria. The step-wise experimental approach allowed to narrow down the factors of interest from high-resolution single-driver designs to specific relevant multi-driver conditions over simple growth assays to complex multi-omics approaches. The following synthesis discussion integrates the results of the previous chapters by highlighting overarching patterns, contradictory findings, and potential ecological implications. Key outcomes directly related to the thesis objectives (see chapter 1.6) are highlighted throughout the synthesis subchapters. Subsequently, future research perspectives are outlined, building upon the knowledge generated by this thesis.

6.1 Revisiting diatom adaptive potentials and poleward range shifts

6.1.1 Thermal patterns and opportunities

I studied *T. gravida* as a typical Arctic diatom and *T. rotula* as a typical temperate diatom. Their thermal traits, identified mainly in publications I and II mirror the biogeographic origin of their respective populations and highlight opportunities but also bottlenecks for adaptation to climate warming and associated poleward range shifts.

In the single-driver context in publication I, both Arctic and temperate diatoms showed thermal optima several degrees higher than the average water temperature of their natural environment as predicted by global patterns of phytoplankton thermal traits suggested by Thomas et al. (2012). Regarding the potential of the studied Arctic diatom *T. gravida* to cope with current warming rates in its Arctic habitat, the single-driver thermal reaction norms suggest that thermal stress (i.e., temperatures beyond its T_{opt}) in the Arctic is currently out of reach. Even under high-emission scenarios, increasing summer sea surface temperatures in the central Arctic Ocean are projected to be around ~5°C by the end of the century (Han et al., 2023). However, known interactive effects with nutrient availability (Thomas et al., 2017) or light intensity (Edwards et al., 2016) may lower their T_{opt} by several degrees and thereby may push the Arctic *T. gravida* beyond their thermal limits. Additionally, the interactive effect of temperature with photoperiod and bacterial presence identified in publication II (i.e., negative growth effects under combined

thermal stress, 24h photoperiods and the presence of bacteria) could further constrain Arctic diatom growth under warming. In publication III, however, this interactive effect was buffered by diatom holobiont resilience, suggesting a context dependency of the observed microbial tipping points that govern this negative effect on host growth (further discussed below).

One possible mechanism of how Arctic diatoms could increase their thermal range in accordance with the warming rate in their habitat is solely by genetic adaptations within their population, also known as the 'evolutionary rescue' concept (Carlson et al., 2014). Although experimental evolution demonstrated a high potential of diatoms for rapid thermal adaptation in laboratory experiments under simplified selection regimes (Reusch and Boyd, 2013), more realistic estimates of the speed of such adaptations in T_{opt} for a temperate diatom were an order of magnitude slower (1°C during the last 60 years, Hattich et al., 2024). However, given the much faster temperature increase in the Arctic (Shu et al., 2022, Han et al., 2023), it remains unclear, whether thermal adaptation in Arctic diatom populations can keep track with the warming rate in their habitat. Moreover, the success of these adaptations is not only depending on the rate of temperature increase but also on the standing genetic variation of the population. The finding of much more conserved adaptive key genes carrying convergent amino acid substitutions in Arctic diatoms compared to temperate diatoms (publication I) indicates a lower degree of genetic variation in Arctic diatoms particularly in genes that likely contribute to their thermal adaptation. This lowered genetic variation in adaptive key genes may further decelerate their thermal adaptation because genetic variation is often considered as a currency for an organism's adaptive potential (Carlson et al., 2014, Lai et al., 2019, Chaturvedi et al., 2021). However, for cosmopolitan diatom species that exist not only in the Arctic but also in temperate regions, poleward range shifts of temperate populations could represent a new source of genetic variation that is boosting their adaptive potential. This ecological idea is also known as the 'genetic rescue' concept (Carlson et al., 2014).

For the temperate diatom *T. rotula*, publications I and II demonstrated its thermal potential for poleward range shifts. Although temperate diatoms have a competitive disadvantage in terms of growth rates under current Arctic temperatures, the increased warming rates due to Arctic amplification and interactive effects with further drivers could change competitive outcomes in their favor. For instance, interactive effects imposed by resource limitation could lower diatom T_{opt} (Edwards et al., 2016, Thomas et al., 2017) and thereby cause detrimental effects for Arctic diatoms but will not push poleward shifting temperate species beyond their T_{opt}. Therefore, in a commonly discussed scenario of warming and stratification-induced resource limitation

(Steinacher et al., 2010), the competitive ability of temperate diatoms may be enhanced. Beyond thermal adaptation, however, publications I and II suggest other obstacles that could compromise the expansive success of temperate diatoms towards the Arctic, such as Arctic-specific genetic adaptations (e.g., in the membrane-bound acyltransferase) or the extreme photoperiods in polar regions.

Key Outcomes

- The broad thermal ranges of the temperate *T. rotula* demonstrate a potential for distributional range expansions towards high latitudes. *(Objective I)*
- Despite having a T_{opt} that is much higher than average water temperatures in their habitat, the Arctic *T. gravida* could be at risk due to fast warming rates and interactive effects with further drivers lowering its T_{opt}. *(Objective I/II)*
- Hard selection pressure in the extreme Arctic environment led to convergent and conserved genetic modifications in several adaptive key genes of Arctic diatoms that are more variable in temperate diatoms. *(Objective I)*
- The low genetic variability in those likely adaptive key genes in Arctic diatoms may constrain their thermal adaptative potential. *(Objective I)*

6.1.2 Adaptation to extreme polar light regimes

Generally, the observed growth responses to different photoperiods match the reported biogeographic distribution patterns of *T. gravida* and *T. rotula* (Semina, 2004, Sar et al., 2011, Supraha et al., 2022). Publications I and II revealed a constrained growth performance of the temperate *T. rotula* at both extreme short and extreme long photoperiods but a preference for intermediate photoperiods. However, as these only correspond to a short transitional phase at high-latitude habitats, the extreme photoperiods imposed by polar night and polar day could pose an obstacle for potential poleward range shifts of *T. rotula*. So far, the existence of such

photoperiodic barriers has only been discussed in theory (Tougeron, 2021). For the Arctic *T. gravida*, habitat-specific adaptations were particularly evident in terms of their tolerance for these extreme photoperiods throughout publications I, II, and III. The general physiological response to photoperiod and its interaction with temperature is clearest in the axenic diatom cultures in publication II, as microbiome bacteria substantially modulate the light response of the studied diatoms in the xenic cultures in publication II and III (further discussed below).

The fact that these strong adaptive signals to the respective light regimes of temperate and Arctic regions can be found even after years of laboratory cultivation at constant intermediate photoperiods suggests that photoperiodic adaptation is beyond phenotypic plasticity but requires adjustments on the genetic level. The identified habitat-specific molecular adaptations in 22 Arctic-specific diatom gene candidates in publication I could therefore play important roles in these genetic adjustments. For instance, the convergent amino acid substation in the all-trans-retinol 13,14-reductase, which likely contributes to photobiological regulative processes (e.g., photoprotection, Moise et al., 2004) could contribute to the previously reported flexibility of the photosynthetic machinery in Arctic diatoms (Croteau et al., 2021, Svenning et al., 2024). In contrast, temperate diatoms may rely on the dark phase more strongly than Arctic diatoms to reduce excess electrons and thereby prevent oxidative stress (Fukai et al., 2022) as they lack the potentially photoprotective genetic adaptations found in their Arctic relatives in publication I. Evolving these genetic adaptations is a long-term process that might be particularly important for strictly photoautotrophic organisms that rely on high photosynthetic performance to maintain their competitiveness (Tittel et al., 2003). Therefore, the potential necessity of these adaptations for temperate diatoms in order to thrive in high-latitude habitats could hamper their poleward movements. In fact, this hypothesis is supported by field observations that found dinoflagellates to closely track marine isotherm shifts poleward while temperate diatom distributional ranges showed no significant correlation with these poleward isotherm shifts (Chivers et al., 2017). This could be due to the higher degree of mixotrophy among dinoflagellates which are potentially less affected by light stress than autotrophs (Cheung et al., 1998, Ong et al., 2023). These discrepancies in the ability of different phytoplankton functional groups for poleward movements so far cannot be explained by species distribution models (Benedetti et al., 2021). The findings about strong habitat-specific photoperiod responses of temperate and Arctic diatoms in publication I, II, and III throughout this thesis contribute to the underlying explanation of this pattern.

Despite urgently needed, monitoring data about phytoplankton range shifts towards higher latitudes are largely missing. In the case of diatoms, this information could be generated by monitoring ratios of temperate to Arctic molecular adaptations in the identified gene candidates from publication I, obtained from field metatranscriptomics samples. However, due to the faster range shifts of dinoflagellates (Chivers et al., 2017), monitoring the ratios of diatoms to dinoflagellates as routinely conducted in the Baltic Sea (Bergström et al., 2018), could also be a useful indicator for phytoplankton community changes in the Arctic (as further explained below).

Key Outcomes

- Diatom growth responses to different photoperiods depend on temperature (and vice-versa). *(Objective II)*
- The studied Arctic and temperate diatoms show strong adaptive signals to the respective photoperiodic ranges of their habitat that are beyond phenotypic plasticity. *(Objective I)*
- Extreme photoperiods at high latitudes could slow down poleward range shifts of temperate phototrophic phytoplankton such as diatoms. *(Objective I)*

6.1.3 Ecological implications of diatom thermal and photoperiodic responses

The here-found thermal and photoperiodic responses (publication I and II) allow to construct basic scenarios of diatom adaptive success and to discuss potential ecological implications. However, a simplified selection regime must be assumed in which the temperate diatoms mainly have to adapt to the Arctic light regime to expand their distributional range poleward and the Arctic diatoms mainly have to adapt their thermal plasticity to withstand warming under Arctic amplification. With differing degrees of adaptive potential for Arctic and temperate diatoms, possible scenarios range from the adaptive success of both groups or only one group, to the inability of both groups to adapt.

A scenario in which both groups exhibit adaptive success would likely result in increased competition between Arctic endemic and temperate diatom species. The afore-discussed higher genetic variability of temperate diatom species could possibly give them a competitive advantage. Although poleward range shifts of temperate species may temporally result in a higher alpha diversity in the Arctic habitat (Benedetti et al., 2021, Hodapp et al., 2023), it also brings the risk of losing Arctic endemic species and their highly specialized functions (Olden, 2006). Due to the important contribution of endemic species to global biodiversity, this could mean negative consequences on the global biodiversity level and contribute to the biotic homogenization of different ecosystems which refers to the increasing genetic, taxonomic, or functional similarity of biotas with potentially far-reaching ecological consequences (Olden, 2006). For example, the poorly understood ability of Arctic diatoms for overwintering the polar night could be such an endemic function that is essential for the phenology of the Arctic spring bloom and thereby steers important bottom-up ecological processes in the Arctic.

Even stronger ecological implications, however, can be expected in a scenario in which the temperate diatoms cannot expand their range further poleward while the Arctic diatoms are unable to adapt fast enough to keep track with the thermal changes in their habitat. This could lead to a smaller proportion of photoautotrophic phytoplankton as mixotrophic organisms are potentially less constrained by an extreme light regime (Cheung et al., 1998, Ong et al., 2023) and have already been shown to more closely track isotherm shifts poleward (Chivers et al., 2017). The consequences could be decreased primary productivity and also a less effective biological carbon pump due to less fixation and increased recycling of carbon by mixotrophs. Moreover, a decreasing proportion of photoautotrophic diatoms could also affect the bloom phenology of the system with potential attenuated bloom signals due to a lower growth response to alleviated light limitation in spring (Rumyantseva et al., 2019), and a decreasing importance of light as a driver for bloom dynamics relative to other abiotic and biotic drivers. This may lead to temporal mismatches between phytoplankton and zooplankton with cascading effects up the food-web.

Although in nature certainly further environmental factors contribute to shaping Arctic adaptation and associated poleward range shifts (e.g., light spectrum and intensity (Hoppe et al., 2024), zinc micronutrient concentrations (Ye et al., 2022), ocean acidification (Hoppe et al., 2018)), these outlined extreme scenarios highlight the potential ecological consequences. Understanding the full selection regimes of diatoms and estimating their adaptive capabilities for temperature and photoperiod are therefore a crucial next step to more realistically predict

the ecological implications of the here-found biogeographic adaptations. To this, publication II showed that thermal and photoperiodic responses can also be enhanced by biotic interactions with associated bacteria. By supporting diatom growth performance even in the margins of their fundamental niche, bacterial microbiomes can play a key role in diatom adaptation, thus reducing the likelihood of the outlined ecological 'worst-case' scenario.

Key Outcomes

Overcoming adaptive constraints towards extreme photoperiods (in temperate diatoms) and fast warming rates (in Arctic diatoms) can have important implications for trophic interactions and the effectivity of the biological carbon pump in the Arctic. *(Objective I)*

6.2 Bacteria as facilitators or gatekeepers of Arctic adaptation

6.2.1 Microbiome effects on diatom growth

Publications II and III highlighted the large contribution of the bacterial microbiome to diatom growth. Although the general existence of this growth-supporting effect was already demonstrated in other studies (Scholz, 2014, Mönnich et al., 2020), the experiments conducted here were able to show that the degree to which the bacterial microbiome supports the host diatom's growth substantially depends on environmental conditions in terms of temperature and photoperiod. On the molecular level, this is demonstrated in publication III by various tightly coupled diatom-bacteria gene expression patterns that follow distinct microbiome member-specific trajectories in response to the main and interactive effects of temperature and photoperiod.

In publication II, the general growth patterns of the studied Arctic and temperate diatoms in response to temperature and photoperiod were modified interactively by bacterial presence. Precisely, the findings suggest that the relative contribution of the bacterial microbiome to their host diatom's growth was largest in the margins of the respective diatom's fundamental niche. This could be due to the fact that under optimal growth conditions, enzymatic processes that ultimately limit diatom cell doublings are capped and thus cannot be further increased (Flynn

and Raven, 2023), whereas, under non-optimal or resource-limited conditions, relative growth performance may be enhanced by metabolic exchanges with beneficial associated bacteria. This was particularly evident in publication III where the relative growth contribution of the bacteria at photoperiods of 16:8h was much larger compared to the photoperiod of 24:0h which was determined as their optimum in publication I. Also, publication IV suggests specific bacterial microbiome members to be fostered in the microbiome community under nitrate or vitamin resource limitations indicating their role in alleviating these limitations and thereby contributing to diatom growth (Shibl et al., 2020). Although the effect of the microbiome on diatom growth was positive under most tested experimental treatments, publication II also demonstrated that under species-specific stressful abiotic conditions, this positive net effect may turn negative. This is highlighting the risk for possible tipping points from overall beneficial to antagonistic relationships in algae microbiomes that have shown to be dependent on host cell viability (Seyedsayamdost et al., 2011, Wang et al., 2022). These antagonistic switches are often associated with a stochastic reassembly of the microbiome termed 'dysbiosis' (Arnault et al., 2023). However, in publication III, the same treatment condition did not result in this previously observed negative growth effect for *T. gravida*. This apparent discrepancy between publications II and III is most likely explained by the different culture environments (i.e., nanocosms vs. microcosms), which could have led to differences in host cell viability. As a consequence, in publication III, this could have prevented triggering antagonistic mechanisms of opportunistic microbiome bacteria and, thereby also the associated negative effects on diatom growth rates (Wang et al., 2022). Host cell viability-dependent bacterial strategies may thereby indirectly contribute to the speed of genotypic sorting as less adapted host genotypes are effectively removed from the population.

As the relative growth supporting effect of the bacterial microbiome for the temperate *T. rotula* in publication II was particularly large at cold temperatures in combination with very short or long photoperiods, the bacteria of the temperate diatom may play a key role in supporting their host in an Arctic environment to which it is currently not well adapted (publication I). Therefore, host-microbiome interactions may represent an important biotic process governing the potential for poleward range shifts of temperate diatoms in the future. Considering context-dependent biological interactions in species distribution models could therefore improve the precision for poleward moving species ranges, which has already demonstrated value in the context of other marine organisms (Lany et al., 2017). However, data for other diatom species than the here studied *T. gravida* and *T. rotula* is needed to reliably implement the found mechanisms in species distribution models (further discussed below).

Key Outcomes

- The positive net effect of the bacterial microbiome on host diatom growth depends on environmental conditions and shows distinct patterns for the studied Arctic and temperate diatoms *(Objective II)*

- By facilitating a wider realized niche space of their host diatom, the microbiome appears to be essential to buffer environmental perturbations and support the host in adapting to new or challenging environments. *(Objective II)*

- Multifactorial environmental stress increases the risk for microbiome dysbiosis, leading to negative net effects on host growth when the host's physiological state is impaired. *(Objective II/III)*

6.2.2 Plasticity of microbiome community composition

Due to the profound effect of the bacterial microbiome on diatom growth and its realized niche, evaluating overarching principles of microbiome community dynamics is of crucial importance for understanding the adaptive potential of diatoms. This thesis gives insights into the bacterial microbiome community composition of *T. gravida* in different environmental conditions in terms of temperature and photoperiod (publication III) and shed light on bacterial community dynamics under macro- or micronutrient limitations and different host genotypes (publication IV).

As demonstrated in publication IV, the bacterial microbiome community is genotype-specific and therein largely conserved even down to the individual host-cell level. Although globally it is rather unlikely that cosmopolitan diatom species have a core microbiome due to different habitat characteristics that select for different microbial communities based on the respective imposed metabolic needs of the holobiont (Ahern et al., 2021, Martin et al., 2021), the three Arctic *T. gravida* genotypes studied in publication IV shared eight microbiome bacterial genera. Certain bacterial groups were unique for the microbiome of specific *T. gravida* host genotypes.

Compared to free-living microbial communities, diatom-associated microbiomes likely have a higher compositional stability, as both the host (Shibl et al., 2020) and the bacteria (Isaac et al., 2024) actively structure the microbiome community in the phycosphere to maintain a specific mutualistic state (Mönnich et al., 2020). This was not only reflected in coordinated host-microbiome transcriptomics in publication III but also in publication IV, where the microbiome community composition was largely unaffected by macro- or micronutrient limitations and only a few specific microbiome bacteria increased in relative abundance. This indicates their potential role in alleviating these limitations for their host diatom. In publication III, the microbiome community composition was tracked under different combinations of temperature and photoperiod. The outcome suggests that at temperatures below T_{opt}, photoperiodic differences did not affect microbiome community composition. However, under thermal stress, it becomes increasingly difficult for the holobiont to maintain this mutualistic state, increasing the risk for microbiome dysbiosis (Arnault et al., 2023). Initial signs for microbiome dysbiosis under thermal stress were visible in terms of negative microbiome effects on host growth performance in publication II as well as in publication III based on compositional shifts coinciding with the loss of key microbiome members such as the *Sulfitobacter* clade that is essential for microbiome assembly itself (Isaac et al., 2024). Of course, in such closed-system laboratory studies microbiome dysbiosis is limited in its extent due to the inability of new antagonistic bacteria to enter the diatom phycosphere. This underlines the need for in-situ data on diatom microbiomes to give more realistic insights into natural microbiome community dynamics. The new methodological approach developed in publication IV will substantially contribute to the collection of this data.

To further study the effect of temperature and host cell viability on microbiome composition more generally, I conducted an additional study (Giesler et al., in prep., not included in this thesis)that tracked the bacterial microbiome community composition and host growth performance of the Arctic *T. gravida* and the temperate *T. rotula* along a thermal gradient (Fig. 11). The outcome suggests that for the temperate *T. rotula*, temperature affects the microbiome community composition more strongly and results in an almost complete bacterial turnover across the thermal gradient. In contrast, the Arctic. *T. gravida* microbiome was much less affected by temperature and remained comparably stable in bacterial family composition across the tested temperatures. In an ecological context, the found higher microbiome compositional flexibility in the temperate diatoms indicate both, risks and opportunities for their adaptation to novel environments. On the one hand, they may be able to recruit new microbiome bacteria that favor their adaptation (e.g., in an Arctic habitat), but on the other hand, this high

compositional flexibility may also increase the chance for antagonistic bacteria to establish in the phycosphere with potentially negative consequences for the holobiont. Vice-versa, for the Arctic diatoms which hold more strongly onto their bacterial microbiome members, the increased compositional stability means a lower potential for gaining novel microbiome functions but also a lower risk for antagonistic bacterial interactions. The observed higher microbiome compositional stability in the Arctic diatom could be a consequence of co-evolution under hard selection in an extreme environment (Chen and Kassen, 2020, Gallet et al., 2018) like the Arctic Ocean. Under hard selection pressure, individuals that do not possess a certain advantageous trait are eliminated, in contrast to soft selection where the fitness of an individual is determined relative to its population (Bell et al., 2021). Extreme abiotic conditions like those in the Arctic predominantly exert hard selective pressure and may therefore favor the survival of specific diatom holobionts that are well-adapted to this harsh environment (Gallet et al., 2018). This could likely lead to the observed stable species associations in the Arctic diatom displayed in Fig. 6.1 that are also visible in the respective Arctic microbiome community compositions in publications III and IV.

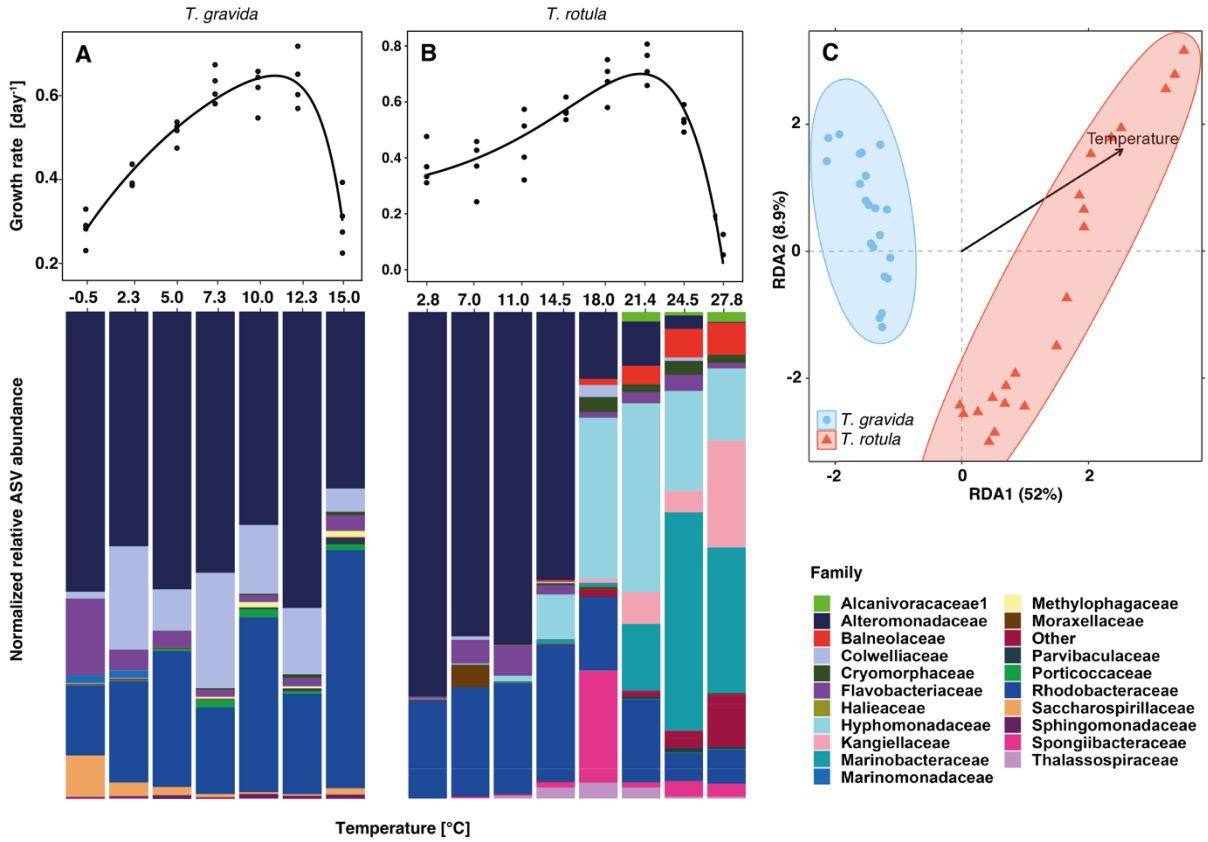

Fig. 6.1: Thermal reaction norms of *T. gravida* (A, top) and *T. rotula* (B, top) with growth rates (day^{-1}) on the y-axis across the tested temperatures (°C) on the x-axis. Black points represent measured data points and the black line refers to fitted temperature performance curves. Experimental conditions, data processing, and curve fitting were identical as reported in publication I. For each of the tested temperatures, the normalized relative ASV abundance of the diatom-associated bacterial fraction is displayed as stacked bar plots on the family level for *T. gravida* (A, bottom) and *T. rotula* (B, bottom). Sample processing and bioinformatics for microbiome community composition were identical to the workflow described in detail in publication III. A redundancy analysis (panel C) demonstrates the effect of temperature on the microbiome community composition that is more pronounced for the temperate diatom-associated microbiome community composition.

Key Outcomes

- Microbiome and host (meta-)transcriptomes are tightly coupled systems that respond in a coordinated manner to abiotic changes even down to the individual host cell level. *(Objective III/IV)*
- Interactions of diatoms and their microbiome bacteria are context-dependent processes, driven by main- and interactive effects of temperature and photoperiod that differ in their direction among bacterial microbiome members. *(Objective III)*
- Coevolution under hard selection resulted in particularly tight species associations in Arctic diatom holobionts that are relatively resistant to thermal changes compared to temperate diatoms. *(Objective III)*
- Differences in microbiome compositional plasticity of temperate and Arctic diatoms could affect their adaptive capabilities due to differences in their ability to recruit new microbiome bacteria but also their vulnerability to antagonistic bacteria entering their phycosphere. *(Objective I/III)*

6.2.3 The diatom microbiome as an extended genotype

This thesis demonstrated the tight link between *T. gravida* and its microbiome bacteria. This is not only reflected in the relatively high compositional stability of the bacterial microbiome community (see above) but also in the found synchronous host-microbiome gene expression patterns. Precisely, publication III showed that almost half of all differentially expressed bacterial genes were highly correlated with almost 90% of diatom host genes of interest. These intertwined host-microbiome cellular processes jointly responded to environmental stimuli and hence might further translate to the level of metabolic exchanges. Furthermore, the SCHoCO-seq approach that enabled high-resolution host-specific microbiome profiling (publication IV) demonstrated that the microbiome community dynamics under different nutrient limitations were largely reproducible across individual diatom host cells. This suggests that strongly

conserved coevolutive mechanisms are at play that are coordinated between the host genotype and its microbiome. Thereby the microbiome acts as an extended genotype as it provides genetic functions that can be accessed by the host when necessary. Even though the relative community composition is more flexible in temperate diatoms (see above), the diversity of temperate diatom microbiomes is reportedly still largely conserved (Mönnich et al., 2020, Ahern et al., 2021), thus the presence enabling similar coevolutive mechanisms.

The overall mostly mutualistic outcome of this tightly linked diatom holobiont (publication II and III) is in strong support of the 'hologenome theory of evolution' which posits that the host and its microbiome act as one 'unit of selection', i.e., all genomes contained in the holobiont are undergoing selective pressure together as an entity (Rosenberg and Zilber-Rosenberg, 2018). While classically, biotic interactions are considered to constrain an organism's fundamental niche and plasticity, thus shaping its realized niche (Soberón and Arroyo-Peña, 2017), microbiomes have a positive effect on the realized niche and enhance the holobiont's plasticity and adaptation (Petersen et al., 2023). The underlying reason for this is that the sum of genetic functions of the holobiont and its genetic variability (i.e., its hologenome) is larger than that of the host alone and thereby enhances its potential for higher plasticity (Bordenstein and Theis, 2015). Although the hologenome concept was originally formulated only for metazoan organisms, it should also be considered as an evolutionary framework for diatoms (and other protists). It could be argued that compared to e.g., metazoan holobionts and their gut microbiomes, diatom holobionts are not a discrete 'metaorganism' as their microbiomes are rather a continuum from tightly attached to free-living bacteria. Nevertheless, the publications II, III, and IV of this thesis demonstrate that diatom-bacteria assemblages are mostly mutualistic and conserved species associations with strong metabolic links, suggesting that their coevolution follows the same overarching principle as proposed for metazoans by the hologenome theory of evolution (Simon et al., 2019).

Key Outcomes

- Microbiome and host (meta-)transcriptomes are tightly coupled systems that respond in a coordinated manner to abiotic changes even down to the individual host cell level. *(Objective III/IV)*
- Synchronized host-microbiome transcriptomic responses with a synergistic outcome and reproducible bacterial community dynamics across individual host diatoms (enabled by novel single-cell microbiome profiling techniques) suggest a common coevolutive history in line with the hologenome theory of evolution. *(Objective III/IV)*

6.3 Future perspectives

6.3.1 Validation by follow-up experiments

Publications I and II gave insights into the different responses of the studied temperate and Arctic diatoms to different photoperiods, highlighting the role of the extreme Arctic light regime for adaptation and the potential for poleward range shifts. However, to improve ecosystem-scale predictions about diatom species distributional shifts and ecological consequences in the future, the applicability of this finding needs to be tested and validated for further Arctic and temperate phytoplankton species. Ideally, these photoperiodic assays would not only be conducted with other Arctic and temperate diatoms but also with other phytoplankton groups, including mixotrophic organisms which potentially are less constrained by extreme light regimes (Cheung et al., 1998, Ong et al., 2023). Therefore, in laboratory experiments, mixed communities of temperate and Arctic phytoplankton could be exposed to different temperature-photoperiod combinations to study their competitive ability under Arctic spring bloom or polar day conditions. A more realistic light setting could be employed mimicking the intensity and spectrum for these different scenarios over the course of the day. Besides growth rates, also photo-physiological parameters such as photosynthetic efficiency, non-photochemical quenching, and ROS production could be measured to understand the underlying cellular processes at play. Subsequently, a simple mathematical model that is flexible enough to account for the observed variability in photoperiod reaction norms in publication I could be developed

to implement this driver in species distribution models. Due to the interactive nature of photoperiod as a driver with temperature and likely also light intensity (Theus et al., 2022), the mathematical integration of these interactions, similarly as demonstrated for temperature-nutrient interactions (Thomas et al., 2017), would be an important next step.

Additionally, long-term experiments under extreme photoperiods could be conducted to estimate the adaptative capabilities of temperate diatoms to extreme photoperiods. Complementary, to estimate the maximum thermal adaptation speed of Arctic diatoms under warming rates corresponding to Arctic amplification, thermal reaction norms could be conducted with Arctic diatoms resurrected from resting stages in different Arctic sediment layers of the last 100 years, similarly as already demonstrated by Hattich et al (2024) for temperate species. Transcriptomic profiling in these experiments could provide valuable insights into the genes involved and thus potentially disentangle which of the candidate genes identified in publication I (as potentially carrying habitat-specific adaptation) contribute to thermal or photoperiodic adaptation, respectively.

As shown in publications II and III, the diatom-associated microbiome bacteria substantially modulate the host's growth responses to temperature and photoperiod. Yet, it is currently unknown, whether temperate and Arctic diatoms could potentially exchange parts of their microbiome to improve their performance under thermal or photoperiodic stress. Although multiple previous studies demonstrated the strong host-specificity of diatom microbiome communities (Baker and Kemp, 2014, Behringer et al., 2018, Mönnich et al., 2020, Ahern et al., 2021), none of these studies tested the host's potential for the recruitment of novel microbiome bacteria under challenging environmental conditions. Therefore, another interesting follow-up experiment could be a co-culture experiment, in which Arctic and temperate diatom hosts are separated by a membrane that is permeable to bacteria. After exposing these co-cultures to different combinations of temperature and photoperiod, their microbiome composition could be examined for microbial exchanges and their performance could be compared to monoculture control treatments in order to determine the net effect of potential bacterial exchanges on host growth performance.

6.3.2 From lab to field: Plasticity of natural diatom holobionts

To more realistically study the diversity and plasticity of diatom microbiomes it is necessary to apply the newly developed method presented in publication IV (Objective IV) in the field context to obtain diatom species-specific in-situ data of their microbiome community

composition. The qualitative advantage of this is that biases due to cultivation (i.e., loss of unculturable bacteria) or filtration (only mixed host community samples) are avoided.

To implemented this approach, I received the Bremen IDEA grant which allowed me to take part in an expedition in southwest Greenland in 2023 during the spring bloom as part of a monitoring program of the Greenland Climate Research Center (GCRC). To investigate how abiotic drivers shape microbiomes of different diatom species in a more realistic setting, I sampled ~700 diatom single-cell holobionts at a total of 20 stations along three transects that characterize different environmental gradients from high or low glacial impact towards the open ocean (Fig. 6.2). Additionally, a one-month time series station was sampled repeatedly to study the diatom holobiont response to the transition phase of the fast-changing light regime during early spring. CTD profiles and nutrient samples that were produced as part of the monitoring cruise will be used to correlate changes in microbiome community compositions to environmental drivers. At the three most distant stations of the three sampled transects, bulk RNA samples were taken to investigate how the different habitat characteristics of these stations (i.e., open ocean vs. glacial ice edge vs. fjord with low glacial impact) affect interactions of diatoms and bacteria on the community level. The samples produced for this project are currently processed.

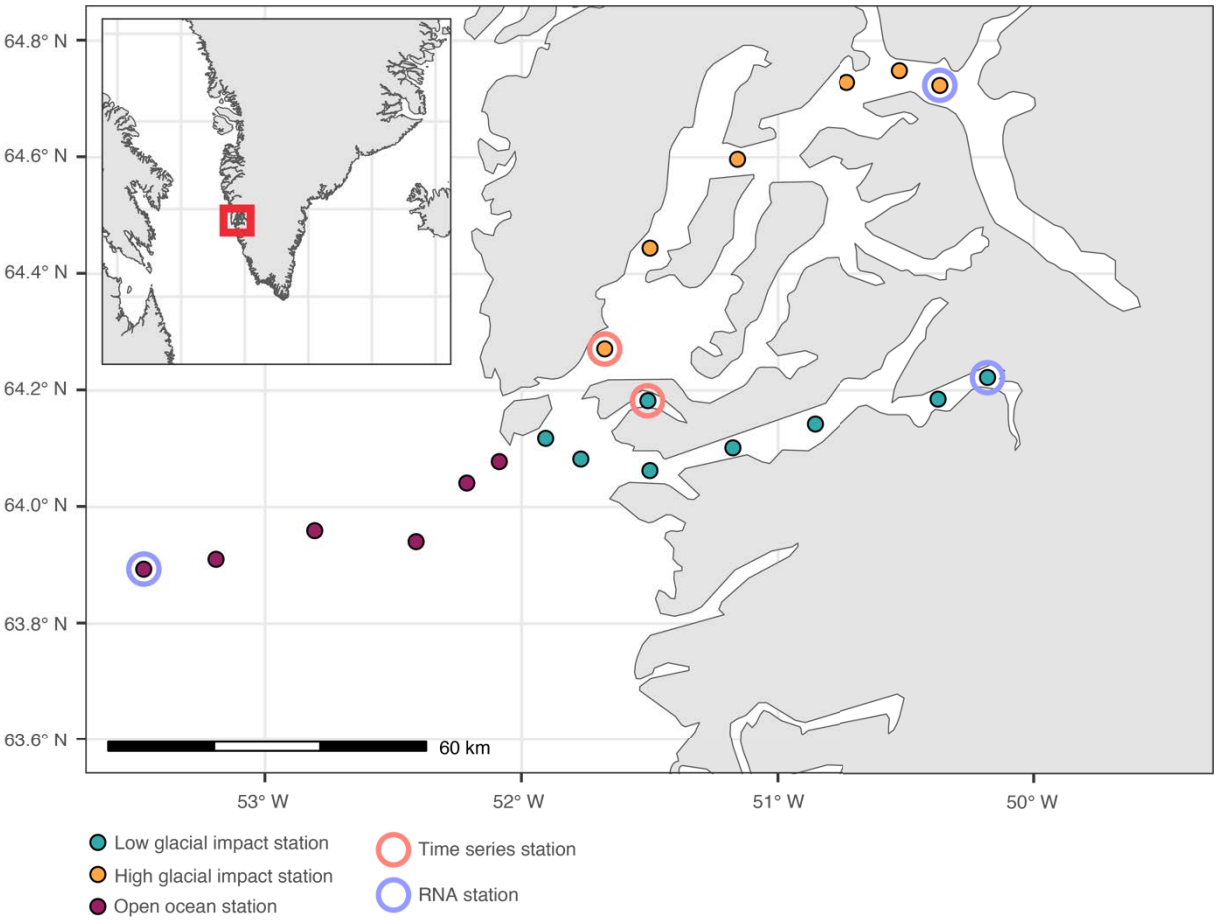

Fig. 6.2.: Sampling plan of the MIDIDARC expedition 2023 to study microbial diversity and plasticity of natural diatom microbiomes in southeast Greenland. Points show the location of the sampling stations for diatom single-cells and bulk samples for community composition. The color code in the legend illustrates the environmental differences of the three transects. At the end of each transect, RNA bulk samples were taken (purple circle). Time series stations are marked with a red circle.

Based on the outcome of publications II, III, and IV, within a respective diatom species, I expect to find a core microbiome that is complemented by unique bacterial taxa for different subpopulations. I further hypothesize that different habitat characteristics in terms of nutrient concentrations (e.g., subglacial nutrient upwelling at the glacial ice edge) will lead to compositional differences across diatom subpopulations at the three stations, driven by host and bacterial metabolic demands.

6.3.3 Functional redundancy in microbiomes as insurance for perturbations

Despite the finding of mutualistic and relatively stable species associations in the here studied diatom microbiomes, this thesis also demonstrated that diatom holobionts are not always able to buffer abiotic stress. In some cases, this might lead to dysbiosis with potential negative

consequences for holobiont survival as indicated in publication II under specific conditions. Furthermore, when microbiomes are shifted out of balance this may result in the loss of key bacterial groups as for instance, the *Sulfitobacter* clade in publication III with cascading effects on other microbiome bacteria (Isaac et al., 2024). Considered in the context of the hologenome theory, this is bringing the risk of potentially losing a genetic property that could be essential to holobiont survival in a given habitat (Petersen et al., 2023). Therefore, quantifying the redundancy of essential microbiome functions would be an important next step toward understanding the vulnerability of diatom holobionts in different ocean provinces. For instance, a study by Zoccarato et al. (2022) showed in a comparative genomic approach, that of 412 studied marine bacterial genomes, 57-70 % of bacterial taxa produce different B vitamins but only 10% are capable of siderophore production. Yet, in iron-limited regions such as the Southern Ocean, this function might be of crucial importance and its redundancy could determine holobiont survival after a disturbance of the microbiome community. Moreover, identifying biogeographic region-specific highly redundant functions could give important insights into which genetic traits are essential for holobiont proliferation in the respective habitat (Zoccarato et al., 2022). Due to the pronounced host-specificity of microbiome communities (Baker and Kemp, 2014), to study their functional redundancy in different ocean provinces, it is necessary to determine the microbiome community on the individual host cell level as proposed in publication IV. However, to obtain host-specific information not only about bacterial diversity but also about the functional properties of algae-associated microbiomes, additional metagenome-assembled-genomes (MAGs) obtained from bulk samples could be used to assign the resulting bacterial genomes to the respective amplicons of the bacteria attached to individual diatom host cells (Fig. 6.3). This would allow to determine the functional redundancy within microbiomes of diatoms that could serve as an insurance for environmental perturbations.

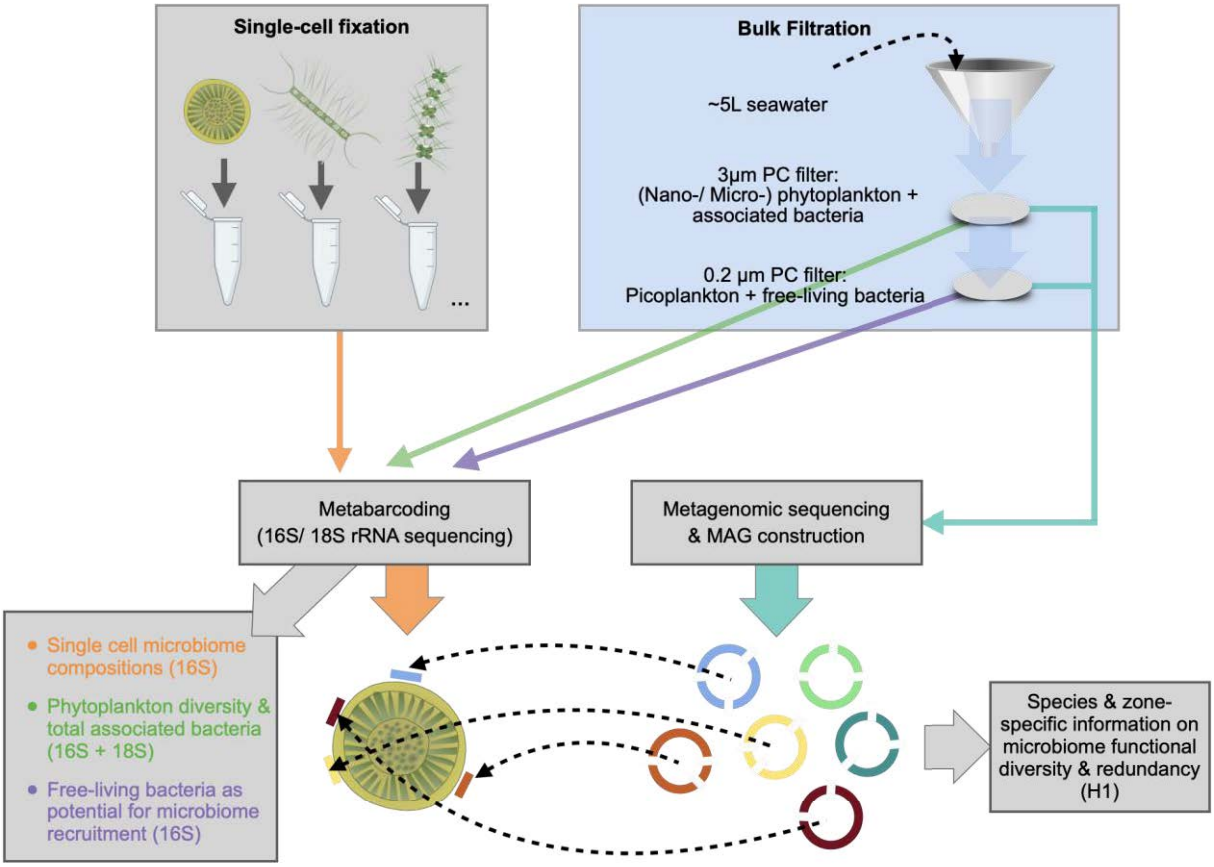

Fig. 6.3: Conceptual figure to study functional redundancy in natural diatom microbiomes. The methodological approach involves single-cell microbiome community analysis as developed in publication IV. Moreover, 16S and 18S amplicon sequencing of size-fractioned bulk samples could give insights into phytoplankton community composition as well as particle-associated and free-living bacterial communities. The same bulk samples could further be used for metagenomic sequencing, allowing for the construction of MAGs that enable the assignment of bacterial functions to individual host diatoms. *Figure contains elements from BioRender.com*

6.4 Concluding remarks

The intricate relationship within the phytoplankton holobiont and its sophisticated host-microbiome interactions have fascinated a growing community of researchers over many decades (Helliwell et al., 2022). However, the fact that climate change affects phytoplankton distributional ranges and challenges their ability for adaptation with potentially far reaching ecological and biogeochemical implications raises the need to understand the role of the phytoplankton holobiont in a multifactorial setting. This thesis contributes to this understanding by studying the biogeographic adaptation of two closely related Arctic and temperate diatoms from a holobiont perspective.

I demonstrated that a common temperate diatom is currently limited in its ability for poleward range expansions due to impaired performance under the extreme photoperiods that are characteristic for high latitudes. However, its microbiome was shown to play an important role in adapting the host to the relevant environmental conditions (i.e., cold temperatures combined with extreme photoperiods) while showing a high compositional plasticity. Furthermore, I demonstrated that Arctic diatoms evolved to their extreme environment by means of conserved genetic modifications at the cost of lowered genetic variability with potential constraints for their thermal adaptation under Arctic amplification. The bacterial microbiome of the studied Arctic diatom is compositionally more stable and exerts a mostly positive net effect on its host diatom's growth, depending on abiotic conditions. However, under thermal stress it also brings risks of shifting from an overall mutualistic to an antagonistic net effect, likely depending on host cell viability. Moreover, this thesis revealed that the underlying tightly linked host-microbiome interactions are not uncoupled from environmental conditions but show coordinated responses between the host and its microbiome to temperature and photoperiod with unique expression trajectories for different microbiome members. This underlines the need for future studies to consider that the probability to identify a specific host-microbiome process is depending on interacting abiotic factors. Eventually, a novel method was introduced to profile diatom microbiomes at a high resolution on the single host cell level, paving the road for more realistic investigations of diatom holobionts in the coming years.

Ultimately, this thesis highlights the value of stepwise experimental designs, by narrowing down highly resolved single drivers to relevant and carefully chosen multifactorial conditions. Combined with multi-omics techniques this approach enabled to study how diatoms and their microbiomes jointly respond and adapt to a multifactorial world that is rapidly changing, particularly in the unique Arctic habitat

References

AHERN, O. M., WHITTAKER, K. A., WILLIAMS, T. C., HUNT, D. E. & RYNEARSON, T. A. 2021. Host genotype structures the microbiome of a globally dispersed marine phytoplankton. *Proceedings of the National Academy of Sciences of the United States of America,* 118.

ALEXANDER, H., JENKINS, B. D., RYNEARSON, T. A. & DYHRMAN, S. T. 2016. Metatranscriptome analyses indicate resource partitioning between diatoms in the field (vol 112, pg E2182, 2015). *Proceedings of the National Academy of Sciences of the United States of America,* 113**,** E3589-E3589.

AMIN, S. A., GREEN, D. H., KÜPPER, F. C. & CARRANO, C. J. 2009. Vibrioferrin, an Unusual Marine Siderophore: Iron Binding, Photochemistry, and Biological Implications. *Inorganic Chemistry,* 48**,** 11451-11458.

AMIN, S. A., HMELO, L. R., VAN TOL, H. M., DURHAM, B. P., CARLSON, L. T., HEAL, K. R., MORALES, R. L., BERTHIAUME, C. T., PARKER, M. S., DJUNAEDI, B., INGALLS, A. E., PARSEK, M. R., MORAN, M. A. & ARMBRUST, E. V. 2015. Interaction and signalling between a cosmopolitan phytoplankton and associated bacteria. *Nature,* 522**,** 98-U253.

AMIN, S. A., PARKER, M. S. & ARMBRUST, E. V. 2012. Interactions between Diatoms and Bacteria. *Microbiology and Molecular Biology Reviews,* 76**,** 667.

ANNUNZIATA, R., RITTER, A., FORTUNATO, A. E., MANZOTTI, A., CHEMINANT-NAVARRO, S., AGIER, N., HUYSMAN, M. J. J., WINGE, P., BONES, A. M., BOUGET, F. Y., LAGOMARSINO, M. C., BOULY, J. P. & FALCIATORE, A. 2019. bHLH-PAS protein RITMO1 regulates diel biological rhythms in the marine diatom. *Proceedings of the National Academy of Sciences of the United States of America,* 116**,** 13137-13142.

ANTAO, L., BATES, A., BLOWES, S., WALDOCK, C., SUPP, S., MAGURRAN, A., DORNELAS, M. & SCHIPPER, A. 2020. Temperature-related biodiversity change across temperate marine and terrestrial systems. *Nature Ecology & Evolution,* 4.

ARMBRUST, E. V. 2009. The life of diatoms in the world's oceans. *Nature,* 459**,** 185-192.

ARMBRUST, E. V., BERGES, J. A., BOWLER, C., GREEN, B. R., MARTINEZ, D., PUTNAM, N. H., ZHOU, S. G., ALLEN, A. E., APT, K. E., BECHNER, M., BRZEZINSKI, M. A., CHAAL, B. K., CHIOVITTI, A., DAVIS, A. K., DEMAREST, M. S., DETTER, J. C., GLAVINA, T., GOODSTEIN, D., HADI, M. Z., HELLSTEN, U., HILDEBRAND, M., JENKINS, B. D., JURKA, J., KAPITONOV, V. V., KRÖGER, N., LAU, W. W. Y., LANE, T. W., LARIMER, F. W., LIPPMEIER, J. C., LUCAS, S., MEDINA, M., MONTSANT, A., OBORNIK, M., PARKER, M. S., PALENIK, B., PAZOUR, G. J., RICHARDSON, P. M., RYNEARSON, T. A., SAITO, M. A., SCHWARTZ, D. C., THAMATRAKOLN, K., VALENTIN, K., VARDI, A., WILKERSON, F. P. & ROKHSAR, D. S. 2004. The genome of the diatom *Thalassiosira pseudonana*: Ecology, evolution, and metabolism. *Science,* 306**,** 79-86.

ARNAULT, G., MONY, C. & VANDENKOORNHUYSE, P. 2023. Plant microbiota dysbiosis and the Anna Karenina Principle. *Trends in Plant Science,* 28**,** 18-30.

REFERENCES

AZAM, F., FENCHEL, T., FIELD, J. G., GRAY, J. S., MEYERREIL, L. A. & THINGSTAD, F. 1983. The Ecological Role of Water-Column Microbes in the Sea. *Marine Ecology Progress Series,* 10**,** 257-263.

AZAM, F. & MALFATTI, F. 2007. Microbial structuring of marine ecosystems. *Nature Reviews Microbiology,* 5**,** 782-791.

BAKER, L. J. & KEMP, P. F. 2014. Exploring bacteria-diatom associations using single-cell whole genome amplification. *Aquatic Microbial Ecology,* 72**,** 73-88.

BAR-ON, Y. M., PHILLIPS, R. & MILO, R. 2018. The biomass distribution on Earth. *Proceedings of the National Academy of Sciences of the United States of America,* 115**,** 6506-6511.

BARRETO, M. M., WALKER, M., ASHWORTH, M. P. & MORRIS, J. J. 2021. Structure and Long-Term Stability of the Microbiome in Diverse Diatom Cultures. *Microbiology Spectrum,* 9.

BARTHOLOMEW, G. A. 1958. The role of physiology in the distribution of terrestrial vertebrates. *American Association for the Advancement of Science,* 51**,** 81-95.

BEHRENFELD, M. J., HALSEY, K. H. & MILLIGAN, A. J. 2008. Evolved physiological responses of phytoplankton to their integrated growth environment. *Philosophical Transactions of the Royal Society B-Biological Sciences,* 363**,** 2687-2703.

BEHRINGER, G., OCHSENKUHN, M. A., FEI, C., FANNING, J., KOESTER, J. A. & AMIN, S. A. 2018. Bacterial Communities of Diatoms Display Strong Conservation Across Strains and Time. *Frontiers in Microbiology,* 9.

BELL, D. A., KOVACH, R. P., ROBINSON, Z. L., WHITELEY, A. R. & REED, T. E. 2021. The ecological causes and consequences of hard and soft selection. *Ecology Letters,* 24**,** 1505-1521.

BELL, W. & MITCHELL, R. 1972. Chemotactic and Growth Responses of Marine Bacteria to Algal Extracellular Products. *Biological Bulletin,* 143**,** 265-&.

BENDER, S. J., DURKIN, C. A., BERTHIAUME, C. T., MORALES, R. L. & ARMBRUST, E. V. 2014. Transcriptional responses of three model diatoms to nitrate limitation of growth. *Frontiers in Marine Science,* 1.

BENEDETTI, F., VOGT, M., ELIZONDO, U. H., RIGHETTI, D., ZIMMERMANN, N. E. & GRUBER, N. 2021. Major restructuring of marine plankton assemblages under global warming. *Nat Commun,* 12**,** 5226.

BENOISTON, A. S., IBARBALZ, F. M., BITTNER, L., GUIDI, L., JAHN, O., DUTKIEWICZ, S. & BOWLER, C. 2017. The evolution of diatoms and their biogeochemical functions. *Philosophical Transactions of the Royal Society B-Biological Sciences,* 372.

BERGSTRÖM, L., AHTIAINEN, H., AVELLAN, L., ESTLANDER, S., HAAPANIEMI, J., HALDIN, J., HOIKKALA, L., RUIZ, M., ROWE, O. & ZWEIFEL, U. 2018. *HELCOM State-of-the-Baltic-Sea Second-HELCOM-holistic-assessment-2011-2016*.

BERTRAND, E. M., MCCROW, J. P., MOUSTAFA, A., ZHENG, H., MCQUAID, J. B., DELMONT, T. O., POST, A. F., SIPLER, R. E., SPACKEEN, J. L., XU, K., BRONK, D. A., HUTCHINS, D. A. & ALLEN, A. E. 2015. Phytoplankton-bacterial interactions mediate micronutrient colimitation at the coastal Antarctic sea ice edge. *Proceedings of the National Academy of Sciences of the United States of America,* 112**,** 9938-9943.

BIDDANDA, B. & BENNER, R. 1997. Carbon, nitrogen, and carbohydrate fluxes during the production of particulate and dissolved organic matter by marine phytoplankton. *Limnology and Oceanography,* 42**,** 506-518.

BINTANJA, R. & KRIKKEN, F. 2016. Magnitude and pattern of Arctic warming governed by the seasonality of radiative forcing. *Scientific Reports,* 6.

BJORNSEN, P. K. 1988. Phytoplankton Exudation of Organic-Matter - Why Do Healthy Cells Do It. *Limnology and Oceanography,* 33**,** 151-154.

BORDENSTEIN, S. R. & THEIS, K. R. 2015. Host Biology in Light of the Microbiome: Ten Principles of Holobionts and Hologenomes. *Plos Biology,* 13.

BOWLER, C., ALLEN, A. E., BADGER, J. H., GRIMWOOD, J., JABBARI, K., KUO, A., MAHESWARI, U., MARTENS, C., MAUMUS, F., OTILLAR, R. P., RAYKO, E., SALAMOV, A., VANDEPOELE, K., BESZTERI, B., GRUBER, A., HEIJDE, M., KATINKA, M., MOCK, T., VALENTIN, K., VERRET, F., BERGES, J. A., BROWNLEE, C., CADORET, J. P., CHIOVITTI, A., CHOI, C. J., COESEL, S., DE MARTINO, A., DETTER, J. C., DURKIN, C., FALCIATORE, A., FOURNET, J., HARUTA, M., HUYSMAN, M. J. J., JENKINS, B. D., JIROUTOVA, K., JORGENSEN, R. E., JOUBERT, Y., KAPLAN, A., KRÖGER, N., KROTH, P. G., LA ROCHE, J., LINDQUIST, E., LOMMER, M., MARTIN-JÉZÉQUEL, V., LOPEZ, P. J., LUCAS, S., MANGOGNA, M., MCGINNIS, K., MEDLIN, L. K., MONTSANT, A., OUDOT-LE SECQ, M. P., NAPOLI, C., OBORNIK, M., PARKER, M. S., PETIT, J. L., PORCEL, B. M., POULSEN, N., ROBISON, M., RYCHLEWSKI, L., RYNEARSON, T. A., SCHMUTZ, J., SHAPIRO, H., SIAUT, M., STANLEY, M., SUSSMAN, M. R., TAYLOR, A. R., VARDI, A., VON DASSOW, P., VYVERMAN, W., WILLIS, A., WYRWICZ, L. S., ROKHSAR, D. S., WEISSENBACH, J., ARMBRUST, E. V., GREEN, B. R., VAN DE PEER, Y. & GRIGORIEV, I. V. 2008. The *Phaeodactylum* genome reveals the evolutionary history of diatom genomes. *Nature,* 456**,** 239-244.

BOYD, P. W., DILLINGHAM, P. W., MCGRAW, C. M., ARMSTRONG, E. A., CORNWALL, C. E., FENG, Y. Y., HURD, C. L., GAULT-RINGOLD, M., ROLEDA, M. Y., TIMMINS-SCHIFFMAN, E. & NUNN, B. L. 2016. Physiological responses of a Southern Ocean diatom to complex future ocean conditions. *Nature Climate Change,* 6**,** 207-+.

BOYD, P. W., RYNEARSON, T. A., ARMSTRONG, E. A., FU, F., HAYASHI, K., HU, Z., HUTCHINS, D. A., KUDELA, R. M., LITCHMAN, E., MULHOLLAND, M. R., PASSOW, U., STRZEPEK, R. F., WHITTAKER, K. A., YU, E. & THOMAS, M. K. 2013. Marine Phytoplankton Temperature versus Growth Responses from Polar to Tropical Waters – Outcome of a Scientific Community-Wide Study. *PLOS ONE,* 8**,** e63091.

BRENNAN, G. & COLLINS, S. 2015. Growth responses of a green alga to multiple environmental drivers. *Nature Climate Change,* 5**,** 892-+.

BRUCKNER, C. G., BAHULIKAR, R., RAHALKAR, M., SCHINK, B. & KROTH, P. G. 2008. Bacteria Associated with Benthic Diatoms from Lake Constance: Phylogeny and Influences on Diatom Growth and Secretion of Extracellular Polymeric Substances. *Applied and Environmental Microbiology,* 74**,** 7740-7749.

BRUN, P., STAMIESZKIN, K., VISSER, A. W., LICANDRO, P., PAYNE, M. R. & KIORBOE, T. 2019. Climate change has altered zooplankton-fuelled carbon export in the North Atlantic. *Nature Ecology & Evolution,* 3**,** 416-+.

BUCHAN, A., LECLEIR, G. R., GULVIK, C. A. & GONZÁLEZ, J. M. 2014. Master recyclers: features and functions of bacteria associated with phytoplankton blooms. *Nature Reviews Microbiology,* 12**,** 686-698.

BURKE, C., STEINBERG, P., RUSCH, D., KJELLEBERG, S. & THOMAS, T. 2011. Bacterial community assembly based on functional genes rather than species. *Proceedings of the National Academy of Sciences of the United States of America,* 108**,** 14288-14293.

BURROWS, M., SCHOEMAN, D., BUCKLEY, L., MOORE, P., POLOCZANSKA, E., BRANDER, K., BROWN, C., BRUNO, J., DUARTE, C., HALPERN, B., HOLDING, J., KAPPEL, C., KIESSLING, W., O'CONNOR, M., PANDOLFI, J., PARMESAN, C., SCHWING, F., SYDEMAN, W. & RICHARDSON, A. 2011. The Pace of Shifting Climate in Marine and Terrestrial Ecosystems. *Science (New York, N.Y.),* 334**,** 652-5.

BURROWS, M. T., SCHOEMAN, D. S., RICHARDSON, A. J., MOLINOS, J. G., HOFFMANN, A., BUCKLEY, L. B., MOORE, P. J., BROWN, C. J., BRUNO, J. F., DUARTE, C. M., HALPERN, B. S., HOEGH-GULDBERG, O., KAPPEL, C. V., KIESSLING, W., O'CONNOR, M. I., PANDOLFI, J. M., PARMESAN, C., SYDEMAN, W., FERRIER, S., WILLIAMS, K. J. & POLOCZANSKA, E. S. 2014. Geographical limits to species-range shifts are suggested by climate velocity. *Nature,* 507**,** 492-+.

CAPUTI, L., CARRADEC, Q., EVEILLARD, D., KIRILOVSKY, A., PELLETIER, E., KARLUSICH, J. J. P., VIEIRA, F. R. J., VILLAR, E., CHAFFRON, S., MALVIYA, S., SCALCO, E., ACINAS, S. G., ALBERTI, A., AURY, J. M., BENOISTON, A. S., BERTRAND, A., BIARD, T., BITTNER, L., BOCCARA, M., BRUM, J. R., BRUNET, C., BUSSENI, G., CARRATALÀ, A., CLAUSTRE, H., COELHO, L. P., COLIN, S., D'ANIELLO, S., DA SILVA, C., DEL CORE, M., DORÉ, H., GASPARINI, S., KOKOSZKA, F., JAMET, J. L., LEJEUSNE, C., LEPOIVRE, C., LESCOT, M., LIMA-MENDEZ, G., LOMBARD, F., LUKES, J., MAILLET, N., MADOUI, M. A., MARTINEZ, E., MAZZOCCHI, M. G., NÉOU, M. B., PAZ-YEPES, J., POULAIN, J., RAMONDENC, S., ROMAGNAN, J. B., ROUX, S., MANTA, D. S., SANGES, R., SPEICH, S., SPROVIERI, M., SUNAGAWA, S., TAILLANDIER, V., TANAKA, A., TIRICHINE, L., TROTTIER, C., UITZ, J., VELUCHAMY, A., VESELÁ, J., VINCENT, F., YAU, S., KANDELS-LEWIS, S., SEARSON, S., DIMIER, C., PICHERAL, M., BORK, P., BOSS, E., DE VARGAS, C., FOLLOWS, M. J., GRIMSLEY, N., GUIDI, L., HINGAMP, P., KARSENTI, E., SORDINO, P., STEMMANN, L., SULLIVAN, M. B., TAGLIABUE, A., ZINGONE, A., GARCZAREK, L., D'ORTENZIO, F., TESTOR, P., NOT, F., D'ALCALÀ, M. R.,

WINCKER, P., BOWLER, C., IUDICONE, D., GORSKY, G., JAILLON, O., KARP-BOSS, L., KRZIC, U., OGATA, H., PESANT, S., RAES, J., REYNAUD, E. G., SARDET, C., SIERACKI, M., VELAYOUDON, D., WEISSENBACH, J., et al. 2019. Community-Level Responses to Iron Availability in Open Ocean Plankton Ecosystems. *Global Biogeochemical Cycles,* 33**,** 391-419.

CARLSON, S. M., CUNNINGHAM, C. J. & WESTLEY, P. A. H. 2014. Evolutionary rescue in a changing world. *Trends in Ecology & Evolution,* 29**,** 521-530.

CERMEÑO, P., DUTKIEWICZ, S., HARRIS, R. P., FOLLOWS, M., SCHOFIELD, O. & FALKOWSKI, P. G. 2008. The role of nutricline depth in regulating the ocean carbon cycle. *Proceedings of the National Academy of Sciences of the United States of America,* 105**,** 20344-20349.

CHAPPELL, P. D., WHITNEY, L. P., HADDOCK, T. L., MENDEN-DEUER, S., ROY, E. G., WELLS, M. L. & JENKINS, B. D. 2013. *Thalassiosira* spp. community composition shifts in response to chemical and physical forcing in the northeast Pacific Ocean. *Frontiers in Microbiology,* 4.

CHATURVEDI, A., ZHOU, J. R., RAEYMAEKERS, J. A. M., CZYPIONKA, T., ORSINI, L., JACKSON, C. E., SPANIER, K. I., SHAW, J. R., COLBOURNE, J. K. & DE MEESTER, L. 2021. Extensive standing genetic variation from a small number of founders enables rapid adaptation in. *Nature Communications,* 12.

CHEN, B. Z. 2015. Patterns of thermal limits of phytoplankton. *Journal of Plankton Research,* 37**,** 285-292.

CHEN, J. W., GUO, Y. Q., LU, Y. J., WANG, B. X., SUN, J. D., ZHANG, H. W. & WANG, H. 2019. Chemistry and Biology of Siderophores from Marine Microbes. *Marine Drugs,* 17.

CHEN, P. & KASSEN, R. 2020. The evolution and fate of diversity under hard and soft selection. *Proceedings of the Royal Society B-Biological Sciences,* 287.

CHEUNG, S., VONSHAK, A. & CHEN, F. 1998. Photoinhibition and Its Recovery of Spirulina Platensis in Photoautotrophic and Mixotrophic Cultures.

CHISHOLM, S. W. 2000. Oceanography - Stirring times in the Southern Ocean. *Nature,* 407**,** 685-687.

CHIVERS, W. J., WALNE, A. W. & HAYS, G. C. 2017. Mismatch between marine plankton range movements and the velocity of climate change. *Nature Communications,* 8.

CLEVE, P. T. 1873. On diatoms from the Arctic Sea. *Bihang till Kongliga Svenska Vetenskaps-Akademiens Handlingar,* 1**,** 1-28.

CLOERN, J. E. 1999. The relative importance of light and nutrient limitation of phytoplankton growth: a simple index of coastal ecosystem sensitivity to nutrient enrichment. *Aquatic Ecology,* 33**,** 3-15.

COLE, J. J. 1982. Interactions between Bacteria and Algae in Aquatic Ecosystems. *Annual Review of Ecology and Systematics,* 13**,** 291-314.

CROFT, M. T., LAWRENCE, A. D., RAUX-DEERY, E., WARREN, M. J. & SMITH, A. G. 2005. Algae acquire vitamin B12 through a symbiotic relationship with bacteria. *Nature,* 438**,** 90-93.

CROTEAU, D., GUÉRIN, S., BRUYANT, F., FERLAND, J., CAMPBELL, D. A., BABIN, M. & LAVAUD, J. 2021. Contrasting nonphotochemical quenching patterns under high light and darkness aligns with light niche occupancy in Arctic diatoms. *Limnology and Oceanography,* 66**,** S231-S245.

DESCAMPS-JULIEN, B. & GONZALEZ, A. 2005. Stable coexistence in a fluctuating environment: An experimental demonstration. *Ecology,* 86**,** 2815-2824.

DEVRIES, T. 2022. The Ocean Carbon Cycle. *Annual Review of Environment and Resources,* 47**,** 317-341.

DICKMAN, E. M., VANNI, M. J. & HORGAN, M. J. 2006. Interactive effects of light and nutrients on phytoplankton stoichiometry. *Oecologia,* 149**,** 676-689.

DORRELL, R. G., VILLAIN, A., PEREZ-LAMARQUE, B., DE KERDREL, G. A., MCCALLUM, G., WATSON, A. K., AIT-MOHAMED, O., ALBERTI, A., CORRE, E., FRISCHKORN, K. R., KARLUSICH, J. J. P., PELLETIER, E., MORLON, H., BOWLER, C. & BLANC, G. 2021. Phylogenomic fingerprinting of tempo and functions of horizontal gene transfer within ochrophytes. *Proceedings of the National Academy of Sciences of the United States of America,* 118.

DURHAM, B. P., SHARMA, S., LUO, H. W., SMITH, C. B., AMIN, S. A., BENDER, S. J., DEARTH, S. P., VAN MOOY, B. A. S., CAMPAGNA, S. R., KUJAWINSKI, E. B., ARMBRUST, E. V. & MORAN, M. A. 2015. Cryptic carbon and sulfur cycling between surface ocean plankton. *Proceedings of the National Academy of Sciences of the United States of America,* 112**,** 453-457.

DYHRMAN, S. T., JENKINS, B. D., RYNEARSON, T. A., SAITO, M. A., MERCIER, M. L., ALEXANDER, H., WHITNEY, L. P., DRZEWIANOWSKI, A., BULYGIN, V. V., BERTRAND, E. M., WU, Z. J., BENITEZ-NELSON, C. & HEITHOFF, A. 2012. The Transcriptome and Proteome of the Diatom *Thalassiosira pseudonana* Reveal a Diverse Phosphorus Stress Response. *Plos One,* 7.

ECKHART, V., GEBER, M., WF, M., TIFFIN, P., FABIO, E. & DA, M. 2011. Eckhart VM, Geber MA, Morris WF, Tiffin P, Fabio ES, Moeller DA (2011) The geography of demography: Long-term demographic studies and species distribution models reveal a species border limited by adaptation. American Naturalist 178: S26-S43. *The American Naturalist,* 178.

EDWARDS, K. F., THOMAS, M. K., KLAUSMEIER, C. A. & LITCHMAN, E. 2016. Phytoplankton growth and the interaction of light and temperature: A synthesis at the species and community level. *Limnology and Oceanography,* 61**,** 1232-1244.

ELLEGAARD, M. & RIBEIRO, S. 2018. The long-term persistence of phytoplankton resting stages in aquatic 'seed banks'. *Biological Reviews,* 93**,** 166-183.

EPPLEY, R. W. 1972. Temperature and Phytoplankton Growth in Sea. *Fishery Bulletin,* 70**,** 1063-1085.

EPPLEY, R. W. & THOMAS, W. H. 1969. Comparison of half-saturation constants for growth and nitrate uptake of marine phytoplankton. *Journal of Phycology,* 5**,** 375-379.

FALCIATORE, A., JAUBERT, M., BOULY, J.-P., BAILLEUL, B. & MOCK, T. 2020. Diatom Molecular Research Comes of Age: Model Species for Studying Phytoplankton Biology and Diversity[OPEN]. *The Plant Cell,* 32**,** 547-572.

FALKOWSKI, P. G. 1994. The Role of Phytoplankton Photosynthesis in Global Biogeochemical Cycles. *Photosynthesis Research,* 39**,** 235-258.

FALKOWSKI, P. G. 2015. *Life's engines: how microbes made Earth habitable*, Princeton University Press.

FALKOWSKI, P. G., FENCHEL, T. & DELONG, E. F. 2008. The microbial engines that drive Earth's biogeochemical cycles. *Science,* 320**,** 1034-1039.

FERREIRA, A., SÁ, C., SILVA, N., BELTRÁN, C., DIAS, A. M. & BRITO, A. C. 2020. Phytoplankton response to nutrient pulses in an upwelling system assessed through a microcosm experiment (Algarrobo Bay, Chile). *Ocean & Coastal Management,* 190**,** 105167.

FIELD, C. B., BEHRENFELD, M. J., RANDERSON, J. T. & FALKOWSKI, P. 1998. Primary production of the biosphere: Integrating terrestrial and oceanic components. *Science,* 281**,** 237-240.

FILATOV, D. A. & KIRKPATRICK, M. 2024. How does evolution work in superabundant microbes? *Trends in Microbiology,* 32**,** 836-846.

FLYNN, K. J. & RAVEN, J. A. 2023. Errata and re-visitation of "What is the limit for photoautotrophic plankton growth rates?" (Flynn and Raven, 2017). *Journal of Plankton Research,* 45**,** 597-603.

FRIEDLINGSTEIN, P., O'SULLIVAN, M., JONES, M. W., ANDREW, R. M., GREGOR, L., HAUCK, J., LE QUÉRÉ, C., LUIJKX, I. T., OLSEN, A., PETERS, G. P., PETERS, W., PONGRATZ, J., SCHWINGSHACKL, C., SITCH, S., CANADELL, J. G., CIAIS, P., JACKSON, R. B., ALIN, S. R., ALKAMA, R., ARNETH, A., ARORA, V. K., BATES, N. R., BECKER, M., BELLOUIN, N., BITTIG, H. C., BOPP, L., CHEVALLIER, F., CHINI, L. P., CRONIN, M., EVANS, W., FALK, S., FEELY, R. A., GASSER, T., GEHLEN, M., GKRITZALIS, T., GLOEGE, L., GRASSI, G., GRUBER, N., GÜRSES, Ö., HARRIS, I., HEFNER, M., HOUGHTON, R. A., HURTT, G. C., IIDA, Y., ILYINA, T., JAIN, A. K., JERSILD, A., KADONO, K., KATO, E., KENNEDY, D., GOLDEWIJK, K. K., KNAUER, J., KORSBAKKEN, J. I., LANDSCHÜTZER, P., LEFÈVRE, N., LINDSAY, K., LIU, J. J., LIU, Z., MARLAND, G., MAYOT, N., MCGRATH, M. J., METZL, N., MONACCI, N. M., MUNRO, D. R., NAKAOKA, S. I., NIWA, Y., O'BRIEN, K., ONO, T., PALMER, P., PAN, N. Q., PIERROT, D., POCOCK, K., POULTER, B., RESPLANDY, L., ROBERTSON, E., RÖDENBECK, C., RODRIGUEZ, C., ROSAN, T. M., SCHWINGER, J., SÉFÉRIAN, R., SHUTLER, J. D., SKJELVAN, I., STEINHOFF, T., SUN, Q., SUTTON, A. J., SWEENEY, C., TAKAO, S., TANHUA, T., TANS, P. P., TIAN, X. J., TIAN, H. Q., TILBROOK, B., TSUJINO, H., TUBIELLO, F., VAN DER WERF, G. R., WALKER, A. P., WANNINKHOF, R., WHITEHEAD, C., WRANNE,

A. W., WRIGHT, R., et al. 2022. Global Carbon Budget 2022. *Earth System Science Data,* 14**,** 4811-4900.

FUKAI, Y., MATSUNO, K., FUJIWARA, A. & SUZUKI, K. 2022. Photophysiological response of diatoms in surface sediments to light exposure: A laboratory experiment on a diatom community in sediments from the Chukchi Sea. *Frontiers in Marine Science,* 9.

FUKAO, T., KIMOTO, K. & KOTANI, Y. 2010. Production of transparent exopolymer particles by four diatom species. *Fisheries Science,* 76**,** 755-760.

FURUSAWA, G., YOSHIKAWA, T., YASUDA, A. & SAKATA, T. 2003. Algicidal activity and gliding motility of *Saprospira* sp. SS98-5. *Canadian Journal of Microbiology,* 49**,** 92-100.

GALLET, R., FROISSART, R. & RAVIGNÉ, V. 2018. Experimental demonstration of the impact of hard and soft selection regimes on polymorphism maintenance in spatially heterogeneous environments. *Evolution,* 72**,** 1677-1688.

GÄRDES, A., IVERSEN, M. H., GROSSART, H. P., PASSOW, U. & ULLRICH, M. S. 2011. Diatom-associated bacteria are required for aggregation of *Thalassiosira weissflogii*. *Isme Journal,* 5**,** 436-445.

GASTON, K. J. 1990. Patterns in the Geographical Ranges of Species. *Biological Reviews,* 65**,** 105-129.

GIESLER, J. K., AHME, A. & WOHLRAB, S. in prep. Microbiome compositional plasticity of Arctic and temperate diatoms in response to temperature.

GLEDHILL, M. & BUCK, K. N. 2012. The organic complexation of iron in the marine environment: a review. *Frontiers in Microbiology,* 3.

GRANT, M. A. A., KAZAMIA, E., CICUTA, P. & SMITH, A. G. 2014. Direct exchange of vitamin B is demonstrated by modelling the growth dynamics of algal-bacterial cocultures. *Isme Journal,* 8**,** 1418-1427.

GROSSER, K., ZEDLER, L., SCHMITT, M., DIETZEK, B., POPP, J. & POHNERT, G. 2012. Disruption-free imaging by Raman spectroscopy reveals a chemical sphere with antifouling metabolites around macroalgae. *Biofouling,* 28**,** 687-696.

GUILLARD, R. R. L. 1975. Culture of Phytoplankton for Feeding Marine Invertebrates. *In:* SMITH, W. L. & CHANLEY, M. H. (eds.) *Culture of Marine Invertebrate Animals: Proceedings — 1st Conference on Culture of Marine Invertebrate Animals Greenport.* Boston, MA: Springer US.

HAINES, K. C. & GUILLARD, R. R. 1974. Growth of Vitamin-B12-Requiring Marine Diatoms in Mixed Laboratory Cultures with Vitamin-B12-Producing Marine Bacteria. *Journal of Phycology,* 10**,** 245-252.

HAMM, C. E., MERKEL, R., SPRINGER, O., JURKOJC, P., MAIER, C., PRECHTEL, K. & V, S. 2003. Architecture and material properties of diatom shells provide effective mechanical protection. *Nature,* 421**,** 841-843.

HAN, J. S., PARK, H. S. & CHUNG, E. S. 2023. Projections of central Arctic summer sea surface temperatures in CMIP6. *Environmental Research Letters,* 18.

HASSLER, C. S., SCHOEMANN, V., NICHOLS, C. M., BUTLER, E. C. V. & BOYD, P. W. 2011. Saccharides enhance iron bioavailability to Southern Ocean phytoplankton. *Proceedings of the National Academy of Sciences of the United States of America,* 108**,** 1076-1081.

HATTICH, G. S. I., JOKINEN, S., SILDEVER, S., GAREIS, M., HEIKKINEN, J., JUNGHARDT, N., SEGOVIA, M., MACHADO, M. & SJÖQVIST, C. 2024. Temperature optima of a natural diatom population increases as global warming proceeds. *Nature Climate Change,* 14.

HEARING, T. W., HARVEY, T. H. P., WILLIAMS, M., LENG, M. J., LAMB, A. L., WILBY, P. R., GABBOTT, S. E., POHL, A. & DONNADIEU, Y. 2018. An early Cambrian greenhouse climate. *Science Advances,* 4.

HEINRICHS, A. L., HARDORP, O. J., HILLEBRAND, H., SCHOTT, T. & STRIEBEL, M. 2024. Direct and indirect cumulative effects of temperature, nutrients, and light on phytoplankton growth. *Ecology and Evolution,* 14.

HELLIWELL, K. E., SHIBL, A. A. & AMIN, S. A. 2022. The Diatom Microbiome: New Perspectives for Diatom-Bacteria Symbioses. *In:* FALCIATORE, A. & MÖCK, T. (eds.) *The Molecular Life of Diatoms.* Springer.

HENRY, L. P., BRUIJNING, M., FORSBERG, S. K. G. & AYROLES, J. F. 2021. The microbiome extends host evolutionary potential. *Nature Communications,* 12.

HODAPP, D., ROCA, I. T., FIORENTINO, D., GARILAO, C., KASCHNER, K., KESNER-REYES, K., SCHNEIDER, B., SEGSCHNEIDER, J., KOCSIS, A. T., KIESSLING, W., BREY, T. & FROESE, R. 2023. Climate change disrupts core habitats of marine species. *Glob Chang Biol,* 29**,** 3304-3317.

HOLTERMANN, K. E., BATES, S. S., TRAINER, V. L., ODELL, A. & ARMBRUST, E. V. 2010. Mass Sexual Reproduction in the Toxigenic Diatoms *Pseudo-nitschia australis* and *P. Pungens* (Bacillariophyceae) on the Washington coast, USA. *Journal of Phycology,* 46**,** 41-52.

HONG, T., HUANG, N., MO, J. Z., CHEN, Y. H., LI, T. C. & DU, H. 2023. Transcriptomic and physiological responses of a model diatom (*Phaeodactylum tricornutum*) to heat shock and heat selection. *Ecological Indicators,* 153.

HOPPE, C. J. M., FUCHS, N., NOTZ, D., ANDERSON, P., ASSMY, P., BERGE, J., BRATBAK, G., GUILLOU, G., KRABERG, A., LARSEN, A., LEBRETON, B., LEU, E., LUCASSEN, M., MÜLLER, O., OZIEL, L., ROST, B., SCHARTMÜLLER, B., TORSTENSSON, A. & WLOKA, J. 2024. Photosynthetic light requirement near the theoretical minimum detected in Arctic microalgae. *Nature Communications,* 15**,** 7385.

HOPPE, C. J. M., SCHUBACK, N., SEMENIUK, D., GIESBRECHT, K., MOL, J., THOMAS, H., MALDONADO, M. T., ROST, B., VARELA, D. E. & TORTELL, P. D. 2018. Resistance of Arctic phytoplankton to ocean acidification and enhanced irradiance. *Polar Biology,* 41**,** 399-413.

HUBER, B. T., MACLEOD, K. G., WATKINS, D. K. & COFFIN, M. F. 2018. The rise and fall of the Cretaceous Hot Greenhouse climate. *Global and Planetary Change,* 167**,** 1-23.

HÜNKEN, M., HARDER, J. & KIRST, G. O. 2008. Epiphytic bacteria on the Antarctic ice diatom *Amphiprora kufferathii* (Manguin) cleave hydrogen peroxide produced during algal photosynthesis. *Plant Biology,* 10**,** 519-526.

HUTCHINSON, G. E. 1961. The paradox of the plankton. *American Naturalist,* 95**,** 137-145.

IPCC 2023. Climate Change 2023: Synthesis Report. Contribution of Working Groups I, II and III to the Sixth Assessment Report of the Intergovernmental Panel on Climate Change [Core Writing Team, H. Lee and J. Romero (eds.)]. IPCC, Geneva, Switzerland.

IRWIN, A. J., FINKEL, Z. V., MÜLLER-KARGER, F. E. & GHINAGLIA, L. T. 2015. Phytoplankton adapt to changing ocean environments. *Proceedings of the National Academy of Sciences of the United States of America,* 112**,** 5762-5766.

ISAAC, A., MOHAMED AMIN, R. & AMIN SHADY, A. 2024. Rhodobacteraceae are key players in microbiome assembly of the diatom *Asterionellopsis glacialis*. *Applied and Environmental Microbiology,* 90**,** e00570-24.

JAHREN, A. H. 2007. The Arctic Forest of the Middle Eocene. *Annual Review of Earth and Planetary Sciences,* 35**,** 509-540.

JANZEN, D. H. 1967. Why Mountain Passes are Higher in the Tropics. *The American Naturalist,* 101**,** 233-249.

JEWSON, D. H. 1992. Size-Reduction, Reproductive Strategy and the Life-Cycle of a Centric Diatom. *Philosophical Transactions of the Royal Society of London Series B-Biological Sciences,* 336**,** 191-213.

JIAO, N., HERNDL, G. J., HANSELL, D. A., BENNER, R., KATTNER, G., WILHELM, S. W., KIRCHMAN, D. L., WEINBAUER, M. G., LUO, T., CHEN, F. & AZAM, F. 2010. Microbial production of recalcitrant dissolved organic matter: long-term carbon storage in the global ocean. *Nature Reviews Microbiology,* 8**,** 593-599.

JIAO, N., LUO, T., CHEN, Q., ZHAO, Z., XIAO, X., LIU, J., JIAN, Z., XIE, S., THOMAS, H., HERNDL, G. J., BENNER, R., GONSIOR, M., CHEN, F., CAI, W.-J. & ROBINSON, C. 2024. The microbial carbon pump and climate change. *Nature Reviews Microbiology,* 22**,** 408-419.

JIN, X., GRUBER, N., DUNNE, J. P., SARMIENTO, J. L. & ARMSTRONG, R. A. 2006. Diagnosing the contribution of phytoplankton functional groups to the production and export of particulate organic carbon, CaCO3, and opal from global nutrient and alkalinity distributions. *Global Biogeochemical Cycles,* 20.

KANDA, J., ZIEMANN, D. A., CONQUEST, L. D. & BIENFANG, P. K. 1989. Light-Dependency of Nitrate Uptake by Phytoplankton over the Spring Bloom in Auke Bay, Alaska. *Marine Biology,* 103**,** 563-569.

KIM, D., PÉREZ-CARRASCAL, O. M., DESOUSA, C., JUNG, D. K., BOHLEY, S., WIJAYA, L., TRANG, K., KHOURY, S. & SHAPIRA, M. 2023. Microbiome remodeling through bacterial competition and host behavior enables rapid adaptation to environmental toxins. *bioRxiv*.

KOEDOODER, C., STOCK, W., WILLEMS, A., MANGELINCKX, S., DE TROCH, M., VYVERMAN, W. & SABBE, K. 2019. Diatom-Bacteria Interactions Modulate the Composition and Productivity of Benthic Diatom Biofilms. *Frontiers in Microbiology,* 10.

KOLUNDZIJA, S., CHENG, D. Q. & LAURO, F. M. 2022. RNA Viruses in Aquatic Ecosystems through the Lens of Ecological Genomics and Transcriptomics. *Viruses-Basel,* 14.

KOOISTRA, W. H. C. F. & MEDLIN, L. K. 2007. Species concepts in diatoms: A clarification. *Diatom Research,* 22**,** 227-228.

KRAUSE, J. W., SCHULZ, I. K., ROWE, K. A., DOBBINS, W., WINDING, M. H. S., SEJR, M. K., DUARTE, C. M. & AGUSTÍ, S. 2019. Silicic acid limitation drives bloom termination and potential carbon sequestration in an Arctic bloom. *Scientific Reports,* 9.

KROTH, P. G., CHIOVITTI, A., GRUBER, A., MARTIN-JEZEQUEL, V., MOCK, T., PARKER, M. S., STANLEY, M. S., KAPLAN, A., CARON, L., WEBER, T., MAHESWARI, U., ARMBRUST, E. V. & BOWLER, C. 2008. A Model for Carbohydrate Metabolism in the Diatom *Phaeodactylum tricornutum* Deduced from Comparative Whole Genome Analysis. *Plos One,* 3.

LAI, Y. T., YEUNG, C. K. L., OMLAND, K. E., PANG, E. L., HAO, Y., LIAO, B. Y., CAO, H. F., ZHANG, B. W., YEH, C. F., HUNG, C. M., HUNG, H. Y., YANG, M. Y., LIANG, W., HSU, Y. C., YAO, C. T., DONG, L., LIN, K. & LI, S. H. 2019. Standing genetic variation as the predominant source for adaptation of a songbird. *Proceedings of the National Academy of Sciences of the United States of America,* 116**,** 2152-2157.

LANE, N., ALLEN, J. F. & MARTIN, W. 2010. How did LUCA make a living? Chemiosmosis in the origin of life. *Bioessays,* 32**,** 271-280.

LANY, N. K., ZARNETSKE, P. L., GOUHIER, T. C. & MENGE, B. A. 2017. Incorporating Context Dependency of Species Interactions in Species Distribution Models. *Integrative and Comparative Biology,* 57**,** 159-167.

LENSSEN, N. J. L., SCHMIDT, G. A., HANSEN, J. E., MENNE, M. J., PERSIN, A., RUEDY, R. & ZYSS, D. 2019. Improvements in the GISTEMP Uncertainty Model. *Journal of Geophysical Research: Atmospheres,* 124**,** 6307-6326.

LEVITAN, O., DINAMARCA, J., ZELZION, E., LUN, D. S., GUERRA, L. T., KIM, M. K., KIM, J., VAN MOOY, B. A. S., BHATTACHARYA, D. & FALKOWSKI, P. G. 2015. Remodeling of intermediate metabolism in the diatom *Phaeodactylum tricornutum* under nitrogen stress. *Proceedings of the National Academy of Sciences of the United States of America,* 112**,** 412-417.

LI, X. F., ROEVROS, N., DEHAIRS, F. & CHOU, L. 2017. Biological responses of the marine diatom *Chaetoceros socialis* to changing environmental conditions: A laboratory experiment. *Plos One,* 12.

LIEBIG, J. 1840. *Organische Chemie in ihrer Anwendung auf Agricultur und Physiologie,* Braunschweig, Vieweg.

LITCHMAN, E. & KLAUSMEIER, C. A. 2008. Trait-Based Community Ecology of Phytoplankton. *Annual Review of Ecology Evolution and Systematics,* 39**,** 615-639.

LIU, K., LIU, S., CUI, Z., ZHAO, Y. & CHEN, N. 2024. Rich diversity and active spatial–temporal dynamics of *Thalassiosira* species revealed by time-series metabarcoding analysis. *ISME Communications,* 4**,** ycad009.

LOMMER, M., SPECHT, M., ROY, A. S., KRAEMER, L., ANDRESON, R., GUTOWSKA, M. A., WOLF, J., BERGNER, S. V., SCHILHABEL, M. B., KLOSTERMEIER, U. C., BEIKO, R. G., ROSENSTIEL, P., HIPPLER, M. & LAROCHE, J. 2012. Genome and low-iron response of an oceanic diatom adapted to chronic iron limitation. *Genome Biology,* 13.

LONGOBARDI, L., DUBROCA, L., MARGIOTTA, F., SARNO, D. & ZINGONE, A. 2022. Photoperiod-driven rhythms reveal multi-decadal stability of phytoplankton communities in a highly fluctuating coastal environment. *Scientific Reports,* 12.

LUTZ, V. A., SATHYENDARANATH, S., HEAD, E. J. H. & LI, W. K. W. 2001. Changes in the absorption and fluorescence excitation spectra with growth irradiance in three species of phytoplankton. *Journal of Plankton Research,* 23**,** 555-569.

LYNCH, H., RHAINDS, M., CALABRESE, J., CANTRELL, S., COSNER, C. & FAGAN, W. 2014. How climate extremes—Not means—Define a species' geographic range boundary via a demographic tipping point. *Ecological Monographs,* 84**,** 131-149.

MACDONALD, A. M. & WUNSCH, C. 1996. An estimate of global ocean circulation and heat fluxes. *Nature,* 382**,** 436-439.

MALVIYA, S., SCALCO, E., AUDIC, S., VINCENTA, F., VELUCHAMY, A., POULAIN, J., WINCKER, P., IUDICONE, D., DE VARGAS, C., BITTNER, L., ZINGONE, A. & BOWLER, C. 2016. Insights into global diatom distribution and diversity in the world's ocean. *Proceedings of the National Academy of Sciences of the United States of America,* 113**,** E1516-E1525.

MANN, D. 1988. Why didn't Lund see sex in *Asterionella*? A discussion of the diatom life cycle in nature.

MANN, D. G. 1999. The species concept in diatoms. *Phycologia,* 38**,** 437-495.

MANN, D. G. & VANORMELINGEN, P. 2013. An Inordinate Fondness? The Number, Distributions, and Origins of Diatom Species. *Journal of Eukaryotic Microbiology,* 60**,** 414-420.

MARCHETTI, A., SCHRUTH, D. M., DURKIN, C. A., PARKER, M. S., KODNER, R. B., BERTHIAUME, C. T., MORALES, R., ALLEN, A. E. & ARMBRUST, E. V. 2012. Comparative metatranscriptomics identifies molecular bases for the physiological

responses of phytoplankton to varying iron availability. *Proceedings of the National Academy of Sciences of the United States of America,* 109**,** E317-E325.

MARGULIS, L. & FESTER, R. 1991. Symbiosis as a Source of Evolutionary Innovation - Speciation and Morphogenesis - Margulis,L, Fester,R. *Nature,* 352**,** 391-391.

MARTIN, K., SCHMIDT, K., TOSELAND, A., BOULTON, C. A., BARRY, K., BESZTERI, B., BRUSSAARD, C. P. D., CLUM, A., DAUM, C. G., ELOE-FADROSH, E., FONG, A., FOSTER, B., FOSTER, B., GINZBURG, M., HUNTEMANN, M., IVANOVA, N. N., KYRPIDES, N. C., LINDQUIST, E., MUKHERJEE, S., PALANIAPPAN, K., REDDY, T. B. K., RIZKALLAH, M. R., ROUX, S., TIMMERMANS, K., TRINGE, S. G., VAN DE POLL, W. H., VARGHESE, N., VALENTIN, K. U., LENTON, T. M., GRIGORIEV, I. V., LEGGETT, R. M., MOULTON, V. & MOCK, T. 2021. The biogeographic differentiation of algal microbiomes in the upper ocean from pole to pole. *Nature Communications,* 12**,** 5483.

MARTIN, T. L. & HUEY, R. B. 2008. Why "Suboptimal" is optimal: Jensen's inequality and ectotherm thermal preferences. *American Naturalist,* 171**,** E102-E118.

MATURILLI, M., HERBER, A. & KÖNIG-LANGLO, G. 2013. Climatology and time series of surface meteorology in Ny-Ålesund, Svalbard. *Earth System Science Data,* 5**,** 155-163.

MAYALI, X. & AZAM, F. 2004. Algicidal bacteria in the sea and their impact on algal blooms. *Journal of Eukaryotic Microbiology,* 51**,** 139-144.

MEDLIN, L. K., WILLIAMS, D. M. & SIMS, P. A. 1993. The Evolution of the Diatoms (Bacillariophyta) .1. Origin of the Group and Assessment of the Monophyly of Its Major Divisions. *European Journal of Phycology,* 28**,** 261-275.

MILLER, T. R., HNILICKA, K., DZIEDZIC, A., DESPLATS, P. & BELAS, R. 2004. Chemotaxis of *Silicibacter* sp strain TM1040 toward dinoflagellate products. *Applied and Environmental Microbiology,* 70**,** 4692-4701.

MITCHELL, R. 1971. Role of predators in the reversal of imbalances in microbial ecosystems. *Nature,* 230**,** 257–258.

MOCK, T., OTILLAR, R. P., STRAUSS, J., MCMULLAN, M., PAAJANEN, P., SCHMUTZ, J., SALAMOV, A., SANGES, R., TOSELAND, A., WARD, B. J., ALLEN, A. E., DUPONT, C. L., FRICKENHAUS, S., MAUMUS, F., VELUCHAMY, A., WU, T. Y., BARRY, K. W., FALCIATORE, A., FERRANTE, M. I., FORTUNATO, A. E., GLÖCKNER, G., GRUBER, A., HIPKIN, R., JANECH, M. G., KROTH, P. G., LEESE, F., LINDQUIST, E. A., LYON, B. R., MARTIN, J., MAYER, C., PARKER, M., QUESNEVILLE, H., RAYMOND, J. A., UHLIG, C., VALAS, R. E., VALENTIN, K. U., WORDEN, A. Z., ARMBRUST, E. V., CLARK, M. D., BOWLER, C., GREEN, B. R., MOULTON, V., VAN OOSTERHOUT, C. & GRIGORIEV, I. V. 2017. Evolutionary genomics of the cold-adapted diatom. *Nature,* 541**,** 536-540.

MOCK, T., SAMANTA, M. P., IVERSON, V., BERTHIAUME, C., ROBISON, M., HOLTERMANN, K., DURKIN, C., BONDURANT, S. S., RICHMOND, K., RODESCH, M., KALLAS, T., HUTTLIN, E. L., CERRINA, F., SUSSMANN, M. R. & ARMBRUST, E. V. 2008. Whole-genome expression profiling of the marine diatom *Thalassiosira pseudonana* identifies genes involved in silicon bioprocesses.

Proceedings of the National Academy of Sciences of the United States of America, 105**,** 1579-1584.

MOISE, A. R., KUKSA, V., IMANISHI, Y. & PALCZEWSKI, K. 2004. Identification of all-trans-retinol:: All-trans-13,14-dihydroretinol saturase. *Journal of Biological Chemistry,* 279**,** 50230-50242.

MÖNNICH, J., TEBBEN, J., BERGEMANN, J., CASE, R., WOHLRAB, S. & HARDER, T. 2020. Niche-based assembly of bacterial consortia on the diatom *Thalassiosira rotula* is stable and reproducible. *Isme Journal,* 14**,** 1614-1625.

MONTSANT, A., ALLEN, A. E., COESEL, S., DE MARTINO, A., FALCIATORE, A., MANGOGNA, M., SIAUT, M., HEIJDE, M., JABBARI, K., MAHESWARI, U., RAYKO, E., VARDI, A., APT, K. E., BERGES, J. A., CHIOVITTI, A., DAVIS, A. K., THAMATRAKOLN, K., HADI, M. Z., LANE, T. W., LIPPMEIER, J. C., MARTINEZ, D., PARKER, M. S., PAZOUR, G. J., SAITO, M. A., ROKHSAR, D. S., ARMBRUST, E. V. & BOWLER, C. 2007. Identification and comparative genomic analysis of signaling and regulatory components in the diatom. *Journal of Phycology,* 43**,** 585-604.

MONTSANT, A., JABBARI, K., MAHESWARI, U. & BOWLER, C. 2005. Comparative genomics of the pennate diatom. *Plant Physiology,* 137**,** 500-513.

MORAN, N. A. 2002. Microbial minimalism: Genome reduction in bacterial pathogens. *Cell,* 108**,** 583-586.

MOSKOVITS, G. 1961. *Studies on diatom-bacteria interactions.*, Texas A&M University.

MOUGET, J.-L., GASTINEAU, R., DAVIDOVICH, O., GAUDIN, P. & DAVIDOVICH, N. A. 2009. Light is a key factor in triggering sexual reproduction in the pennate diatom *Haslea ostrearia*. *FEMS Microbiology Ecology,* 69**,** 194-201.

MÜHLENBRUCH, M., GROSSART, H. P., EIGEMANN, F. & VOSS, M. 2018. Mini-review: Phytoplankton-derived polysaccharides in the marine environment and their interactions with heterotrophic bacteria. *Environmental Microbiology,* 20**,** 2671-2685.

MUNDAY, P., WARNER, R., MONRO, K., PANDOLFI, J. & MARSHALL, D. 2013. Predicting evolutionary responses to climate change in the sea. *Ecology letters,* 16.

NISBET, R. E. R., KILIAN, O. & MCFADDEN, G. I. 2004. Diatom genomics: Genetic acquisitions and mergers. *Current Biology,* 14**,** R1048-R1050.

NOAA 2024. Dr. Xin Lan, NOAA/GML (gml.noaa.gov/ccgg/trends/) and Dr. Ralph Keeling, Scripps Institution of Oceanography (scrippsco2.ucsd.edu/).

NOWICKI, M., DEVRIES, T. & SIEGEL, D. 2022. Quantifying the Carbon Export and Sequestration Pathways of the Ocean's Biological Carbon Pump. *Global Biogeochemical Cycles,* 36.

OGURA, A., AKIZUKI, Y., IMODA, H., MINETA, K., GOJOBORI, T. & NAGAI, S. 2018. Comparative genome and transcriptome analysis of diatom, *Skeletonema costatum*, reveals evolution of genes for harmful algal bloom. *Bmc Genomics,* 19.

OLDEN, J. D. 2006. Biotic homogenization: a new research agenda for conservation biogeography. *Journal of Biogeography,* 33**,** 2027-2039.

ONG, L. K., LAUW, V. V., TANG, S., ARIFIN, Y. & RIADI, L. 2023. Application of solar photovoltaic for the cultivation of *Arthospira platensis* (Spirulina). *International Journal of Applied Science and Engineering,* 20**,** 1-7.

OOMEN, R. A. & HUTCHINGS, J. A. 2022. Genomic reaction norms inform predictions of plastic and adaptive responses to climate change. *Journal of Animal Ecology,* 91**,** 1073-1087.

OSTENFELD, C. S., J. 1901. Plankton fra det Røde hav og Adenbugten, Vidensk. Meddel. Naturh. Forening i Kbhvn. *Marine pelagic cyanobacteria: Trichodesmium and other Diazotrophs.*: Springer Science & Business Media.

PADFIELD, D., YVON-DUROCHER, G., BUCKLING, A., JENNINGS, S. & YVON-DUROCHER, G. 2016. Rapid evolution of metabolic traits explains thermal adaptation in phytoplankton. *Ecology Letters,* 19**,** 133-142.

PARFREY, L. W., LAHR, D. J. G., KNOLL, A. H. & KATZ, L. A. 2011. Estimating the timing of early eukaryotic diversification with multigene molecular clocks. *Proceedings of the National Academy of Sciences of the United States of America,* 108**,** 13624-13629.

PAUL, C. & POHNERT, G. 2011. Interactions of the Algicidal Bacterium *Kordia algicida* with Diatoms: Regulated Protease Excretion for Specific Algal Lysis. *Plos One,* 6.

PEARSON, G. A., LAGO-LESTON, A., CÁNOVAS, F., COX, C. J., VERRET, F., LASTERNAS, S., DUARTE, C. M., AGUSTI, S. & SERRAO, E. A. 2015. Metatranscriptomes reveal functional variation in diatom communities from the Antarctic Peninsula. *Isme Journal,* 9**,** 2275-2289.

PETERSEN, C., HAMERICH, I. K., ADAIR, K. L., GRIEM-KREY, H., OLIVA, M. T., HOEPPNER, M. P., BOHANNAN, B. J. M. & SCHULENBURG, H. 2023. Host and microbiome jointly contribute to environmental adaptation. *Isme Journal,* 17**,** 1953-1965.

PINSKY, M., EIKESET, A. M., MCCAULEY, D., PAYNE, J. & SUNDAY, J. 2019. Greater vulnerability to warming of marine versus terrestrial ectotherms. *Nature,* 569**,** 1-4.

POLOCZANSKA, E. S., BROWN, C. J., SYDEMAN, W. J., KIESSLING, W., SCHOEMAN, D. S., MOORE, P. J., BRANDER, K., BRUNO, J. F., BUCKLEY, L. B., BURROWS, M. T., DUARTE, C. M., HALPERN, B. S., HOLDING, J., KAPPEL, C. V., O'CONNOR, M. I., PANDOLFI, J. M., PARMESAN, C., SCHWING, F., THOMPSON, S. A. & RICHARDSON, A. J. 2013. Global imprint of climate change on marine life. *Nature Climate Change,* 3**,** 919-925.

POULÍČKOVÁ, A. & MANN, D. 2019. Diatom Sexual Reproduction and Life Cycles.

RANTANEN, M., KARPECHKO, A. Y., LIPPONEN, A., NORDLING, K., HYVÄRINEN, O., RUOSTEENOJA, K., VIHMA, T. & LAAKSONEN, A. 2022. The Arctic has warmed nearly four times faster than the globe since 1979. *Communications Earth & Environment,* 3.

RASTOGI, A., VIEIRA, F. R. J., DETON-CABANILLAS, A. F., VELUCHAMY, A., CANTREL, C., WANG, G. H., VANORMELINGEN, P., BOWLER, C., PIGANEAU, G., HU, H. H. & TIRICHINE, L. 2020. A genomics approach reveals the global genetic polymorphism, structure, and functional diversity of ten accessions of the marine model diatom. *Isme Journal,* 14**,** 347-363.

RETALLACK, G. J. 2013. Permian and Triassic greenhouse crises. *Gondwana Research,* 24**,** 90-103.

REUSCH, T. B. H. & BOYD, P. W. 2013. Experimental Evolution Meets Marine Phytoplankton. *Evolution,* 67**,** 1849-1859.

RICHON, C. & TAGLIABUE, A. 2021. Biogeochemical feedbacks associated with the response of micronutrient recycling by zooplankton to climate change. *Global Change Biology,* 27**,** 4758-4770.

ROSENBERG, E. & ZILBER-ROSENBERG, I. 2018. The hologenome concept of evolution after 10 years. *Microbiome,* 6.

ROSENZWEIG, C., KAROLY, D., VICARELLI, M., NEOFOTIS, P., WU, Q. G., CASASSA, G., MENZEL, A., ROOT, T. L., ESTRELLA, N., SEGUIN, B., TRYJANOWSKI, P., LIU, C. Z., RAWLINS, S. & IMESON, A. 2008. Attributing physical and biological impacts to anthropogenic climate change. *Nature,* 453**,** 353-U20.

RUMYANTSEVA, A., HENSON, S., MARTIN, A., THOMPSON, A. F., DAMERELL, G. M., KAISER, J. & HEYWOOD, K. J. 2019. Phytoplankton spring bloom initiation: The impact of atmospheric forcing and light in the temperate North Atlantic Ocean. *Progress in Oceanography,* 178.

RYTHER, J. H. 1956. Photosynthesis in the Ocean as a Function of Light Intensity. *Limnology and Oceanography,* 1**,** 61-70.

SAGAN, L. 1967. On the origin of mitosing cells. *Journal of Theoretical Biology,* 14**,** 225-IN6.

SAR, E. A., SUNESEN, I., LAVIGNE, A. S. & LOFEUDO, S. 2011. Thalassiosira gravida, a heterotypic synonym of *Thalassiosira rotula*: morphological evidence. *Diatom Research,* 26**,** 109-119.

SAYANOVA, O., MIMOUNI, V., ULMANN, L., MORANT-MANCEAU, A., PASQUET, V., SCHOEFS, B. & NAPIER, J. A. 2017. Modulation of lipid biosynthesis by stress in diatoms. *Philosophical Transactions of the Royal Society B-Biological Sciences,* 372.

SCHAUM, C. E., BUCKLING, A., SMIRNOFF, N. & YVON-DUROCHER, G. 2022. Evolution of thermal tolerance and phenotypic plasticity under rapid and slow temperature fluctuations. *Proceedings of the Royal Society B-Biological Sciences,* 289.

SCHOLZ, B. 2014. Purification and Culture Characteristics of 36 Benthic Marine Diatoms Isolated from the Solthorn Tidal Flat (Southern North Sea). *Journal of Phycology,* 50**,** 685-697.

SEMINA, G. I. 2004. *SEM-studied diatom of different regions of the world ocean*, Ruggell Liechtenstein.

SEYEDSAYAMDOST, M. R., CASE, R. J., KOLTER, R. & CLARDY, J. 2011. The Jekyll-and-Hyde chemistry of *Phaeobacter gallaeciensis*. *Nature Chemistry,* 3**,** 331-335.

SEYMOUR, J. R., AHMED, T., DURHAM, W. M. & STOCKER, R. 2010. Chemotactic response of marine bacteria to the extracellular products of *Synechococcus* and *Prochlorococcus*. *Aquatic Microbial Ecology,* 59**,** 161-168.

SEYMOUR, J. R., AMIN, S. A., RAINA, J. B. & STOCKER, R. 2017. Zooming in on the phycosphere: the ecological interface for phytoplankton-bacteria relationships. *Nature Microbiology,* 2.

SHIBL, A. A., ISAAC, A., OCHSENKÜHN, M. A., CÁRDENAS, A., FEI, C., BEHRINGER, G., ARNOUX, M., DROU, N., SANTOS, M. P., GUNSALUS, K. C., VOOLSTRA, C. R. & AMIN, S. A. 2020. Diatom modulation of select bacteria through use of two unique secondary metabolites. *Proceedings of the National Academy of Sciences of the United States of America,* 117**,** 27445-27455.

SHILOVA, I. N., MAGASIN, J. D., MILLS, M. M., ROBIDART, J. C., TURK-KUBO, K. A. & ZEHR, J. P. 2020. Phytoplankton transcriptomic and physiological responses to fixed nitrogen in the California current system. *Plos One,* 15.

SHRESTHA, R. P., TESSON, B., NORDEN-KRICHMAR, T., FEDEROWICZ, S., HILDEBRAND, M. & ALLEN, A. E. 2012. Whole transcriptome analysis of the silicon response of the diatom. *Bmc Genomics,* 13.

SHU, Q., WANG, Q., ÅRTHUN, M., WANG, S., SONG, Z., ZHANG, M. & QIAO, F. 2022. Arctic Ocean Amplification in a warming climate in CMIP6 models. *Science Advances,* 8**,** eabn9755.

SIMON, J. C., MARCHESI, J. R., MOUGEL, C. & SELOSSE, M. A. 2019. Host-microbiota interactions: from holobiont theory to analysis. *Microbiome,* 7.

SMETACEK, V. S. 1985. Role of Sinking in Diatom Life-History Cycles - Ecological, Evolutionary and Geological Significance. *Marine Biology,* 84**,** 239-251.

SMITH, D. C., STEWARD, G. F., LONG, R. A. & AZAM, F. 1995. Bacterial Mediation of Carbon Fluxes during a Diatom Bloom in a Mesocosm. *Deep-Sea Research Part Ii-Topical Studies in Oceanography,* 42**,** 75-97.

SMITH, D. F. & WIEBE, W. J. 1976. Constant Release of Photosynthate from Marine-Phytoplankton. *Applied and Environmental Microbiology,* 32**,** 75-79.

SMRIGA, S., FERNANDEZ, V. I., MITCHELL, J. G. & STOCKER, R. 2016. Chemotaxis toward phytoplankton drives organic matter partitioning among marine bacteria. *Proceedings of the National Academy of Sciences of the United States of America,* 113**,** 1576-1581.

SOBERÓN, J. & ARROYO-PEÑA, B. 2017. Are fundamental niches larger than the realized? Testing a 50-year-old prediction by Hutchinson. *PLOS ONE,* 12.

SOMMER, U. 1996. Plankton ecology: The past two decades of progress. *Naturwissenschaften,* 83**,** 293-301.

SONNENSCHEIN, E. C., SYIT, D. A., GROSSART, H. P. & ULLRICH, M. S. 2012. Chemotaxis of *Marinobacter adhaerens* and Its Impact on Attachment to the Diatom Thalassiosira weissflogii. *Applied and Environmental Microbiology,* 78**,** 6900-6907.

SORTE, C. J. B., WILLIAMS, S. L. & CARLTON, J. T. 2010. Marine range shifts and species introductions: comparative spread rates and community impacts. *Global Ecology and Biogeography,* 19**,** 303-316.

SPILLING, K., YLÖSTALO, P., SIMIS, S. & SEPPÄLÄ, J. 2015. Interaction Effects of Light, Temperature and Nutrient Limitations (N, P and Si) on Growth, Stoichiometry and Photosynthetic Parameters of the Cold-Water Diatom. *Plos One,* 10.

STEINACHER, M., JOOS, F., FRÖLICHER, T., BOPP, L., CADULE, P., COCCO, V., DONEY, S., GEHLEN, M., LINDSAY, K., MOORE, J., SCHNEIDER, B. & SEGSCHNEIDER, J. 2010. Projected 21st century decrease in marine productivity: A multi-model analysis. *Biogeosciences,* 7**,** 979-1005.

STOCK, F., BILCKE, G., DE DECKER, S., OSUNA-CRUZ, C., VAN DEN BERGE, K., VANCAESTER, E., VEYLDER, L., VANDEPOELE, K., MANGELINCKX, S. & VYVERMAN, W. 2020. Distinctive Growth and Transcriptional Changes of the Diatom *Seminavis robusta* in Response to Quorum Sensing Related Compounds. *Frontiers in Microbiology,* 11.

STOCKER, R. 2015. The 100 µm length scale in the microbial ocean. *Aquatic Microbial Ecology,* 76**,** 189-194.

SULEIMAN, M., ZECHER, K., YÜCEL, O., JAGMANN, N. & PHILIPP, B. 2016. Interkingdom Cross-Feeding of Ammonium from Marine Methylamine-Degrading Bacteria to the Diatom. *Applied and Environmental Microbiology,* 82**,** 7113-7122.

SULTANA, S., BRUNS, S., WILKES, H., SIMON, M. & WIENHAUSEN, G. 2023. Vitamin B12 is not shared by all marine prototrophic bacteria with their environment. *The ISME Journal,* 17**,** 836-845.

SUPRAHA, L., KLEMM, K., GRAN-STADNICZEÑKO, S., HÖRSTMANN, C., VAULOT, D., EDVARDSEN, B. & JOHN, U. 2022. Diversity and biogeography of planktonic diatoms in Svalbard fjords: The role of dispersal and Arctic endemism in phytoplankton community structuring. *Elementa-Science of the Anthropocene,* 10.

SVENNING, J. B., VASSKOG, T., CAMPBELL, K., BAEVERUD, A. H., MYHRE, T. N., DALHEIM, L., FORGEREAU, Z. L., OSANEN, J. E., HANSEN, E. H. & BERNSTEIN, H. C. 2024. Lipidome Plasticity Enables Unusual Photosynthetic Flexibility in Arctic vs. Temperate Diatoms. *Marine Drugs,* 22.

THEUS, M. E., LAYDEN, T. J., MCWILLIAMS, N., CRAFTON-TEMPEL, S., KREMER, C. T. & FEY, S. B. 2022. Photoperiod influences the shape and scaling of freshwater phytoplankton responses to light and temperature. *Oikos,* 2022.

THOMAS, M. K., ARANGUREN-GASSIS, M., KREMER, C. T., GOULD, M. R., ANDERSON, K., KLAUSMEIER, C. A. & LITCHMAN, E. 2017. Temperature-

nutrient interactions exacerbate sensitivity to warming in phytoplankton. *Global Change Biology,* 23**,** 3269-3280.

THOMAS, M. K., KREMER, C. T., KLAUSMEIER, C. A. & LITCHMAN, E. 2012. A Global Pattern of Thermal Adaptation in Marine Phytoplankton. *Science,* 338**,** 1085-1088.

THOMAS, M. K., KREMER, C. T. & LITCHMAN, E. 2016. Environment and evolutionary history determine the global biogeography of phytoplankton temperature traits. *Global Ecology and Biogeography,* 25**,** 75-86.

TILMAN, D. 1977. Resource Competition between Planktonic Algae - Experimental and Theoretical Approach. *Ecology,* 58**,** 338-348.

TITTEL, J., BISSINGER, V., ZIPPEL, B., GAEDKE, U., BELL, E., LORKE, A. & KAMJUNKE, N. 2003. Mixotrophs combine resource use to outcompete specialists: Implications for aquatic food webs. *Proceedings of the National Academy of Sciences of the United States of America,* 100**,** 12776-12781.

TOUGERON, K. 2021. How Constraining are Photic Barriers to Poleward Range-Shifts? *Trends in Ecology & Evolution,* 36**,** 478-479.

TOULZA, E., TAGLIABUE, A., BLAIN, S. & PIGANEAU, G. 2012. Analysis of the Global Ocean Sampling (GOS) Project for Trends in Iron Uptake by Surface Ocean Microbes. *Plos One,* 7.

TRALLER, J. C., COKUS, S. J., LOPEZ, D. A., GAIDARENKO, O., SMITH, S. R., MCCROW, J. P., GALLAHER, S. D., PODELL, S., THOMPSON, M., COOK, O., MORSELLI, M., JAROSZEWICZ, A., ALLEN, E. E., ALLEN, A. E., MERCHANT, S. S., PELLEGRINI, M. & HILDEBRAND, M. 2016. Genome and methylome of the oleaginous diatom *Cyclotella cryptica* reveal genetic flexibility toward a high lipid phenotype. *Biotechnology for Biofuels,* 9.

VANCAESTER, E., DEPUYDT, T., OSUNA-CRUZ, C. M. & VANDEPOELE, K. 2020. Comprehensive and Functional Analysis of Horizontal Gene Transfer Events in Diatoms. *Molecular Biology and Evolution,* 37**,** 3243-3257.

VELUCHAMY, A., LIN, X., MAUMUS, F., RIVAROLA, M., BHAVSAR, J., CREASY, T., O'BRIEN, K., SENGAMALAY, N. A., TALLON, L. J., SMITH, A. D., RAYKO, E., AHMED, I., LE CROM, S., FARRANT, G. K., SGRO, J. Y., OLSON, S. A., BONDURANT, S. S., ALLEN, A. E., RABINOWICZ, P. D., SUSSMAN, M. R., BOWLER, C. & TIRICHINE, L. 2014. Insights into the role of DNA methylation in diatoms by genome-wide profiling in Phaeodactylum tricornutum. *Nature Communications,* 5.

VON DASSOW, P. & MONTRESOR, M. 2011. Unveiling the mysteries of phytoplankton life cycles: patterns and opportunities behind complexity. *Journal of Plankton Research,* 33**,** 3-12.

WAKSMAN, S. A. R., C. E. 1936. Decomposition of organic matter in sea water by bacteria: iii. Factors influencing the rate of decomposition. *Biol Bull,* 70**,** 472–483.

WANG, R. R., GALLANT, É., WILSON, M. Z., WU, Y. H., LI, A. R., GITAI, Z. & SEYEDSAYAMDOST, M. R. 2022. Algal -coumaric acid induces oxidative stress and siderophore biosynthesis in the bacterial symbiont *Phaeobacer inhibens*. *Cell Chemical Biology,* 29**,** 670-+.

WEISSE, T., GRÖSCHL, B. & BERGKEMPER, V. 2016. Phytoplankton response to short-term temperature and nutrient changes. *Limnologica,* 59**,** 78-89.

WHITTAKER, K. A., RIGNANESE, D. R., OLSON, R. J. & RYNEARSON, T. A. 2012. Molecular subdivision of the marine diatom *Thalassiosira rotula* in relation to geographic distribution, genome size, and physiology. *Bmc Evolutionary Biology,* 12.

WIGGLESWORTH-COOKSEY, B. & COOKSEY, K. E. 2005. Use of fluorophore-conjugated lectins to study cell-cell interactions in model marine biofilms. *Applied and Environmental Microbiology,* 71**,** 428-435.

WILHELM, S. W. & SUTTLE, C. A. 1999. Viruses and Nutrient Cycles in the Sea - Viruses play critical roles in the structure and function of aquatic food webs. *Bioscience,* 49**,** 781-788.

WINDLER, M., TSYMBAL, D., KRYVENDA, A., STRAILE, D., GRUBER, A. & KROTH, P. 2014. Influence of bacteria on cell size development and morphology of cultivated diatoms. *Phycological Research,* 62**,** 269-281.

WISZ, M., POTTIER, J., KISSLING, W., PELLISSIER, L., LENOIR, J., DAMGAARD, C., DORMANN, C., FORCHHAMMER, M., GRYTNES, J. A., GUISAN, A., HEIKKINEN, R., HØYE, T., KÜHN, I., LUOTO, M., MAIORANO, L., NILSSON, M.-C., NORMAND, S., ÖCKINGER, E., SCHMIDT, N. & SVENNING, J.-C. 2013. The role of biotic interactions in shaping distributions and realised assemblages of species: Implications for species distribution modelling. *Biological reviews of the Cambridge Philosophical Society,* 88**,** 15-30.

WORDEN, A. Z., FOLLOWS, M. J., GIOVANNONI, S. J., WILKEN, S., ZIMMERMAN, A. E. & KEELING, P. J. 2015. Rethinking the marine carbon cycle: Factoring in the multifarious lifestyles of microbes. *Science,* 347.

YE, N. H., HAN, W. T., TOSELAND, A., WANG, Y. T., FAN, X., XU, D., VAN OOSTERHOUT, C., GRIGORIEV, I. V., TAGLIABUE, A., ZHANG, J., ZHANG, Y., MA, J., QIU, H., LI, Y. X., ZHANG, X. W., MOCK, T. & CONSORTIUM, S. C. 2022. The role of zinc in the adaptive evolution of polar phytoplankton. *Nature Ecology & Evolution,* 6**,** 965-+.

YOSHIKAWA, T., NAKAHARA, M., TABATA, A., KOKUMAI, S., FURUSAWA, G. & SAKATA, T. 2008. Characterization and expression of *Saprospira* cytoplasmic fibril protein (SCFP) gene from algicidal *Saprospira* spp. strains. *Fisheries Science,* 74**,** 1109-1117.

ZEHR, J. P. 2015. How single cells work together. *Science,* 349**,** 1163-1164.

ZOCCARATO, L., SHER, D., MIKI, T., SEGRÈ, D. & GROSSART, H.-P. 2022. A comparative whole-genome approach identifies bacterial traits for marine microbial interactions. *Communications Biology,* 5**,** 276.

Appendix Publication I

What does it mean to be(come) Arctic? Functional and genetic traits of Arctic- and temperate-adapted diatoms

Supplementary material

Table S2.1: Detailed available information about the diatom strains used in this study. Information contains species name, strain name as used throughout the manuscript (ID), the official strain name as used in the respective culture collections where the strains originated from (strain name), isolation date, and the sampling location (latitude, longitude) in decimal degrees (if available). Moreover, culture conditions during long-term cultivation in the respective culture collections are given, showing that both Arctic and temperate strains were kept at rather intermediate photoperiods before they were obtained for this study.

species	ID	Strain name	isolation date	latitude	longitude	culture collection temperature	culture collection photoperiod
T. gravida	A1	UiO478	2018-08-20	83.33	29.29	4°C	14:10h
T. gravida	A2	UiO483	2018-08-05	83.15	31.46	4°C	14:10h
T. gravida	A3	UiO484	2018-08-05	83.15	31.46	4°C	14:10h
T. gravida	A4	UIO447	2017-09-12	79.99	14.97	4°C	14:10h
T. gravida	A5	UiO448	2017-09-12	79.99	14.97	4°C	14:10h
T. rotula	T1	t_rotula_S16	unknown	54.183333	7.9	15°C	16:8h
T. rotula	T2	strain_WHV	2022-03-06	54.183333	7.9	15°C	16:8h
T. rotula	T3	strain_Sylt	2021-09-01	55.0300	8.46	15°C	16:8h
T. rotula	T4	RCC_778	unknown	English channel		13°C	12:12h
T. rotula	T5	RCC_290	unknown	English channel		20°C	12:12h

Table S2.2: Details and references for RNA-seq input data for CAAStools analysis. For each RNA-seq data set location code number in Figure 4 of the main manuscript is given, as well as RNA-seq type (i.e., obtained from culture isolate or metatranscriptomic field sample), species and strain (in case of culture isolates), origin and specific sampling or isolation coordinates and data references. Coordinates marked with an asterisk (*) indicate approxim ate coordinates as exact location could not be identified.

Location Code (Fig.4)	RNA-seq type	Species	Strain	Origin	Lat	Long	Reference
1	Isolate	*Thalassiosira gravida*	NORCCA UIO478 (A1)	Arctic	83.33	29.29	this study
2	Isolate	*Thalassiosira gravida*	NORCCA UIO483 (A2)	Arctic	83.15	31.46	this study
3	Isolate	*Thalassiosira gravida*	NORCCA UIO484 (A3)	Arctic	83.15	31.46	this study
4	Isolate	*Thalassiosira gravida*	NORCCA UIO447 (A4)	Arctic	79.99	14.97	this study
5	Isolate	*Thalassiosira gravida*	NORCCA UIO448 (A5)	Arctic	79.99	14.97	this study
6	Isolate	*Thalassiosira rotula*	Harder Lab t.rotula S16 (T1)	Temperate	54.18	7.90	this study
7	Isolate	*Thalassiosira rotula*	WHV (T2)	Temperate	54.18	7.90	this study
8	Isolate	*Thalassiosira rotula*	Sylt (T3)	Temperate	55.03	8.46	this study
9	Isolate	*Thalassiosira rotula*	RCC290 (T4)	Temperate	49.79*	-2.57*	this study
10	Isolate	*Shionodiscus bioculatus*	-	Arctic	78.98	9.48	this study
11	Isolate	*Minidiscus spinulatus*	RCC4659	Temperate	49.79*	-2.57*	https://zenodo.org/records/5256603
12	Isolate	*Minidiscus variabilis*	RCC4665	Temperate	49.79*	-2.57*	https://zenodo.org/records/5256603
13	Isolate	*Minutocellus polymorphus*	-	Temperate	-17.50	11.25	https://evocellbio.com/eukprot/
14	Isolate	*Fragilariopsis sp.*	-	Arctic	69.07	-52.41	https://doi.org/10.1186/s12867-019-0124-0
15	Isolate	*Pseudo-Nitzschia turgidula*	-	Arctic	69.07	-52.41	https://doi.org/10.1186/s12867-019-0124-0
16	Isolate	*Arcocellulus cornucervis*	-	Arctic	71.18	-159.42	https://evocellbio.com/eukprot/
17	Isolate	*Chaetoceros diaderma*	-	Arctic	78.98	9.48	this study
18	Isolate	*Pseudo-Nitzschia turgidula*	-	Arctic	78.98	9.48	this study
19	Isolate	*Dactyliosolen fragilissimus*	-	Temperate	41.33	-70.57	https://evocellbio.com/eukprot/
20	Isolate	*Detonula confervaceae*	-	Temperate	41.60	-71.40	https://evocellbio.com/eukprot/
21	Metatranscriptome	-	-	Temperate	44.28	-12.61	DOI: 10.46936/10.25585/60000951
22	Metatranscriptome	-	-	Temperate	45.53	-12.43	DOI: 10.46936/10.25585/60000951
23	Metatranscriptome	-	-	Temperate	47.57	-12.11	DOI: 10.46936/10.25585/60000951
24	Metatranscriptome	-	-	Arctic	78.85	9.23	DOI: 10.46936/10.25585/60000951
25	Metatranscriptome	-	-	Arctic	78.87	8.11	DOI: 10.46936/10.25585/60000951
26	Metatranscriptome	-	-	Arctic	79.02	-9.52	DOI: 10.46936/10.25585/60000951
27	Metatranscriptome	-	-	Arctic	79.04	-7.67	DOI: 10.46936/10.25585/60000951
28	Metatranscriptome	-	-	Arctic	79.07	7.08	DOI: 10.46936/10.25585/60000951
29	Metatranscriptome	-	-	Arctic	79.08	-8.52	DOI: 10.46936/10.25585/60000951
30	Metatranscriptome	-	-	Temperate	41.50	-71.33	https://doi.org/10.1073/pnas.1421993112
31	Isolate	Minidiscus comicus	-	Temperate	49.79*	-2.57*	https://zenodo.org/records/5256603

Table S2.3: ANOVA results testing for differences of GAM shape as a response of photoperiod and the interaction of photoperiod and strain origin. Reference degrees of freedom (Ref. df), F-, and p-values are reported for each effect. Values marked with an asterisk (*) indicate significant effects ($p < 0.05$).

		GAM shape		
	Ref. df	*F*	*p*	
photoperiod	3	420.53	<0.001	*
photoperiod*origin	3	49.96	<0.001	*

Figure S2.1: Phylogenetic tree of ITS1 sequences for the *T. rotula* and *T. gravida* strains used in this study and respective reference sequences for both species (strains JX074…) identified by Whittaker et al (2012).

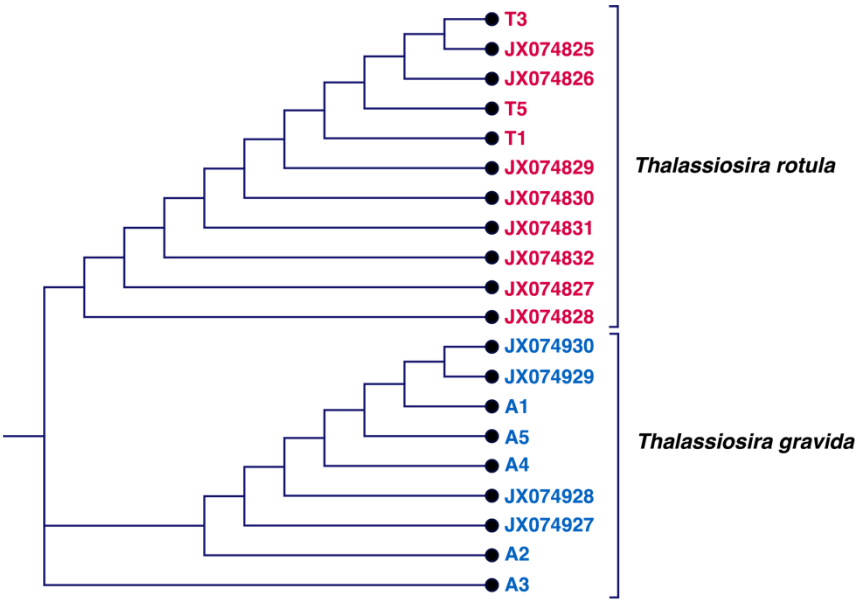

Appendix Publication II

Microbiome and photoperiod interactively determine thermal sensitivity of polar and temperate diatoms

Supplementary material

Table S1: Pairwise Post-hoc results for all treatment combinations on the maximum growth rate (μ_{max}) for *T. gravida* (polar)

	diff	ci.lo	ci.hi	t	p
9.axenic.4-4.axenic.4	-0.0594	-0.07920	-0.03958	10.78	<.01
13.5.axenic.4-4.axenic.4	-0.1075	-0.13205	-0.08295	15.83	<.01
4.xenic.4-4.axenic.4	0.0857	0.07070	0.10072	20.53	<.01
9.xenic.4-4.axenic.4	0.3021	0.28345	0.32071	58.23	<.01
13.5.xenic.4-4.axenic.4	0.3078	0.29026	0.32537	62.93	<.01
4.axenic.16-4.axenic.4	0.3522	0.32295	0.38154	43.66	<.01
9.axenic.16-4.axenic.4	0.3501	0.30099	0.39917	26.14	<.01
13.5.axenic.16-4.axenic.4	0.1826	0.14194	0.22335	16.40	<.01
4.xenic.16-4.axenic.4	0.3344	0.30216	0.36673	37.70	<.01
9.xenic.16-4.axenic.4	0.5922	0.56587	0.61848	81.52	<.01
13.5.xenic.16-4.axenic.4	0.5257	0.50563	0.54569	94.36	<.01
4.axenic.24-4.axenic.4	0.3211	0.30210	0.34011	60.69	<.01
9.axenic.24-4.axenic.4	0.4130	0.38246	0.44345	49.40	<.01
13.5.axenic.24-4.axenic.4	0.4201	0.39920	0.44100	72.36	<.01
4.xenic.24-4.axenic.4	0.3425	0.32073	0.36429	56.66	<.01
9.xenic.24-4.axenic.4	0.5463	0.50944	0.58310	54.13	<.01
13.5.xenic.24-4.axenic.4	0.2547	0.22272	0.28658	29.02	<.01
13.5.axenic.4-9.axenic.4	-0.0481	-0.07462	-0.02160	6.53	<.01
4.xenic.4-9.axenic.4	0.1451	0.12680	0.16340	28.65	<.01
9.xenic.4-9.axenic.4	0.3615	0.34020	0.38274	60.99	<.01
13.5.xenic.4-9.axenic.4	0.3672	0.34684	0.38757	64.77	<.01
4.axenic.16-9.axenic.4	0.4116	0.38073	0.44255	48.08	<.01
9.axenic.16-9.axenic.4	0.4095	0.35946	0.45948	29.89	<.01
13.5.axenic.16-9.axenic.4	0.2420	0.20021	0.28387	21.05	<.01
4.xenic.16-9.axenic.4	0.3938	0.36010	0.42758	42.24	<.01
9.xenic.16-9.axenic.4	0.6516	0.62344	0.67969	83.44	<.01
13.5.xenic.16-9.axenic.4	0.5851	0.56257	0.60753	93.38	<.01
4.axenic.24-9.axenic.4	0.3805	0.35891	0.40209	63.23	<.01
9.axenic.24-9.axenic.4	0.4723	0.44032	0.50437	53.45	<.01
13.5.axenic.24-9.axenic.4	0.4795	0.45626	0.50273	74.06	<.01
4.xenic.24-9.axenic.4	0.4019	0.37788	0.42592	60.07	<.01
9.xenic.24-9.axenic.4	0.6057	0.56758	0.64375	57.73	<.01
13.5.xenic.24-9.axenic.4	0.3140	0.28065	0.34744	34.02	<.01
4.xenic.4-13.5.axenic.4	0.1932	0.16981	0.21661	30.02	<.01
9.xenic.4-13.5.axenic.4	0.4096	0.38389	0.43528	57.41	<.01
13.5.xenic.4-13.5.axenic.4	0.4153	0.39034	0.44030	60.00	<.01
4.axenic.16-13.5.axenic.4	0.4598	0.42585	0.49366	48.72	<.01
9.axenic.16-13.5.axenic.4	0.4576	0.40580	0.50936	32.08	<.01
13.5.axenic.16-13.5.axenic.4	0.2902	0.24617	0.33413	23.85	<.01

4.xenic.16-13.5.axenic.4	0.4419	0.40549	0.47841	43.61	<.01
9.xenic.16-13.5.axenic.4	0.6997	0.66824	0.73112	79.87	<.01
13.5.xenic.16-13.5.axenic.4	0.6332	0.60650	0.65983	85.36	<.01
4.axenic.24-13.5.axenic.4	0.4286	0.40266	0.45457	59.45	<.01
9.axenic.24-13.5.axenic.4	0.5205	0.48556	0.55535	53.72	<.01
13.5.axenic.24-13.5.axenic.4	0.5276	0.50032	0.55489	69.46	<.01
4.xenic.24-13.5.axenic.4	0.4500	0.42208	0.47794	57.84	<.01
9.xenic.24-13.5.axenic.4	0.6538	0.61331	0.69424	58.28	<.01
13.5.xenic.24-13.5.axenic.4	0.3622	0.32601	0.39831	36.04	<.01
9.xenic.4-4.xenic.4	0.2164	0.19938	0.23336	45.93	<.01
13.5.xenic.4-4.xenic.4	0.2221	0.20633	0.23788	50.67	<.01
4.axenic.16-4.xenic.4	0.2665	0.23818	0.29490	34.31	<.01
9.axenic.16-4.xenic.4	0.2644	0.21581	0.31293	20.00	<.01
13.5.axenic.16-4.xenic.4	0.0969	0.05688	0.13700	8.88	<.01
4.xenic.16-4.xenic.4	0.2487	0.21728	0.28019	28.92	<.01
9.xenic.16-4.xenic.4	0.5065	0.48122	0.53171	73.06	<.01
13.5.xenic.16-4.xenic.4	0.4400	0.42141	0.45850	85.75	<.01
4.axenic.24-4.xenic.4	0.2354	0.21799	0.25281	48.79	<.01
9.axenic.24-4.xenic.4	0.3272	0.29763	0.35686	40.53	<.01
13.5.axenic.24-4.xenic.4	0.3344	0.31491	0.35388	62.11	<.01
4.xenic.24-4.xenic.4	0.2568	0.23635	0.27724	45.52	<.01
9.xenic.24-4.xenic.4	0.4606	0.42446	0.49667	46.73	<.01
13.5.xenic.24-4.xenic.4	0.1689	0.13786	0.20003	19.87	<.01
13.5.xenic.4-9.xenic.4	0.0057	-0.01349	0.02496	1.07	1
4.axenic.16-9.xenic.4	0.0502	0.01993	0.08040	6.00	<.01
9.axenic.16-9.xenic.4	0.0480	-0.00163	0.09762	3.54	.07
13.5.axenic.16-9.xenic.4	-0.1194	-0.16079	-0.07808	10.53	<.01
4.xenic.16-9.xenic.4	0.0324	-0.00077	0.06550	3.54	.06
9.xenic.16-9.xenic.4	0.2901	0.26273	0.31746	38.25	<.01
13.5.xenic.16-9.xenic.4	0.2236	0.20210	0.24506	37.37	<.01
4.axenic.24-9.xenic.4	0.0190	-0.00151	0.03956	3.32	.1
9.axenic.24-9.xenic.4	0.1109	0.07948	0.14226	12.83	<.01
13.5.axenic.24-9.xenic.4	0.1180	0.09575	0.14029	19.03	<.01
4.xenic.24-9.xenic.4	0.0404	0.01733	0.06352	6.29	<.01
9.xenic.24-9.xenic.4	0.2442	0.20663	0.28175	23.65	<.01
13.5.xenic.24-9.xenic.4	-0.0474	-0.08021	-0.01464	5.24	<.01
4.axenic.16-13.5.xenic.4	0.0444	0.01479	0.07408	5.43	<.01
9.axenic.16-13.5.xenic.4	0.0423	-0.00703	0.09155	3.14	.18
13.5.axenic.16-13.5.xenic.4	-0.1252	-0.16612	-0.08422	11.16	<.01
4.xenic.16-13.5.xenic.4	0.0266	-0.00597	0.05924	2.97	.25
9.xenic.16-13.5.xenic.4	0.2844	0.25765	0.31106	38.50	<.01
13.5.xenic.16-13.5.xenic.4	0.2178	0.19727	0.23843	38.03	<.01
4.axenic.24-13.5.xenic.4	0.0133	-0.00630	0.03288	2.44	.58
9.axenic.24-13.5.xenic.4	0.1051	0.07431	0.13597	12.42	<.01

13.5.axenic.24-13.5.xenic.4	0.1123	0.09087	0.13370	18.85	<.01
4.xenic.24-13.5.xenic.4	0.0347	0.01241	0.05697	5.60	<.01
9.xenic.24-13.5.xenic.4	0.2385	0.20136	0.27556	23.42	<.01
13.5.xenic.24-13.5.xenic.4	-0.0532	-0.08541	-0.02091	5.99	<.01
9.axenic.16-4.axenic.16	-0.0022	-0.05607	0.05172	0.15	1
13.5.axenic.16-4.axenic.16	-0.1696	-0.21612	-0.12309	13.13	<.01
4.xenic.16-4.axenic.16	-0.0178	-0.05739	0.02178	1.61	.98
9.xenic.16-4.axenic.16	0.2399	0.20481	0.27504	24.53	<.01
13.5.xenic.16-4.axenic.16	0.1734	0.14237	0.20445	20.16	<.01
4.axenic.24-4.axenic.16	-0.0311	-0.06159	-0.00069	3.70	.04
9.axenic.24-4.axenic.16	0.0607	0.02254	0.09887	5.71	<.01
13.5.axenic.24-4.axenic.16	0.0679	0.03630	0.09941	7.75	<.01
4.xenic.24-4.axenic.16	-0.0097	-0.04184	0.02236	1.09	1
9.xenic.24-4.axenic.16	0.1940	0.15077	0.23727	16.12	<.01
13.5.xenic.24-4.axenic.16	-0.0976	-0.13690	-0.05829	8.91	<.01
13.5.axenic.16-9.axenic.16	-0.1674	-0.22767	-0.10719	9.98	<.01
4.xenic.16-9.axenic.16	-0.0156	-0.07103	0.03976	1.02	1
9.xenic.16-9.axenic.16	0.2421	0.18957	0.29462	16.70	<.01
13.5.xenic.16-9.axenic.16	0.1756	0.12549	0.22567	12.80	<.01
4.axenic.24-9.axenic.16	-0.0290	-0.07872	0.02078	2.13	.79
9.axenic.24-9.axenic.16	0.0629	0.00843	0.11732	4.17	.01
13.5.axenic.24-9.axenic.16	0.0700	0.01964	0.12041	5.07	<.01
4.xenic.24-9.axenic.16	-0.0076	-0.05828	0.04314	0.54	1
9.xenic.24-9.axenic.16	0.1962	0.13830	0.25410	12.19	<.01
13.5.xenic.24-9.axenic.16	-0.0954	-0.15063	-0.04021	6.23	<.01
4.xenic.16-13.5.axenic.16	0.1518	0.10350	0.20009	11.30	<.01
9.xenic.16-13.5.axenic.16	0.4095	0.36465	0.45440	32.93	<.01
13.5.xenic.16-13.5.axenic.16	0.3430	0.30109	0.38494	29.76	<.01
4.axenic.24-13.5.axenic.16	0.1385	0.09695	0.17997	12.15	<.01
9.axenic.24-13.5.axenic.16	0.2303	0.18313	0.27748	17.57	<.01
13.5.axenic.24-13.5.axenic.16	0.2375	0.19516	0.27974	20.39	<.01
4.xenic.24-13.5.axenic.16	0.1599	0.11718	0.20254	13.59	<.01
9.xenic.24-13.5.axenic.16	0.3636	0.31240	0.41485	25.48	<.01
13.5.xenic.24-13.5.axenic.16	0.0720	0.02393	0.12008	5.38	<.01
9.xenic.16-4.xenic.16	0.2577	0.22016	0.29530	24.65	<.01
13.5.xenic.16-4.xenic.16	0.1912	0.15736	0.22507	20.43	<.01
4.axenic.24-4.xenic.16	-0.0133	-0.04666	0.01999	1.45	.99
9.axenic.24-4.xenic.16	0.0785	0.03811	0.11890	6.98	<.01
13.5.axenic.24-4.xenic.16	0.0857	0.05133	0.11998	9.02	<.01
4.xenic.24-4.xenic.16	0.0081	-0.02676	0.04288	0.84	1
9.xenic.24-4.xenic.16	0.2118	0.16664	0.25701	16.83	<.01
13.5.xenic.24-4.xenic.16	-0.0798	-0.12126	-0.03833	6.90	<.01
13.5.xenic.16-9.xenic.16	-0.0665	-0.09478	-0.03824	8.47	<.01
4.axenic.24-9.xenic.16	-0.2711	-0.29867	-0.24346	35.40	<.01

9.axenic.24-9.xenic.16	-0.1792	-0.21529	-0.14316	17.88	<.01
13.5.axenic.24-9.xenic.16	-0.1721	-0.20092	-0.14323	21.45	<.01
4.xenic.24-9.xenic.16	-0.2497	-0.27912	-0.22022	30.46	<.01
9.xenic.24-9.xenic.16	-0.0459	-0.08735	-0.00445	3.99	.02
13.5.xenic.24-9.xenic.16	-0.3375	-0.37479	-0.30025	32.53	<.01
4.axenic.24-13.5.xenic.16	-0.2046	-0.22635	-0.18276	33.68	<.01
9.axenic.24-13.5.xenic.16	-0.1127	-0.14486	-0.08055	12.70	<.01
13.5.axenic.24-13.5.xenic.16	-0.1056	-0.12898	-0.08214	16.17	<.01
4.xenic.24-13.5.xenic.16	-0.1832	-0.20735	-0.15896	27.17	<.01
9.xenic.24-13.5.xenic.16	0.0206	-0.01758	0.05880	1.96	.88
13.5.xenic.24-13.5.xenic.16	-0.2710	-0.30452	-0.23749	29.24	<.01
9.axenic.24-4.axenic.24	0.0918	0.06025	0.12343	10.55	<.01
13.5.axenic.24-4.axenic.24	0.0990	0.07642	0.12157	15.74	<.01
4.xenic.24-4.axenic.24	0.0214	-0.00199	0.04479	3.29	.11
9.xenic.24-4.axenic.24	0.2252	0.18744	0.26289	21.70	<.01
13.5.xenic.24-4.axenic.24	-0.0665	-0.09943	-0.03348	7.30	<.01
13.5.axenic.24-9.axenic.24	0.0071	-0.02550	0.03980	0.79	1
4.xenic.24-9.axenic.24	-0.0704	-0.10361	-0.03728	7.67	<.01
9.xenic.24-9.axenic.24	0.1333	0.08935	0.17730	10.90	<.01
13.5.xenic.24-9.axenic.24	-0.1583	-0.19842	-0.11817	14.17	<.01
4.xenic.24-13.5.axenic.24	-0.0776	-0.10248	-0.05271	11.19	<.01
9.xenic.24-13.5.axenic.24	0.1262	0.08758	0.16477	11.85	<.01
13.5.xenic.24-13.5.axenic.24	-0.1654	-0.19944	-0.13146	17.58	<.01
9.xenic.24-4.xenic.24	0.2038	0.16474	0.24279	18.90	<.01
13.5.xenic.24-4.xenic.24	-0.0879	-0.12234	-0.05336	9.19	<.01
13.5.xenic.24-9.xenic.24	-0.2916	-0.33656	-0.24667	23.29	<.01

Table S2: Pairwise Post-hoc results for all treatment combinations on the maximum growth rate (μ_{max}) for *T. gravida* (polar) for *T. rotula* (temperate)

comparison	**diff**	**ci.lo**	**ci.hi**	**t**	**p**
9.axenic.4-4.axenic.4	0.17532	0.1568	0.19386	33974	<.01
13.5.axenic.4-4.axenic.4	0.32314	0.3005	0.34574	51596	<.01
4.xenic.4-4.axenic.4	0.17281	0.1533	0.19237	31769	<.01
9.xenic.4-4.axenic.4	0.29927	0.2812	0.31736	59388	<.01
13.5.xenic.4-4.axenic.4	0.41709	0.4011	0.43310	93475	<.01
4.axenic.16-4.axenic.4	0.17326	0.1571	0.18939	38551	<.01
9.axenic.16-4.axenic.4	0.47771	0.4545	0.50097	74181	<.01
13.5.axenic.16-4.axenic.4	0.65728	0.6317	0.68290	92920	<.01
4.xenic.16-4.axenic.4	0.38755	0.3607	0.41435	52410	<.01
9.xenic.16-4.axenic.4	0.60603	0.5546	0.65746	43212	<.01
13.5.xenic.16-4.axenic.4	0.70803	0.6698	0.74623	67697	<.01

4.axenic.24-4.axenic.4	-0.00577	-0.0198	0.00823	1486	.99
9.axenic.24-4.axenic.4	0.05855	0.0400	0.07710	11339	<.01
13.5.axenic.24-4.axenic.4	0.39745	0.3645	0.43042	43913	<.01
4.xenic.24-4.axenic.4	0.11264	0.0970	0.12824	25921	<.01
9.xenic.24-4.axenic.4	0.51715	0.4913	0.54304	72350	<.01
13.5.xenic.24-4.axenic.4	0.25312	0.2215	0.28478	29101	<.01
13.5.axenic.4-9.axenic.4	0.14782	0.1238	0.17180	22161	<.01
4.xenic.4-9.axenic.4	-0.00251	-0.0237	0.01867	0.426	1
9.xenic.4-9.axenic.4	0.12394	0.1041	0.14381	22384	<.01
13.5.xenic.4-9.axenic.4	0.24176	0.2237	0.25980	48182	<.01
4.axenic.16-9.axenic.4	-0.00206	-0.0202	0.01608	0.408	1
9.axenic.16-9.axenic.4	0.30239	0.2778	0.32698	44231	<.01
13.5.axenic.16-9.axenic.4	0.48196	0.4551	0.50877	64808	<.01
4.xenic.16-9.axenic.4	0.21222	0.1843	0.24017	27410	<.01
9.xenic.16-9.axenic.4	0.43070	0.3787	0.48270	30307	<.01
13.5.xenic.16-9.axenic.4	0.53270	0.4937	0.57168	49750	<.01
4.axenic.24-9.axenic.4	-0.18109	-0.1974	-0.16477	40150	<.01
9.axenic.24-9.axenic.4	-0.11677	-0.1370	-0.09650	20664	<.01
13.5.axenic.24-9.axenic.4	0.22213	0.1882	0.25600	23789	<.01
4.xenic.24-9.axenic.4	-0.06268	-0.0804	-0.04500	12754	<.01
9.xenic.24-9.axenic.4	0.34183	0.3148	0.36891	45533	<.01
13.5.xenic.24-9.axenic.4	0.07780	0.0452	0.11040	8648	<.01
4.xenic.4-13.5.axenic.4	-0.15033	-0.1751	-0.12559	21824	<.01
9.xenic.4-13.5.axenic.4	-0.02387	-0.0475	-0.00021	3630	.05
13.5.xenic.4-13.5.axenic.4	0.09394	0.0717	0.11616	15286	<.01
4.axenic.16-13.5.axenic.4	-0.14988	-0.1722	-0.12759	24294	<.01
9.axenic.16-13.5.axenic.4	0.15457	0.1269	0.18221	20067	<.01
13.5.axenic.16-13.5.axenic.4	0.33414	0.3046	0.36373	40551	<.01
4.xenic.16-13.5.axenic.4	0.06441	0.0338	0.09500	7562	<.01
9.xenic.16-13.5.axenic.4	0.28288	0.2295	0.33623	19313	<.01
13.5.xenic.16-13.5.axenic.4	0.38488	0.3441	0.42570	34120	<.01
4.axenic.24-13.5.axenic.4	-0.32891	-0.3498	-0.30801	57309	<.01
9.axenic.24-13.5.axenic.4	-0.26459	-0.2886	-0.24059	39651	<.01
13.5.axenic.24-13.5.axenic.4	0.07431	0.0383	0.11033	7439	<.01
4.xenic.24-13.5.axenic.4	-0.21050	-0.2324	-0.18856	34725	<.01
9.xenic.24-13.5.axenic.4	0.19401	0.1642	0.22383	23364	<.01
13.5.xenic.24-13.5.axenic.4	-0.07002	-0.1049	-0.03518	7241	<.01
9.xenic.4-4.xenic.4	0.12646	0.1056	0.14727	21810	<.01
13.5.xenic.4-4.xenic.4	0.24427	0.2252	0.26337	46053	<.01
4.axenic.16-4.xenic.4	0.00045	-0.0187	0.01964	0.085	1
9.axenic.16-4.xenic.4	0.30490	0.2796	0.33023	43251	<.01
13.5.axenic.16-4.xenic.4	0.48447	0.4570	0.51195	63471	<.01
4.xenic.16-4.xenic.4	0.21474	0.1862	0.24332	27075	<.01
9.xenic.16-4.xenic.4	0.43321	0.3809	0.48553	30263	<.01

13.5.xenic.16-4.xenic.4	0.53521	0.4958	0.57462	49352	<.01
4.axenic.24-4.xenic.4	-0.17858	-0.1961	-0.16107	36994	<.01
9.axenic.24-4.xenic.4	-0.11426	-0.1355	-0.09306	19343	<.01
13.5.axenic.24-4.xenic.4	0.22464	0.1903	0.25902	23660	<.01
4.xenic.24-4.xenic.4	-0.06017	-0.0789	-0.04141	11556	<.01
9.xenic.24-4.xenic.4	0.34434	0.3166	0.37208	44709	<.01
13.5.xenic.24-4.xenic.4	0.08031	0.0472	0.11345	8769	<.01
13.5.xenic.4-9.xenic.4	0.11782	0.1002	0.13540	24080	<.01
4.axenic.16-9.xenic.4	-0.12600	-0.1437	-0.10832	25598	<.01
9.axenic.16-9.xenic.4	0.17844	0.1542	0.20273	26454	<.01
13.5.axenic.16-9.xenic.4	0.35802	0.3315	0.38455	48690	<.01
4.xenic.16-9.xenic.4	0.08828	0.0606	0.11596	11521	<.01
9.xenic.16-9.xenic.4	0.30676	0.2549	0.35862	21652	<.01
13.5.xenic.16-9.xenic.4	0.40876	0.3700	0.44755	38382	<.01
4.axenic.24-9.xenic.4	-0.30504	-0.3208	-0.28923	69784	<.01
9.axenic.24-9.xenic.4	-0.24071	-0.2606	-0.22084	43447	<.01
13.5.axenic.24-9.xenic.4	0.09818	0.0645	0.13185	10590	<.01
4.xenic.24-9.xenic.4	-0.18662	-0.2038	-0.16941	38986	<.01
9.xenic.24-9.xenic.4	0.21789	0.1911	0.24469	29347	<.01
13.5.xenic.24-9.xenic.4	-0.04615	-0.0785	-0.01376	5169	<.01
4.axenic.16-13.5.xenic.4	-0.24382	-0.2594	-0.22829	56315	<.01
9.axenic.16-13.5.xenic.4	0.06063	0.0377	0.08350	9584	<.01
13.5.axenic.16-13.5.xenic.4	0.24020	0.2149	0.26547	34461	<.01
4.xenic.16-13.5.xenic.4	-0.02954	-0.0560	-0.00305	4049	.01
9.xenic.16-13.5.xenic.4	0.18894	0.1377	0.24022	13522	<.01
13.5.xenic.16-13.5.xenic.4	0.29094	0.2529	0.32893	28005	<.01
4.axenic.24-13.5.xenic.4	-0.42286	-0.4361	-0.40957	114565	<.01
9.axenic.24-13.5.xenic.4	-0.35853	-0.3766	-0.34048	71404	<.01
13.5.axenic.24-13.5.xenic.4	-0.01964	-0.0524	0.01308	2189	.75
4.xenic.24-13.5.xenic.4	-0.30444	-0.3194	-0.28946	72921	<.01
9.xenic.24-13.5.xenic.4	0.10007	0.0745	0.12562	14203	<.01
13.5.xenic.24-13.5.xenic.4	-0.16396	-0.1954	-0.13257	19035	<.01
9.axenic.16-4.axenic.16	0.30445	0.2815	0.32740	47954	<.01
13.5.axenic.16-4.axenic.16	0.48402	0.4587	0.50936	69235	<.01
4.xenic.16-4.axenic.16	0.21428	0.1877	0.24083	29292	<.01
9.xenic.16-4.axenic.16	0.43276	0.3814	0.48407	30949	<.01
13.5.xenic.16-4.axenic.16	0.53476	0.4967	0.57279	51405	<.01
4.axenic.24-4.axenic.16	-0.17903	-0.1925	-0.16560	47998	<.01
9.axenic.24-4.axenic.16	-0.11471	-0.1329	-0.09656	22715	<.01
13.5.axenic.24-4.axenic.16	0.22418	0.1914	0.25695	24947	<.01
4.xenic.24-4.axenic.16	-0.06062	-0.0757	-0.04552	14401	<.01
9.xenic.24-4.axenic.16	0.34389	0.3183	0.36951	48668	<.01
13.5.xenic.24-4.axenic.16	0.07986	0.0484	0.11130	9253	<.01
13.5.axenic.16-9.axenic.16	0.17957	0.1495	0.20963	21441	<.01

4.xenic.16-9.axenic.16	-0.09016	-0.1212	-0.05911	10426	<.01
9.xenic.16-9.axenic.16	0.12831	0.0747	0.18190	8715	<.01
13.5.xenic.16-9.axenic.16	0.23031	0.1892	0.27145	20240	<.01
4.axenic.24-9.axenic.16	-0.48348	-0.5051	-0.46186	81509	<.01
9.axenic.24-9.axenic.16	-0.41916	-0.4438	-0.39455	61288	<.01
13.5.axenic.24-9.axenic.16	-0.08026	-0.1167	-0.04386	7946	<.01
4.xenic.24-9.axenic.16	-0.36507	-0.3877	-0.34245	58464	<.01
9.xenic.24-9.axenic.16	0.03944	0.0092	0.06973	4674	<.01
13.5.xenic.24-9.axenic.16	-0.22459	-0.2598	-0.18935	22951	<.01
4.xenic.16-13.5.axenic.16	-0.26974	-0.3025	-0.23698	29545	<.01
9.xenic.16-13.5.axenic.16	-0.05126	-0.1058	0.00324	3414	.09
13.5.xenic.16-13.5.axenic.16	0.05074	0.0084	0.09311	4318	.01
4.axenic.24-13.5.axenic.16	-0.66305	-0.6872	-0.63890	100243	<.01
9.axenic.24-13.5.axenic.16	-0.59873	-0.6256	-0.57191	80484	<.01
13.5.axenic.24-13.5.axenic.16	-0.25983	-0.2977	-0.22202	24708	<.01
4.xenic.24-13.5.axenic.16	-0.54464	-0.5697	-0.51960	78976	<.01
9.xenic.24-13.5.axenic.16	-0.14013	-0.1722	-0.10809	15690	<.01
13.5.xenic.24-13.5.axenic.16	-0.40416	-0.4409	-0.36745	39569	<.01
9.xenic.16-4.xenic.16	0.21848	0.1635	0.27347	14406	<.01
13.5.xenic.16-4.xenic.16	0.32048	0.2774	0.36351	26828	<.01
4.axenic.24-4.xenic.16	-0.39332	-0.4187	-0.36789	56540	<.01
9.axenic.24-4.xenic.16	-0.32899	-0.3569	-0.30104	42479	<.01
13.5.axenic.24-4.xenic.16	0.00990	-0.0287	0.04848	0.923	1
4.xenic.24-4.xenic.16	-0.27490	-0.3012	-0.24864	38049	<.01
9.xenic.24-4.xenic.16	0.12961	0.0966	0.16257	14107	<.01
13.5.xenic.24-4.xenic.16	-0.13442	-0.1719	-0.09693	12877	<.01
13.5.xenic.16-9.xenic.16	0.10200	0.0413	0.16270	6045	<.01
4.axenic.24-9.xenic.16	-0.61179	-0.6626	-0.56103	44337	<.01
9.axenic.24-9.xenic.16	-0.54747	-0.5995	-0.49547	38521	<.01
13.5.axenic.24-9.xenic.16	-0.20858	-0.2664	-0.15071	13004	<.01
4.xenic.24-9.xenic.16	-0.49338	-0.5446	-0.44221	35404	<.01
9.xenic.24-9.xenic.16	-0.08887	-0.1435	-0.03426	5906	<.01
13.5.xenic.24-9.xenic.16	-0.35290	-0.4101	-0.29570	22276	<.01
4.axenic.24-13.5.xenic.16	-0.71379	-0.7511	-0.67651	70299	<.01
9.axenic.24-13.5.xenic.16	-0.64947	-0.6885	-0.61049	60646	<.01
13.5.axenic.24-13.5.xenic.16	-0.31058	-0.3574	-0.26377	23824	<.01
4.xenic.24-13.5.xenic.16	-0.59538	-0.6332	-0.55754	57583	<.01
9.xenic.24-13.5.xenic.16	-0.19087	-0.2334	-0.14835	16183	<.01
13.5.xenic.24-13.5.xenic.16	-0.45490	-0.5009	-0.40895	35557	<.01
9.axenic.24-4.axenic.24	0.06432	0.0480	0.08067	14248	<.01
13.5.axenic.24-4.axenic.24	0.40322	0.3713	0.43510	46365	<.01
4.xenic.24-4.axenic.24	0.11841	0.1056	0.13118	33361	<.01
9.xenic.24-4.axenic.24	0.52292	0.4985	0.54737	78120	<.01
13.5.xenic.24-4.axenic.24	0.25889	0.2284	0.28941	31084	<.01

13.5.axenic.24-9.axenic.24	0.33890	0.3050	0.37278	36287	<.01
4.xenic.24-9.axenic.24	0.05409	0.0364	0.07179	10998	<.01
9.xenic.24-9.axenic.24	0.45860	0.4315	0.48569	61067	<.01
13.5.xenic.24-9.axenic.24	0.19457	0.1620	0.22718	21625	<.01
4.xenic.24-13.5.axenic.24	-0.28481	-0.3173	-0.25227	31954	<.01
9.xenic.24-13.5.axenic.24	0.11970	0.0817	0.15770	11329	<.01
13.5.xenic.24-13.5.axenic.24	-0.14433	-0.1862	-0.10245	12366	<.01
9.xenic.24-4.xenic.24	0.40451	0.3792	0.42983	58016	<.01
13.5.xenic.24-4.xenic.24	0.14048	0.1093	0.17169	16422	<.01
13.5.xenic.24-9.xenic.24	-0.26403	-0.3009	-0.22714	25720	<.01

Table S3: Maximum growth rate (μ_{max}) means and standard deviations for all treatment combinations of axenic and xenic *T. gravida* (polar) and *T. rotula* (temperate) cultures.

species	bacteria	temperature	photoperiod	mean μ	sd μ
T_gravida	axenic	4	4	0.086	0.023
T_gravida	axenic	4	16	0.439	0.051
T_gravida	axenic	4	24	0.407	0.029
T_gravida	axenic	9	4	0.027	0.030
T_gravida	axenic	9	16	0.436	0.090
T_gravida	axenic	9	24	0.457	0.150
T_gravida	axenic	13.5	4	-0.021	0.041
T_gravida	axenic	13.5	16	0.269	0.074
T_gravida	axenic	13.5	24	0.506	0.033
T_gravida	xenic	4	4	0.172	0.017
T_gravida	xenic	4	16	0.421	0.057
T_gravida	xenic	4	24	0.429	0.035
T_gravida	xenic	9	4	0.388	0.028
T_gravida	xenic	9	16	0.678	0.045
T_gravida	xenic	9	24	0.633	0.066
T_gravida	xenic	13.5	4	0.394	0.025
T_gravida	xenic	13.5	16	0.612	0.031
T_gravida	xenic	13.5	24	0.341	0.056
T_rotula	axenic	4	4	-0.017	0.023
T_rotula	axenic	4	16	0.157	0.021
T_rotula	axenic	4	24	-0.022	0.015
T_rotula	axenic	9	4	0.159	0.028
T_rotula	axenic	9	16	0.461	0.038
T_rotula	axenic	9	24	0.042	0.028
T_rotula	axenic	13.5	4	0.307	0.037
T_rotula	axenic	13.5	16	0.641	0.043
T_rotula	axenic	13.5	24	0.381	0.058
T_rotula	xenic	4	4	0.156	0.030
T_rotula	xenic	4	16	0.371	0.046
T_rotula	xenic	4	24	0.096	0.020
T_rotula	xenic	9	4	0.283	0.027
T_rotula	xenic	9	16	0.589	0.094
T_rotula	xenic	9	24	0.501	0.044
T_rotula	xenic	13.5	4	0.400	0.021
T_rotula	xenic	13.5	16	0.691	0.069
T_rotula	xenic	13.5	24	0.237	0.056

Figure S1: ITS1 sequences for the *T. rotula* (T. rotula_S16) and *T. gravida* (T.gravida_UiO478) strains used in this study and 3 reference sequences for both species (strains JX07…) identified by Whittaker et al (2012)

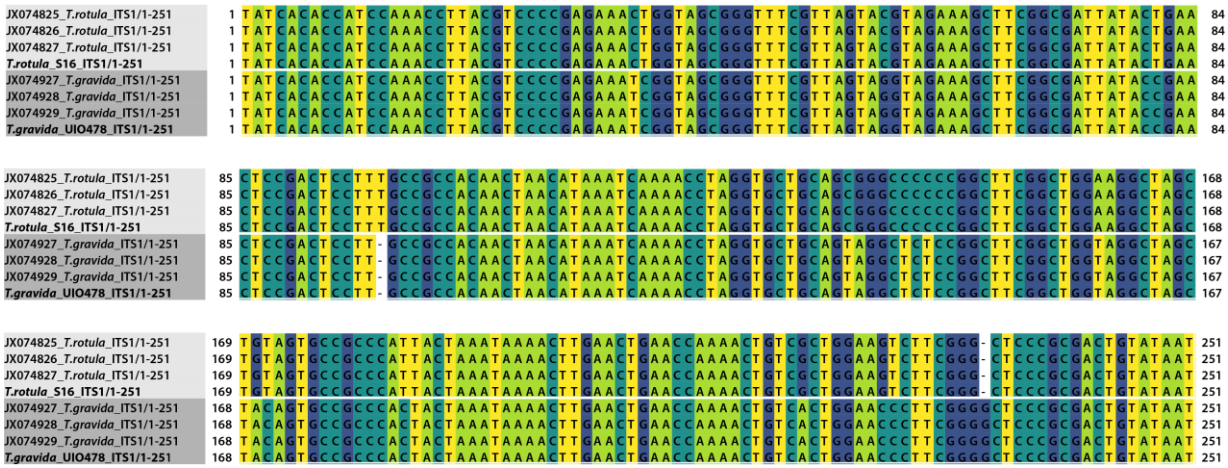

Figure S2: Exemplary images of CYBR green stained xenic (left) and axenic (right) *T. gravida* cultures at 200X (bottom) and 400X (top) magnification. Please note that CYBR green is a DNA-specific dye and that the large green staining inside the cells are the nucleus and not a contamination.

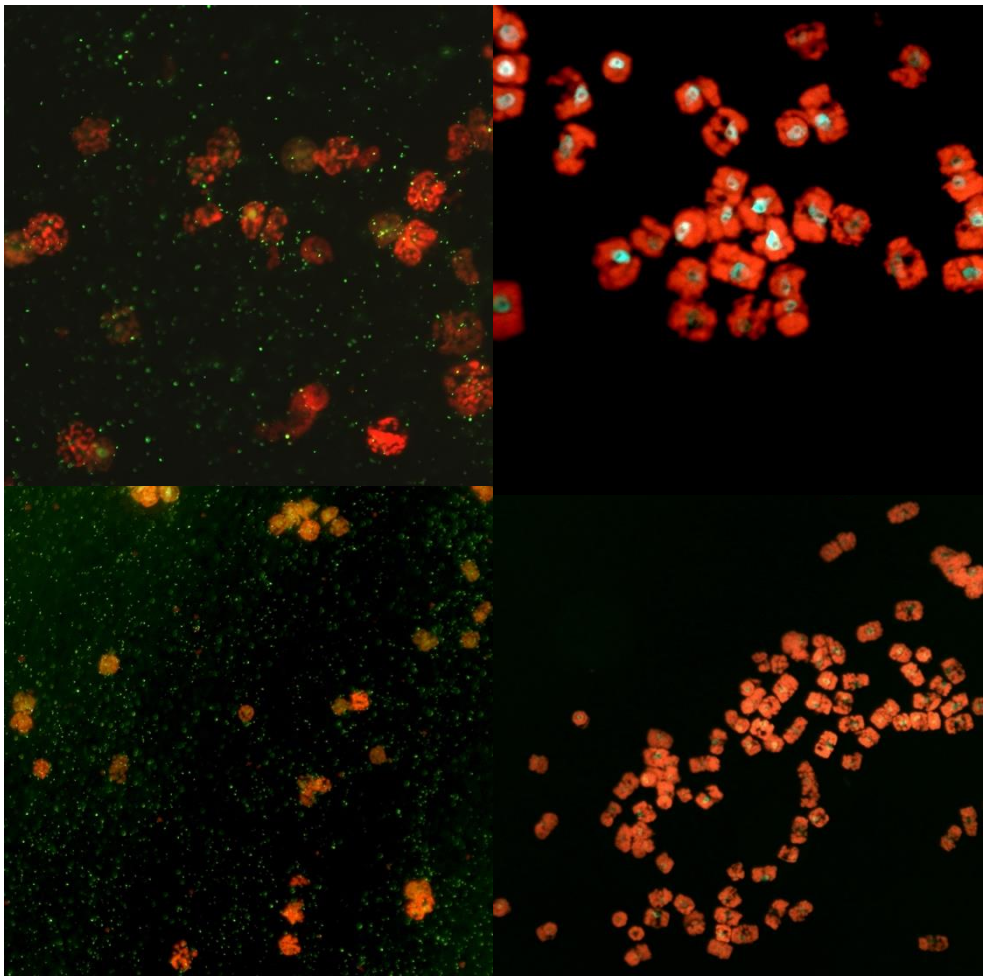

Figure S3: Maximum growth rates (μ max) of the xenic *T. gravida* (polar) on the y-axis across the three tested temperatures of 4°C; 9°C and 13.5°C on the x-axis in combination with the three photoperiods 4h; 16h and 24h indicated by color.

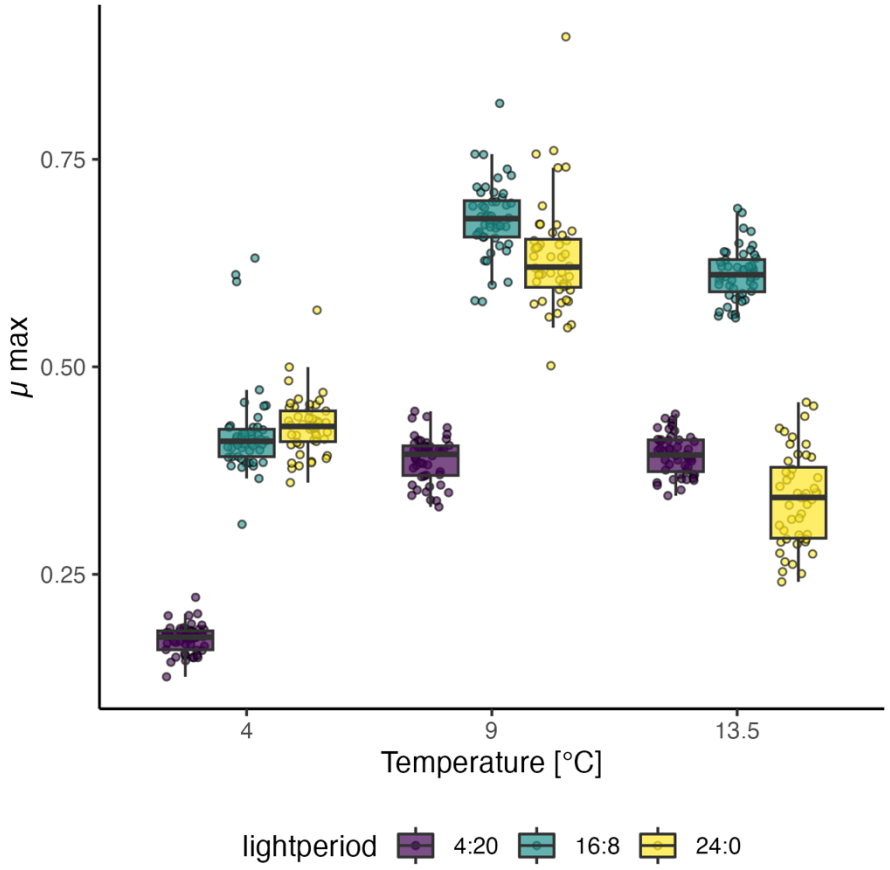

Figure S4: Maximum growth rates (μ max) of the xenic *T. rotula* (temperate) on the y-axis across the three tested temperatures of 4°C; 9°C and 13.5°C on the x-axis in combination with the three photoperiods 4h; 16h and 24h indicated by color.

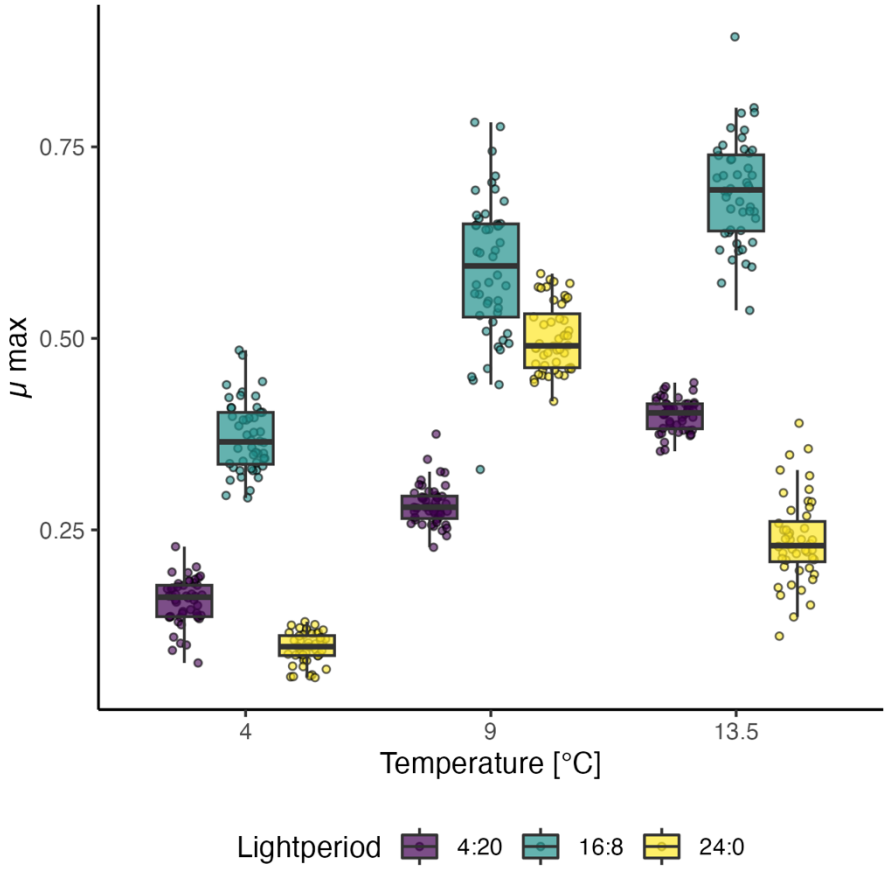

Figure S5: Maximum growth rates (μ max) of the axenic *T. gravida* (polar) on the y-axis across the three tested temperatures of 4°C; 9°C and 13.5°C on the x-axis in combination with the three photoperiods 4h; 16h and 24h indicated by color.

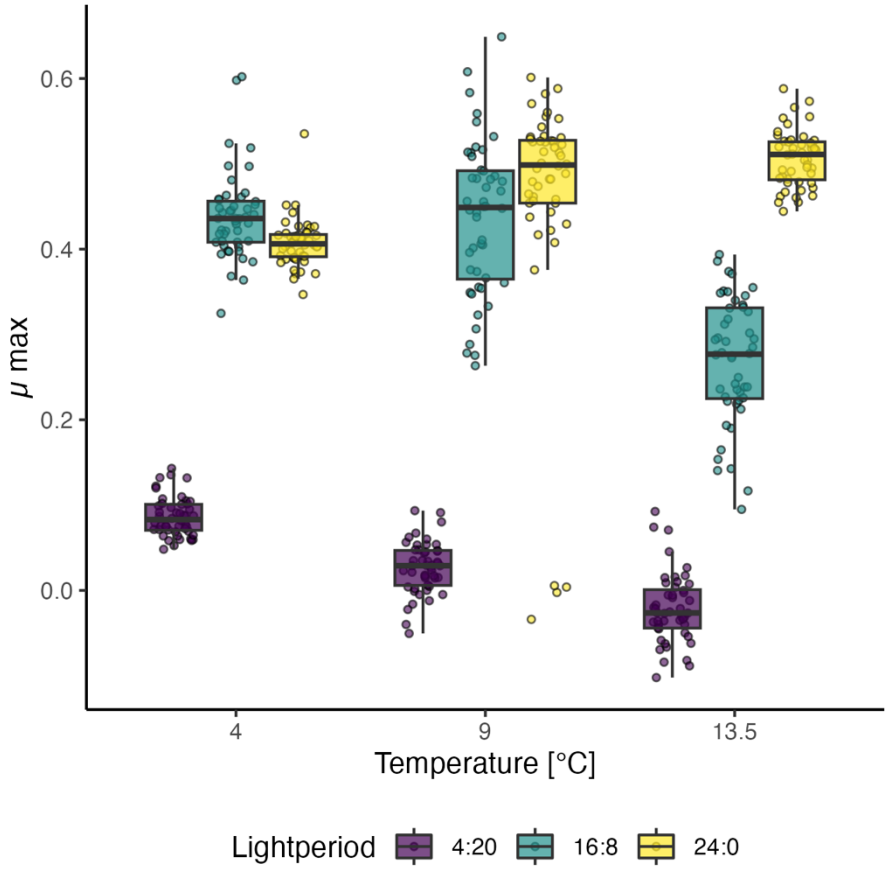

Figure S6: Maximum growth rates (μ max) of the axenic *T. rotula* (temperate) on the y-axis across the three tested temperatures of 4°C; 9°C and 13.5°C on the x-axis in combination with the three photoperiods 4h; 16h and 24h indicated by color.

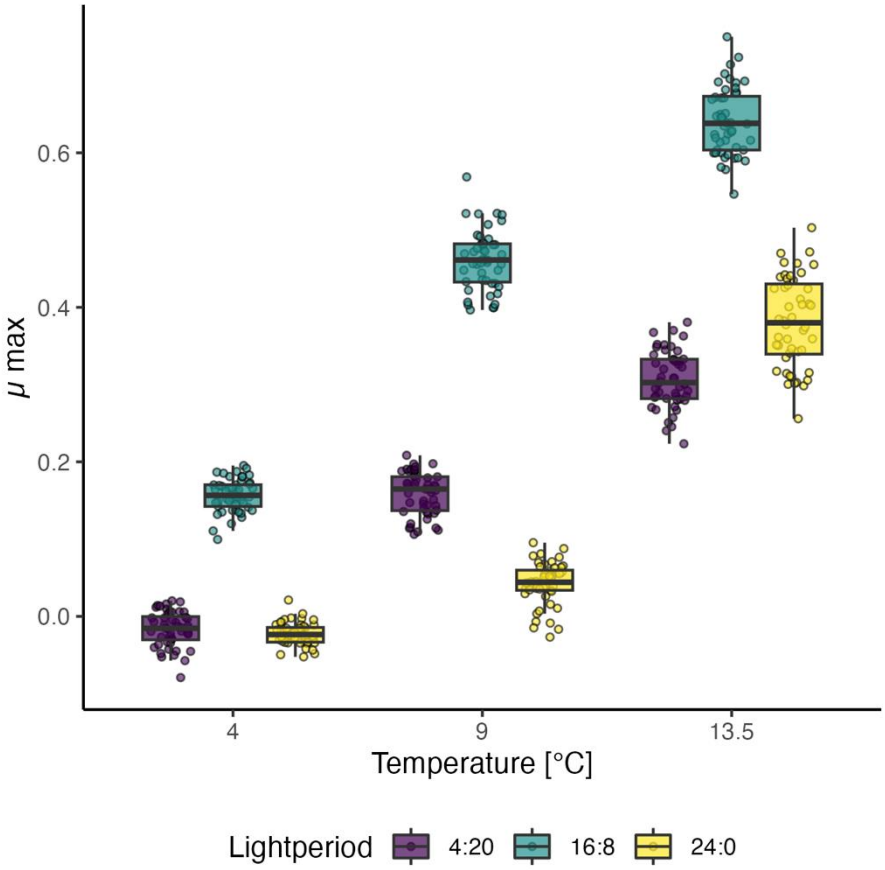

Figure S7: Raw fluorescence intensity of the polar *Thalassiosira gravida* on the y-axis against time in days on the x-axis. Bacterial presence is indicated by color. Vertical facets represent the applied photoperiod in hours, horizontal facets represent the applied temperature.

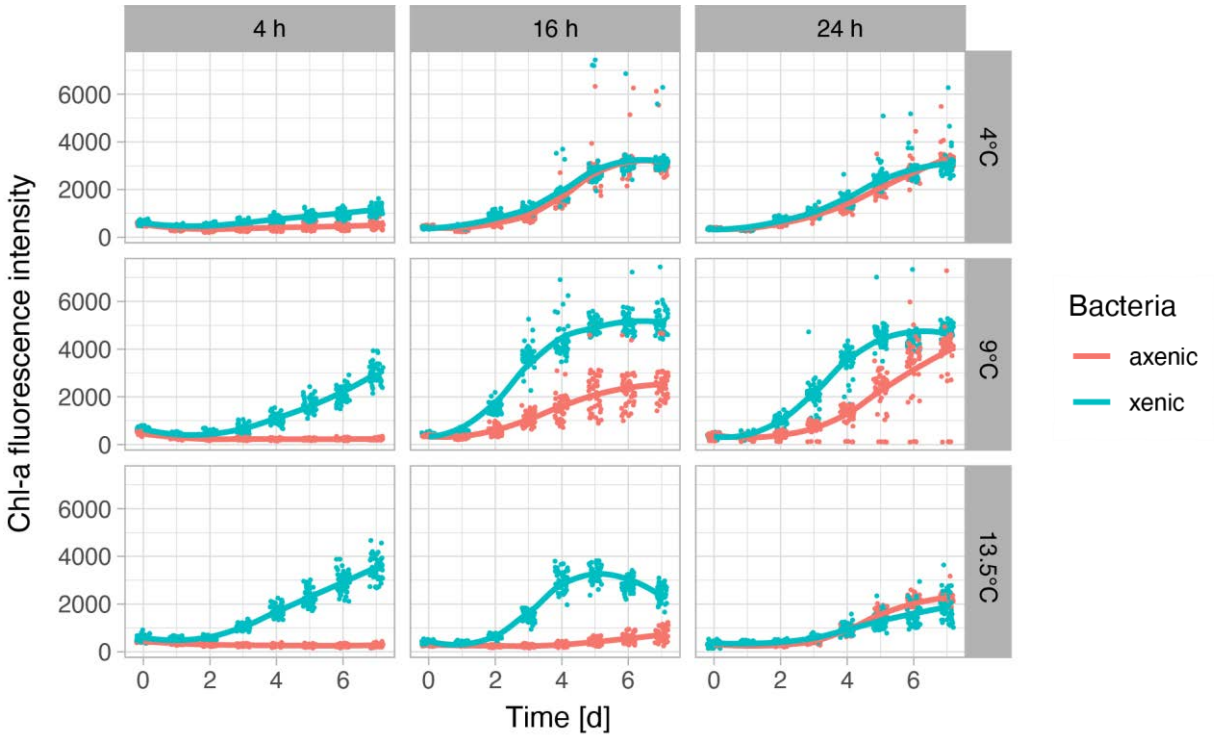

Figure S8: Raw fluorescence intensity of the temperate *Thalassiosira rotula* on the y-axis against time in days on the x-axis. Bacterial presence is indicated by color. Vertical facets represent the applied photoperiod in hours, horizontal facets represent the applied temperature.

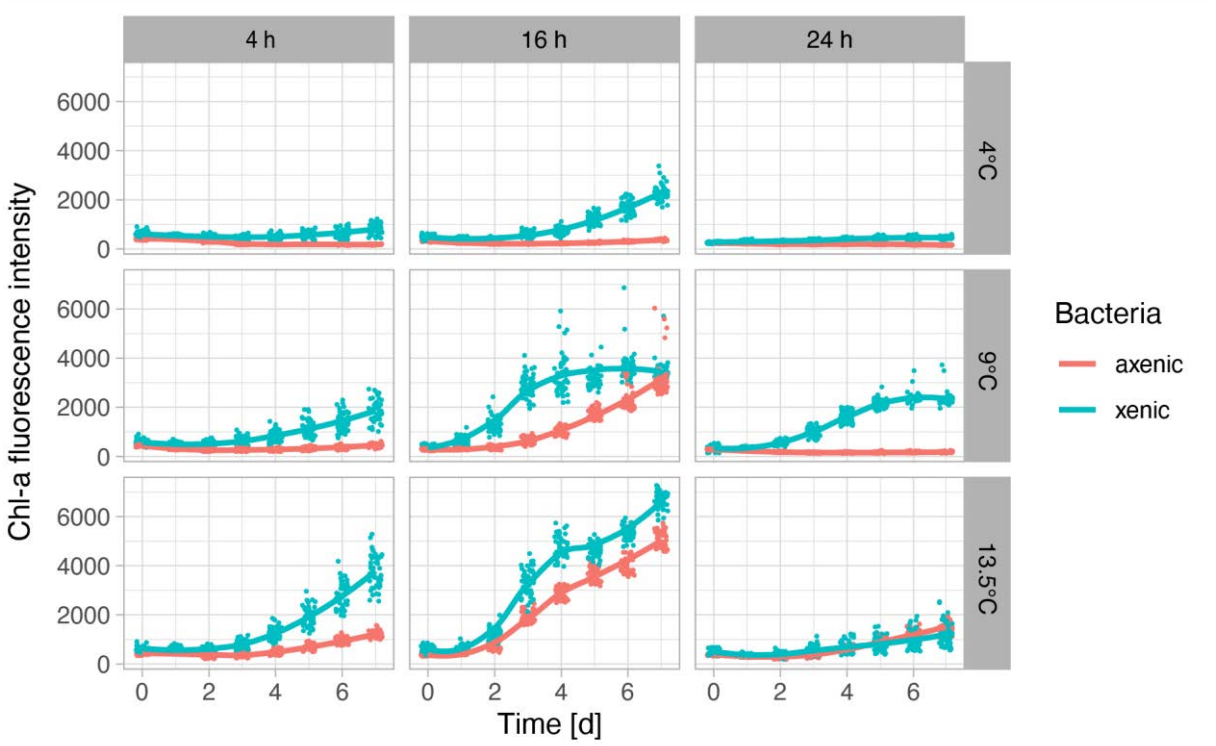

Appendix Publication III

Co-expression of Arctic diatoms and their bacterial microbiomes under thermal and photoperiodic stress

Supplementary material

Table S4.1: ANOVA results for main and interactive effects of bacterial presence (bac), temperature (temp) and photoperiod (light) on the specific growth rate of *Thalassiosira gravida* cultures. Degrees of freedom (Df), sums of squares (Sum Sq), mean squares (Mean Sq), as well as F- and p-values are given for each effect. Asterisks (*) indicate significant effects ($p < 0.05$).

	Df	Sum Sq	Mean Sq	F value	Pr(>F)	
bac	1	1.614	1.614	1148.2	< 0.001	*
temp	1	0.088	0.088	62.2	< 0.001	*
light	1	0.409	0.409	290.9	< 0.001	*
bac*temp	1	0.001	0.001	0.5	0.4691	
bac*light	1	0.060	0.060	42.8	< 0.001	*
temp*light	1	0.009	0.009	6.0	0.0197	*
bac*temp*light	1	0.034	0.034	24.1	< 0.001	*

Table S4.2: Host gene IDs (Gene ID) that were significantly different expressed in response to bacterial presence and significantly enriched/depleted in their respective COG-category (COG). The description for each gene and the respective Pfam domain (PFAMs) obtained from eggNOG-mapper v2 are given. Moreover, the assigned cluster ID from the K-means clustering is given (Cluster. ID).

Gene ID	COG	Description	PFAMs	Clust. ID
euk_1	A	Angel homolog	-	H1
euk_2	F	Involved in maintaining the homeostasis of cellular nucleotides by catalyzing the interconversion of nucleoside phosphates. Has GTP AMP phosphotransferase and ITP AMP phosphotransferase activities	ADK,ADK_lid	H1
euk_3	F	Involved in maintaining the homeostasis of cellular nucleotides by catalyzing the interconversion of nucleoside phosphates. Has GTP AMP phosphotransferase and ITP AMP phosphotransferase activities	ADK,ADK_lid	H1
euk_4	F	Involved in maintaining the homeostasis of cellular nucleotides by catalyzing the interconversion of nucleoside phosphates. Has GTP AMP phosphotransferase and ITP AMP phosphotransferase activities	ADK,ADK_lid	H1
euk_5	J	Methyltransferase FkbM domain	Methyltransf_21	H1
euk_6	J	Methyltransferase FkbM domain	Methyltransf_21	H1
euk_7	O	peptide-methionine (R)-S-oxide reductase activity	-	H1
euk_8	O	protein folding	DUF1977	H1
euk_9	O	DnaJ C terminal domain	DnaJ_C,DnaJ_CXXCXGXG	H1
euk_10	O	Peptidase S8	Peptidase_S8	H1
euk_11	P	fucoxanthin chlorophyll a c protein	Chloroa_b-bind	H1
euk_12	P	Sodium/hydrogen exchanger family	Na_H_Exchanger	H1
euk_13	A	BING4CT (NUC141) domain	-	H2
euk_14	A	Helicase associated domain (HA2) Add an annotation	DEAD,HA2,Helicase_C,OB_NTP_bind,zf-RanBP	H2
euk_15	A	helicase superfamily c-terminal domain	DEAD,GUCT,Helicase_C	H2
euk_16	A	DUF4217	DEAD,DUF4217,Helicase_C	H2
euk_17	L	AAA domain	-	H2
euk_18	L	AAA domain	-	H2
euk_19	L	AAA domain	AAA_11,AAA_12	H2
euk_20	L	AAA domain	AAA_12	H2
euk_21	O	positive regulation of hematopoietic stem cell proliferation	PDCD2_C	H2
euk_22	O	Belongs to the heat shock protein 70 family	HSP70	H2
euk_23	O	PIN domain of ribonuclease	NOB1_Zn_bind,PIN_6	H2
euk_24	O	Peptidase family M3	Peptidase_M3	H2
euk_25	O	Thioredoxin	Thioredoxin	H2
euk_26	P	Sodium:dicarboxylate symporter family	SDF	H2

euk_27	P	Sodium:dicarboxylate symporter family	SDF	H2
euk_28	B	Williams-Beuren syndrome DDT (WSD), D-TOX E motif	WSD	H3
euk_29	I	long-chain-3-hydroxyacyl-CoA dehydrogenase activity	Thiolase_C,Thiolase_N	H3
euk_30	I	3-hydroxyacyl-CoA dehydrogenase, NAD binding domain	3HCDH,3HCDH_N	H3
euk_31	I	Domain of unknown function (DUF3336)	Patatin	H3
euk_32	I	Domain of unknown function (DUF3336)	-	H3
euk_33	I	3-hydroxyacyl-CoA dehydrogenase, NAD binding domain	3HCDH,3HCDH_N	H3
euk_34	I	Domain of unknown function (DUF3336)	DUF3336,Patatin	H3
euk_35	I	Belongs to the enoyl-CoA hydratase isomerase family	ECH_1	H3
euk_36	I	Enoyl-CoA hydratase/isomerase	ECH_1	H3
euk_37	I	Enoyl-CoA hydratase/isomerase	ECH_1	H3
euk_38	I	long-chain-3-hydroxyacyl-CoA dehydrogenase activity	Thiolase_N	H3
euk_39	I	AMP-binding enzyme	AMP-binding	H3
euk_40	J	Catalyzes the formation of 2'O-methylated cytidine (Cm32) or 2'O-methylated uridine (Um32) at position 32 in tRNA	SpoU_methylase	H3
euk_41	L	BRCA2, oligonucleotide/oligosaccharide-binding, domain 1	BRCA-2_OB1,BRCA-2_helical	H3
euk_42	L	HELICc2	DEAD_2,Helicase_C_2	H3
euk_43	M	tail specific protease	-	H3
euk_44	A	RNA recognition motif. (a.k.a. RRM, RBD, or RNP domain)	RRM_1	H4
euk_45	A	helicase superfamily c-terminal domain	DEAD	H4
euk_46	I	Belongs to the CDP-alcohol phosphatidyltransferase class-I family	CDP-OH_P_transf	H4
euk_47	J	structural constituent of ribosome	ubiquitin	H4
euk_48	M	Mechanosensitive ion channel	-	H4
euk_49	M	Mechanosensitive ion channel	-	H4
euk_50	O	Belongs to the peptidase S1 family	Trypsin	H4
euk_51	O	Serine carboxypeptidase S28	Peptidase_S28	H4
euk_52	O	peptide-methionine (S)-S-oxide reductase activity	PMSR	H4
euk_53	Q	ABC transporter	ABC2_membrane,ABC_tran	H4
euk_54	A	helicase superfamily c-terminal domain	DEAD	H5
euk_55	O	N-terminal domain of galactosyltransferase	Glyco_transf_7C,Glycos_transf_2	H5
euk_56	O	N-terminal domain of galactosyltransferase	Glyco_transf_7C,Glycos_transf_2	H5
euk_57	O	AAA domain (Cdc48 subfamily)	AAA	H5
euk_58	O	PIN domain of ribonuclease	NOB1_Zn_bind,PIN_6	H5
euk_59	Q	ABC transporter	ABC_tran	H5
euk_60	Q	ABC transporter	ABC_tran,Fer4,RLI	H5
euk_61	A	RNA recognition motif	RRM_1	H6
euk_62	O	DnaJ C terminal domain	DnaJ,DnaJ_C,DnaJ_CXXCXGXG	H6

euk_63	O	peptide-methionine (R)-S-oxide reductase activity	-	H6
euk_64	O	Belongs to the peptidase S1 family	Trypsin	H6
euk_65	O	Protein prenyltransferase alpha subunit repeat	PPTA	H6
euk_66	O	Protein prenyltransferase alpha subunit repeat	PPTA	H6
euk_67	O	Trypsin-like serine protease	Trypsin	H6
euk_68	O	protein folding	DnaJ	H6
euk_69	O	Trypsin-like serine protease	Trypsin	H6
euk_70	O	peptide-methionine (R)-S-oxide reductase activity	-	H6
euk_71	O	Belongs to the peptidase S1 family	Trypsin	H6
euk_72	O	PFAM Beta-propeller repeat	-	H6
euk_73	O	Chitin recognition protein	Chitin_bind_1	H6
euk_74	O	Belongs to the peptidase S1 family	Trypsin	H6
euk_75	O	Chitin recognition protein	Chitin_bind_1	H6
euk_76	O	Belongs to the peptidase S8 family	Peptidase_S8	H6
euk_77	O	ATP-binding cassette subfamily B	ABC_tran	H6
euk_78	O	Peptidase S8 and S53, subtilisin, kexin, sedolisin	Peptidase_S8	H6
euk_79	O	Belongs to the GST superfamily	Peptidase_M11	H6
euk_80	O	Chitin recognition protein	Chitin_bind_1	H6
euk_81	O	positive regulation of hematopoietic stem cell proliferation	-	H6
euk_82	P	Cation transporter/ATPase, N-terminus	Cation_ATPase_C,Cation_ATPase_N,E1-E2_ATPase,Hydrolase,Hydrolase_3	H6
euk_83	P	Protein of unknown function (DUF3494)	DUF3494	H6
euk_84	P	Protein of unknown function (DUF3494)	DUF3494	H6
euk_85	P	alginic acid biosynthetic process	DUF3494	H6
euk_86	Q	repeat protein	-	H6
euk_87	Q	repeat protein	-	H6
euk_88	Q	Flavin containing amine oxidoreductase	Amino_oxidase	H6
euk_89	M	BCCT, betaine/carnitine/choline family transporter	BCCT	H7
euk_90	M	BCCT, betaine/carnitine/choline family transporter	BCCT	H7
euk_91	M	BCCT, betaine/carnitine/choline family transporter	BCCT	H7
euk_92	M	BCCT, betaine/carnitine/choline family transporter	BCCT	H7
euk_93	M	BCCT, betaine/carnitine/choline family transporter	BCCT	H7
euk_94	M	BCCT, betaine/carnitine/choline family transporter	BCCT	H7
euk_95	M	BCCT, betaine/carnitine/choline family transporter	BCCT	H7
euk_96	O	Belongs to the peptidase S1 family	Trypsin	H7
euk_97	O	protein folding	DnaJ	H7

euk_98	O	Belongs to the heat shock protein 70 family	HSP70	H7
euk_99	O	Plasmin dissolves the fibrin of blood clots and acts as a proteolytic factor in a variety of other processes including embryonic development, tissue remodeling, tumor invasion, and inflammation. In ovulation, weakens the walls of the Graafian follicle. It activates the urokinase-type plasminogen activator, collagenases and several complement zymogens, such as C1 and C5. Cleavage of fibronectin and laminin leads to cell detachment and apoptosis. Also cleaves fibrin, thrombospondin and von Willebrand factor. Its role in tissue remodeling and tumor invasion may be modulated by CSPG4. Binds to cells	DUF285,Kringle	H7
euk_100	O	Belongs to the peptidase C1 family	Inhibitor_I29	H7
euk_101	O	protein folding	-	H7
euk_102	O	Serine carboxypeptidase S28	Peptidase_S28	H7
euk_103	O	Belongs to the peptidase S1 family	Trypsin	H7
euk_104	O	Thioredoxin	Thioredoxin	H7
euk_105	O	Belongs to the peptidase S8 family	Peptidase_S8	H7
euk_106	A	basic region leucin zipper	bZIP_1	H8
euk_107	A	basic region leucin zipper	bZIP_1	H8
euk_108	O	Proteasome subunit	Proteasome	H8
euk_109	O	PPIases accelerate the folding of proteins. It catalyzes the cis-trans isomerization of proline imidic peptide bonds in oligopeptides	Pro_isomerase	H8
euk_110	O	Redoxin	Redoxin	H8
euk_111	O	Redoxin	Redoxin	H8
euk_112	P	Sodium/hydrogen exchanger family	Na_H_Exchanger	H8
euk_113	A	EF-hand domain pair	EF-hand_7	H9
euk_114	B	Control of topological states of DNA by transient breakage and subsequent rejoining of DNA strands. Topoisomerase II makes double-strand breaks	DNA_gyraseB,DNA_topoisoIV,HATPase_c,TOPRIM_C,Toprim	H9
euk_115	B	Histone H2B	Histone	H9
euk_116	B	Chromatin organization modifier domain	Chromo,Cupin_8	H9
euk_117	B	Histone deacetylase domain	Hist_deacetyl	H9
euk_118	F	Ribonucleotide reductase, small chain	-	H9
euk_119	I	Diacylglycerol acyltransferase	DAGAT	H9
euk_120	I	NAD-binding of NADP-dependent 3-hydroxyisobutyrate dehydrogenase	NAD_binding_11,NAD_binding_2	H9
euk_121	J	FkbM family	Met_10	H9
euk_122	L	helicase activity	DEAD,Helicase_C	H9
euk_123	M	tail specific protease	-	H9
euk_124	M	Glycosyltransferase family 9 (heptosyltransferase)	Methyltransf_21	H9
euk_125	O	Subtilase family	-	H9
euk_126	O	regulation of protein catabolic process	PC_rep	H9

euk_127	O	Belongs to the peptidase S8 family	Trypsin	H9
euk_128	O	RNA-binding, Nab2-type zinc finger	-	H9
euk_129	O	CAP_GLY	CAP_GLY,Ubiquitin_2	H9
euk_130	O	Peptidase family M48	Peptidase_M48	H9
euk_131	O	Tubulin folding cofactor D C terminal	-	H9
euk_132	P	fucoxanthin chlorophyll a c protein	Chloroa_b-bind	H9
euk_133	I	Belongs to the membrane-bound acyltransferase family	PH	H10
euk_134	I	Belongs to the membrane-bound acyltransferase family	MBOAT,PH	H10
euk_135	O	serine-type endopeptidase activity	Trypsin	H10
euk_136	O	ubiquitin-protein transferase activity	zf-RING_2	H10
euk_137	O	peptide-methionine (R)-S-oxide reductase activity	-	H10
euk_138	O	peptide-methionine (R)-S-oxide reductase activity	-	H10
euk_139	O	ATP-binding cassette subfamily B	ABC_membrane,ABC_tran	H10
euk_140	O	Peptidase family M3	Peptidase_M3	H10
euk_141	P	Chlorophyll A-B binding protein	Chloroa_b-bind	H10
euk_142	P	Chlorophyll A-B binding protein	Chloroa_b-bind	H10
euk_143	P	Chlorophyll A-B binding protein	Chloroa_b-bind	H10
euk_144	P	Heme oxygenase	Heme_oxygenase	H10
euk_145	Q	repeat protein	FG-GAP_2	H10
euk_146	B	Histone 2A	Histone,Histone_H2A_C	H11
euk_147	B	Domain in histone families 1 and 5	Linker_histone	H11
euk_148	B	Williams-Beuren syndrome DDT (WSD), D-TOX E motif	WSD	H11
euk_149	B	Chromatin organization modifier domain	Chromo,Cupin_8	H11
euk_150	B	Domain in histone families 1 and 5	Linker_histone	H11
euk_151	F	Ribonucleotide reductase, small chain	Ribonuc_red_sm	H11
euk_152	F	Ribonucleotide reductase, small chain	Ribonuc_red_sm	H11
euk_153	F	Ribonucleotide reductase, small chain	Ribonuc_red_sm	H11
euk_154	F	dUTPase	dUTPase	H11
euk_155	F	Ribonucleotide reductase, small chain	Ribonuc_red_sm	H11
euk_156	F	Provides the precursors necessary for DNA synthesis. Catalyzes the biosynthesis of deoxyribonucleotides from the corresponding ribonucleotides	ATP-cone,Ribonuc_red_lgC,Ribonuc_red_lgN	H11
euk_157	I	Myo-inositol-1-phosphate synthase	Inos-1-P_synth,NAD_binding_5	H11
euk_158	I	Myo-inositol-1-phosphate synthase	Inos-1-P_synth,NAD_binding_5	H11
euk_159	I	Myo-inositol-1-phosphate synthase	Inos-1-P_synth,NAD_binding_5	H11
euk_160	L	Belongs to the eukaryotic-type primase small subunit family	DNA_primase_S	H11
euk_161	L	Pfam:KaiC	Rad51	H11
euk_162	L	Domain of unknown function (DUF1744)	DNA_pol_B,DNA_pol_B_exo1,DUF1744	H11

euk_163	L	Belongs to the eukaryotic-type primase small subunit family	DNA_primase_S	H11
euk_164	L	This protein is an auxiliary protein of DNA polymerase delta and is involved in the control of eukaryotic DNA replication by increasing the polymerase's processibility during elongation of the leading strand	PCNA_C	H11
euk_165	L	base-excision repair, AP site formation via deaminated base removal	UDG	H11
euk_166	L	Endonuclease/Exonuclease/phosphatase family	Exo_endo_phos	H11
euk_167	L	nuclear-transcribed mRNA catabolic process, nonsense-mediated decay	AAA_11,AAA_12,UPF1_Zn_bind	H11
euk_168	L	Origin recognition complex subunit 2	ORC2	H11
euk_169	L	DNA polymerase family B	DNA_pol_B,zf-C4pol	H11
euk_170	L	Replication protein A C terminal	tRNA_anti-codon	H11
euk_171	L	ATPase family associated with various cellular activities (AAA)	-	H11
euk_172	L	chromatin organization	WD40	H11
euk_173	L	ATPase family associated with various cellular activities (AAA)	-	H11
euk_174	L	Replication protein A C terminal	tRNA_anti-codon	H11
euk_175	L	This protein is an auxiliary protein of DNA polymerase delta and is involved in the control of eukaryotic DNA replication by increasing the polymerase's processibility during elongation of the leading strand	PCNA_C	H11
euk_176	L	DNA polymerase family B	DNA_pol_B,DNA_pol_B_exo1	H11
euk_177	L	Type IIB DNA topoisomerase	TP6A_N	H11
euk_178	L	Prokaryotic RING finger family 4	Helicase_C_2,zf-C3HC4_3	H11
euk_179	M	tail specific protease	Peptidase_S41	H11
euk_180	O	Belongs to the peptidase S1 family	Trypsin	H11
euk_181	O	Zinc-ribbon	zf-CHY,zf-RING_2,zinc_ribbon_6	H11
euk_182	O	SUMO activating enzyme activity	ThiF	H11
euk_183	O	Belongs to the ubiquitin-conjugating enzyme family	UQ_con	H11
euk_184	O	SUMO activating enzyme activity	ThiF	H11
euk_185	O	Tubulin folding cofactor D C terminal	TFCD_C	H11
euk_186	O	N-acetylglucosaminyldiphosphodolichol N-acetylglucosaminyltransferase activity	Glyco_tran_28_C	H11

Table S4.3: Bacterial gene IDs (Gene ID) of microbiome clusters (Cluster ID) which significantly correlated with host gene clusters beyond a correlation coefficient threshold of ≥ 0.8 and ≤ -0.8. For each microbiome gene cluster, only those genes are given whose COG-subcategory (COG) was significantly enriched in the respective microbiome cluster. Maximum annotation levels (Max annot. Level), the respective Pfam domain (PFAMs) obtained from eggNOG-mapper v2 are given.

Gene ID	Max annotation level	COG	PFAMs	Cluster ID
bac_1	Rhodospirillales	Q	Methyltransf_21	M1
bac_2	Rhodospirillales	Q	Methyltransf_21	M1
bac_3	Aquificae	G	PEP-utilizers,PEP-utilizers_C,PPDK_N	M1
bac_4	Aquificae	G	PEP-utilizers,PEP-utilizers_C,PPDK_N	M1
bac_5	Clostridia	G	PEP-utilizers,PEP-utilizers_C,PPDK_N	M1
bac_6	Actinobacteria	GL	His_Phos_1,RVT_3	M1
bac_7	Alphaproteobacteria	G	SBP_bac_1,SBP_bac_8	M1
bac_8	Actinobacteria	IQ	adh_short	M1
bac_9	Actinobacteria	Q	Cu-oxidase,Cu-oxidase_2,Cu-oxidase_3	M1
bac_10	Cyanobacteria	GM	NmrA	M1
bac_11	Gammaproteobacteria	IQ	AMP-binding,AMP-binding_C,Acyl_transf_3,FSH1	M1
bac_12	Bacteroidetes	J	Ribosomal_S11	M3
bac_13	Chromatiales	C	Oxidored_q2	M3
bac_14	Rhodospirillales	C	NADHdh	M3
bac_15	Bacteroidetes	M	CHU_C,Calx-beta,DUF11,HYR,SprB	M3
bac_16	Gammaproteobacteria	M	CMAS	M3
bac_17	Gammaproteobacteria	J	Ribosomal_S4,S4	M3
bac_18	Gammaproteobacteria	J	Ribosomal_S11	M3
bac_19	Gammaproteobacteria	J	Ribosomal_S13	M3
bac_20	Gammaproteobacteria	J	Ribosomal_S5,Ribosomal_S5_C	M3
bac_21	Alphaproteobacteria	C	Fer4,Fer4_11,Fer4_7	M3
bac_22	Alphaproteobacteria	C	Molybdop_Fe4S4,Molybdopterin,Molydop_binding	M3
bac_23	Bacteroidetes	C	Rnf-Nqr	M3
bac_24	Gammaproteobacteria	J	Ribosomal_L4	M3
bac_25	Gammaproteobacteria	J	Ribosomal_L2,Ribosomal_L2_C	M3
bac_26	Gammaproteobacteria	J	KH_2,Ribosomal_S3_C	M3
bac_27	Bacteroidetes	C	ATP-synt_C	M3
bac_28	Gammaproteobacteria	C	ATP-synt_ab,ATP-synt_ab_C,ATP-synt_ab_N	M3
bac_29	Gammaproteobacteria	C	ATP-synt_B	M3
bac_30	Alphaproteobacteria	M	UDPG_MGDP_dh,UDPG_MGDP_dh_C,UDPG_MGDP_dh_N	M3
bac_31	Gammaproteobacteria	C	CoA_transf_3	M3
bac_32	Bacteroidetes	C	COX3	M3
bac_33	Thiotrichales	C	Fe-S_biosyn	M3
bac_34	Alphaproteobacteria	M	OmpH	M3

bac_35	Gammaproteobacteria	J	Ribosomal_L10	M3
bac_36	Gammaproteobacteria	J	Ribosomal_L1	M3
bac_37	Thiotrichales	M	Poly_export,SLBB	M3
bac_38	Gammaproteobacteria	C	FAD_binding_2,Succ_DH_flav_C	M3
bac_39	Gammaproteobacteria	M	Slp	M3
bac_40	Gammaproteobacteria	C	Cytochrom_B_C,Cytochrom_C1,Cytochrome_B	M3
bac_41	Bacteroidetes	M	Glycos_transf_2	M3
bac_42	Gammaproteobacteria	C	COX1	M3
bac_43	Gammaproteobacteria	C	IDH	M3
bac_44	Gammaproteobacteria	C	ATP-grasp_2,Ligase_CoA	M3
bac_45	Alphaproteobacteria	C	COX3	M3
bac_46	Gammaproteobacteria	M	OmpA	M3
bac_47	Gammaproteobacteria	C	COX3	M3
bac_48	Gammaproteobacteria	J	Ribosom_S12_S23	M3
bac_49	Alphaproteobacteria	M	OmpA	M3
bac_50	Alphaproteobacteria	M	Porin_4	M3
bac_51	Gammaproteobacteria	J	Ribosomal_S9	M3
bac_52	Gammaproteobacteria	J	Ribosomal_L13	M3
bac_53	Alphaproteobacteria	J	Ribosomal_L2,Ribosomal_L2_C	M3
bac_54	Thiotrichales	M	17kDa_Anti_2,Rick_17kDa_Anti	M3
bac_55	Alphaproteobacteria	C	Fer4	M3
bac_56	Proteobacteria	M	-	M3
bac_57	Bacteria	J	B3_4,B5,FDX-ACB,tRNA_bind	M3
bac_58	Gammaproteobacteria	J	Ribosomal_L28	M3
bac_59	Bacteroidetes	O	Cu-binding_MopE,HYR,MAM,P_protein,SprB	M6
bac_60	Alphaproteobacteria	O	Cpn60_TCP1	M6
bac_61	Alphaproteobacteria	O	Cpn10	M6
bac_62	Alphaproteobacteria	O	Band_7	M6
bac_63	Alphaproteobacteria	O	Met_10,Methyltransf_21	M6
bac_64	Thiotrichales	O	GSHPx	M6
bac_65	Bacteroidetes	O	Peptidase_M48	M6
bac_66	Rhodospirillales	O	Redoxin	M6
bac_67	Bacteroidetes	O	Cu-binding_MopE,HYR,MAM,P_protein,SprB	M6
bac_68	Alphaproteobacteria	O	GST_C,GST_C_2,GST_N	M6
bac_69	Alphaproteobacteria	O	Band_7,Band_7_C	M6
bac_70	Kinetoplastida	O	Pro_isomerase	M6
bac_71	Alphaproteobacteria	O	META,YscW	M6
bac_72	Alphaproteobacteria	O	Nfu_N,NifU	M6
bac_73	Gammaproteobacteria	O	1-cysPrx_C,AhpC-TSA	M6
bac_74	Alphaproteobacteria	O	Redoxin	M6
bac_75	Alphaproteobacteria	O	Thioredoxin	M6
bac_76	Gammaproteobacteria	M	-	M7
bac_77	Bacteroidetes	NU	-	M7

bac_78	Bacteroidetes	M	23S_rRNA_IVP	M7
bac_79	Bacteroidetes	EU	DPPIV_N,Peptidase_S9	M7
bac_80	Bacteroidetes	EM	ANF_receptor,LysM,Peripla_BP_6	M7
bac_81	Bacteroidetes	M	CarboxypepD_reg,OmpA,PD40	M7
bac_82	Gammaproteobacteria	M	DUF11	M7
bac_83	Bacteroidetes	M	EFG_C,GTP_EFTU,GTP_EFTU_D2,LepA_C	M7
bac_84	Bacteroidetes	M	EPSP_synthase	M7
bac_85	Gammaproteobacteria	U	ExbD	M7
bac_86	Bacteroidetes	U	ExbD	M7
bac_87	Bacteroidetes	U	ExbD	M7
bac_88	Bacteroidetes	IM	FabA,LpxC	M7
bac_89	Gammaproteobacteria	U	FHA,T2SSE	M7
bac_90	Bacteroidetes	M	FKBP_C,Pro_isomerase	M7
bac_91	Bacteroidetes	M	Glycos_transf_1	M7
bac_92	Bacteroidetes	M	Glycos_transf_2	M7
bac_93	Bacteroidetes	U	Helicase_C,SEC-C,SecA_DEAD,SecA_PP_bind,SecA_SW	M7
bac_94	Bacteroidetes	U	MotA_ExbB	M7
bac_95	Bacteroidetes	U	MotA_ExbB	M7
bac_96	Bacteroidetes	M	Mur_ligase_C,Mur_ligase_M	M7
bac_97	Bacteroidetes	M	Mur_ligase,Mur_ligase_C,Mur_ligase_M	M7
bac_98	Bacteroidetes	M	NTP_transf_4	M7
bac_99	Bacteroidetes	M	NTP_transferase	M7
bac_100	Bacteroidetes	MU	OEP	M7
bac_101	Bacteroidetes	M	OMP_b-brl	M7
bac_102	Bacteroidetes	M	OMP_b-brl,OmpA,TSP_3	M7
bac_103	Alphaproteobacteria	M	OmpA	M7
bac_104	Bacteroidetes	M	OmpH	M7
bac_105	Bacteroidetes	M	PGA_cap	M7
bac_106	Proteobacteria	M	Porin_4	M7
bac_107	Bacteroidetes	GM	ABC2_membrane	M7
bac_108	Bacteroidetes	M	PorP_SprF	M7
bac_109	Bacteroidetes	U	SecD_SecF,Sec_GG	M7
bac_110	Bacteroidetes	U	SecE	M7
bac_111	Bacteroidetes	U	SecY	M7
bac_112	Oceanospirillales	U	SecY	M7
bac_113	Bacteroidetes	M	SusD-like_3,SusD_RagB	M7
bac_114	Bacteroidetes	M	Glyco_trans_4_2,Glyco_trans_4_4,Glyco_transf_4,Glycos_transf_1	M9
bac_115	Bacteroidetes	M	Glyco_transf_64,Glycos_transf_2	M9
bac_116	Bacteroidetes	K	Sigma70_r2,Sigma70_r4_2	M9
bac_117	Gammaproteobacteria	K	RNA_pol_A_CTD,RNA_pol_A_bac,RNA_pol_L	M9
bac_118	Bacteroidetes	M	WD40	M9
bac_119	Bacteroidetes	M	Epimerase,NAD_binding_4	M9
bac_120	Bacteroidetes	K	HTH_3	M9

bac_121	Bacteroidetes	M	Peptidase_M23	M9
bac_122	Bacteroidetes	M	GDP_Man_Dehyd	M9
bac_123	Bacteroidetes	M	GDP_Man_Dehyd	M9
bac_124	Bacteroidetes	MU	OEP	M9
bac_125	Bacteroidetes	M	Bac_transf,Response_reg	M9
bac_126	Bacteroidetes	KT	Response_reg	M9
bac_127	Bacteroidetes	M	Glyco_trans_1_4	M9
bac_128	Bacteroidetes	M	-	M9
bac_129	Bacteroidetes	M	Glycos_transf_2	M9
bac_130	Bacteria	M	Cadherin_3,Fasciclin	M9
bac_131	Bacteria	M	TonB_C	M9
bac_132	Bacteroidetes	M	adh_short	M9
bac_133	Bacteroidetes	M	DAHP_synth_1	M9
bac_134	Alphaproteobacteria	K	Sigma70_r2,Sigma70_r4,Sigma70_r4_2	M9
bac_135	Alphaproteobacteria	M	Fasciclin	M9
bac_136	Gammaproteobacteria	KLT	WG_beta_rep	M9
bac_137	Bacteroidetes	M	Glyco_transf_4,Glycos_transf_1	M9
bac_138	Bacteroidetes	K	HTH_1,LysR_substrate	M9
bac_139	Bacteroidetes	K	AraC_binding,HTH_18	M9
bac_140	Bacteroidetes	K	Sigma70_r2,Sigma70_r4,Sigma70_r4_2	M9
bac_141	Bacteroidetes	K	LytTR,Response_reg	M9
bac_142	Bacteroidetes	K	LytTR,Response_reg	M9
bac_143	Gammaproteobacteria	M	UDPG_MGDP_dh,UDPG_MGDP_dh_C,UDPG_MGDP_dh_N	M9
bac_144	Gammaproteobacteria	KT	PspA_IM30	M9
bac_145	Bacteroidetes	K	OMP_b-brl_2	M9
bac_146	Gammaproteobacteria	K	Sigma70_r2,Sigma70_r4,Sigma70_r4_2	M9
bac_147	Gammaproteobacteria	M	Porin_2	M9
bac_148	Bacteroidetes	M	Hexapep,NTP_transferase	M9
bac_149	Bacteroidetes	M	Glyco_tranf_2_3,Glycos_transf_2	M9
bac_150	Gammaproteobacteria	M	Porin_2	M9
bac_151	Bacteroidetes	M	Fasciclin	M9
bac_152	Gammaproteobacteria	M	Fasciclin,Lipoprotein_15	M9
bac_153	Bacteroidetes	K	MarR,MarR_2	M9
bac_154	Gammaproteobacteria	M	CMAS	M9
bac_155	Bacteroidetes	K	MraZ	M9
bac_156	Bacteroidetes	J	Ribosomal_S4,S4	M10
bac_157	Rickettsiales	J	Ribosom_S12_S23	M10
bac_158	Clostridia	J	Ribosomal_L5,Ribosomal_L5_C	M10
bac_159	Bacilli	J	Ribosomal_L2,Ribosomal_L2_C	M10
bac_160	Bacteroidetes	J	KH_2,Ribosomal_S3_C	M10
bac_161	Rickettsiales	J	Ribosomal_S14	M10
bac_162	Tenericutes	J	Ribosomal_L6	M10
bac_163	Rickettsiales	J	Ribosomal_S13	M10
bac_164	Gammaproteobacteria	J	tRNA-synt_1c	M10

bac_165	Bacteroidetes	J	DNA_pol_A_exo1	M10
bac_166	Gammaproteobacteria	J	PseudoU_synth_2	M10
bac_167	Bacteroidetes	J	DNA_pol_A_exo1	M10
bac_168	Bacteroidetes	J	DNA_pol_A_exo1	M10
bac_169	Bacilli	J	Anticodon_1,tRNA-synt_1,tRNA-synt_1_2	M10
bac_170	Actinobacteria	HJ	ATPgrasp_TupA	M10
bac_171	Bacteroidetes	J	GTP_EFTU,GTP_EFTU_D2,RF3_C	M10
bac_172	Actinobacteria	J	GTP_EFTU,RF3_C	M10
bac_173	Thiotrichales	J	SpoU_methylase	M10
bac_174	Bacteroidetes	GM	Epimerase	M13
bac_175	Alphaproteobacteria	EGP	MFS_1	M13
bac_176	Gammaproteobacteria	EG	ILVD_EDD	M13
bac_177	Cyanobacteria	G	DUF563	M13
bac_178	Bacteria	G	CBM_4_9,CBM_6,F5_F8_type_C,Glyco_hydro_16,Glyco_hydro_cc,PKD,SKN1	M13
bac_179	Cyanobacteria	G	DUF563	M13
bac_180	Bacteroidetes	GM	Epimerase	M13
bac_181	Bacteria	GM	Epimerase,NAD_binding_10,Semialdhyde_dh	M13
bac_182	Bacteroidetes	EGP	MFS_1	M13
bac_183	Clostridia	J	Ribosomal_L5,Ribosomal_L5_C	M14
bac_184	Bacteroidetes	G	-	M14
bac_185	Bacteroidetes	J	Ribosomal_S8	M14
bac_186	Bacteroidetes	O	Redoxin	M14
bac_187	Bacteroidetes	CO	Thioredoxin	M14
bac_188	Alphaproteobacteria	J	Ribosomal_L5,Ribosomal_L5_C	M14
bac_189	Bacteroidetes	O	-	M14
bac_190	Alphaproteobacteria	J	Ribosomal_L6	M14
bac_191	Alphaproteobacteria	J	Ribosomal_S5,Ribosomal_S5_C	M14
bac_192	Bacteroidetes	O	CcmF_C,Cytochrom_C_asm	M14
bac_193	Bacteroidetes	J	GatB_N,GatB_Yqey	M14
bac_194	Alphaproteobacteria	J	Ribosomal_S19	M14
bac_195	Alphaproteobacteria	J	Ribosomal_L22	M14
bac_196	Bacteroidetes	O	NifU	M14
bac_197	Bacteria	CO	DUF4842,HYR	M14
bac_198	Actinobacteria	G	Transket_pyr,Transketolase_C,Transketolase_N	M14
bac_199	Actinobacteria	O	He_PIG,Inhibitor_I9,P_proprotein,Peptidase_S8	M14
bac_200	Bacteroidetes	G	GDPD,Glyco_hydro_16	M14
bac_201	Thiotrichales	G	RuBisCO_large,RuBisCO_large_N	M14
bac_202	Alphaproteobacteria	O	HSP70	M14
bac_203	Actinobacteria	G	Lactonase	M14
bac_204	Gammaproteobacteria	G	PQQ,PQQ_2	M14
bac_205	Alphaproteobacteria	O	Band_7	M14
bac_206	Alphaproteobacteria	J	Ribosomal_L3	M14
bac_207	Alphaproteobacteria	J	Ribosomal_S10	M14

bac_208	Actinobacteria	G	Lactonase	M14
bac_209	Proteobacteria	G	Lactonase	M14
bac_210	Alphaproteobacteria	G	DctP	M14
bac_211	Alphaproteobacteria	O	GSHPx	M14
bac_212	Proteobacteria	G	Lactonase	M14
bac_213	Proteobacteria	G	Lactonase	M14
bac_214	Actinobacteria	G	Lactonase	M14
bac_215	Actinobacteria	G	Lactonase	M14
bac_216	Actinobacteria	GM	Epimerase	M14
bac_217	Bacteroidetes	O	AhpC-TSA	M14
bac_218	Alphaproteobacteria	O	Thioredoxin_4	M14
bac_219	Alphaproteobacteria	J	HHH_5,Ribosomal_L21p	M14
bac_220	Alphaproteobacteria	GM	CIA30	M14
bac_221	Alphaproteobacteria	O	AAA,LON_substr_bdg,Lon_C	M14
bac_222	Alphaproteobacteria	J	Ribosom_S30AE_C,Ribosomal_S30AE	M14
bac_223	Alphaproteobacteria	O	Glutaredoxin	M14
bac_224	Bacteroidetes	O	Band_7	M14
bac_225	Alphaproteobacteria	O	1-cysPrx_C,AhpC-TSA	M14
bac_226	Kinetoplastida	O	Pro_isomerase	M14
bac_227	Alphaproteobacteria	J	Ribosomal_L10	M14
bac_228	Alphaproteobacteria	G	SBP_bac_1,SBP_bac_8	M14
bac_229	Alphaproteobacteria	J	Ribosomal_L19	M14
bac_230	Bacteroidetes	O	DSBA,Thioredoxin_5	M14
bac_231	Alphaproteobacteria	O	PMSR	M14
bac_232	Alphaproteobacteria	J	Ribosomal_S15	M14
bac_233	Alphaproteobacteria	J	eIF-1a	M14
bac_234	Cyanobacteria	E	GMC_oxred_C,GMC_oxred_N	M16
bac_235	Cyanobacteria	E	GMC_oxred_C,GMC_oxred_N	M16
bac_236	Cyanobacteria	KLT	AAA_16, GAF, HATPase_c, HisKA, PAS_3, Pkinase, Response_reg	M16
bac_237	Vibrionales	L	CBM_4_9, Endonuclease_1	M16
bac_238	Actinobacteria	Q	Cu-oxidase, Cu-oxidase_2, Cu-oxidase_3	M16
bac_239	Bacteria	L	AAA_11, AAA_12, AAA_30,HA, Helicase_C, NERD, ResIII, UvrD_C_2	M16
bac_240	Cyanobacteria	Q	Big_3_3, DUF4347, FG-GAP_2,VCBS	M16
bac_241	Alphaproteobacteria	EGP	MFS_1	M16
bac_242	Cyanobacteria	KLT	AAA_16, GAF, HATPase_c, HisKA, PAS_3,Pkinase,Response_reg	M16
bac_243	Cyanobacteria	KLT	AAA_16, GAF, Guanylate_cyc, HATPase_c, HisKA, PAS_4, Pkinase	M16
bac_244	Bacteria	Q	MerR, MerR_1, Methyltransf_11, Methyltransf_2, Methyltransf_23, Methyltransf_25,Methyltransf_31	M16
bac_245	Gammaproteobacteria	E	Amino_oxidase	M16
bac_246	Gammaproteobacteria	E	Amino_oxidase	M16
bac_247	Gammaproteobacteria	E	Amino_oxidase	M16
bac_248	Gammaproteobacteria	E	Amino_oxidase	M16

bac_249	Vibrionales	L	CBM_4_9, Endonuclease_1	M16
bac_250	Bacteria	EGP	MFS_1	M16
bac_251	Gammaproteobacteria	E	Amino_oxidase	M16
bac_252	Clostridia	L	RVT_3	M16
bac_253	Alphaproteobacteria	E	PALP	M16
bac_254	Alphaproteobacteria	E	PALP	M16
bac_255	Bacilli	Q	Acetyltransf_2	M16
bac_256	Rhodospirillales	Q	Methyltransf_21	M16
bac_257	Cyanobacteria	Q	LCM	M16
bac_258	Alphaproteobacteria	E	FMN_red	M16
bac_259	Gammaproteobacteria	L	CBM_4_9, Endonuclease_1	M16
bac_260	Bacteria	Q	Methyltransf_11, Methyltransf_23, Methyltransf_25,TPMT	M16
bac_261	Cyanobacteria	KLT	AAA_16, GAF, Guanylate_cyc, HATPase_c, HisKA, PAS_3, Pkinase	M16
bac_262	Bacteroidetes	E	CAP	M16

Appendix Publication IV

A CRISPR-Cas9 assisted analysis of single-cell microbiomes for identifying rare bacterial taxa in phycospheres of diatoms

Supplementary material

Table S5.1: Detailed information about *Thalassiosira gravida* strains used in this study.

name	NORCCA strain number	isolation date	lat	lon
A1	UIO478	20.08.17	83.33	29.29
A2	UIO483	05.09.17	83.15	31.46
A5	UIO448	12.09.17	79.99	14.97

Table S5.2: Recipe for full (modified) K – seawater medium. Final concentrations refer to the addition of the respective components and do not consider potential background concentration in seawater.

Full (modified) K - medium	
Component	Final concentration
Enrichments	
$NaNO_3$	8.82×10^{-4} M
$NaH_2PO_4 \times H_2O$	1.00×10^{-5} M
$Na_2SiO_3 \times 9\ H_2O$	$1{,}06 \times 10^{-4}$ M
H_2SeO_3	1.00×10^{-8} M
Tris Base	1.00×10^{-3} M
Supplements (trace metals)	
$Na_2EDTA \times 2\ H_2O$	1.12×10^{-4} M
$FeCl_3 \times 6\ H_2O$	1.17×10^{-5} M
$Na_2MoO_4 \times 2H_2O$	2.60×10^{-8} M
$ZnSO_4 \times 7\ H_2O$	7.65×10^{-8} M
$CoCl_2 \times 6\ H_2O$	4.20×10^{-8} M
$MnCl_2 \times 4\ H_2O$	9.10×10^{-7} M
$CuSO_4 \times 5\ H_2O$	1.96×10^{-8} M
Supplements (vitamins)	
Vitamin B12	3.69×10^{-10} M
Biotin	2.05×10^{-9} M
Thiamin HCl	2.96×10^{-7} M

Table S5.3: Recipe for nitrogen limited (modified) K – seawater medium. Final concentrations refer to the addition of the respective components and do not include background concentration in the seawater. By omitting the addition of inorganic nitrogen sources to the medium, the final nitrogen concentration is limited to the background concentration in the seawater (~ 5 µM $NaNO_3$; ~ 5 µM NH_4).

Nitrogen limited (modified) K - Medium	
Component	Final concentration
Enrichments	
$NaNO_3$	-
$NaH_2PO_4 \times H_2O$	1.00×10^{-5} M
$Na_2SiO_3 \times 9\ H_2O$	$1{,}06 \times 10^{-4}$ M
H_2SeO_3	1.00×10^{-8} M
Tris Base	1.00×10^{-3} M
Supplements (trace metals)	
$Na_2EDTA \times 2\ H_2O$	1.12×10^{-4} M
$FeCl_3 \times 6\ H_2O$	1.17×10^{-5} M
$Na_2MoO_4 \times 2H_2O$	2.60×10^{-8} M
$ZnSO_4 \times 7\ H_2O$	7.65×10^{-8} M
$CoCl_2 \times 6\ H_2O$	4.20×10^{-8} M
$MnCl_2 \times 4\ H_2O$	9.10×10^{-7} M
$CuSO_4 \times 5\ H_2O$	1.96×10^{-8} M
Supplements (vitamins)	
Vitamin B12	3.69×10^{-10} M
Biotin	2.05×10^{-9} M
Thiamin HCl	2.96×10^{-7} M

Table S5.4: Recipe for vitamin limited (modified) K – seawater medium. Final concentrations refer to the addition of the respective components and do not include background concentration in the seawater. However, due to autoclaving, vitamin concentrations in the seawater were negligible.

Vitamin limited (modified) K - Medium	
Component	Final concentration
Enrichments	
$NaNO_3$	8.82×10^{-4} M
$NaH_2PO_4 \times H_2O$	1.00×10^{-5} M
$Na_2SiO_3 \times 9\ H_2O$	$1{,}06 \times 10^{-4}$ M
H_2SeO_3	1.00×10^{-8} M
Tris Base	1.00×10^{-3} M
Supplements (trace metals)	
$Na_2EDTA \times 2\ H_2O$	1.12×10^{-4} M
$FeCl_3 \times 6\ H_2O$	1.17×10^{-5} M
$Na_2MoO_4 \times 2H_2O$	2.60×10^{-8} M
$ZnSO_4 \times 7\ H_2O$	7.65×10^{-8} M
$CoCl_2 \times 6\ H_2O$	4.20×10^{-8} M
$MnCl_2 \times 4\ H_2O$	9.10×10^{-7} M
$CuSO_4 \times 5\ H_2O$	1.96×10^{-8} M
Supplements (vitamins)	
Vitamin B12	-
Biotin	-
Thiamin HCl	-

Table S5.5: Modified DNA Extraction Protocol based on DNA MasterPure Complete DNA & RNA Purification Kit for fluid samples.

Step	Procedure
1	Thaw frozen samples (sample in 30 µL of 2xT&C Lysis buffer) at 50°C
2	Add 30 µL ultrapure H_2O
3	Add 30 µL mastermix (prepared as 30 µL 2xT&C Lysis Buffer + 0.2 µL Protease K per sample) at room temperature
4	Incubate for 15 min at 65°C and 1,000 rpm; cool for 5 min on ice
5	Add 45 µL MPC protein precipitation reagent; vortex for 10 s Centrifuge at 10,000 x g, 4°C for 10 min; transfer supernatant to new 1.5 mL reaction vile
6	Add 150 µL isopropanol and 0.7 µL Pellet Paint NF Co-Precipitant to each sample
7	Centrifuge at 15,000 x g, 4°C for 10 min; discard supernatant
8	Wash DNA pellet twice with 150 µL of 70% ethanol
9	Dissolve DNA pellet in 12.5 µL TE buffer
10	Store at -20°C

Table S5.6: List of common contaminants according to Sheik et al. (2018) and other non-marine bacteria that were excluded from analysis (if present).

Contaminant (Genus)			
Abiotrophia	*Cloacibacterium*	*Klebsiella*	*Polaromonas*
Acidobacteria Gp2	*Comamonas*	*Kocuria*	*Prevotella*
Acidovorax	*Corynebacterium*	*Lactobacillus*	*Prevotella_7*
Acinetobacter	*Craurococcus*	*Lawsonella*	*Propionibacterium*
Acinetobactera	*Cupriavidus*	*Leptothrix*	*Pseudomonas*
Actinomyces	*Curtobacterium*	*Limnobacter*	*Pseudoxanthomonas*
Aerococcus	*Curvibacter*	*Massilia*	*Psychrobacter*
Aeromicrobium	*Cutibacterium*	*Mesorhizobium*	*Ralstonia*
Afipia	*Deinococcus*	*Methylobacterium*	*Rhizobium*
Alloprevotella	*Delftiae*	*Methylophilus*	*Rhodococcus*
Anaerococcus	*Devosia*	*Methyloversatilis*	*Roseomonas*
Aquabacterium	*Dietzia*	*Microbacterium*	*Rothia*
Arthrobacter	*Duganella*	*Micrococcus*	*Ruminococcus*
Asticcacaulis	*Dyadobacter*	*Microlunatus*	*Schlegelella*
Aurantimonas	*Enhydrobacter*	*Neisseria*	*Sphingobium*
Azoarcus	*Enterobacter*	*Nevskia*	*Sphingomonas*
Azospira	*Escherichia*	*Niastella*	*Sphingopyxis*
Bacillus	*Escherichia-Shigella*	*Novosphingobium*	*Staphylococcus*
Beijerinckia	*Escherichia/Shigella*	*Ochrobactrum*	*Stenotrophomonas*
Beutenbergia	*Facklamia*	*Olivibacter*	*Streptococcus*
Bosea	*Finegoldia*	*Oxalobacter*	*Sulfuritalea*
Bradyrhizobium	*Flavobacterium*	*Paenibacillus*	*Tsukamurella*
Brevibacillus	*Fusobacterium*	*Parabacteroides*	*Turicella*
Brevibacterium	*Geodermatophilus*	*Paracoccus*	*Undibacterium*
Brevundimonas	*Haemophilus*	*Pasteurella*	*Variovorax*
Brochothrix	*Herbaspirillum*	*Patulibacter*	*Veillonella*
Burkholderia	*Hoefleae*	*Pedobacter*	*Wautersiella*
Capnocytophaga	*Hydrotalea*	*Pedomicrobium*	*Xanthomonas*
Cardiobacterium	*Janibacter*	*Pelomonas*	
Caulobacter	*Janthinobacterium*	*Peptoniphilus*	
Chryseobacterium	*Kingella*	*Phyllobacterium*	

Table S5.7: ANOVA results testing differences in bacterial richness and Shannon diversity of *T. gravida* single cell microbiomes as a response of strain identity, culture condition and DNA processing method. F and p-values are reported for each effect. Values marked with an asterisk (*) indicate significant effects ($p < 0.05$).

		Richness			Shannon		
Effect	*Df*	*F*	*p*		*F*	*p*	
Strain	2	27.525	<0.001	*	27.905	<0.001	*
Condition	2	4.965	0.008	*	6.283	0.003	*
Method	1	0.476	0.492		0.488	0.486	
Strain*Condition	4	3.424	0.011	*	4.108	0.004	*

Table S5.8: PERMANOVA results testing differences in bacterial community composition of *T. gravida* single cell microbiomes as a response of strain identity and culture condition. F and p-values are reported for each effect. Values marked with an asterisk (*) indicate significant effects ($p < 0.05$).

		microbiome composition			
Effect	*Df*	R^2	*F*	*p*	
Strain	2	0.700	199.9	<0.001	*
Condition	2	0.042	12.1	<0.001	*
Strain*Condition	4	0.048	6.9	<0.001	*

Table S5.9: Multiple ANOVA results on normalized ASV read counts summarized on the genus level as a response to strain identity, culture condition and their respective interactive effect. Combinations of bacterial genera and respective effects marked with an asterisk indicate significant effects (significance code: * = $p < 0.05$ & > 0.01; ** = $p < 0.01$ & > 0.001; *** = $p < 0.001$).

Genus	strain	condition	strain*condition
Adhaeribacter			
Alloiococcus			
Amaricoccus			
Aurantivirga	***	**	***
Balneola	**	***	***
Candidatus Phaeomarinobacter			
Celeribacter	***	***	*
Colwellia	***	***	**
Croceibacter			
Fimbriiglobus			
Friedmanniella			
Gemella			
Glaciecola	***	***	***
Granulicatella			
Ilumatobacter			
Lentilitoribacter	***	***	***
Luteimonas			
Maribacter			
Marinobacter	***	***	***
Marinomonas	***	***	***
Methylobacterium-Methylorubrum			
Methylophaga			*
Mf105b01	***		
NS3a marine group	***		
Octadecabacter	***	***	***
Oleiphilus	*		
Owenweeksia	***		
Pacificibacter			
Paraglaciecola	***	***	***
Peredibacter	***		
Phaeobacter			
Polaribacter	***		
Porticoccus		*	
Pseudohongiella		**	
Reichenbachiella			
Romboutsia			
Roseivirga			*
Roseobacter clade NAC11-7 lineage	***		**
Sedimentitalea	***		***
Segetibacter			
Sphingorhabdus	***		
Spirosoma			
Sulfitobacter	***	**	
Thalassospira			*
Treponema			
Verticiella			
Zhongshania			

Table S5.10: Results of ANOVA testing the effects of SCHoCO-seq treatment on bacterial ASV richness for microbiomes of *T. gravida* single cells. Single cell ID was treated as random factor. Degrees of freedom (df), mean squares (Mean Sq), F-, and p-values are given. Values marked with an asterisk (*) indicate significant effects ($p < 0.05$).

			Richness		
Main Effect	Df	Mean Sq	*F*	*p*	
SCHoCO-seq	1	282.01	81.34	< 0.001	*
Random Effect					
Single-Cell ID	61	29.68	-	-	

Fig. S5.1: Gel-electrophoresis of 16S rDNA Amplicons. Single Cell Samples from Strain A1 (top), A2 (middle) and A5 (bottom). Eight single cells from full medium (left), from vitamin depleted medium (middle) and from nitrogen depleted medium (right). Culture blanks (culture samples without diatom cells) on the left of each row for all three strains. Size of Amplicons is around 1.5 kb according to the 1 kb DNA Ladder (Gold Biotechnology Inc, USA).

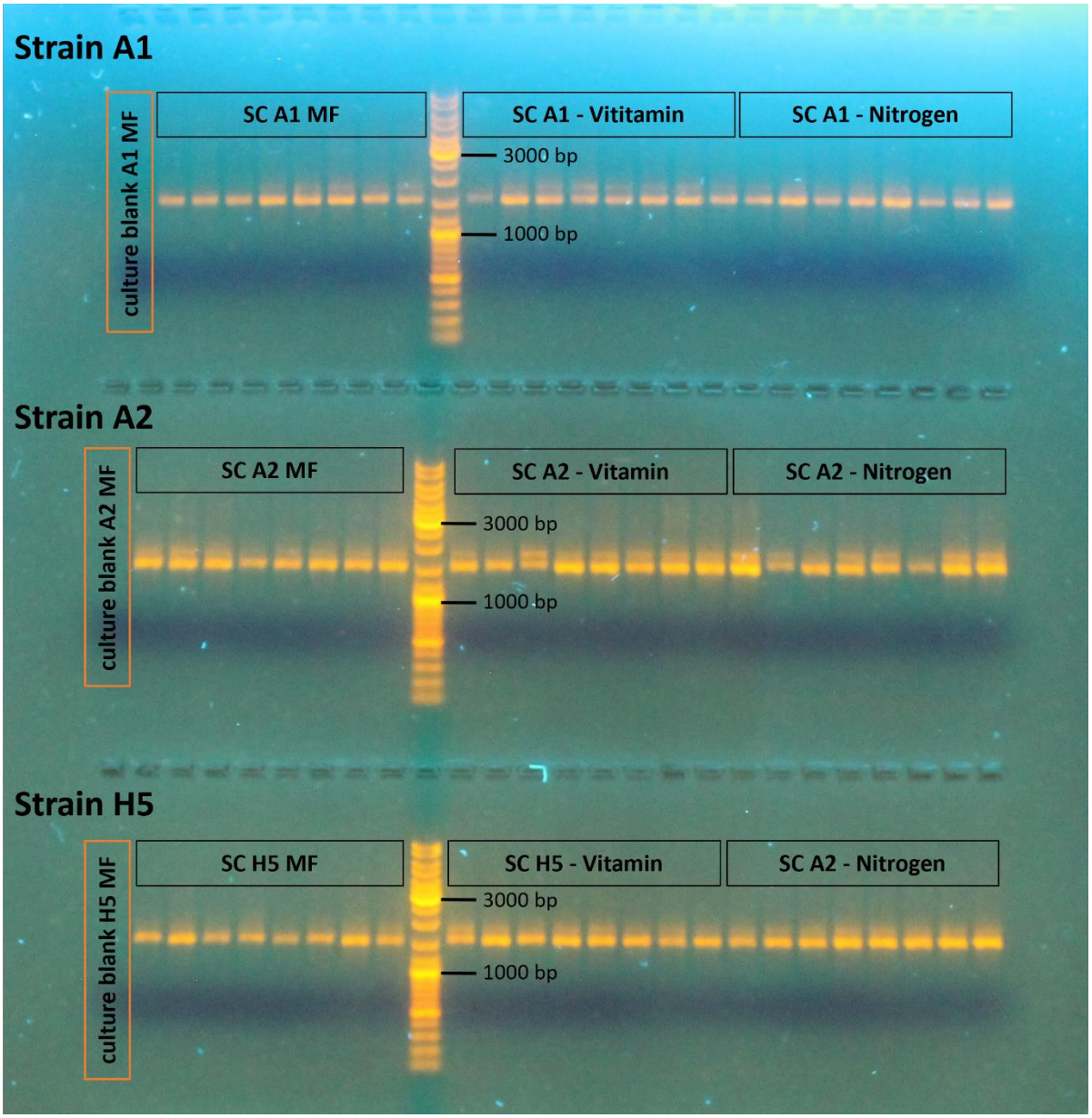

Fig. S5.2: Design of gRNA from four oligonucleotides. Primer F and Primer R are needed to generate full length gDNA copies during PCR. The Specific oligo #7 contains the target binding sequence (red) and is linked to the universal oligo containing the Cas9 Nuclease binding site by the linker region (green).

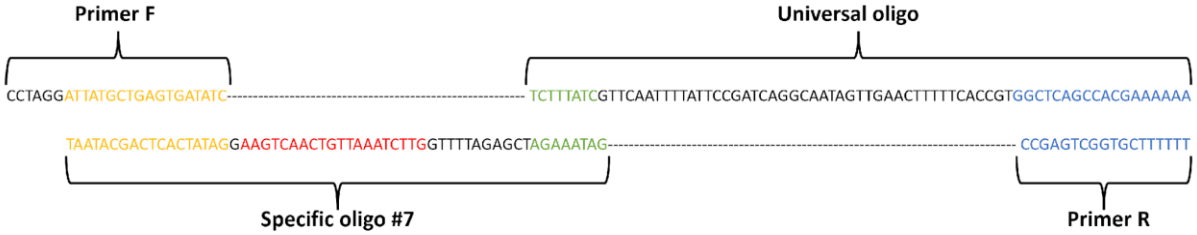

Fig. S5.3: Bacterial richness (right) and Shannon diversity (left) of *T. gravida* single cell microbiomes across two different DNA processing methods (i.e., extracted DNA vs. direct PCR).

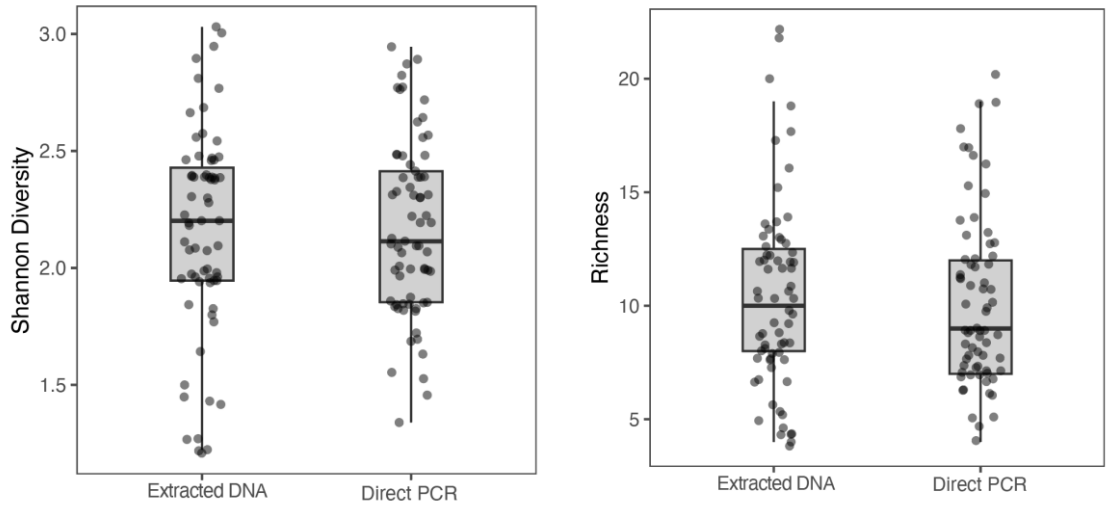

Fig. S5.4: Bacterial richness (top row) and Shannon diversity (bottom row) of T. *gravida* single cell microbiomes across strains and culture conditions represented as horizontal facets.

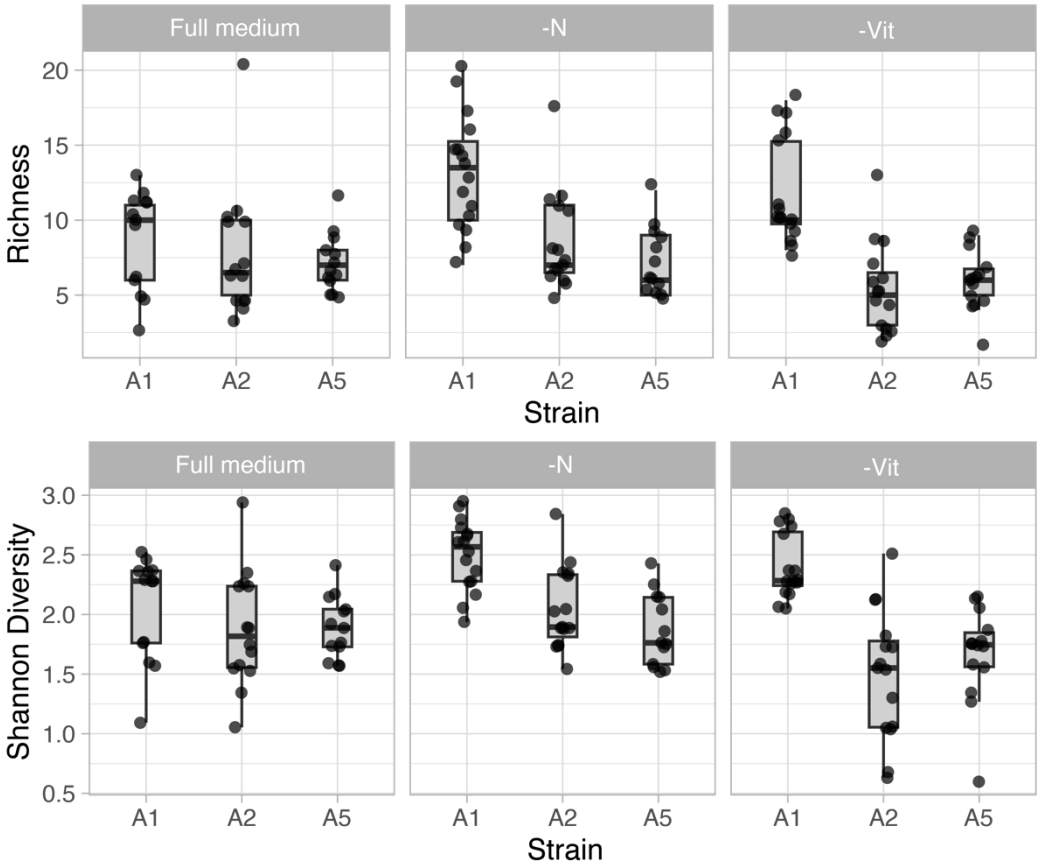

Declaration

Versicherung an Eides Statt

Name, Vorname	Giesler, Jakob
Matrikel-Nr.	6156286

Ich, Jakob Giesler,

versichere an Eides Statt durch meine Unterschrift, dass ich die vorstehende Arbeit selbständig und ohne fremde Hilfe angefertigt und alle Stellen, die ich wörtlich dem Sinne nach aus Veröffentlichungen entnommen habe, als solche kenntlich gemacht habe, mich auch keiner anderen als der angegebenen Literatur oder sonstiger Hilfsmittel bedient habe.

Ich versichere an Eides Statt, dass ich die vorgenannten Angaben nach bestem Wissen und Gewissen gemacht habe und dass die Angaben der Wahrheit entsprechen und ich nichts verschwiegen habe.

Die Strafbarkeit einer falschen eidesstattlichen Versicherung ist mir bekannt, namentlich die Strafandrohung gemäß §156 StGB bis zu drei Jahren Freiheitsstrafe oder Geldstrafe bei vorsätzlicher Begehung der Tat bzw. gemäß §161 Abs. 1 StGB bis zu einem Jahr Freiheitsstrafe oder Geldstrafe bei fahrlässiger Begehung.

_____ _____

Ort, Datum Unterschrift

Contribution

Declaration on the contribution of the candidate to a multi-author article/manuscript. Contribution of the candidate in % of the total workload (up to 100% for each of the following categories).

Chapter 2, Publication I

Experimental concept and design: ca. 70%

Experimental work and/or acquisition of (experimental) data: ca. 95%

Data analysis and interpretation: ca. 70%

Preparation of Figures and Tables: ca. 95%

Drafting of the manuscript: ca. 85%

Chapter 3, Publication II

Experimental concept and design: ca. 95%

Experimental work and/or acquisition of (experimental) data: ca. 100%

Data analysis and interpretation: ca. 80%

Preparation of Figures and Tables: ca. 100%

Drafting of the manuscript: ca. 75%

Chapter 4, Publication III

Experimental concept and design: ca. 90%

Experimental work and/or acquisition of (experimental) data: ca. 80%

Data analysis and interpretation: ca. 75%

Preparation of Figures and Tables: ca. 80%

Drafting of the manuscript: ca. 90%

Chapter 5, Publication IV

Experimental concept and design: ca. 35%

Experimental work and/or acquisition of (experimental) data: ca. 35%

Data analysis and interpretation: ca. 50%

Preparation of Figures and Tables: ca. 65%

Drafting of the manuscript: ca. 70%

2024

JAKOB K. GIESLER